



**University of
Nottingham**
UK | CHINA | MALAYSIA

Targeting HOXA in engineered iPSCs and pre-clinical leukaemia models

Mays Abuhantash MSc, BSc (Hons)
School of Medicine
Biodiscovery Institute
The University of Nottingham

Thesis submitted to the University of Nottingham for the Degree
of Doctor of Philosophy

March 2023

Acknowledgements

I would like to thank my principal supervisor Dr Alexander Thompson for being a mentor, a friend and a father during my postgraduate education. His ongoing support, guidance and motivation has helped me in all stages of my MSc and PhD projects. His humble approach to science and dedication to research is an inspiration. I would also like to acknowledge my secondary supervisor, Dr Claire Seedhouse, for her significant advice and immense knowledge.

I must thank the technical and administrative staff at the Biodiscovery Institute, especially Paula Olsen, who has helped me with invaluable help and support. I thank Dr Emma Collins (EC) for her help and advice with haematopoietic differentiation experiments. I would also like to thank Dr Kenton Arkill for his advice and help with confocal microscopy and imaging. I thank Dr William Hotham for his assistance with fluorescence imaging. I also thank Dr Alexander Kondrashov for his insightful discussions and guidance on gene editing. I also thank Dr David Onion and Dr Nicola Croxall for their help at the flow cytometry facility.

I would like to sincerely thank the BCASC group, you have made my time truly enjoyable. Dr Kate Butcher and Lara Doolan, thank you for all the happy memories in the lab. Thank you for your kind words during the stressful times. It has truly made a difference in my PhD journey.

Last but not least, words cannot express my deepest gratitude to my support system; my family. Without them, this PhD would not have been possible. My heroes, mom and dad, I am forever thankful for your never-ending love, encouragement and prayers in my life. I owe you all that I have accomplished so far. My sister, you have been with me every step of the way and I am forever lucky to have you. My brothers, your presence was what sustained me this far. I promise to make your patience and efforts during my journey abroad worthwhile.

Declaration

I hereby declare that this thesis has been composed by myself and has not been submitted for any other degree previously. This project was supervised by Dr Alexander Thompson and Dr Claire Seedhouse. Acknowledgments of specific procedures not performed by myself are stated; otherwise, the work described is my own.

Abstract

Haematopoiesis is a highly regulated process governed by a complex network of transcription factors and signalling molecules. *HOXA* genes are master regulators of embryonic development and haematopoiesis. In normal haematopoiesis, expression of *HOXA* is high in haematopoietic stem and progenitor cells (HSPCs) and decreases upon differentiation and maturation. Aberrant expression of the *HOXA* cluster, particularly *HOXA9*, is associated with malignant haematopoiesis.

To enable routine and efficient production of iPSC-derived HSPCs, two haematopoietic differentiation systems mimicking the stages of haematopoietic development and specification *in vivo* were tested. The monolayer-based differentiation was improved using a single-cell derived approach. Embryoid body (EB) differentiation was found to be more efficient and reproducible. Cells were characterised at key stages of the process by flow cytometry, qRT-PCR and methylcellulose colony assays. To monitor *HOXA9* expression, an endogenous *HOXA9*-mScarlet reporter (eA9^m) iPSC line was generated using CRISPR/Cas9 system and validated by Sanger sequencing. The functionality of eA9^m was assessed using EB differentiation and confocal microscopy. Fluctuations in *HOXA9* expression were coincident with *mScarlet-H* expression, particularly at early stages of the EB differentiation. Proof-of-principle studies revealed that exposure of eA9^m iPSCs or EBs to oncogenic *MLL::AF9* results in deregulation of key haematopoietic genes, including *HOXA* genes.

In malignant haematopoiesis, *MLL*-rearranged leukaemias are a hallmark for aggressive paediatric blood cancer. *MLL* fusion proteins, particularly *MLL::AF9*, contribute to disease pathogenesis through upregulation of transcription factors, in particular *HOXA9*, which is associated with poor clinical outcome and a high incidence of relapse. A *HOXA*^{del} signature from a conditional transgenic mouse model was used to identify and validate potential anti-*HOXA* FDA-approved drugs. These drugs were found to possess variable anti-leukaemic properties *in vitro*, as shown by RNA sequencing analysis which should be further investigated. This highlights the importance of using advanced models for drug

discovery. Thus, eA9^m iPSCs can be used to generate isogenic models of diseases involving dysregulated expression of *HOXA9* such as leukaemia.

Table of Contents

Chapter 1	Introduction	1
1.1	Haematopoiesis	1
1.1.1	Embryonic haematopoietic development	1
1.1.2	Waves of haematopoiesis	3
1.1.3	Haematopoietic differentiation of human iPSCs	4
1.1.4	Characterisation of iPSC-derived HSPCs	6
1.1.5	Role of HOXA genes in normal haematopoiesis	8
1.2	Malignant haematopoiesis	10
1.2.1	Acute leukaemias	10
1.3	Mixed lineage leukaemia	12
1.3.1	MLL/KMT2A gene in leukaemia	12
1.3.2	Disease models of MLL-rearranged leukaemia	13
1.3.3	Role of HOXA genes in malignant haematopoiesis	15
1.4	Drug discovery	17
1.4.1	Leukaemic stem cells	17
1.4.2	iPSC-based drug discovery	18
1.4.3	Drug repurposing	19
1.5	Genome editing	20
1.5.1	CRISPR/Cas9-mediated genome editing	20
1.5.2	CRISPR/Cas9 in haematopoiesis	21
1.6	Hypothesis and aims	23
Chapter 2	Materials and Methods	24
2.1	Cell culture	24
2.1.1	Human iPSCs maintenance and cryopreservation	24
2.1.2	iPSC-derived HSPCs culture	24
2.1.3	Leukaemic cell lines maintenance	24
2.2	Haematopoietic differentiation	25
2.2.1	STEMdiff™ haematopoietic kit	25
2.2.2	Spin Embryoid Body haematopoietic differentiation	25

2.2.3	Colony-forming unit assay	27
2.3	SB/CHIR/RA treatment.....	27
2.3.1	Cell culture and treatment on coverslips	27
2.3.2	Immunofluorescence.....	28
2.4	DNA integration.....	28
2.4.1	Lentiviral production	28
2.4.2	Lentiviral transduction	29
2.4.3	Plasmid transfection/ Nucleofection	29
2.5	Molecular biology.....	30
2.5.1	Genomic DNA extraction	30
2.5.2	RNA extraction.....	30
2.5.3	cDNA synthesis	31
2.5.4	Quantitative real-time polymerase chain reaction (qRT-PCR)	31
2.6	Flow cytometry.....	32
2.7	Genetic engineering of HOXA9 reporter line, eA9^m	33
2.7.1	Plasmid design and eA9 ^m generation.....	33
2.7.2	Polymerase chain reaction (PCR).....	34
2.7.3	Primer design.....	34
2.7.4	Agarose gel electrophoresis.....	35
2.7.5	Sanger sequencing	35
2.8	Microscopy	36
2.9	Anti-leukaemic drug treatment.....	36
2.9.1	Dose response assay	36
2.9.2	RNA sequencing.....	37
2.9.3	RNA sequencing analysis	37
2.9.4	Statistical analysis.....	37
Chapter 3	<i>Haematopoietic differentiation of human iPSCs</i>	38
3.1	Brief background	38
3.2	Monolayer differentiation using the STEMdiff™ kit	39
3.2.1	iPSC passaging and seeding for haematopoietic differentiation.....	39
3.2.2	Single cell eA9 ^m iPSCs seeding yields CD34+CD43/CD45+ using the STEMdiff™ kit.....	43
3.2.3	Extended differentiation culture on viability	44
3.2.4	Extended differentiation culture does not affect the clonogenicity of eA9 ^m -derived HSPCs	
	46	
3.3	Spin EB differentiation	46

3.3.1	Overview of HSPCs derivation from iPSCs using the spin EB method.....	46
3.3.2	Mesodermal and haemogenic endothelial cell generation from eA9 ^m iPSCs	47
3.3.3	eA9 ^m cells can differentiate to HSPCs using the spin EB method	49
3.3.4	Formation of multipotent HSPCs from eA9 ^m cells through HE specification.....	51
3.4	Streamlining the timing of mesoderm patterning and endothelial induction in spin EB differentiation.....	54
3.4.1	Mesoderm patterning timing affects CD34 and CD90 expression of day 7 EBs.....	55
3.4.2	Induction of mesoderm at 38h hinders HSPCs production	57
3.4.3	Increased mesoderm induction enhances HSPC production	59
3.5	Summary of results	61
Chapter 4 Generation of a HOXA9-mScarlet reporter cell line		63
4.1	Brief background	63
4.2	Gene targeting strategy of the endogenous HOXA9 locus in iPSCs.....	63
4.3	Molecular validation of HOXA9 targeting.....	66
4.4	Functional validation through HOXA9 upregulation	73
4.4.1	Upregulation of HOXA9 using Wnt pathway-related molecules.....	73
4.4.2	Haematopoietic differentiation: HOXA9 vs RUNX1	75
4.5	MLL::AF9 treatment of eA9^m cells.....	79
4.5.1	MLL::AF9 nucleofection of eA9 ^m iPSCs.....	79
4.5.2	MLL::AF9 lentiviral transduction of eA9 ^m iPSCs.....	81
4.5.3	LVp addition during spin EB differentiation	87
4.5.4	Effect of LVp addition on gene expression during the spin EB differentiation	90
4.5.5	LVp exposure enhances production of HSPCs with myeloid lineage bias	92
4.5.6	EBs show mScarlet-H fluorescence at varying intensities.....	94
4.6	Summary of results	96
Chapter 5 Investigation of the efficacy of FDA-approved drugs in AML 98		
5.1	Brief background	98
5.2	Effect of FDA-approved drugs on cell viability of leukaemic cell lines..	99
5.2.1	Homoharringtonine (HHT)	99
5.2.2	Atorvastatin (ATV)	100
5.3	Effect of atorvastatin and homoharringtonine on colony formation....	103
5.4	Gene expression profiling of IC50-treated leukaemic cell lines.....	104
5.5	Differential expression in IC50-treated leukaemic cell lines	106
5.6	Pathway analysis of IC50-treated leukaemic cell lines	109

5.7	Validation of DEGs identified using RNA sequencing by qPCR	115
5.8	Discussion	119
Chapter 6	General Discussion	122

List of figures

Figure 1.1	Haematopoietic development during embryogenesis.....	2
Figure 1.2	Structure of a human HOXA gene and protein.	9
Figure 1.3	An overview of the role of HOXA in normal and malignant haematopoiesis.....	16
Figure 1.4	A schematic of the conventional and iPSCs drug discovery routes.	19
Figure 1.5	Applications of CRISPR/Cas9 in haematology.	22
Figure 3.1	Aggregate passaging of RPATs or eA9 ^m results in high variability in HSPC formation using the STEMdiff™ kit.	41
Figure 3.2	Single cell seeding of RPATs for STEMdiff™ differentiation.....	43
Figure 3.3	Culture and characterisation of single cell-derived eA9 ^m -derived HSPCs using the STEMdiff™ kit.....	45
Figure 3.4	Lineage committed haematopoietic progenitors formed from eA9 ^m -derived HSPCs using the CFU assay.	46
Figure 3.5	Overview of the spin EB haematopoietic differentiation method.....	47
Figure 3.6	eA9 ^m can differentiate to mesodermal and haemogenic endothelial cells.	49
Figure 3.7	Surface marker analysis of iPSC-HSPCs derived using the spin EB differentiation.	51
Figure 3.8	Changes in key haematopoietic gene expression during the spin EB differentiation.	53
Figure 3.9	Lineage committed haematopoietic progenitors formed from eA9 ^m spin EB-derived HSPCs using the CFU assay.....	54
Figure 3.10	Comparative analysis of the effect of 38h or 40h SB/CHIR treatment on morphology and surface marker expression in day 7 EBs.....	56
Figure 3.11	Comparative analysis of the effect of 38h and 40h SB/CHIR treatment on surface marker co-expression and viability in day 7 EBs.....	57
Figure 3.12	Comparative analysis of the effect of SB/CHIR treatment timing on generation and colony formation of day 14 and day 18 suspension cells.	58

Figure 3.13 Analysis of HSPCs characterisation and viability derived from 40h-treated EBs.	60
Figure 4.1 Strategy for the footprint-free targeting of the endogenous HOXA9 locus.	65
Figure 4.2 CRISPR/Cas9 targeting plasmid map.	66
Figure 4.3 Validation of 5' integration and presence of mScarlet-H in HOXA9 locus.	67
Figure 4.4 Validation of integration and excision of the PB cassette from the HOXA9 locus.	68
Figure 4.5 Validation of PB cassette excision after transposase treatment.	69
Figure 4.6 Validation of post excision clones by Sanger sequencing.	70
Figure 4.7 PiggyBac cassette elements are retained post-excision in eA9 ^m cells.	72
Figure 4.8 eA9 ^m are not resistant to puromycin.	72
Figure 4.9 eA9 ^m retain a copy of the wildtype HOXA9 allele.	73
Figure 4.10 iPSC seeding and attachment on coverslips.	74
Figure 4.11 eA9 ^m cells show mScarlet-H fluorescence upon HOXA9 stimulation.	75
Figure 4.12 Differential gene expression of eA9 ^m and RPATs during EB differentiation.	77
Figure 4.13 Nucleofection of MLL::AF9 plasmids in eA9 ^m cells.	80
Figure 4.14 Measure of LVp using Lenti-X TM GoStix TM Plus.	82
Figure 4.15 High-titre MLL::AF9 LVp transduction causes stress of eA9 ^m cells.	83
Figure 4.16 Effect of polybrene and LVp on morphology of eA9 ^m	84
Figure 4.17 Effect of LVp transduction on gene expression in eA9 ^m	85
Figure 4.18 Expression of mScarlet after MLL::AF9 lentiviral transduction in eA9 ^m cells.	87
Figure 4.19 Effect of lentiviral transduction on morphology, haematopoietic markers expression and viability of EBs.	90
Figure 4.20 Differential gene expression following LVp induction of eA9 ^m -derived EBs during generation of HSPCs.	91
Figure 4.21 Colony forming potential of HSPCs after LVp exposure.	93
Figure 4.22 mScarlet-H expression in eA9 ^m EBs during spin EB haematopoietic differentiation.	95

Figure 5.1 Effect of HHT on the viability of leukaemic cell lines.	100
Figure 5.2 Effect of ATV on the viability of leukaemic cell lines.....	102
Figure 5.3 Effect of HHT and ATV treatment on colony formation in leukaemic cell lines.	104
Figure 5.4 Gene expression relationship between treated leukaemic cell lines.	105
Figure 5.5 Differential gene expression of leukaemic cell lines treated with HHT.	107
Figure 5.6 Differential gene expression of leukaemic cell lines treated with ATV.	108
Figure 5.7 Schematic representation of co-expressed genes in treated leukaemic cell lines.	109
Figure 5.8 Pathway analysis of differentially expressed genes in THP1 treated with HHT or ATV.....	111
Figure 5.9 Pathway analysis of differentially expressed genes in MV4-11 treated with HHT or ATV.....	112
Figure 5.10 Pathway analysis of differentially expressed genes in OCI-AML3 treated with HHT or ATV.	113
Figure 5.11 Pathway analysis of differentially expressed genes in HL60 treated with HHT or ATV.....	114
Figure 5.12 Validation of DEGs in treated leukaemic cell lines by qPCR.....	118

List of tables

Table 2.1 Components of the Spin EB differentiation medium.	26
Table 2.2 Plasmids used in transfection	29
Table 2.3 qPCR primers used for haematopoietic differentiation characterisation	31
Table 2.4 qPCR primers used for RNA sequencing results validation	32
Table 2.5 Conjugated antibodies used for flow cytometry	33
Table 2.6 PCR thermocycling conditions	34
Table 2.7 Genotyping primers used in genomic PCR	34
Table 3.1 Stage-specific surface markers of cells during haematopoietic differentiation	39
Table 3.2 Comparison between two different iPSCs passaging methods tested.	42
Table 3.3 Number of HSPCs derived from RPATs and eA9 ^m	59
Table 4.1 Intensity of mScarlet-H fluorescence in eA9 ^m EBs.....	96
Table 5.1 Common mutations in AML cell lines	99
Table 5.2 Significance of KEGG pathways selected for validation	115
Table 5.3 Genes from four pathways and at least 3 cell lines were selected for validation by qPCR	116
Table 5.4 Gene expression changes identified from RNA sequencing data ...	116

Abbreviations

AGM	Aorta-gonad-mesonephros
ALL	Acute lymphoid leukaemia
AML	Acute myeloid leukaemia
ATV	Atorvastatin
BFU-E	Blood forming unit-erythroid
BMP4	Bone morphogenic protein 4
CAR	Chimeric antigen receptor
CAS	Crispr-associated
CFU	Colony forming-unit
CFU-E	Colony forming-unit-erythroid
CR RNA	Crispr RNA
CRISPR	Clustered regularly interspaced palindromic repeats
DEGs	Differentially expressed genes
DSB	Double strand breaks
E	Embryonic day
E8	Essential 8
EB	Embryoid body
EHT	Endothelial-to-haematopoietic transition
EMPs	Erythromyeloid progenitors
FBS	Foetal bovine serum
FGF2	Fibroblast growth factor 2
FPKM	Fragments per kilobase of exon per million mapped
GCDR	Gentle cell dissociation reagent
GEMM	Granulocyte erythroid macrophage monocyte
GM	Granulocyte macrophage
GRNA	guideRNA
HDR	Homology directed repair
HE	Hemogenic endothelium
HEK	Human embryonic kidney
hESC	Human embryonic stem cells
HHT	Homoharringtonine

HMT	Histone methyl transferase
HOXA	Homeobox A
HR	Homologous repair
HSCs	Haematopoietic stem cells
HSPC	Haematopoietic stem and progenitor cells
HMG-CoA	Hydroxymethylglutaryl coenzyme A
IDH2	Isocitrate dehydrogenase 2
iPSCs	Induced pluripotent stem cells
KDR	Kinase insert domain receptor
KEGG	Kyoto Encyclopedia of Genes and Genomes
KMT2A	Lysine-specific methyltransferase 2A
LSC	Leukaemic stem cells
LVp	Lentivirus particle
MLL	Mixed lineage leukaemia
MLLr	Mixed lineage leukaemia rearrangement
NHEJ	Non-homologous end joining
PAM	Protospacer adjacent motif
PCA	Principal component analysis
pcw	Post-conception weeks
PD1	Programmed cell death 1
PFA	Paraformaldehyde
PB	PiggyBac
PP1A	Protein phosphatase 1A
PSCs	Pluripotent stem cells
RA	Retinoic acid
RC	Revitacell
RI	Rock inhibitor
RPATs	ReBI-Pats
RQ	Relative quantification
RT	Reverse transcriptase
TAE	Tris-acetate-EDTA
TALE	Three-amino-acid-loop-extension motif
TALENS	Transcription activator-like effector nucleases
TFs	Transcription factors
tracrRNA	Transactivating crispr RNA
ZFN	Zinc finger nucleases

Chapter 1 Introduction

1.1 Haematopoiesis

1.1.1 Embryonic haematopoietic development

Haematopoiesis is a tightly regulated multi-step process, giving rise to the formation of peripheral blood. In adult humans, peripheral blood comprises of approximately one trillion cells arising daily from the human bone marrow (Doulatov et al., 2012). Haematopoiesis leads to the formation of mature functional blood cells of all lineages by differentiation of haematopoietic stem cells (HSCs). These self-renewing, multipotent HSCs were previously thought to be a distinct, homogenous population at the top of a hierarchical tree-like model. Here, the first branch point bifurcates into a strict separation of myeloid and lymphoid lineages that progresses to unipotent progenitor cells and finally gives rise to mature haematopoietic cells (Belyavsky et al., 2021; Laurenti and Göttgens, 2018). Although the classical model provides better understanding for the process of HSCs differentiation, it does not fully reveal the complexity of the process. This is because it is mainly based on bulk cell analysis. Over the past years, the classical model has been challenged and a more complex version emerged, in part due to technologies such as single cell transcriptomics and genetic mouse models (Laurenti and Göttgens, 2018). Several studies have shown that the haematopoietic differentiation is continuous, rather than a discrete, step-wise process (reviewed in Cheng et al., 2020). The current biological model indicates that the HSCs compartment is a molecularly and functionally heterogenous continuum of low-primed undifferentiated HSPCs undergoing several transient states of differentiation (Cheng et al., 2020). Recently, more biological models for mammalian stem cell homeostasis are being investigated (Nakamuta et al., 2022).

The process of haematopoietic development has been extensively studied in the mouse, which closely recapitulates the human process (Frame et al., 2013). During embryogenesis, haematopoiesis occurs in temporally and spatially distinct waves, generating progenitors that vary in their haematopoietic potential (reviewed in Belyavsky et al., 2021). An overview of the location of haematopoietic sites and distinct timings is presented in Figure 1.1. Primitive

haematopoiesis, the first wave, occurs in the extra-embryonic yolk sac from embryonic day 7 (E7.0) and 2-3 post-conception weeks (pcw) in mouse and human embryos, respectively (Canu and Ruhrberg, 2021; Palis et al., 1999; Ivanovs et al., 2017; Soares-da-Silva et al., 2021). It is marked by the emergence of the first detectable haematopoietic progenitors, which have limited potential and predominantly give rise to primitive erythrocytes (Palis and Yoder, 2001). Definitive haematopoiesis comprises the second and third waves of haematopoiesis, and gives rise to erythro-myeloid progenitors (EMPs) and HSCs, respectively. The second wave is termed as pro-definitive and the third wave is definitive haematopoiesis (Canu and Ruhrberg, 2021). In the mouse embryo, the second wave takes place in the extra-embryonic yolk sac at E9.5, while the third wave begins in the intra-embryonic embryo proper at E10.5 (Palis et al., 1999; reviewed in Canu and Ruhrberg, 2021). In the same way, the second wave occurs at 4-5 pcw in the yolk sac, followed by the third wave at 6-7 pcw in the human embryo (Tavian et al., 2001; Baron et al., 2012; Canu and Ruhrberg, 2021).

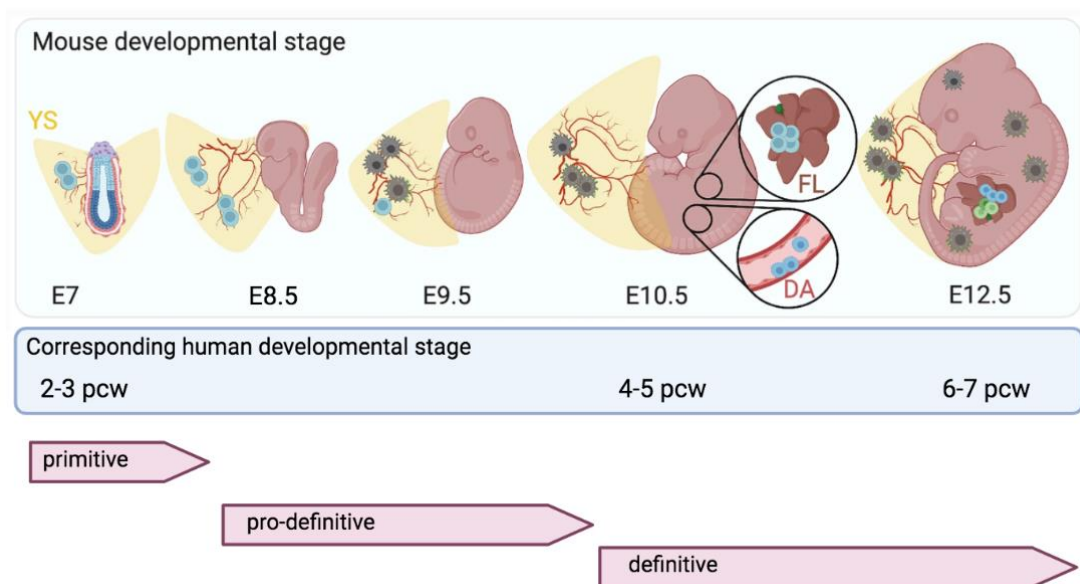


Figure 1.1 Haematopoietic development during embryogenesis.

Three developmental waves of haematopoiesis indicated as primitive, pro-definitive and definitive. These waves are spatiotemporally overlapping, producing distinct haematopoietic progenitors. The primitive and pro-definitive wave occur in the yolk sac (YS), whereas definitive wave arises in the AGM. Definitive wave produces HSCs from the haemogenic endothelium within the dorsal aorta (DA). Haematopoietic progenitors from the pro-definitive and definitive waves populate the foetal liver (FL), making it the main blood cell production until around birth. Timing of the initiation of these waves in mouse and

human embryo is indicated. Figure modified from Canu and Ruhrberg, 2021, using biorender.com

1.1.2 Waves of haematopoiesis

During haematopoietic development, a complex network of intrinsic factors and environmental cues govern the continuous process of lineage-commitment through the activation and repression of distinct signalling pathways (Belyavsky et al., 2021). In the embryo, combined bone morphogenic protein 4 (BMP4), fibroblast growth factor 2 (FGF2), Wnt and Nodal signalling regulates the first critical wave of haematopoiesis (Canu and Ruhrberg, 2021). Ingression of the primitive streak occurs next, as surface ectoderm cells undergo an epithelial-mesenchymal transition and migrate to the yolk sac, forming mesodermal cells (Conlon et al., 1994; Flamme et al., 1995; Winnier et al., 1995; Liu et al., 1999; Canu and Ruhrberg, 2021). Within the blood islands of the yolk sac, kinase insert domain receptor (KDR) and Brachury- expressing mesodermal progenitors, with restricted potential, give rise to the first haematopoietic cells (foetal haemoglobin expressing-erythroblasts, embryonic macrophages, and megakaryocytes) (Canu and Ruhrberg, 2021; Ferkowicz and Yoder, 2005). This transient wave is required for the continued rapid growth of the embryo as it functions to meet tissue oxygen requirements for a brief period prior to the onset of blood circulation from the definite wave (Frame et al., 2013).

The second wave of haematopoiesis generates EMPs from the haemogenic endothelium (HE). This is a specialized population of endothelial cells present in the blood island capillaries of the yolk sac (Canu and Ruhrberg, 2021). In mice, EMPs seed the foetal liver after detaching from the blood island and entering the bloodstream (Palis et al., 1999). These progenitors, not only express adult globin proteins, but also have multilineage potential and can generate B and T lymphoid progenitors (Boiers et al., 2013). However, definitive HSCs are not yet developed.

HSCs are functionally characterized by their ability to self-renew and reconstitute the entire blood system following transplantation into immunodeficient mice (Zovein et al., 2008). The first emergence of definitive adult-repopulating HSCs are produced in the third and last wave of haematopoiesis (reviewed in Canu and Ruhrberg, 2021). This takes place in the dorsal aorta of the aorta-gonad-mesonephros (AGM) region and is regulated by several specific signalling events that result in the formation of haematopoietic cells from endothelial cells of the

HE (termed endothelial-to-haematopoietic transition; EHT) (Gao et al., 2018). Notch, adenosine and *Runx1* play important roles in EHT (North et al., 2002; Gori et al. 2015; Jang et al., 2015; Jing et al., 2015; Lin et al., 2015; Canu and Ruhrberg, 2021). *RUNX1*, upregulated by HE cells, coordinates the transcriptional activation program driving EHT (North et al., 1999; Canu and Ruhrberg, 2021). HSCs are temporarily produced in the AGM (Rybtsov et al., 2016), before they leave the dorsal aorta after specification and migrate towards the placenta and foetal liver where they proliferate transiently, before fully colonizing the bone marrow, making it the most important haematopoietic organ in adults (Gao et al., 2018). The first HSCs are detected at E10.5 and 4-5 pcw in the mouse and human embryos, respectively (Canu and Ruhrberg, 2021). By E18.5 and 10.5 pcw, in mouse and human embryos respectively, bone marrow colonization is complete (Baron et al., 2012).

1.1.3 Haematopoietic differentiation of human iPSCs

The interest in the expansion and production of HSCs has increased, partly due to potential application to cellular therapy of a large number of blood diseases (namely blood cancers) and immune disorders. Building on the success in murine studies, vast efforts have been made to mimic the distinct haematopoietic signalling cascade occurring during human embryogenesis *in vitro*. Insights into the mechanisms by which transcription factors and signalling molecules direct haematopoietic commitment and differentiation have been provided through lineage tracing and transplantation studies of *in vitro* models and the mouse embryo. Despite murine haematopoiesis being similar to humans, there are key physiological differences e.g. mice peripheral blood is highly enriched for lymphocytes, whereas in humans neutrophils are enriched (Mestas and Hughes, 2004).

In haematology research, murine models are invaluable, but do not always fully represent human pathophysiology. Thus, the use of human pluripotent stem cells (PSCs), namely induced PSCs (iPSCs), and their ability to differentiate to various cell types is an essential complement to research along with animal models of disease. Using iPSC technology greatly reduces the translational issues accompanying human embryonic stem cell (hESC)-based therapies. In the clinical setting, utilisation of promising cell therapies is heavily hindered by shortage of immunocompatible HSCs, poor HSC *ex vivo* expansion and

heterogenous response to therapy (Lim et al., 2013; Takizawa et al., 2011; Campos-Sanchez et al., 2019). *Bona fide* HSCs, arising during definitive haematopoiesis, can generate multi lineage cells and have long-term engraftment potential *in vivo* (Yoder, 2014). To generate *de novo* HSCs from PSCs, lineage commitment is induced using a combination of transcription factors (TFs) and signalling molecules in a controlled, defined manner (Kennedy et al., 2012; Sturgeon et al., 2014; Ng et al., 2016; Sugimura et al., 2017; Ruiz et al., 2019).

Established human PSC-derived haematopoietic differentiation protocols, including co-culture feeder-dependent methods, conventional monolayer cultivation or three-dimensional (3D) embryoid-body (EB) differentiation are extremely variable in terms of efficiency and quality of HSPCs produced (Alsayegh et al., 2019). Maintenance and retention of PSCs presents another challenge in these approaches. Overall, these protocols encompass 3 main stages of PSC differentiation: 1) mesoderm induction and patterning, 2) HE formation, 3) EHT and HSCs specification (Lancrin et al., 2012; Tursky et al., 2020; Ackermann et al., 2021). In brief, mesoderm specification and primitive streak formation are directed by TGF β , Wnt and BMP signalling pathways. The primitive wave depends on BMP4 which acts synergistically with Activin/Nodal and Wnt (Sumi et al., 2008; Alsayegh et al., 2019; Zhang et al., 2008; Kennedy et al., 2012). Suppression of primitive haematopoiesis during *in vitro* differentiation is achieved by inhibition of Activin/Nodal and activation of Wnt, which upregulates *CDX* genes (Sturgeon et al., 2014; Kennedy et al., 2012). *In vitro*, the precise timing of this regulation affects the generation and quality of HSPCs produced (Ng et al., 2016). This is achieved using a combination of the key molecules SB431542 (Activin/Nodal/TGF β antagonist) and CHIR9901 (Wnt agonist) (Ruiz et al., 2019). Simultaneous modulation of these pathways in mesodermal precursors increases arterial endothelium formation, restores the expression of haematopoietic *HOXA* gene cluster and promotes definitive haematopoiesis (Ng et al., 2016). In turn, *CDX* genes sustain the expression of Homeobox A (*HOXA*) genes that also direct cells away from extra-embryonic haematopoiesis and towards intra-embryonic haematopoiesis. Notably, retinoic acid is required during EHT, to upregulate these HSC-specific factors and increase chromatin accessibility of the *HOXA* cluster (Dou et al., 2016).

Regulation of these genes results in the production of multipotent HSPCs as in the definitive program (Ng et al., 2016). Key factors shown to be indispensable for multilineage engraftment and reconstitution of HSCs include *HOXA* genes (*HOXA5*, *HOXA9*, *HOXA10*), *RUNX1*, *SPII*, *LCOR* and *ERG* (Sugimura et al., 2017). Several studies have shown that *HOXA* expression alone is insufficient for generating of long-term repopulating HSCs (Sugimura et al., 2017; Zeng et al., 2021; Ramos-Mejía et al., 2014). This highlights the significance of acquiring a *HOXA* gene signature, along with creating the correct combination of signalling pathways, during haematopoietic differentiation to generate self-renewing, repopulating HSCs from human PSCs (Sugimura et al., 2017; Lis et al., 2017).

1.1.4 Characterisation of iPSC-derived HSPCs

Directed haematopoietic differentiation is governed by a large number of regulatory networks that orchestrate epigenetic and transcription modifications (Li et al., 2017). The presence of certain TFs and cell surface markers endows cell identity during haematopoietic specification. Figure 1.2 shows an illustration of the classical human haematopoiesis model encompassing key surface markers used to characterise differentiation cell types in this project (Doulatov et al., 2012). At early stages of the *in vitro* differentiation, NCAM expression marks acquisition of mesodermal fate from which multiple lineages are specified such as the haematopoietic lineage (Evseenko et al., 2010). Double positive expression of NCAM and KDR are indicative of correct mesoderm patterning and endothelial induction (Pearson et al., 2008; Scialdone et al., 2016). Similar to the early human embryo, where expression of KDR and lack of CD34 denotes presence of NCAM+ mesoderm precursors that generate HE cells (Cortes et al., 1999; Pearson et al., 2015). In humans, the early haematopoietic progenitors are phenotypically defined by several surface markers including CD34, CD43, CD90, CD45 and lack of/low CD38 (Tavian et al., 1999; Ivanovs et al., 2014; Zhang et al., 2022). Haemato-vascular phenotype is commonly marked by a CD34+CD90+CD43- profile (Lange et al., 2021). Upregulation of CD43 is indicative of formation of pre-HSCs from HE cells (Lange et al., 2021). Expression of CD34 and CD90 is acquired by HSPCs and endothelial cells (Gomes et al., 2018; Zhang et al., 2022).

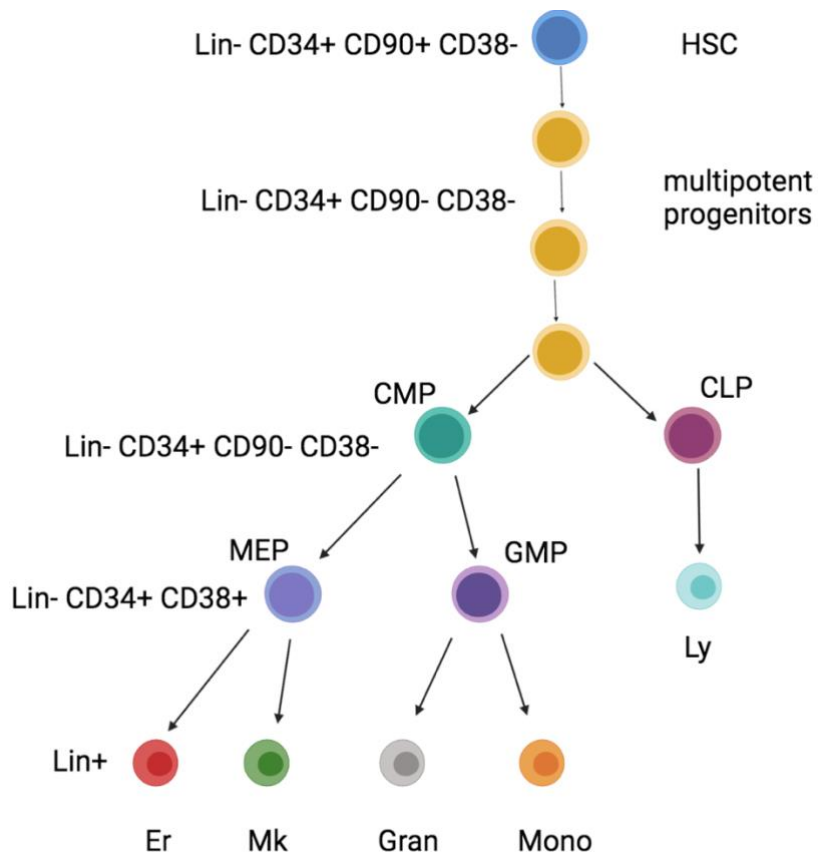


Figure 1.2 Classical model of human haematopoietic developmental hierarchy.

Cells can be defined majorly by cell surface markers listed next to each population horizontally. HSCs give rise to transiently engrafting multipotent progenitors. These give rise to oligopotent progenitors, CMP and CLP, that ultimately give rise to mature cells. In this schema, CMP and CLP can be distinguished from HSCs and their multipotent progenitors using CD90. HSC: haematopoietic stem cells; CMP: common myeloid progenitor; CLP: common lymphoid progenitor; MEP: megakaryocyte-erythroid progenitors; GMP: granulocyte-macrophage progenitors; Er: erythrocytes; Mk: megakaryocytes; Gran: granulocytes; Mono: monocytes; Ly: lymphocytes. Illustration created using biorender.com.

Table 1.1 Stage-specific surface markers of cells during haematopoietic differentiation

Cells population	Surface markers
Mesoderm	NCAM+ KDR+ CD34-
Haemogenic mesoderm	CD34+ KDR+ CD43-
Hemato-vascular mesoderm	CD34+ CD90+

Haemogenic endothelium (HE)	CD34+ CD90+/- CD43-
Haematopoietic progenitors	CD34+ CD90+ CD43+ CD45+ CD38-

Molecularly, downregulation of endothelial cells and upregulation of haematopoietic-specific TFs such as RUNX1 and GATA2 illustrates EHT and haematopoietic commitment (Kang et al., 2018; Lange et al., 2021). *HOXA9*, which is a master regulator of haematopoiesis, and its cofactor *MEIS1* are expressed in HSPCs and is downregulated as they become fully mature (Aryal et al., 2021; Argiropoulos and Humphries, 2007). In haematopoietic differentiation, *HOXA9* and *MEIS1* downregulation confirms correct progression to haematopoietic cell fate, through haemato-endothelial specification (Zhang et al., 2022).

Following the generation of iPSC-HSPCs, assessing their self-renewal ability and multi-potentiality using the colony forming-unit (CFU) assay is a gold-standard method (Frisch and Calvi, 2014).

1.1.5 Role of HOXA genes in normal haematopoiesis

The *HOX* family is a highly conserved set of genes, situated in four clusters (*HOXA*, *HOXB*, *HOXC* and *HOXD*) on chromosome 7 in humans (Mark et al., 1997). Mammalian *HOX* genes normally possess two exons and one intron Figure 1.3. The homeobox is located in the second exon and translates to a 60-61 amino acid homeodomain that interacts with DNA through a helix-turn-helix DNA-binding motif (Grier et al., 2005). Upstream of the homeodomain is a three-amino-acid-loop-extension motif (TALE) binding site that permits interaction of TALE proteins, namely MEIS and PBX family members, which are the most important HOX co-factors (Grier et al., 2005). HOX proteins depend on interactions with these co-factors to increase their DNA-binding specificity. *HOX* genes encode DNA-binding TFs that play a critical role in cellular differentiation during embryogenesis, and are master regulators of haematopoiesis (Aryal et al., 2021; Slany, 2009).

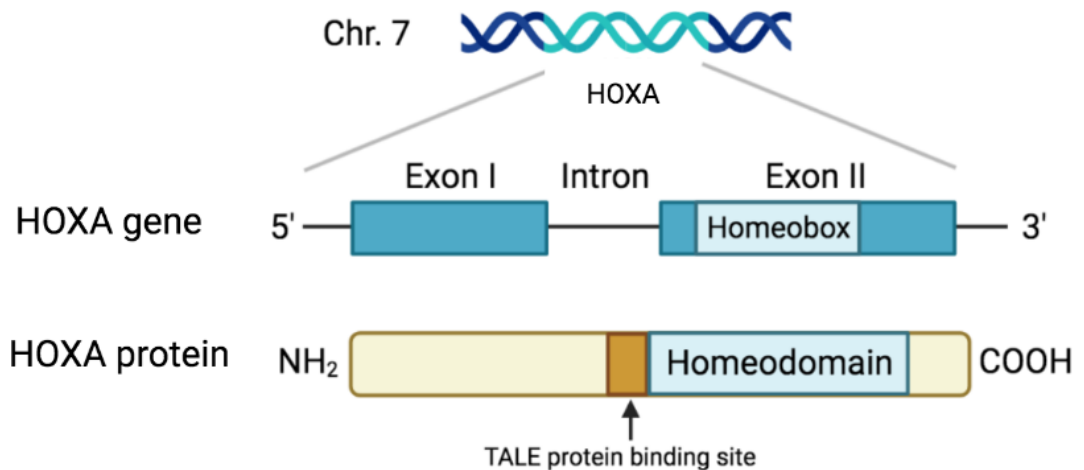


Figure 1.3 Structure of a human HOXA gene and protein.

HOXA genes are located on chromosome 7 and normally consist of two exons and one intron. A 60-61 amino acid DNA-binding homeodomain is encoded by the homeobox in exon 2. In HOX proteins, a TALE (three-amino-acid-loop-extension) binding site lies upstream of the homeodomain, enabling interactions with co-factors such as MEIS and PBX. Figure created using biorender.com

During embryogenesis, *HOX* genes play an integral role in the formation of the body plan. *HOX* genes exhibit spatio-temporal activity, indicating their key functions in hierarchical commitment of cell fate in embryonic development and early haematopoiesis (Aryal et al., 2021; Argiropoulos and Humphries, 2007). Whilst *HOXC* genes play a role in erythropoiesis, *HOXD* genes are not involved in haematopoietic development (Daga et al., 2000; Alharbi et al., 2013). Of all clusters, *HOXA* and *HOXB* genes are the most dominant in haematopoiesis, with *HOXA* genes mainly expressed in myeloid lineages. Expression of *HOXA* is high in human HSPCs and downregulated upon differentiation and maturation (Aryal et al., 2021; Sauvageau et al., 1994). Despite this, knockdown of *HOXA5* and/or *HOXA7* in CD34+ fetal liver halts multilineage differentiation in vivo (Dou et al., 2016). Overexpression and knock-out studies have also demonstrated that *HOXA9* in particular is the most abundant *HOX* gene in HSCs and has the most significant effect on haematopoietic development (Lawrence et al., 2005; Huang et al., 2012; Doulatov et al., 2013). *Hoxa* deficient mice exhibit impaired HSPCs activity, which is partially rescued by *Hoxa9* alone (Lebert-Ghali et al., 2016). Functional co-operation between *HOXA9* and HSC-specific TFs is observed. In particular, *HOXA9* interacts with enhancers of *SPII* and targets *ERG* (Huang et

al., 2012). *HOXA9* also works together with *HOXB4* in HSCs to maintain potency (Alsayegh et al., 2019).

Haematopoietic differentiation of hESCs is also enhanced by *HOXA9* overexpression, as it commits HE precursor cells into primitive blood cells (Ramos-Mejía et al., 2014). Other studies have also demonstrated that *HOXA9* particularly is a crucial factor in obtaining long-term repopulating HSCs (Lawrence et al., 2005; Huang et al., 2012; Doulatov et al., 2013). On the contrary, differentiation of HSCs to mature blood cells is associated with downregulation of *HOXA9* (Dou et al., 2016; Lawrence et al., 2005). Indeed, the progressive loss of *HOX* gene expression is a vital signal for HSCs proliferation and the start of lymphoid and myeloid differentiation (Aryal et al., 2021; Lawrence et al., 2005). Overall, manipulation of *HOXA* expression leads to lineage bias through a combination of altered lineage commitment and blocked differentiation. Therefore, deregulation of *HOXA* genes is a common feature of malignant haematopoiesis, primarily leukaemia,.

1.2 Malignant haematopoiesis

In malignant haematopoiesis, a block of the differentiation process accompanied by uncontrolled proliferation of HSPCs takes place due to acquisition of genetic alterations. This results in the accumulation of abnormal immature leukaemic blasts at the expense of normal blood cell production from HSCs. Consequently, competition for niche resources along with creation of an abnormal bone marrow microenvironment eventually leads to bone marrow failure (Pelayo et al., 2012). Clinically, leukaemia falls within four broad categories based on the lineage (myeloid or lymphoid) and subtype (acute or chronic). The latter categorization helps dictate the treatment regimen and indicates the onset and aggressiveness of disease. Emergence of leukaemic cells is highly efficient, particularly in the acute phase of leukaemias, owing to the motility and easy trafficking of the blood cells throughout the body (Whiteley et al., 2021).

1.2.1 Acute leukaemias

In children, leukaemia is the most prevalent cancer accounting for around a third of new paediatric cases each year in the UK (Cancer Research UK). Abnormal myeloid and lymphoid progenitors give rise to haematological diseases including acute myeloid leukaemia (AML) and acute lymphoid leukaemia (ALL),

respectively (Enciso et al., 2015). AML is a biologically and clinically heterogeneous malignancy, which is predominant in adults (Kouchkovsky & Abdul-Hay, 2016). In the UK, AML accounts for 2% of all cancer deaths in the UK (Cancer Research UK). According to the World Health Organization, one of the most important prognostic factors in AML is the identification of recurring genetic abnormalities, which has helped classify AML into cytogenetic and molecular disease entities (Arber et al., 2016). In 1970s, the French, American and British (FAB) classification of acute leukaemias was introduced based on morphology, cytochemistry and cell-surface markers (reviewed in Zini and Bennett, 2023). According to the International Consensus Classification of AML, it is mainly classified based on genetic aberrations and further classified into subgroups based on blast thresholds (Arber et al., 2022). Despite advances in prognostic risk stratification in combination with optimized therapeutic approaches such as allogeneic HSC transplantation, intensive chemotherapy and improved supportive care, overall clinical outcome of patients remains poor (Kumar et al., 2018). The standard of care treatment involves is known as the “3 + 7 regimen”, which involves 3 days of daunorubicin and 7 days of cytarabine (reviewed in Kantarjian et al., 2021). In older patients (age 60 years and older), the intensive chemotherapy regimens result in 5-year survival rates of <10-15% (Löwenberg et al., 2009). In younger patients (up to the age of 60 years), the 5-year survival rate is slightly higher, 30-35%.

In AML, 20-25% of patients with refractory AML never achieve complete remission. Amongst the 65% of patients that achieve complete remission, only 15-30% remain disease free for 5 years due to a high incidence of relapse (cited in Advani, 2006). Unlike AML, ALL is the most common acute leukaemia in children, accounting for 80% of all leukaemia cases in children (Redaelli et al., 2005). More than 80% of ALL cases originate from B-cell haematopoietic progenitors, and around 20% is derived from T-cell precursors. Although almost all ALL cases in children achieve complete remission, event-free survival is still limited (Chiaretti et al., 2014).

1.3 Mixed lineage leukaemia

1.3.1 MLL/KMT2A gene in leukaemia

A subset of acute leukaemias is characterized by recurring genetic alterations such as chromosomal translocations, resulting in fusion oncoproteins. Some of the driver translocations that result in *HOXA* overexpression include *MOZ::TIF*, *FTL3::ITD*, *MOZ::CBP*, *CALM::AF10*, *E2A::PBX*, *ETV6::9RUNX1* and the most common mixed lineage leukaemia (*MLL*) gene rearrangements (*MLLr*). (Aryal et al., 2021; Alharbi et al., 2013; Collins and Hess, 2016; De braekeleer et al., 2014; Metzeler et al., 2016; Studd et al., 2021).

The human *MLL* gene is located on chromosome band 11q23 and functions as a global epigenetic regulator first characterized as a histone methyl transferase (HMT) (Tsakaneli and Williams, 2021; Erfurth et al., 2008). *MLL* gene is now regarded as Lysine [K]-specific MethylTransferase 2A (KMT2A) (El Chaer et al., 2020; Winters and Bernt, 2017). It contains a DNA methyl transferase homologue domain CxxC, which binds to unmethylated CpG residues in genes like *HOXA9* locus and protects it from potential DNA methylation. Chromosomal rearrangements in *MLL* is a hallmark for aggressive high-risk acute leukaemias, *MLL*-rearranged leukaemias, possessing unique clinical and biological characteristics (Tsakaneli and Williams, 2021; Slany, 2009). Translocations in *MLL* are found in approximately 10% of all leukaemias (Schwaller, 2020; Winters and Bernt, 2017). *MLL* is a human homologue of the *trithorax* gene in *Drosophila melanogaster*, which is ubiquitously expressed in human HSPCs (El Chaer et al., 2020; Kristov and Armstrong, 2007). Hence, knockout of *Mll* causes deficiencies in proliferation and/or self-renewal of *Mll*^{-/-} HSPCs (Hess et al., 1997). The human *MLL* HMT positively regulates the expression of downstream genes (Muntean and Hess, 2012). For instance, *MLL* can directly bind to DNA or through interactions with menin (a tumour suppressor protein), to deposit H3K4 methylation marks on developmental genes such as *HOX* genes. In absence of menin, *HOXA9* expression is dysregulated (Yokoyama et al., 2005). In mice, it was shown that *Mll* is important for the maintenance of *Hox* gene expression.

MLLr likely result from a failure of repairing DNA double strand breaks (DSB) during the development of haematopoietic cells (Richardson and Jasin, 2000). *MLL* fusions are found in paediatric, adult and therapy-related acute leukaemias

that show an unfavourable clinical outcome (Muntean and Hess, 2012). They are present in >70% of infant ALL, and between 35-50% of infant AML (Kristov and Armstrong, 2007). Hence, predominantly (>90%) seen in infants. However, *MLLr* rare in children and adults, accounting for approximately 2-5% of cases (Chiaretti et al., 2014). Balanced chromosomal translocations at 11q23 result in fusion of the *MLL* gene with over 130 partner genes (Meyer et al., 2018). Despite the vast number of potential *MLL* partner genes, *MLL* preferentially recombines with five genes, which are found in approximately 80% of all *MLLr* leukaemias. These are *MLL::AF9* t(9;11)(p22;q23), *MLL::AF4* t(4;11)(q21;q23), *MLL::AF10* t(10;11)(p12;q23), *MLL-ENL* t(11;19)(q23;p13.3), and *MLL::AF6* t(6;11)(q27;q23) (El Chaer et al., 2020; Meyer et al., 2013). It is believed that *MLL* translocation partners are non-randomly selected as they encode nuclear proteins involved in histone H3K79 methylation (Meyer et al., 2006). These events fuse the N-terminus of *MLL* with a partner gene, thus destroying the normal histone methyltransferase function and replacing it with aberrant functions that enhance their transcriptional activity (Slany, 2009; Chiaretti et al., 2014). The major *MLL* fusion proteins present in AML and ALL are *MLL::AF9* and *MLL- AF4*, respectively (El Chaer et al., 2020; Kristov and Armstrong, 2007). A key functional feature of the resulting chimeric proteins is their ability to induce leukaemic activity by altering the self-renewal and growth properties of HSPCs (Argiropoulos and Humphries, 2007).

1.3.2 Disease models of *MLL*-rearranged leukaemia

From a study of 200 *de novo* AML patients, *MLL* fusions were found to be the main driving mutation with few additional mutations needed for disease onset (The Cancer Genome Atlas, 2013). The group of patient samples with *MLL* fusions had the least recurrent mutations compared to other AML-initiating events, with some samples without any recurring coding mutations. The early occurrence of these *MLL* translocations is accompanied with poor clinical outcome of patients. Taken together, this has generated much interest in modelling common translocations like *MLL::AF9* fusion in AML (Schwaller, 2020). The earliest model of *MLL::AF9* fusion generated knock-in mice, wherein in-frame fusion of exon 8 of endogenous *MLL* to the 3' end of *AF9* was developed using homologous recombination in embryonic stem cells by targeting vectors (Corral et al., 1996). Despite developing leukaemia in mice with a long latency, it did not

represent the true translocation in humans. Expression of the fusion gene in this model depended on widespread activity of the *Mll* promoter. To better recapitulate *de novo* generation of *MLL* translocations, mice models were developed using the Cre-loxP system. In 2000, a proof of principle study reported Cre recombinase-mediated inter-chromosomal rearrangement of *MLL::AF9* in mice, by inserting loxP sites into introns of endogenous *Mll* and *Af9* at common breakpoint sites (Collins et al., 2000). However, no leukaemias were reported in these translocator mice models. Endogenous targeting of *MLL* lacks tissue specificity and results in the formation of the fusion gene product in all *MLL*-expressing tissues, which could have an impact on leukaemia development. Another similar model involving the haematopoietic regulator *Lmo2* to drive the expression of *Cre* resulted in *Mll-Enl*-mediated leukaemogenesis (Forster et al., 2003). Similarly, expression of *Cre* under the control of *Lmo2* to induce *MLL::AF9* fusion in primitive progenitor cells generated AML. However, T cell-specific *Lck* promoter did not induce leukaemia following *Cre* expression in T cells despite the presence of the translocations (Drynan et al., 2005). In contrast, the same translocator model, but in *Mll-Enl*, produced both lymphoid and myeloid tumors driven by *Lmo2-Cre* and *Lck-Cre* expression (Drynan et al., 2005). This demonstrates that the target cell type where the translocation occurs plays a crucial role in the development of haematopoietic malignancies, and *Af9* and *Enl* partner proteins are functionally distinct (Milne, 2017). However, to study the expression of *MLL::AF9* in different haematopoietic populations, viral transduction of *MLL::AF9* oncogene has been used to directly transform specific cell types such as haematopoietic progenitors, HSCs and *ckit+* mouse BM stem and progenitor cells (Krivtsov et al., 2006; Somervaille and Cleary, 2006; Krivtsov et al., 2013). These models resulted in transplantable leukaemias. Interestingly, HSC-derived leukaemias were much more aggressive compared to leukaemias initiated in haematopoietic progenitors, by retroviral transduction (Krivtsov et al., 2013). Variation in gene expression signatures, epigenetic status and chemotherapy drug responses from these leukaemias were also observed. Nevertheless, viral transduction results in expression of the oncogene at non-physiological levels by random integration at different sites. Viral studies also maintain the presence of two normal copies of the gene.

Another knock-in, lineage-restricted mouse model of *MLL::AF9*, wherein expression of the fusion gene is under the control of endogenous *Mll* promoter,

further highlights the importance of cell-specific transformation ability (Chen et al., 2008). The authors also conclude that oncogene dosage (physiologically relevant levels in knock-in models vs. supraphysiological levels in transduced models) affects transformation ability. This is because leukaemia was observed in mice transplanted with MLL::AF9 transduced HSCs (where *Mll* expression is highest in wildtype (Jude et al., 2007), but not in granulocyte-macrophage progenitors (Chen et al., 2008). More recently, a doxycycline-induced *MLLr* mouse model emphasized that the phenotype of leukaemia is influenced by cell of origin (Stavropoulou et al., 2016).

Although using mouse models to accurately recapitulate the human disease remains controversial, together these data highlight developmental stage of target cells, and oncogene dosage as critical factors in modelling MLL-rearranged leukaemias. In attempts to faithfully model the human disease, the Cleary lab used transcription activator-like effector nucleases (TALENs) to generate endogenous *MLL::AF9* and *MLL-ENL* oncogenes through insertional mutagenesis from primary HSPCs derived from human umbilical cord blood (Buechele et al., 2015; Schneidawind et al., 2018). These particular models recapitulate several features of the clinical disease such as phenotype, morphology and molecular features of the induced leukaemias including expression of an MLL-associated transcriptional program. The authors also showed that microenvironment plays a key role in leukaemia development (Buechele et al., 2015). Recently, human HSPCs from umbilical cord blood were also engineered using clustered regularly interspaced palindromic repeats (CRISPR)/CRISPR-associated 9 (Cas9) system to generate the MLL::AF9 translocation *in vitro* prior to transplantation in mice (Jeong et al., 2019). Using CRISPR/Cas9 gene editing, these authors achieved high translocation efficiency and leukaemias of different lineages developed in mice.

1.3.3 Role of HOXA genes in malignant haematopoiesis

Owing to its myeloid lineage bias, aberrant *HOXA* expression primarily leads to myeloid leukaemia. Ectopic expression of *HOXA* will block differentiation and form a pre-leukaemic pool of HSPCs (Slany, 2009) (see Figure 1.4 for overview). Studies assessing the oncogenic potential of the *HoxA* cluster has shown their ability to transform cells in culture, and the sensitivity of adult HSPCs to *HoxA* gene dosage (Lebert- Ghali et al., 2016; Bach et al., 2010). Following retroviral

transduction and transplantation, five of the human *HOXA* genes (*HOXA1*, *HOXA4*, *HOXA6*, *HOXA9* and *HOXA10*) were capable of inducing leukaemia in mice (Buske et al., 2001; Bach et al., 2010). The rest of the genes in the *HOXA* cluster were not as potent as single events.

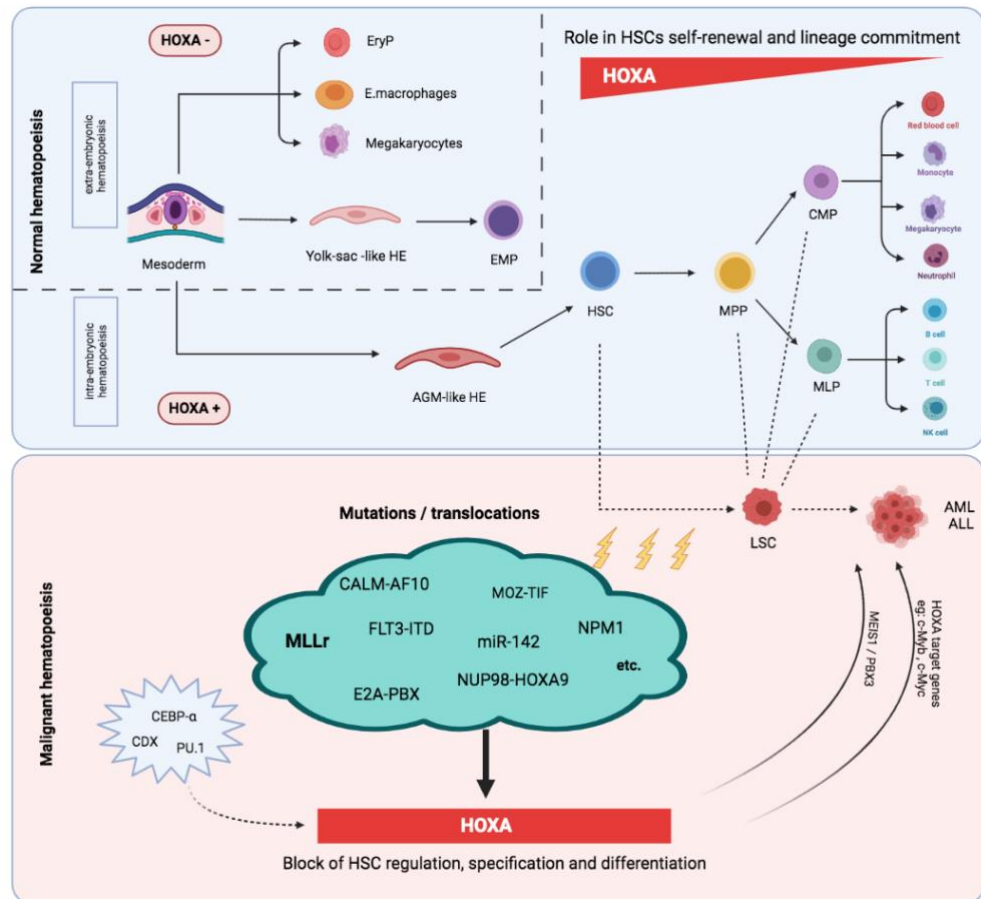


Figure 1.4 An overview of the role of *HOXA* in normal and malignant haematopoiesis.

HOXA is required for intra-embryonic haematopoiesis but dispensable for extra-embryonic haematopoiesis. *HOXA* expression is essential for the formation and maintenance of haematopoietic stem cells (HSC). *HOXA* expression is significantly reduced as HSCs differentiate. Direct mutation or genetic lesion of upstream regulators, including rearrangements of the mixed-lineage-leukaemia gene (*MLLr*), results in *HOXA* dysregulation, which is associated with a malignant phenotype, primarily acute myeloid leukaemia (AML) and acute lymphoid leukaemia (ALL). EryP, erythroid progenitors; E.macrophages, embryonic macrophages; EMP, erythromyeloid progenitors; AGM, aorta-gonad-mesonephros; HE, haemogenic endothelium, MPP, multipotent progenitor; CMP, common myeloid progenitor; MLP, multilymphoid progenitor; NK, natural killer. Figure created using biorender.com

MLL fusion proteins contribute to the pathogenesis of leukaemia mainly through direct upregulation of *HOXA* gene expression (Aryal et al., 2021; Li et al., 2012). Of all the *HOXA* cluster, the most critical downstream targets of MLL fusion proteins are *HOXA9*, and its cofactor *MEIS1* (Aryal et al., 2021; Zeisig et al., 2004; Kroon et al., 1998; Roth et al., 2009). Indeed, *HOXA9* has been known to be the single most highly associated gene (out of 6817) for poor AML prognosis (Golub et al., 1999). Moreover, it is one of the most highly expressed genes in HSCs, suggesting a key role in HSC function (Argiropoulos and Humphries, 2007). This has been demonstrated in a study where overexpressing *Hoxa9* in *Hoxa9*-deficient mice partially rescues HSPCs activity *in vivo*, and restores the expression of several dysregulated genes (Lebert-Ghali et al., 2016). Significant overexpression of *HOXA9* and *MEIS1* is needed to induce and maintain MLL-rearranged leukaemias (Aryal et al., 2021; Roth et al., 2009; Faber et al., 2009). Thus, a critical dependency of *HOXA9* to transform and initiate AML in HSPCs has been demonstrated (Kettyle et al., 2019).

1.4 Drug discovery

1.4.1 Leukaemic stem cells

Despite advances in our molecular understanding of leukaemia over the last two decades, cure rates have for the most part stagnated and treatment remains a challenge. From 2011 to 2021, the FDA approved a total of 52 drugs for the treatment of haematological malignancies (reviewed in Sochacka-Ćwikła et al., 2022). For AML therapeutics, 8 targeted agents have been approved from 2017 to 2020 (Park et al., 2020), which is considered the highest discovery rate to date. Novel targeted therapies have emerged including venetoclax, FLT3 inhibitors (midostaurin, gilteritib) and IDH inhibitors (ivosidenib, enasidenib), and others (reviewed in Kantarjian et al., 2021). However, none of which is targeted for *MLLr* leukaemias in particular. This is largely due to disease resistance and relapse, which is a result of inadequate eradication of a subpopulation of cells termed leukaemia repopulating cells or leukaemic stem cells (LSCs), by conventional therapies (Pollyea et al., 2014). LSCs have self-renewal, disease initiation, and disease propagation properties, hence serving as a reservoir for disease relapse (Lapidot et al., 1994). This is due to LSCs acquiring new pro-survival and pro-proliferative mutations. Therapies that involve directly targeting of mutations or pathways in LSCs are promising because they may lead to disease regression

and possibly complete remission through eradication of the LSC. However, being highly similar to HSCs, the therapeutic challenges lie in selectively targeting LSCs while sparing HSCs, to maintain normal haematopoiesis (Kouchkovsky & Abdul-Hay, 2016; Lapidot et al., 1994).

1.4.2 iPSC-based drug discovery

For decades, one of the main challenges for experimental research and drug discovery is using biologically relevant models/platforms. To date, these include immortalized cell lines and animal models of human disease, followed by clinical trials. However, these approaches are at best approximations of human disease and have well documented limitations (Nicholson et al., 2022; Gunaseeli et al., 2010) . Since the discovery of human iPSCs in 2006, the landscape of drug discovery and the potential of isogenic disease models has started to be realised (Takahashi and Yamanaka, 2006). Firstly, hiPSCs are renewable and scalable, thus offering an unlimited supply for high throughput drug screening and toxicological studies (Nicholson et al., 2022)

Unlike hESCs, patient-specific human iPSCs will not evoke an immune response in the host following transplantation, complimenting stem cell-based cell replacement therapy (Doss and Sachinidis, 2019). Moreover, ethical restrictions around being derived from fertilized human embryos that accompanied hESCs experimentation, is avoided. Therefore, the ability to derive iPSCs from patients becomes an added advantage. In addition, their plasticity and ability to differentiate into diverse cell types allows drug effects to be studied on hard-to-obtain tissues such as cardiac muscle and brain (Nicholson et al., 2022). Using iPSCs allows recapitulation of the earliest stages of diseases, such as cancer, hence identifying significant early molecular events involved in disease initiation and pathogenesis, ultimately improving stratification of patients. This is also useful in studying rare diseases and diseases with multifactorial origin (Ko and Gelb, 2014). This highlights iPSC-derived isogenic models as a valuable resource in the route to accelerated drug discovery (Nicholson et al., 2022). Modelling cancers using iPSCs is important where mutations are too complex to be engineered in a mouse model, or where mouse counterpart of the cancer related human genes is absent (Kim, 2015). A schematic of key steps in conventional vs. iPSC-based drug discovery is illustrated in Figure 1.5. Overall,

human iPSCs are a promising research tool that compliments *in vivo* models by increasing productivity and decreasing the cost and time of drug development.

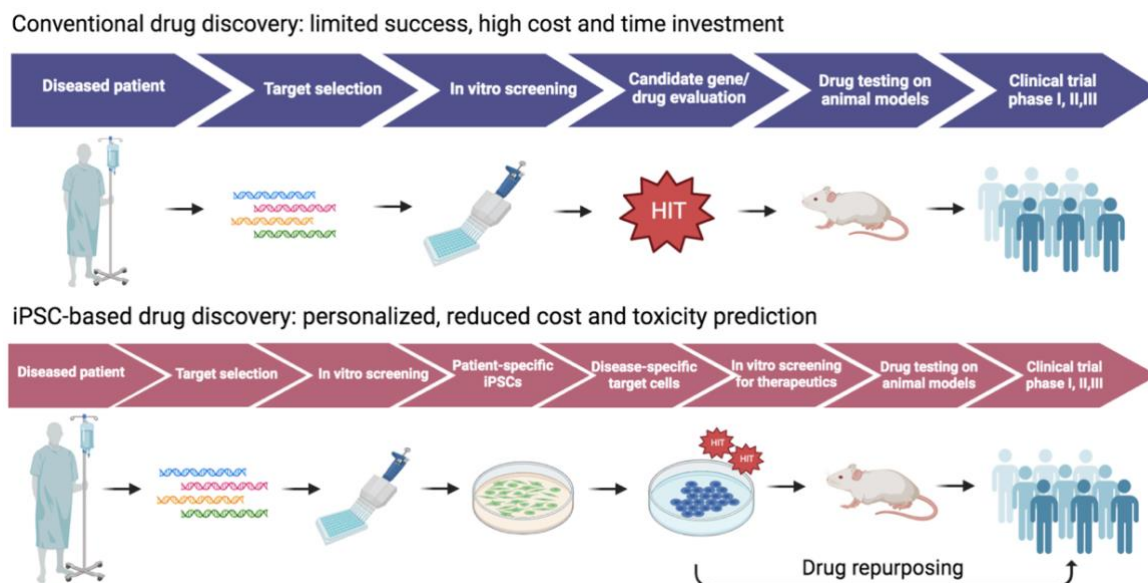


Figure 1.5 A schematic of the conventional and iPSCs drug discovery routes.

Comparatively, the conventional route has high cost and time coupled with low success rates of drugs reaching the clinic. Whereas, iPSC-based discovery is patient-specific, accelerates the process along and lowers associated costs. It can also potentially replace the need for *in vivo* models. Illustration created using biorender.com

1.4.3 Drug repurposing

Drug development, particularly of anti-cancer drugs, is costly, inefficient, and requires several years to obtain clinical approval (Pammoli et al., 2011; Hay et al., 2014). *De novo* cancer drug discovery and development takes longer than a decade, most of which is spent before phase I clinical trials (Zhang et al., 2020). The process of drug discovery for use in the market costs approximately, \$2-3 billion (Tsakaneli and Williams, 2021). The high failure rate for the translation of drug trials from animal models to humans in the clinic is often due to intrinsic species differences, resulting in variable biological response. This includes differences in drug metabolism, toxicity and crossing of the blood-brain barrier (Lawrence et al., 2015). Therefore, the idea of repurposing drugs with known side effects will lower the risk of failure due to unexpected toxicity, thus bypassing major steps in the route to clinical trials (Pantziarka et al., 2014; Tsakaneli and Williams, 2021). This strategy, in the case of cancer, involves screening drugs that are used to treat non-cancer diseases, for anti-cancer properties (Roulston

et al., 2016). To identify these potential drugs, connectivity mapping can be used, which is a systematic approach that detects functional connections between disease-related gene signatures, small molecules and drug actions (Lamb et al., 2006; Pushpakom et al., 2019). Several examples of drug repurposing approaches have proven to be effective (Ishida et al., 2016; Palumbo et al., 2008), most recently for treatment of COVID-19 (Scavone et al., 2020; Singh et al., 2020).

1.5 Genome editing

1.5.1 CRISPR/Cas9-mediated genome editing

In the last decade, genome engineering tools have simultaneously advanced due to their increasing precision and efficiency in editing the genome. Programmable nucleases such as meganucleases, zinc-finger nucleases (ZFNs) and TALENs are able to recognize specific DNA base pair (bp) sequences (González-Romero et al., 2019). The nucleases have been used to induce locus-specific DNA DSBs with a higher homologous recombination (HR) efficiency compared to the pre-nuclease era, which depended heavily on chance (González-Romero et al., 2019). However, targeting these nucleases to specific loci is technically challenging because it relies on predicting DNA-protein interactions (Porteus and Baltimore, 2003). In contrast, the CRISPR/Cas genome engineering approach is based on nucleic acid interactions, making it more widely accessible and the current leading technology. The CRISPR/Cas system is a novel, easy-to-use tool that enables versatile and uncomplicated genome editing irrespective of the complexity of the genome (González-Romero et al., 2019).

CRISPR sequence repeats were first characterized in an archaeon, *Haloflex mediterranei*, (Mojica et al., 1995), before being identified as part of a primitive adaptive prokaryotic immune system (Mojica et al., 2009). The technology is essentially composed of a guide RNA (gRNA) and the Cas enzyme. The gRNA is made from of a combination of CRISPR RNA (crRNA) which recognizes the target sequence and transactivating crRNA (tracrRNA), which binds to the Cas protein. The Cas family of proteins are endonucleases that introduce a DSB, and the most commonly used member for CRISPR technology is Cas9. Altogether, the gRNA brings Cas9 to the sequence of interest (approximately 20 nucleotides long), which is always next to the protospacer adjacent motif (PAM). PAM is a conserved dinucleotide- containing sequence upstream of the target sequence.

For Cas9, the PAM sequence is NGG (González-Romero et al., 2019). Following these conditions, Cas9 cleaves the genome and creates a DSB in eukaryotic cells which is repaired by either non-homologous end joining (NHEJ) or homology-directed repair (HDR). NHEJ is used to generate gene knock-outs by introducing indels (insertions or deletions), whereas HDR allows for gene editing by integrating an engineered template DNA to the system. The simplicity and efficiency of the system revolutionized the field of genome engineering with multiple and broad applications in medicine.

1.5.2 CRISPR/Cas9 in haematopoiesis

The use of CRISPR/Cas9 in the haematopoietic setting has been applied in experimental research and human therapeutics (reviewed in Elliott et al., 2021; Bhat et al., 2022; González-Romero et al., 2019). A summary of key applications is shown in Figure 1.6. In research, due to the simplicity of the CRISPR/Cas9 system coupled with the robustness and easy manipulation of cell lines, it has been largely used to decipher gene function in haematopoietic cells. Studies have used CRISPR/Cas9 not only to create knock-outs upon NHEJ-based disruption, but also to introduce insertions, translocations or point mutations using a DNA template by HDR as mentioned above (Jeong et al., 2019; Li et al., 2022). Unlike RNA interference approaches (Hannon and Rossi, 2004), CRISPR/Cas9 mimics the complete loss-of-function and does not produce hypomorphic phenotypes making it the method of choice for *in vitro* genomic studies. In AML, precise models harbouring driver mutations have been created to help develop novel, targeted therapies using CRISPR/Cas9. For example, a mutation in isocitrate dehydrogenase 2 (*IDH2*), R140Q, causes cells to generate an oncometabolite that disrupts normal epigenetic cell regulation, contributing to malignant transformation (Brabetz et al., 2017). Using RNA-guided CRISPR/Cas9 system, gene edited K562 cells recapitulated the genetic, epigenetic and functional changes observed in *IDH2*-mutated patients (Brabetz et al., 2017). Likewise, gene correction using CRISPR/Cas9 in primary haematopoietic cells and patient-specific iPSCs was also shown to be feasible in proof-of-concept studies (Valletta et al., 2015; Pittermann et al., 2017). CRISPR/Cas9 technologies have been employed in genome-wide functional genetic screens in mammalian cells using lentiviral gRNA libraries for positive and negative selection (Aregger et al., 2019; Bock et al., 2022; Zhou et al., 2014). Another promising application of the

technology is drug discovery and target identification. In the context of haematology, a high-throughput CRISPR screen in murine AML cells has been performed to validate drug targets and discover potential new targets (Shi et al., 2015). Screening using CRISPR/Cas9 also identified that cytarabine resistance in AML cell lines is primarily due to the deoxycytidine kinase gene (Rathe et al., 2014). *In vivo* mouse models were extensively generated using this technology to study early developmental processes, and evaluate the safety and efficacy of novel gene therapies (Horiuchi et al., 2018; Yen et al., 2016; Xiang et al., 2017).

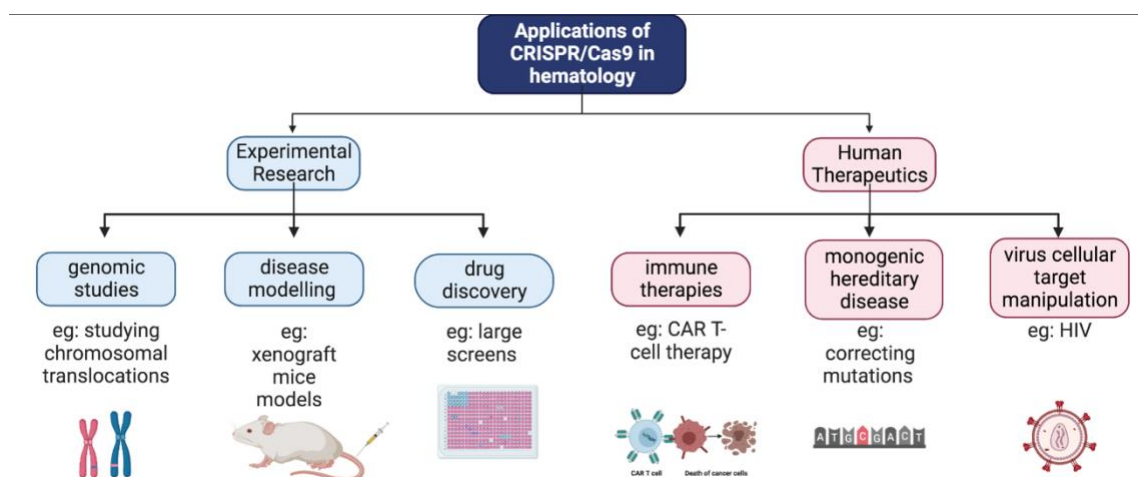


Figure 1.6 Applications of CRISPR/Cas9 in haematology.

Examples of CRISPR/Cas9-mediated genome editing in research and therapy. CAR: chimeric antigen receptor; HIV: human immunodeficiency virus. Figure created using biorender.com

In the clinical setting, CRISPR technology could circumvent the pitfalls associated with *ex vivo* gene editing using integrative viral-based gene therapy followed by autologous HSC transplantation. It has been employed in strategies aiming to treat monogenic inherited disorders. Mutated haematopoietic cells can be isolated from patients, reprogrammed to iPSCs, edited, differentiated to HSC and re-introduced by autologous HSCs transplantation. In hemoglobinopathies like β -thalassemia and sickle cell anaemia, mutations were corrected using CRISPR/Cas9 in patient-specific iPSCs (Song et al., 2015; Huang et al., 2015). Similar strategies have been applied to treat primary and acquired immunodeficiencies as well. More recently, CRISPR/Cas9 has been used to complement cancer immunotherapy (Bhat et al., 2022). Particularly, in chimeric antigen receptor (CAR) T-cells therapy which involves manipulating patient's T

cells *ex vivo* to recognize and attack tumour cells after re-infusion into patients. For instance, the technology was employed to eliminate genes encoding for programmed cell death protein 1 (*PD1*), and other inhibitory T-cell surface receptors to improve the efficiency of the therapy (Xia et al., 2019). Although these studies showed promising results, clinical trials using CRISPR-based treatment is still at an early stage, due to continuing limitations (Bhat et al., 2022). Off-target tumour effects causing potential toxicities remain an obstacle. CAR-T therapy can exhibit fatal, high rates of toxicities, preventing it from becoming a main cancer treatment (Sterner and Sterner, 2021). Another challenge is the inability to traffic and infiltrate CAR-T cells into solid tumours. Application of these therapeutic strategies in multifactorial diseases with complex inheritance such as Alzheimers, arthritis, blood cancer and autoimmune disorders remains a challenge.

1.6 Hypothesis and aims

- 1) Efficiency of iPSC-derived HSPCs generation will be improved using single cell seeding for monolayer haematopoietic differentiation
- 2) Temporal expression of *HOXA9* during iPSC-derived normal and malignant haematopoiesis can be monitored using an engineered reporter model
- 3) Indirect targeting of HOXA signature using FDA-approved drugs is effective in AML

Aim 1: Optimise routine derivation of iPSC-derived HSPCs and generate an endogenous *HOXA9* reporter iPSC line

Aim 2: Evaluate the efficacy of candidate anti-*HOXA* FDA-approved drugs in leukaemia cell lines

Aim 3: Determine key genes and pathways associated with anti-*HOXA* FDA-approved drugs as potential biomarkers of effective drug treatment

Chapter 2 Materials and Methods

2.1 Cell culture

2.1.1 Human iPSCs maintenance and cryopreservation

Human iPSC cell line, ReBL-PAT/RPATs, was gifted by Prof. Chris Denning lab at the University of Nottingham. RPATs and RPAT-derived clones (eA9^m) were routinely cultured as monolayers in Essential 8 (E8) medium (ThermoFisher, A1517001) in tissue culture plastics coated with Matrigel (Corning, 354234). For maintenance, cells were passaged using 0.5mM EDTA (Invitrogen; Ref: 15575-038) for 7 minutes every 3 days after reaching 70-80% confluency. Cells were resuspended and seeded in E8 medium supplemented with 10 mM ROCK Inhibitor (RI) (1:1000) (Y-27632, Tocris, 1254) (E8-RI). Cells were incubated at 37°C in 5% CO₂. For cryopreservation, approximately 1x10⁶ cells were collected and resuspended in 500 µL of 90% filtered foetal bovine serum (FBS) + 10% DMSO. To thaw cells, cryovials were placed in a water bath for 1 min, and cell suspension was added dropwise to 9 mL E8 media. Cell suspension was then centrifuged at 160g for 4 minutes. Supernatant was aspirated and cells were resuspended in E8-RI media. Post thaw, cells were passaged at least twice prior to differentiation to ensure recovery.

2.1.2 iPSC-derived HSPCs culture

iPSC-HSPCs harvested from haematopoietic differentiation was cultured in IMDM media supplemented with 10% FCS, IL3 (10 ng/mL), GM-CSF (10 ng/mL) and SCF (50 ng/mL) in 96-well plates at 1x10⁵ cells/mL. Half media changes were performed every 2 days.

2.1.3 Leukaemic cell lines maintenance

Cell lines (THP1, OCI-AML3, HL60 and MV4-11) were obtained from DSMZ. All cells were cultured in RPMI1640 medium (Gibco, 21875034) supplemented with 10% heat-inactivated FBS and 1% glutaMAX (Gibco, 35050061). Cells were passaged every 3-4 days at a 1:10 ratio using fresh RPMI1640 medium, and incubated at 37°C in 5% CO₂. Cells were frozen with 70% medium, 20% FBS and 10% DMSO.

2.2 Haematopoietic differentiation

2.2.1 STEMdiff™ haematopoietic kit

HiPSCs were differentiated using the STEMdiff™ Haematopoietic kit (StemCell technologies, 05311) according to the kit protocol. For aggregates seeding, cells were passaged using an enzyme-free reagent Gentle Cell Dissociation Reagent (GCDR) (StemCell Technologies, 07174) in 6-well plates. Cells were mechanically dissociated using a cell scraper and resuspended in 1 mL E8 medium, and seeded into 12-well plates at various density ratios (1:60 to 1:160). For single cell seeding, cells were passaged in E8 medium supplemented with RevitaCell (RC) (1:100) (ThermoFisher, A2644501) using 0.5 mM EDTA. RC was used in another single cell-derived haematopoietic differentiation protocol (Hansen et al., 2018). Cells were seeded in Matrigel-coated 12-well plates at low densities (200, 280, 360, 480, 560 or 720 cells/mL) in E8-RC medium. Media was changed to E8 only the following day, and replaced with fresh E8 daily, for 8-9 days. After that, the STEMdiff™ differentiation was started by replacing E8 media to media A provided in the kit. Subsequent media changes were done according to the kit instructions. Cells were incubated at 37°C in 5% CO₂. The process was extended to day 14 by supplementing the adherent cells with fresh media B on day 12 after harvesting the floating cells. Suspension cells harvested on day 12 and day 14 for characterisation using flow cytometry and colony-forming unit (CFU) assay.

2.2.2 Spin Embryoid Body haematopoietic differentiation

Prior to the differentiation, cells were passaged as described previously at 1:1 ratio. Media was changed to E8 the next day, 6 hours before cells were passaged again. RPATs are seeded in Stage I media in round-bottom 96-well plates (ThermoFisher, 268200) at 80 µL/well. A ratio split was used wherein 1 T25 flask with cells at 70-80% confluency seeds approximately 220 wells, forming 1 embryoid body (EB)/well. Plates were centrifuged at 400g for 2 minutes at 4°C to generate EBs. After 40 hours of seeding, Stage I.II media was added (20 µL/well). On day 4, 70 µL/well of media was replaced with 100 µL/well of Stage II media. On day 7, EBs were transferred to Matrigel-coated 6-well plates (20 EBs/well). Media was changed to Stage III media on day 9. Stage III media top up (1 mL/well) was done on day 11 and day 16. iPSC-HSPCs were harvested on day

14 and day 18, and stage III media was replaced. Components of differentiation media are listed in Table 2.1. For downstream assays (flow cytometry and qRT-PCR), EBs were dissociated with Accutase (20 minutes for d4 EBs, 90 minutes for d7 EBs) and incubated at 37 °C. For qRT-PCR (qPCR), 20 EBs were collected, whereas for flow cytometry, 15-20 EBs were collected per sample.

Table 2.1 Components of the Spin EB differentiation medium.

Stage I (days 0-2)		
Component	Reference	Final concentration (ng/mL)
APEL2	StemCell Technologies; Ref: 05275	-
BMP4	R&D Systems 314-BP	5
Activin A	Thermofisher; Ref: PHC9561	7.5
VEGF	Peprotech; Ref: 100-20	25
SCF	Peprotech; Ref: 300-07	25
RI	Tocris; Ref:1254	10 (µM)
Stage I.II SB/CHIR (days 2-4)		
Component	Reference	Final concentration (µM)
APEL2	StemCell Technologies; Ref: 05275	-
SB431542	Sigma; Ref: S4317	4
CHIR99021	Sigma; Ref: SML1046	3
Stage II (days 4-9)		
Component	Reference	Final concentration (ng/mL)
APEL2	StemCell Technologies; Ref: 05275	-
BMP4	R&D Systems 314-BP	5
VEGF	Peprotech; Ref: 100-20	50
SCF	Peprotech; Ref: 300-07	50
FGF2	Peprotech; Ref: 100-18B	10
IGFII	Peprotech; Ref: 100-12	30
Stage III (days 9-18)		

Component	Reference	Final concentration (ng/mL)
APEL2	StemCell Technologies; Ref: 05275	-
VEGF	Peprotech; Ref: 100-20	50
SCF	Peprotech; Ref: 300-07	50
IL3	Peprotech; Ref: 200-03	50
IL6	Peprotech; Ref: 200-06	25
TPO	Peprotech; Ref: 300-18	25
FLT3	Peprotech; Ref:300-19	25
FGF2	Peprotech; Ref: 100-18B	10
IGFII	Peprotech; Ref: 100-12	20

2.2.3 Colony-forming unit assay

Harvested iPSC-derived HSPCs were seeded at 3×10^4 cells/mL in MethoCult™ (Stemcell Technologies, H4434 and H4034), vortexed and plated at 500 μ L/well in 12-well plates. Colonies were observed after 7 and 14 days.

Leukaemic cell lines (THP1, OCI-AML3, HL60 and MV4-11) were seeded in MethoCult™ (StemCell Technologies, H4534) at 1×10^4 cells/mL and treated with either DMSO or the 48-hour IC50 values of Atorvastatin (ATV) (Selleckchem, S5715) or Homoharringtonine (HHT) (Selleckchem, S9015). Cell mixture was vortexed vigorously and plated at 200 μ L/well of a 24-well plate. Cells were incubated at 37°C in 5% CO₂. Colonies were imaged and counted after 7 days.

2.3 SB/CHIR/RA treatment

2.3.1 Cell culture and treatment on coverslips

To prepare for cell seeding, coverslips were washed in 70% sterile ethanol in 12-well plates (1 coverslip/well), followed by two washes using PBS. Coverslips were further sterilised under UV light for 20 minutes and coated with either Matrigel or fibronectin (20 μ g/mL) and stored in 4°C overnight. Passaged iPSCs were seeded at 100,000 cells/well of an empty or coverslip-containing 12-well plate. After 24 hours of seeding, cells were treated with SB431542 (TGF- β inhibitor) (SB, Sigma; S4317) at 4 μ M and CHIR99021 (Wnt agonist) (CHIR, Sigma;

SML1046) at 3 μ M, or in combination with Retinoic Acid (Sigma; Ref: R2625) at 3 μ M. After 24, 48 and 72 hours of treatment with the aforementioned molecules, cells were passaged with EDTA as described previously and pelleted for RNA extraction, or processed for imaging as described below.

2.3.2 Immunofluorescence

Cells attached on coverslips were washed with PBS and fixed with 4% paraformaldehyde (PFA) for 15 minutes. After 2 washes with PBS, cells were incubated with DAPI (Sigma-Merck; Ref: 32670) for 20 minutes. Cells were washed twice with PBS and mounted in slides with Immu-Mount (Fisher; 9990402).

2.4 DNA integration

2.4.1 Lentiviral production

Endofree® prepared plasmids (second generation), pMD2.G (0.1 pmol) and psPAX2 (0.3 pmol), were collected by centrifugation (to remove debris) and incubated with 1.5 mL Opti-MEM® (OM, Life Technologies) in a micro centrifuge tube (1.5 mL) whilst transfection reagent was incubated with 1.5 mL OM in 13 mL polypropylene tube (Becton, Dickinson Limited). Diluted plasmid and transfection reagents were then mixed and further incubated for 30 minutes at room temperature to form complexes. Human embryonic kidney (HEK 293T) cells were washed and overlaid with 6 mL of media. Mixtures were then added dropwise to the target cells and dishes were incubated for 6 hours at 37 °C. After incubation, the supernatant was removed and the cells were washed once with PBS and overlaid with 8 mL culture medium. After 24 hours, the supernatant was removed, discarded and replaced. Viral supernatants were then collected (48 and 72 hours post transfection) and passed through 0.2 μ M low protein binding filter (Merck Millipore). Presence of lentiviral particles was confirmed using Lenti-X™ GoStix™ Plus (Takarabio, USA). The supernatant (20 μ L) was added onto the GoStix cassette with 80 μ L chase buffer. Lenti-X™ GoStix™ Plus is a quantitative lentiviral titre test. The intensity of the band correlates with the amount of lentivirus used. The protocol guidelines were used to qualitatively assess the amount present. The p24 control, lentiviral capsid protein, supplied provided confirmation for the function of the lateral flow test.

2.4.2 Lentiviral transduction

Following routine iPSCs passaging in 12-well plates, cells were allowed to attach for ~ 4 hours in the incubator. LV supernatant was added onto the cells at 1 μ L, 5 μ L, 10 μ L and 20 μ L/well containing 1 mL of E8-RI-polybrene medium. Polybrene was present at 5 μ g/mL. Plates were rocked briefly to distribute the supernatant and placed back in the incubator. Cells were dissociated and analysed after 48 hours.

For EBs, 10 μ L of lentivirus (LV) was added to the Stage II medium present in each well/EB. Plates were rocked to ensure uniform distribution of the LV supernatant, and placed back in the incubator. After 48 hours of incubation (day 9), EBs were collected and dissociated as described previously, for downstream assays (qPCR and flow cytometry). The differentiation was also continued for EBs transduced on day 7 as described by transferring them to Matrigel-coated 6-well plates (refer to 2.2.2). Stage II medium containing LV was replaced on day 9 with Stage III medium. HSPCs derived from treated EBs were harvested on day 14 and assayed by qPCR and CFU assay.

2.4.3 Plasmid transfection/ Nucleofection

Two plasmids harbouring *MLLr* were used to transfect eA9^m cells. These were p2158C and pUMG-LV6MA (pMA9), both of which contain different variations of *MLL::AF9*. An empty vector, pUMG-LV6 (pCTRL), that contains GFP not *MLLr*, was also used. pMA9 and pCTRL were kindly provided by Owen Williams (University College London Institute). Sources of plasmids used are listed in Table 2.2. The P3 Primary Cell 4D nucleofector kit (Lonza, V4XP-3024), was used. For each nucleofection, 1×10^6 cells were collected and resuspended in 100 μ L of P3 buffer. Plasmid DNA was added to cells (1-2 μ g) and mixed prior to transferring to supplied cuvettes. Cuvettes were placed in an AmaxaTM Nucleofector (Lonza) and the CA-137 program was used for iPSCs. Cuvettes were placed in an incubator for 5 minutes before flushing with 900 μ L media (E8-RI for iPSCs and Stage III media, in Table 2.1, for HSPCs), and transferred to Matrigel-coated plates. Fluorescence was captured and quantified using Operetta CLSTM (Perkin Elmer).

Table 2.2 Plasmids used in transfection

Plasmid	Concentration	Reference
pMA9 (pUMG-LV6MA)	0.5 µg/ µL	Chiarella et al., 2014; Osaki et al., 2014
pCTRL (pUMG-LV6)	0.8 µg/ µL	Chiarella et al., 2014
p2158	1 µg/ µL	Gifted by Guy Sauvageau
pGFPmax	1 µg/ µL	Lonza, V4XP-3024

2.5 Molecular biology

2.5.1 Genomic DNA extraction

Total genomic DNA was extracted from cells using the DNEasy® Blood and Tissue kit (Qiagen, 69504) following the manufacturer's protocol. Briefly, cells were lysed using proteinase K and DNA was precipitated using pure ethanol. DNA was purified using two washing buffers. DNA was eluted in 40 µL nuclease-free water instead of Buffer AE (ThermoFisher, AM9930). DNA was quantified using a Nanodrop spectrophotometer.

2.5.2 RNA extraction

For qPCR, total RNA was extracted using NucleoSpin® RNA kit (Macherey Nagel) The manufacturer's protocol was followed. Briefly, lysis buffer was first added to permeate the cell membrane. To precipitate and purify RNA, 70% ethanol was used. DNA was digested using DNase. Ethanol-containing wash buffers were also used to precipitate RNA. RNA was eluted in 30 µL of RNase-free water.

For RNA sequencing, cells were collected and lysed using 1 mL TRI reagent® (Sigma, T9424), and 500 µL chloroform was added. Cells plus mix was shaken vigorously for 1 minute and centrifuged for 15 minutes at 4 °C at max speed. The supernatant (approximately 300-400 µL) was transferred to 550 µL of ice cold isopropanol-containing tubes, and kept at -20 °C for at least 3 hours. Mix was centrifuged at 13000 rpm for 20 minutes at 4 °C, Pellets were washed with 1 mL 75% ethanol and centrifuged again for 20 minutes. RNA pellets were air dried and dissolved in 25 µL RNase free water. RNA was quantified using Nanodrop (for qPCR) and Qubit Tapestation (for sequencing).

2.5.3 cDNA synthesis

RNA was converted to cDNA using SuperScript™ IV Reverse Transcriptase (RT) kit (ThermoFisher, 18091050). To 800-1000 ng of RNA, 1 µL of random primers (Promega, C1181) and 1 µL of 10 mM dNTPs (Invitrogen, 18427088). Reaction mix was made up to 12 µL using nuclease-free water. Samples were heated at 65 °C for 5 minutes before 1 µL SuperScript™ IV RT, 1 µL DTT, and 4 µL first-strand buffer were added to the annealed RNA. Samples were heated to 55 °C for 15 minutes. The enzyme was terminally inactivated by heating to 80 °C for 10 minutes.

2.5.4 Quantitative real-time polymerase chain reaction (qRT-PCR)

Gene expression was measured using SYBR Green for all qPCR reactions (see list of primers in Table 2.3 and Table 2.4) via the Applied Biosystems 7500 Fast Real-time PCR system. Each 10 µL qPCR reaction contained 5 µL GoTaq qPCR master mix (Promega, A6001), 0.25 µL 10 µM forward and reverse primer (Sigma Aldrich) and a cDNA equivalence of 1 µg RNA. Cycling conditions included an initial denaturation at 95°C for 5 minutes followed by 40 cycles at 95°C for 15s, 60°C for 30s and 72°C for 30s. Following amplification, a melt-curve step was performed at 95°C for 15s, 60°C for 1 min, 95°C for 30s and 60°C for 15s. Gene expression was normalised to an endogenous control, protein phosphatase 1A (PP1A). All qPCR reactions were performed in triplicates and data was analysed using the comparative CT method ($2^{-\Delta\Delta C(T)}$) (Livak and Schmittgen, 2001). All gene expression fold changes were calculated relative to undifferentiated and untreated iPSCs collected from maintenance cultures in the lab, unless otherwise stated. All qPCR primers were designed using SnapGene software and purchased from Sigma-Aldrich. Melting temperature of primers were calculating using the Oligonucleotides Property Calculator provided by Northwestern University

Table 2.3 qPCR primers used for haematopoietic differentiation characterisation

Gene	Primer sequence (5'-3')	
	Forward	Reverse
PP1A	TCTTTCACCTTTGCCAAACACC	CATCCTAAAGCATACGGGTCC
HOXA9	GCCGGCCTTATGGCATTAA	CAGGGACAAAGTGTGAGTGTCAA

RUNX1	CCTTCGTACCCACAGTGCT	CAACGCCTCGCTCATCTT
GATA2	TCAGCCACTCCGGACACAT	GTCCTCGACGTCCATCTGTT
MEIS1	TGTA AACGACGGCCAGT	CAGGAAACAGCTATGACC
mScarlet	ATGGTGAGCAAGGGCGAGGC	AACTTGCGGTGCGACGTTGTA
mScarlet-H	GCTGAAGGTGACCAAGGGTG	TCGAAGTTCATCACGCGCTC
HOXA5	TCCCATCGCTTCCCTACCT	GCTTTGGAACAGCCTACAGCTT
HOXA7	AGCTTGGA AATTCTGCTCACTTCT	TCTGATGTCATGGCCAAATTTG
cMYB	TGTA AACGACGGCCAGT	CAGGAAACAGCTATGACC
MECOM	AGTAGGGAGTAGAGCCAGTG	TTCGACGTTGCTTCCTTTTT

Table 2.4 qPCR primers used for RNA sequencing results validation

Gene	Primers sequence (5' -3')	
	Forward	Reverse
CD86	CCCGAGAACCCAAGTGAATCC	CAGTAGAAAGTGAGTAAAACCCACCA
H2AFZ	ACCAACACTGGACAGCTGTTAG	ACTTGAGCTGCATGTTTTTAAAGATACC
HIST1H3H	GCTATCGGCCTGGTACAGTG	TCCTTGGGCATGATAGTCACC
IL1B	CTCAGGTCATTCTCCTGGAAGG	TCTCTGATGTCAAAGCATGGTTCC
CXCL6	CCTGGGTCGTCAACCTTTGT	AATCCTACAGAGAGAATAAGGACATTGTGA
CSF1	TGTGTCATGAGCACCCACTC	ACTGCTAGGGATGGCTTTGG
MMP9	GCTTCTCCAGAAGCAACTGTC	ACAGGACATGTTCCACCGCT
BCL2	TTCATGGTACATCACTGACAATGCATA	GATTTCTCCTGGCTGTCTCTGAA
CDKN1A	CGAGTTCTTCTGTTCTCAGCA	ACACAAACTGAGACTAAGGCAGAAG
EIF4EBP1	CGCACAGGAGACCATGTCC	AATCCGCGATTCCCGATCC
B2M	GGAGAACTGTCTGCAGCTACTT	TTCCCCCAAATTCTAAGCAGAGTAT

2.6 Flow cytometry

Flow cytometric analysis of EBs and suspension cells from the spin EB differentiation were analysed using the Sony ID7000 cytometer. Cell pellets were resuspended in PBS (50 μ L/sample). Cells were first stained for viability using Zombie NIR (Biolegend, 423105) (diluted 1:2000 in PBS) and incubated for 15 minutes at room temperature. Conjugated antibodies were added at room temperature. Isotype, single-stain and unstained controls were prepared by

staining cells with a conjugated isotype antibody a single antibody or no antibodies (unstained). All antibodies are listed in Table 2.5. After 20 minutes, cells were washed twice with 1% PBA and fixed with 4% PFA. Samples were left in PFA and run the following day. Data acquisition was set to 10,000 events per second. Data was analysed using Beckman Coulter Kaluza Analysis software. Events acquired were first analysed using forward and side scatter parameters. Gates were generated to isolate cells from debris, and identify the singlets population of cells. Unstained, isotype and single stained controls were then used to identify non-specific staining, and set background staining thresholds.

Table 2.5 Conjugated antibodies used for flow cytometry

Antibody	Type	Dilution	Reference
NCAM-BV421	Specific	1:20	Biologend, 318328
BV421 Mouse IgG1	Isotype	1:67	Biologend, 400157
KDR-AF647	Specific	1:10	BD Bioscience, 560495
AF647 Mouse IgG1, κ	Isotype	1:80	BD Bioscience, 557714
CD34-FITC	Specific	1:5	BD Bioscience, 555821
FITC Mouse IgG1, κ	Isotype	1:20	BD Bioscience, 555748
CD90-BV421	Specific	1:20	Biologend, 328122
BV421 Mouse IgG1, κ	Isotype	1:20	Biologend, 400157
CD43-APC	Specific	1:40	Biologend, 343206
APC Mouse IgG1, κ	Isotype	1:20	Biologend, 400119
CD38-PerCp-Cy5.5	Specific	1:20	Biologend, 303522
PerCP-Cy5.5 Mouse IgG1	Isotype	1:10	Biologend, 400149

2.7 Genetic engineering of HOXA9 reporter line, eA9^m

2.7.1 Plasmid design and eA9^m generation

Plasmid (pHOXA9-T2A-mScarlet) used for targeting was generated by Genewizz (schematic and validation is discussed in section 4.2). The expression of mScarlet-H is under the control of the endogenous HOXA9 promoter. MScarlet-H was selected because it is more photostable than the original mScarlet protein (Bindels et al., 2016). HOXA9 is linked to mScarlet-H via a self-cleaving T2A peptide (54 base pairs (bp)). The addition of T2A enables the reporter protein to be expressed contemporaneously with HOXA9, without the possible functional effects of a HOXA9-mScarlet fusion protein. HOXA9-T2A-mScarlet-H (1556 bp)

is transcribed and then translated into two separate proteins. To further eliminate possible genetic interference of foreign DNA, the PiggyBac (PB)-driven, foot-print free strategy was chosen for eA9^m generation. This was achieved following a published protocol (Kondrashov et al., 2018). Briefly, the protocol involves a PB transposon approach, followed by a puromycin and delta thymidine kinase (TK) drug selection system that is shorter and simpler than the conventional process. RPATs were nucleofected with the CRISPR/Cas9 elements and treated with puromycin (0.2 µg/mL) for selection.

2.7.2 Polymerase chain reaction (PCR)

DNA was amplified using Phusion High-fidelity DNA polymerase (NEB, M0530). For every PCR reaction, 100 ng of genomic DNA were mixed with 1X GC buffer, 200 µM of dNTPs, 1 µM of primers pair and 1 µL of Phusion polymerase. The reaction was made up to either 20 µL or 50 µL using nuclease-free water. The routine thermocycling conditions are listed in Table 2.6.

Table 2.6 PCR thermocycling conditions

PCR steps	Temperature	Time
Initial denaturation	98	8
Denaturation	98	0.5
Annealing	X*	0.5
Extension	72	X*
Final extension	72	8

*Adjusted according to PCR product length.

2.7.3 Primer design

All primers were designed using SnapGene software and purchased from Sigma-Aldrich. Melting temperature of primers were calculating using the Oligonucleotides Property Calculator provided by Northwestern University. Primers were used at 10 µM in the reaction mix. Genotyping primers are listed in Table 2.7.

Table 2.7 Genotyping primers used in genomic PCR

Primer name	Sequence (5'-3')
A9.int F	AGGAGCCAGAAGTTGGTGTGGGA
Scar F	ATGCAGAAGAAGACAATGGGCTGGG

Scar R	TGTAGGTGGTCTTGAAGTCC
-PB F2	CCACAACGAGGACTACACCG
-PB R2	AGGGGGACGGACAGTTCTTT
PB F1	CCGTGGTGGAACAGTACGAA
PB R1	TTTGA CT CACGCGGTCGTTA
PB F2	TAACGACCGCGTGAGTCAAA
PB R2	TGGATGTGGAATGTGTGCGA
PGK F	AGCTTTGCTCCTTCGCTTTC
PGK R	TGTA CT CGGTCCCCATGGTT
Puro F	AACTAAACCATGGGGACCGAG
Puro R	GTGAGGAAGAGTTCTTGCAGC
TK F	TCCGAGACAATCGCGAACAT
TK R	ATATGAGGAGCCAGAACGGC
polyA F	CTCTATGGCTTCTGAGGCGG
polyA R	GCCCAAATGGCATTAAACCCT
WT fwd	CTTCGGGACGAGCCAAGACTG
WT rev	TACGAGCCAGCCTGAACAGG

2.7.4 Agarose gel electrophoresis

DNA products were electrophoresed on 1.5% agarose gel prepared in 1xTAE buffer (Tris-acetate-EDTA) (ThermoFisher, Ref: B49) at 120 V for 60 minutes. Ethidium bromide (10 mg/mL) was added to visualise DNA and a 1 kb+ DNA ladder was used (NEB, N0550) as a product size reference. Gels were imaged using Gel Doc EZ (Bio-Rad, 1708270EDU).

2.7.5 Sanger sequencing

Amplified DNA was visualised by gel electrophoresis as described previously. DNA bands were extracted from agarose gel using QIAquick Gel Extraction kit (Qiagen, 28706X4). Gel DNA bands were excised using a scalpel under UV light. Gels were heated at 50 °C in buffer QG. DNA was precipitated using isopropanol, and purified using ethanol-containing wash buffers. DNA was eluted in 40 µL buffer EB. Samples were sequenced by Source Bioscience. Sequencing results were analysed using Chromatogram and SnapGene.

2.8 Microscopy

Fluorescence microscopy was performed and intensity quantified using Operetta® high content image analysis system (PerkinElmer) and EVOS M7000 imaging system (Thermofisher). Confocal microscopy was performed using the Leica TCS SPE scanning confocal microscope. Comparative images were always used at the same parameters and settings. To fix EBs for imaging, each EB was transferred from a 96-well in round-bottom plates to a 96-well in a flat-bottom plate, containing PFA. The excitation and emission spectra used was specific to mScarlet-H; 551 nm and 592 nm, respectively (Bindels et al., 2016). We first attempted to image eA9^m and BE31, an iPSC cell line that does not contain a fluorescence reporter, and red fluorescence was visible in both EBs at day 7 of the differentiation. This has shown that EBs possess autofluorescence due to their 3D structure. Day 2 RPATs and eA9^m EBs as a negative control of fluorescence on the dsRed channel. The contrast scale was adjusted to account for autofluorescence and same settings were used for all images taken.

2.9 Anti-leukaemic drug treatment

2.9.1 Dose response assay

Leukaemic cell lines were seeded in flat-bottom 96-well plates at 2×10^5 cells/mL. Cells were treated with ATV, HHT or DMSO and incubated at 37 °C in 5% CO₂ for 72 hours. The ATV concentrations used were 0.01 µM, 0.03 µM, 0.1 µM, 0.3 µM, 1 µM, 3 µM, 10 µM, 30 µM and 100 µM, and 0.0001 µM, 0.0003 µM, 0.001 µM, 0.003 µM, 0.01 µM, 0.03 µM, 0.1 µM, 0.3 µM and 1 µM for HHT. DMSO of the same percentage as the highest drug concentration for each cell line was used as a vehicle control. Drugs were diluted in RPMI1640 medium. Cell viability was assessed using the RealTime-Glo™ kit (Promega, G9711). Briefly, reagents were equilibrated to 37 °C. The cell viability substrate and enzyme were added to the cell suspension at 2X prior to seeding in 96-well plates. Plates were kept in the incubator for 3 days with no media change or further addition of reagents. After 24, 48 and 72 hours incubation times, luminescence was recorded using the FLUOstar® Omega plate reader (BMG Labtech). Statistical analysis and IC50 values were performed using GraphPad Prism.

2.9.2 RNA sequencing

RNA sequencing was performed on leukaemic cell lines (at 2×10^5 cells/mL) that were treated with the 48 hour-IC₅₀ of homoharringtonine (HHT), atorvastatin (ATV) or DMSO for 48h prior to collection. DMSO of the same percentage as the highest drug concentration for each cell line was used as a vehicle control. Total RNA from cells was extracted from two independent biological repeats using phenol-chloroform extraction method as described previously. Samples were submitted to Novogene for quality control, library preparation and total mRNA sequencing using the Illumina platform.

2.9.3 RNA sequencing analysis

Bioinformatics analysis was carried out and figures were generated by Novogene. For quality control, raw data was processed through fastp software, wherein clean data was obtained by removing reads containing adapter, poly-N and low quality reads. Read mapping to the reference genome was generated using Hisat2 as a mapping tool. For gene expression quantification, the common method using FPKM was used, which is based on length and read counts mapped to the gene. For differential expression analysis, genes with an adjusted P-value of ≤ 0.05 found using DESeq2 were assigned as differentially expressed. The clusterProfiler R package was used to test the statistical enrichment of differential expression genes in KEGG pathways. Reactome pathways with corrected P-value < 0.05 were considered significantly enriched.

2.9.4 Statistical analysis

Analysis was performed using GraphPad Prism analysis tools. For dose-response assays, the values were derived using GraphPad prism nonlin-fit agonist vs. response- variable slope (four parameters). For CFU assays, one-way ANOVA analysis was used along with Tukey's multiple comparison test.

Chapter 3 Haematopoietic differentiation of human iPSCs

3.1 Brief background

Haematopoietic differentiation of PSCs has been accomplished following several approaches, producing HSPCs with variable haematopoietic potential and limited *in vivo* engraftment (Hansen et al., 2018; Ng et al., 2016; Doulatov et al., 2013; Ruiz et al., 2019). Despite the availability of several differentiation protocols, discussed in Chapter 1.1.3, the process of differentiating iPSCs to HSPCs, remains challenging and highly inefficient. A pre-requisite to addressing the aims of this thesis is development of a method to routinely generate HSPCs from iPSCs. In this chapter, two protocols were tested and optimised: the commercially available STEMDiff™ Haematopoietic kit (2D culture) and a published spin EB method (Ng et al., 2016; Nafria et al., 2020).

The STEMDiff™ kit is a monolayer directed differentiation method that uses a proprietary chemically defined media containing extrinsic growth factors, cytokines and small molecules to induce differentiation in adherent cultures. In this approach, cells are cultured and passaged as clumps, and differentiated as adherent cells. The spin EB protocol involves administration of defined extrinsic morphogens that mimic endogenous signalling cues. In this method, dissociated iPSCs are initially forced to form aggregates by centrifugation, differentiated to HE cells, and transitioned to adherent cultures which generates a supportive niche for HSPC production.

To summarise, both protocols share a similar stepwise process, aiming to reproduce the spatial organisation of the early embryo.

Step 1: PSCs undergo mesoderm induction and patterning

Step 2: Cells are then directed to haemogenic mesoderm

Step 3: HE specification

Step 4: EHT, giving rise to sprouting of round cells

Step 5: Transition of haematopoietic cells to suspension.

Proof-of-principle (n=1) experiments were done using both protocols to develop a method for routine production of HSPCs in an efficient manner for future differentiation of the HOXA9 reporter iPSC line. Differentiation efficiency and populations produced were assessed using cell surface marker expression by flow cytometry and gene expression profiling by qPCR. Characterisation of the stage-specific cell population markers explained in section 1.1.4 is summarised in Table 3.1. The quality of derived HSPCs was also examined by qPCR and CFU assay. To date, the CFU assay is a key assay demonstrating the repopulating and haematopoietic potential of HSPCs. Two cell lines were used for the haematopoietic differentiations: RPAT, the human iPSC cell line, and eA9^m, a genetically engineered RPATs clone. Detailed generation of eA9^m is discussed in Chapter 4.

Table 3.1 Stage-specific surface markers of cells during haematopoietic differentiation

Cells population	Surface markers
Mesoderm	NCAM+ KDR+ CD34-
Haemogenic mesoderm	CD34+ KDR+ CD43-
Hemato-vascular mesoderm	CD34+ CD90+
Haemogenic endothelium (HE)	CD34+ CD90+/- CD43-
Haematopoietic progenitors	CD34+ CD90+ CD43+ CD45+ CD38-

3.2 Monolayer differentiation using the STEMdiff™ kit

3.2.1 iPSC passaging and seeding for haematopoietic differentiation

An enzyme-free mechanical cell dissociation reagent (GCDR, StemCell Technologies) was used to transition iPSCs from monolayer growth (n=3 passages) to aggregates in preparation of haematopoietic differentiation using the STEMdiff™ kit from StemCell Technologies (in 6 well plates). Aggregates were then routinely dissociated mechanically using a cell scraper and seeded into 12-well plates at a 1:60-1:200 ratio to form colonies of the desired size and colony compaction (100-200 µm in diameter) suitable for differentiation. The STEMdiff™ kit differentiation process is 12 days long, involving two media formulations, media A and media B. Media A was added to the colonies for the first 3 days, after which media was changed to media B (Figure 3.1A). Half media changes were performed on day 2, day 5, day 7 and day 10. During differentiation, cells

underwent marked morphological changes (Figure 3.1B). Colonies possessed flat, compact structures that later formed bursts of large, hollow sacs. The presence of these structures was indicative of successful differentiation. Spherical, potential HSPC buds emerged from colonies on day 10, but remained attached to the surface of the colony. By day 12 these cells had entered suspension and were collected and characterised.

Apart from being time consuming and labour intensive, the aggregate passaging method resulted in variability and inconsistent formation of colonies with the desired size and number for consistent generation of HSPCs. Although derivation of haematopoietic progenitors using the aggregate passaging method was feasible, variability in the CD34⁺/CD38⁻ haematopoietic progenitors fraction was observed (Figure 3.1C). Representative dot plots demonstrate the large variability from four independent differentiations (n=2 for each cell line) (Figure 3.1C). The percentage of CD34⁺/CD38⁻ cells produced were 13.6% and 4.2% for RPATs differentiations, and 58.8% and 12.8% for eA9^m differentiation. Other differentiations failed to produce a measurable number of suspension cells at all (data not shown). It was concluded that aggregation passage of RPATs or eA9^m iPSCs was inefficient for the routine generation of HSPCs by STEMdiff™ kit differentiation.

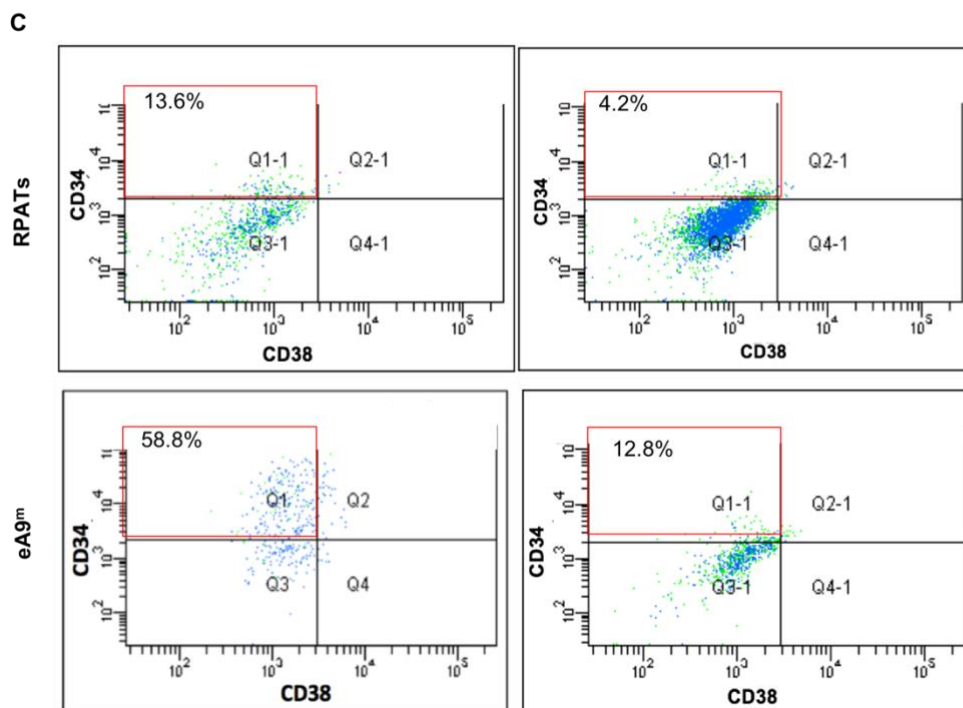
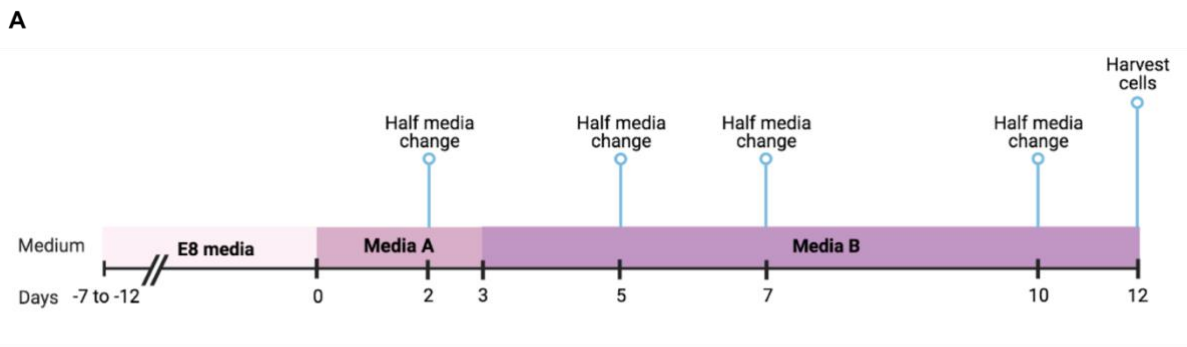


Figure 3.1 Aggregate passaging of RPATs or eA9^m results in high variability in HSPC formation using the STEMdiff™ kit.

A. Schema of the timeline for the STEMdiff™ kit (StemCell Technologies) differentiation process. **B.** Morphological changes during the haematopoietic differentiation of RPAT. Haematopoietic clusters arise from adherent monolayer, and by day 12, suspension haematopoietic cells are seen as small, spherical cells (white box). Scale bar = 200 μ m. **C.** Dot plots showing variable numbers of CD34⁺/CD38⁻ populations generated from RPATs or eA9^m.

The broad range of initial colony size and number was likely a major contributor to the lack of reproducibility observed. Another dissociation reagent, ReLeSR, suggested by the manufacturer was tested but proved to be unsuitable for RPATs by EC. To test this, another passaging and seeding method was used, wherein single cell-derived RPATs colonies were generated. It was hypothesized that initiating aggregate formation from single cells would generate more uniform colony number and size, and thus reduce the observed variation. To achieve this, cells were enzymatically passaged using EDTA and seeded at very low densities (200-720 cells/mL) in RC, which enables maximum cell recovery after single cell passaging, and kept in culture until uniform colonies formed. A comparison between both passaging methods is summarized in Table 3.2.

Table 3.2 Comparison between two different iPSCs passaging methods tested.

Method	Dissociation reagent	Passaging Media	Preparation time	Dissociation	Seeding density	Colony number
Aggregates	GCDR	E8	9-12 days	Mechanical	1:60 – 1:200	16-40
Single cells	EDTA	E8 + RC	7-8 days	Enzymatic	200-440 cells/mL	11-48

Cells were cultured for 7-8 days and formed compact colonies, similar to those derived using the aggregate method, but more consistently, particularly with the lower seeding density (Figure 3.2A). A seeding density of 200-440 cells/mL that resulted in a total number of 11-48 colonies per well was considered optimal for continuing with the haematopoietic differentiation (n=3) (Figure 3.2B). Comparatively, the single cell approach involved one additional preparation step prior to differentiation and the compact colonies formed remained undisturbed in 12-well plates. This removed the mechanical step required for aggregate seeding (scraping), which may also have contributed to variability previously observed. Taken together, the single cell passaging approach subjects the cells to less stress, experimental variation and time taken to generate colonies, making it a more robust and reliable approach for routine HSPCs generation from RPATs and eA9^m using the STEMdiff™ kit.

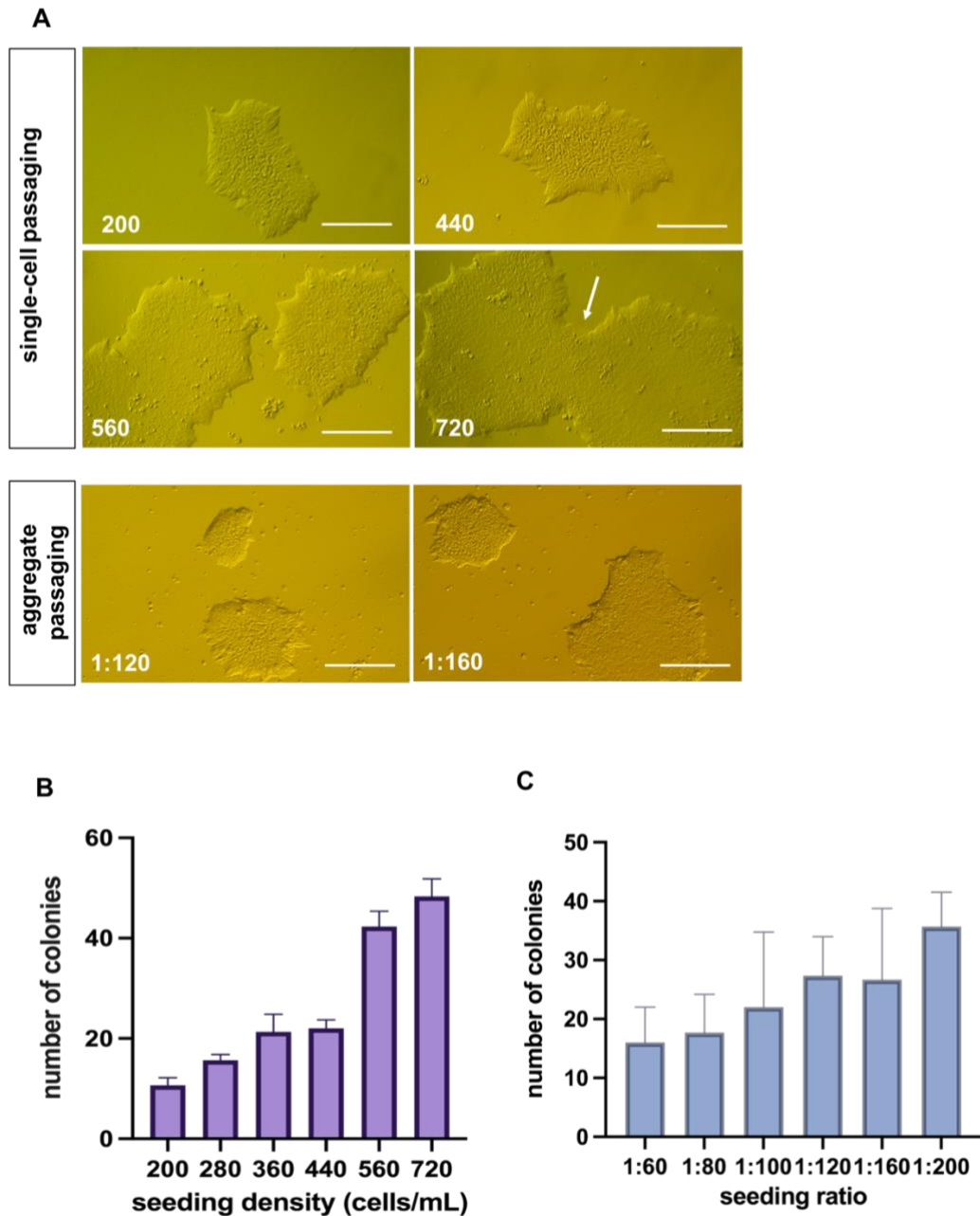


Figure 3.2 Single cell seeding of RPATs for STEMdiff™ differentiation.

A. Representative phase contrast images of RPATs colonies derived from single-cell and aggregate passaging methods after 7 or 3 days in culture respectively. Cell number or ratios are labelled. Colonies started to merge at higher densities (white arrow). Magnification 10x, Scale bar = 200 μ m. Bar graphs show the number of colonies derived using single cell (**B**) and aggregates (**C**) passaging. Numbers are mean \pm SD (n=3).

3.2.2 Single cell eA9^m iPSCs seeding yields CD34+CD43/CD45+ using the STEMdiff™ kit

eA9^m iPSCs were passaged as single cells at low densities as described in 3.2.1. prior to initiating the STEMdiff™ kit differentiation. On day 12, the suspension cells

were harvested (as per the manufacturer's protocol) and characterised for CD34, CD43 and CD45 expression by flow cytometry. In addition, the differentiation process was extended to day 14 to examine whether longer culture time yielded more suspension cells. A total of $\sim 3.5 \times 10^5$ cells ($6.9 \pm 2 \times 10^4$ cells/mL) were harvested on day 12 and $\sim 3 \times 10^5$ cells ($5.5 \pm 1 \times 10^4$ cells/mL) on day 14. Harvested suspension cells were analysed for haematopoietic markers (Figure 3.3A). The proportion of HE cells expressing CD34+CD43- were approximately similar on both days, ranging from 31-33%. The fraction of cells that expressed CD43 only and lacked CD34 also did not vary on either days. Conversely, 55.7% of cells acquired CD34+CD43+ expression (haematopoietic fate) on day 14, compared to only 31.9% CD34+CD43+ on day 12. Interestingly, a slightly lower proportion of CD34+CD45+ cells were seen after extended cell culture (34% vs. 43.9%). However, the CD34+CD45- fraction of cells showed a large increase on day 14, with almost 50% of the population acquiring CD34 expression but still lacking CD45 expression. On day 12, CD34+CD45- cells represented only 17.9% of the population.

To examine the potential to retain eA9^m-derived HSPCs in short-term culture, cells were maintained in supplemented IMDM media (2.1.2) for up to 96 hours. Although cell viability was maintained up to 72 hours the majority of cells exhibited a stressed, apoptotic morphology by day 4 (Figure 3.3B).

3.2.3 Extended differentiation culture on viability

The viability of day 12 vs day 14 eA9^m-derived HSPCs was also assessed by flow cytometry using a fluorescent viability dye that stains dead cells. The viability of CD34+ cells was high (84.6%) on day 12, and decreased to 49.4% on day 14 (n=1) (Figure 3.3C). It is worth noting that more CD34+ cells were collected (13,569) on day 14 compared to day 12 (7,409). In line with the results shown in 3.2.2, the number of CD34+ cells harvested increased, but their viability was compromised.

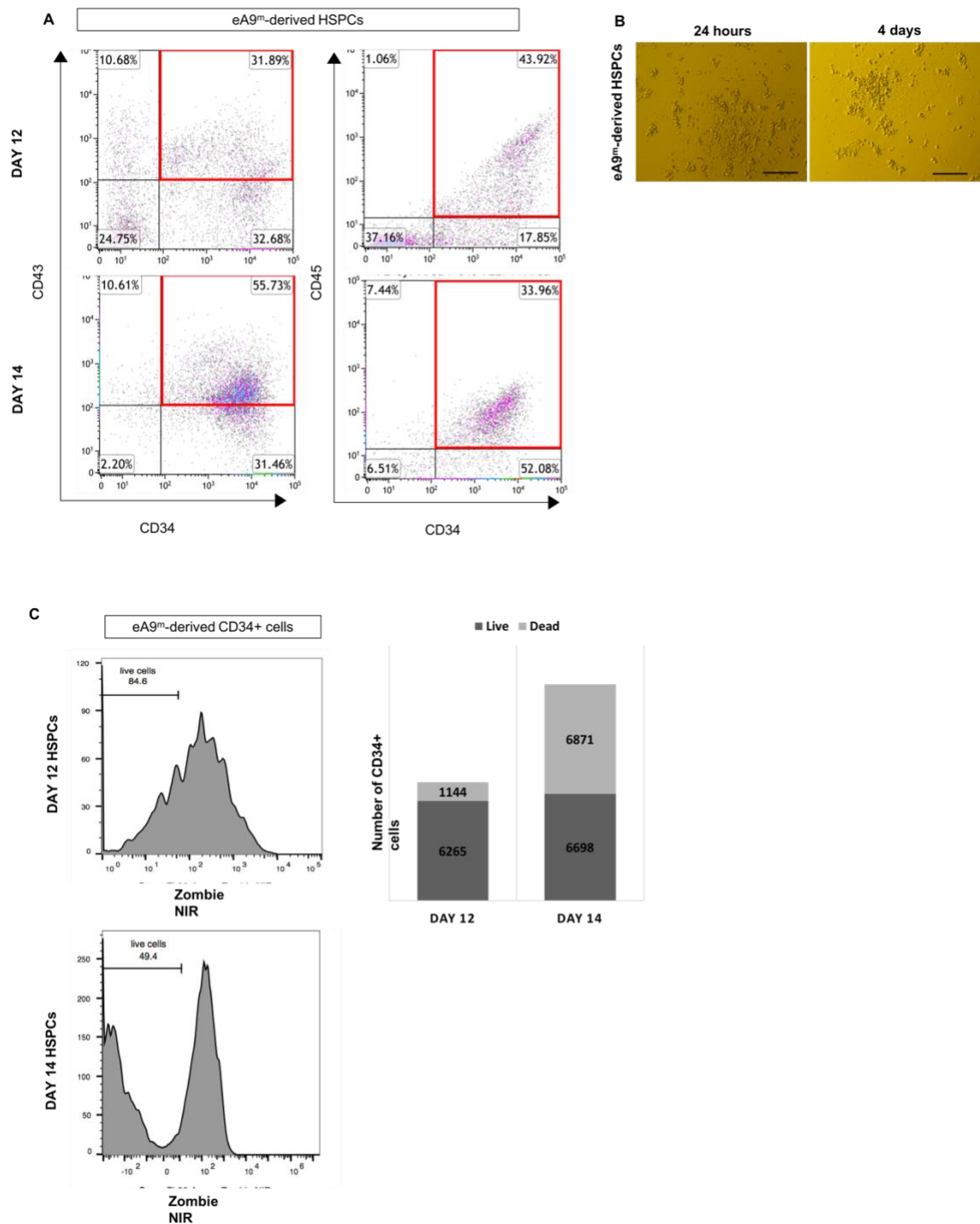


Figure 3.3 Culture and characterisation of single cell-derived eA9^m-derived HSPCs using the STEMdiff™ kit.

A. Representative flow cytometry plots for CD34, CD43 and CD45 expression in eA9^m-derived HSPCs harvested on day 12 and day 14. Results were gated using unstained control and adjusted using single-stained samples. **B.** Representative phase contrast images of harvested potential HSPC suspension cells, seeded in supplemented IMDM liquid culture at 1×10^5 cells/mL. Scale bar = 200 μ m. **C.** Representative flow cytometry analysis of HSPC viability of day 12 and day 14 harvested eA9^m-derived CD34⁺ cells using combined Zombie NIR staining. Stacked bar chart shows the total number of live and dead CD34⁺ cells. (n=1).

3.2.4 Extended differentiation culture does not affect the clonogenicity of eA9^m-derived HSPCs

To functionally assess colony forming and self-renewal capacity, eA9^m-derived HSPCs collected on day 12 and day 14 were seeded into semi-solid, methylcellulose-based medium and observed over 14 days in culture (Figure 3.4). In both samples (day 12 vs. day 14 eA9^m-derived HSPCs), cells cultured in Optimum H4034 medium formed CFU-erythroid (CFU-E) colonies only. In contrast, cells seeded in Classic H4434 medium supported the generation of granulocyte-erythroid-macrophage-monocyte (GEMM), granulocyte-macrophage (GM) and blood forming-unit- erythroid (BFU-E) colonies. GEMM is characterised by a dense core of reddish-brown cells at the core, and loosely packed peripheral cells, whereas BFU-E and CFU-E have a more prominent red centre. Therefore, Classic H4434 medium was chosen for all subsequent eA9^m-derived HSPCs CFU assays.

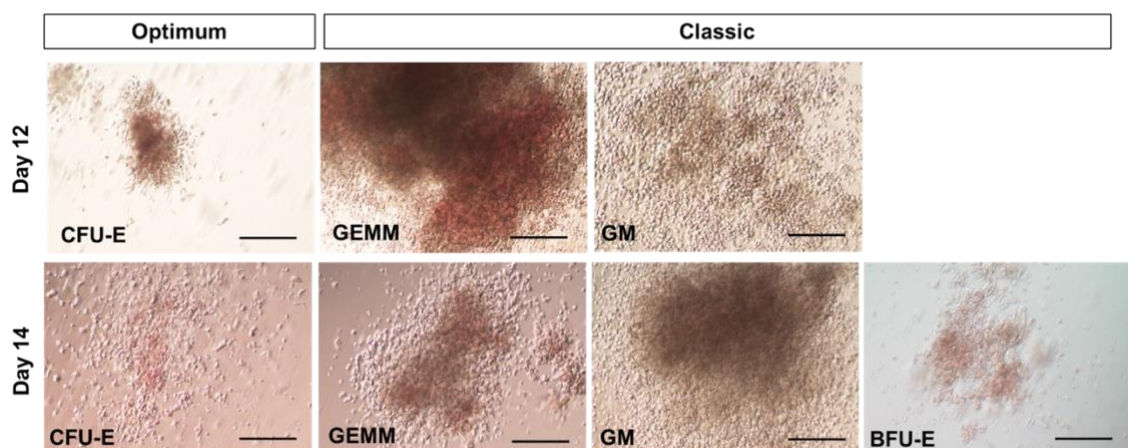


Figure 3.4 Lineage committed haematopoietic progenitors formed from eA9^m-derived HSPCs using the CFU assay.

Representative images of eA9^m-derived HSPCs harvested on day 12 and day 14, and seeded in two different methylcellulose media formulations, Optimum H4034 and Classic H4434. Colonies formed after 10 days in culture, demonstrating colony forming ability of the cells (n=2). BFU; blast-forming unit, G; Granulocyte, M; Macrophage, E; Erythroid, MM; monocyte megakaryocyte. Magnification 10x. Scale bar = 200 μ m.

3.3 Spin EB differentiation

3.3.1 Overview of HSPCs derivation from iPSCs using the spin EB method

It was previously reported that haematopoietic differentiation using the spin EB method allows the formation of reproducible, uniform EBs exhibiting robust

haematopoietic potential (Ng et al., 2016). As previously described (**Error! Reference source not found.2.2.2**), the eA9^m-derived HSPCs were also generated by spin EB differentiation. The published protocol (Ng et al., 2016) was previously optimised in the laboratory for RPAT, to yield more HSPCs compared to the STEMdiff™ kit (EC). A schematic overview of the protocol is shown (Figure 3.5A). Following EB formation in 96-well plates for 7 days, cells were transferred to Matrigel™-coated 6-well plates and grown as adherent cells for the rest of the differentiation. During this process, cells underwent defined morphological changes as represented in Figure 3.5B. Suspension cells emerged on day 14 and day 18 and were harvested for analysis. Herein, we tested the reproducibility and efficiency of the optimised protocol on eA9^m cells.

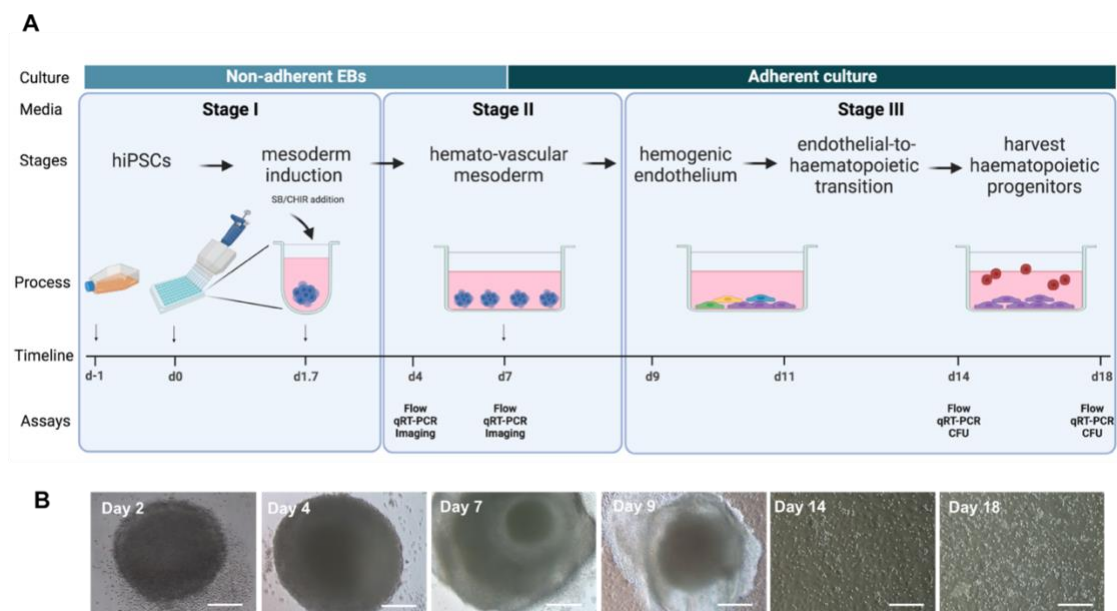


Figure 3.5 Overview of the spin EB haematopoietic differentiation method.

A. Schematic illustration showing the mode of cell culture changing from non-adherent EBs to adherent EBs on day 7 and progress to generation and harvesting of HSPC using 3 different media referred to as Stage I-III (refer to Table 2.1 for components). Human iPSCs are differentiated to mesoderm using Wnt pathway regulators (SB and CHIR), prior to transitioning to adherent EBs. EBs start to gain a haematopoietic profile on Stage II. **B.** Representative images of cell morphology at different stages of spin EB differentiation taken at 10x using a light microscope. Scale bar = 200 μm. Figure generated using biorender.com.

3.3.2 Mesodermal and haemogenic endothelial cell generation from eA9^m iPSCs

To assess whether the first stage of the differentiation process was successful, EBs were collected, dissociated and characterised on day 4 for expression of

pan-mesoderm (NCAM) and mesoderm (KDR) markers by flow cytometry (Figure 3.6). As expected, lack of CD34 expression during the early stages of the differentiation was coupled with high expression of NCAM (69 ± 10 %) and KDR (31 ± 16 %) in day 4 EBs (Figure 3.6A). The majority of cells were viable on day 4 (74 ± 9 %). A similar fraction of the mesodermal double positive NCAM+KDR+ (26 ± 11 %) and earlier mesoderm progenitors that progress to KDR+, NCAM+KDR- cells (38 ± 9 %), cells was also observed at day 4 (Figure 3.6B) .

Prior to transitioning to adherent culture, flow cytometry analysis was used to assess surface marker expression for haematopoietic specification from the haemato-vascular mesoderm on day 7. As cells went through HE specification, CD34 (35 ± 16 %), CD90 (43 ± 2 %), CD43 (6 ± 1 %) expression and viability (66 ± 13 %) was observed on day 7 (Figure 3.6C). Expression of CD34+CD90+CD43- marks the presence of haemato-vascular mesoderm population, as demonstrated in co-expression of CD34+CD90+ (26 ± 16 %) observed in day 7 EBs (Figure 3.6D). CD43 expression distinguishes between endothelial cells and haematopoietic cells. Presence of the double positive CD34+CD43+ population (40 ± 4 %) is indicative of the shift towards a haematopoietic fate and initiation of haematopoiesis. The decrease in viability from day 4 to day 7 samples may be due to the extension in incubation time from 20 minutes (day 4) to 90 minutes (day 7) needed to dissociate the EBs due to the increased cell number and compaction.

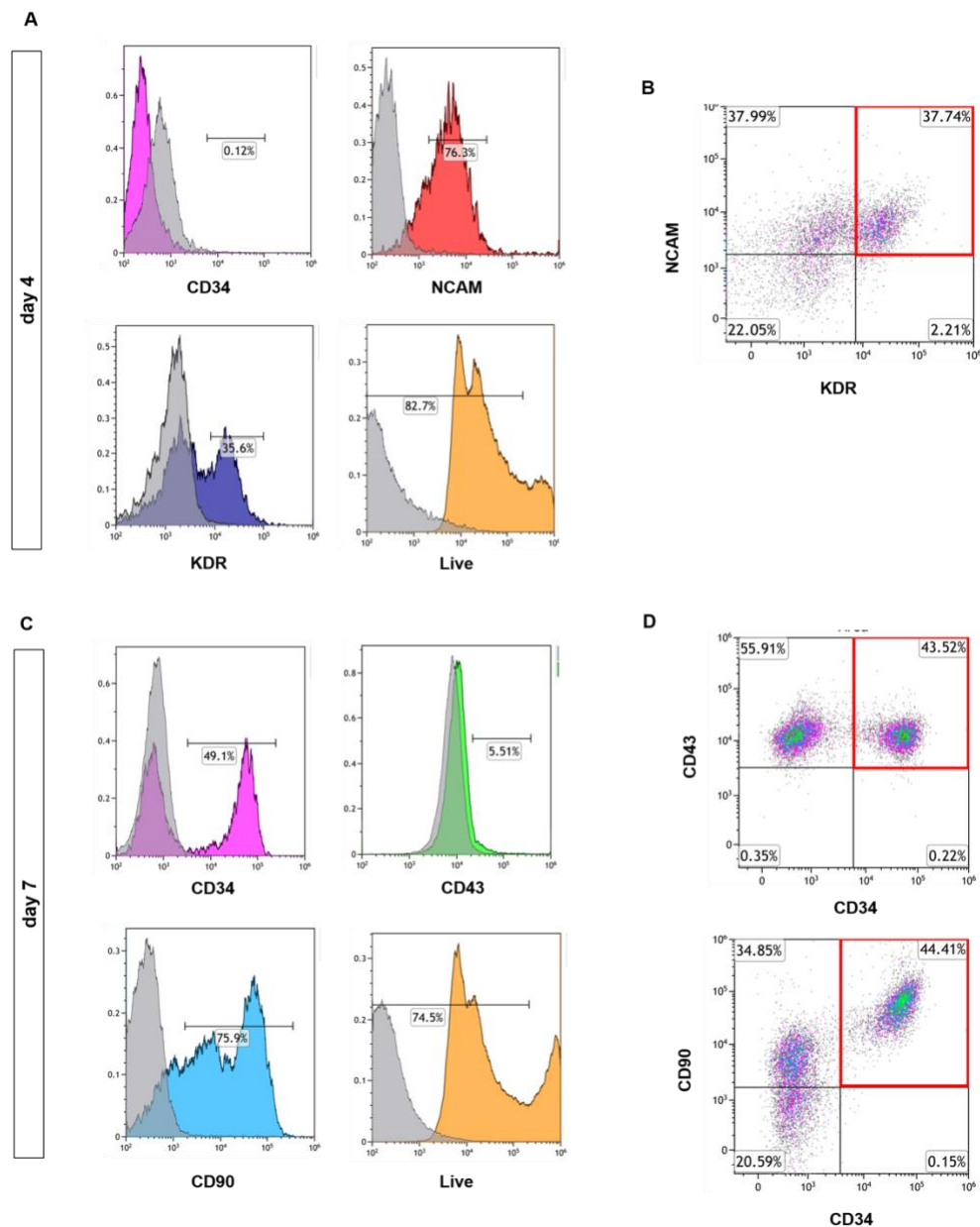


Figure 3.6 *eA9^m* can differentiate to mesodermal and haemogenic endothelial cells.

A. Representative histogram plots of the expression of CD34, NCAM and KDR in day 4 EBs. Cell viability was detected by exclusion of Zombie-positive cells. **B.** Representative dot plots showing the NCAM+KDR+ mesoderm population in day 4 EBs (red box). **C.** Representative histogram plots showing expression of haematopoietic markers (CD34, CD43, CD90) and viability of day 7 EBs. **D.** Co-expression (red box) profiles of CD34+CD43+ and CD34+CD90+ in day 7 EBs. All histogram plots are gated using isotype controls (shown in grey). Dot plots are gated using unstained, single stained, and isotype controls. (n=3).

3.3.3 *eA9^m* cells can differentiate to HSPCs using the spin EB method

The expression of haematopoietic markers was further examined on differentiated cells that had entered suspension by day 14 and day 18.

Characterisation of cells derived from both days is shown in Figure 3.7. Expression of CD34⁺ was similar for cells collected on either day, with a minor decrease on day 18 (28.4% vs. 21.9%) compared to day 14 (Figure 3.7A). Unlike earlier stages of the differentiation, CD43 expression was upregulated to higher levels in suspension cells on these days (40.1% and 67.9% respectively). In contrast, a sharp decrease of ~15 fold in the CD90 fraction (~75% to 5%) of cells was observed on both days. CD38 expression levels were consistent with expected haematopoietic phenotype, being not expressed in day 14 samples and remaining as low as 2.5 % for day 18 samples (Figure 3.7A). This strongly suggests that cells have undergone EHT and lost the HE phenotype. The haematopoietic population, CD34⁺CD43⁺, remains and is similar for both time points (~ 39%). Low expression of CD90 and lack of CD38 in both samples further confirms the presence of HSPCs (Figure 3.7B). The fraction of CD90⁺CD38⁻ cells is higher on day 18 than day 14 (27.19% vs. 13.7%).

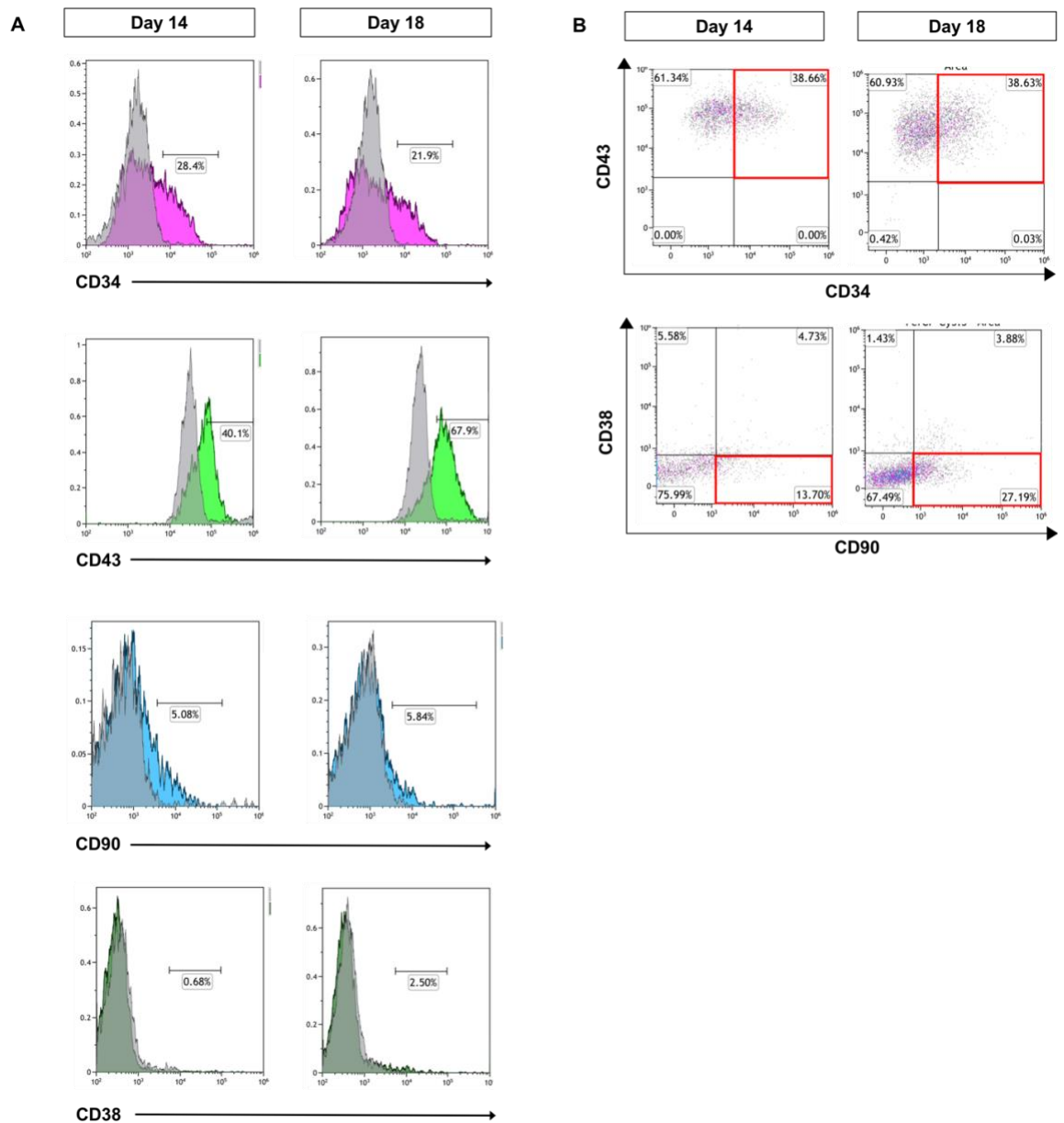


Figure 3.7 Surface marker analysis of iPSC-HSPCs derived using the spin EB differentiation.

A. Representative histogram plots showing expression of haematopoietic markers (CD34, CD43, CD90 and CD38) in iPSC-HSPCs collected on day 14 and day 18 of differentiation. Background threshold was identified using isotype controls shown in grey. **B.** Haematopoietic stem cells populations defined by co-expression of CD34⁺CD43⁺ and CD90⁺CD38⁻ (red boxes).

3.3.4 Formation of multipotent HSPCs from eA9^m cells through HE specification

To assess the expression of key TFs (HOXA9, RUNX1, GATA2 and MEIS1) that regulate haematopoietic development, qPCR analysis was done on samples obtained from days 4, 7, 14 and 18 of the differentiation. The expression of these genes increased on day 7 compared to day 4 across multiple differentiations (n=3) shown in Figure 3.8A. Average relative expression (RQ) values for these

genes, summarised in Figure 3.8B, were determined using undifferentiated eA9^m cell RNA as the comparator. As EHT is initiated, *RUNX1* expression progressively increases from day 4 to day 7. Similarly, *GATA2* expression increases by > 2-fold during EHT. *RUNX1* expression is maintained at later stages and highest expression is observed on day 18 (Figure 3.8C). *GATA2* expression is also maintained throughout differentiation and increases on day 14 and day 18. For comparison, RQ values for all four genes from one representative differentiation is shown in Figure 3.8C. After acquisition of the expected phenotype on day 7, HSPCs were preserved for other downstream experiments, and were not always characterised by qPCR.

Comparatively, EB cells express the least amount of *RUNX1*, with an average of 7.46 ± 2.91 and 31.2 ± 7.10 fold changes on day 4 and day 7, respectively, whereas *HOXA9* and *MEIS1* are expressed at significantly higher levels on either day. Both *HOXA9* and *MEIS1* are highly upregulated on day 7, with an average of 4069 ± 583 for *HOXA9*, and 2935 ± 963 for *MEIS1*.

Comparison between day 14 and day 18 HSPCs indicates increased expression in *HOXA9*, *GATA2* and *RUNX1* but decreased expression of *MEIS1* (Figure 3C). Compared to the EB stages of differentiation, *HOXA9* and *MEIS1* are downregulated by ~1000-fold in suspension cells collected on day 14 and day 18 of the differentiation. Together, this may indicate progression to a haematopoietic cell fate and a degree of HSPC differentiation in the day 14 and day 18 cultures.

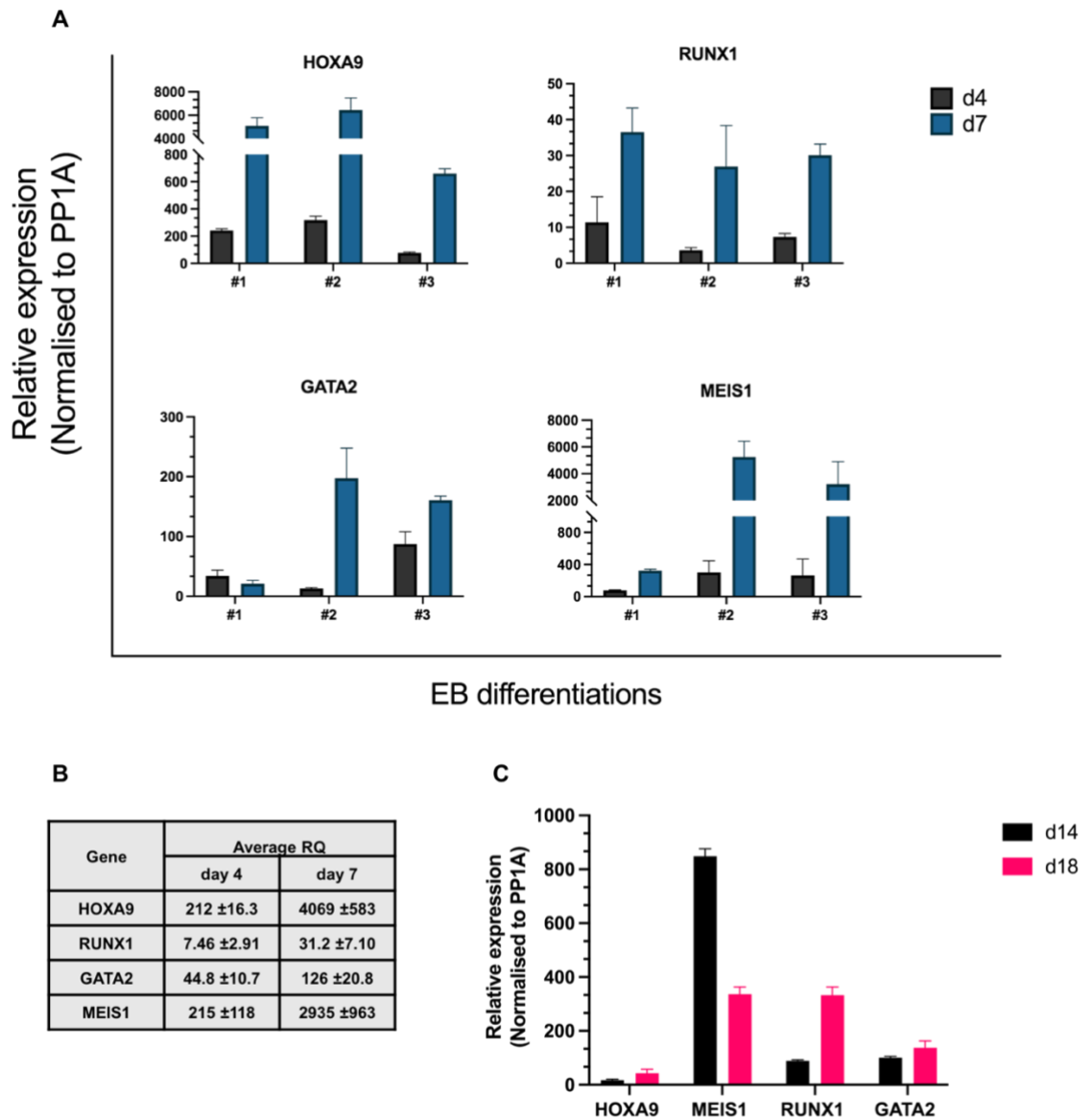


Figure 3.8 Changes in key haematopoietic gene expression during the spin EB differentiation.

A. Bar graphs showing changes of *HOXA9*, *RUNX1*, *GATA2* and *MEIS1* gene expression in day 4 and day 7 EBs derived from eA9^m cells. Results are mean ± SD, of three independent differentiations denoted #1, #2 and #3. An average of relative expression from this data is shown in **B**. Expression is normalized to *PP1A* expression, using undifferentiated eA9^m cells. **C.** qPCR of the TFs in suspension cells harvested on day 14 and day 18. Results are mean ± SD of three technical repeats.

To confirm the colony forming, multipotential ability of the suspension cells derived using the spin EB method, cells from day 14 and day 18 were seeded into Methocult™ for the CFU assay (Figure 3.9). Suspension cells from both timepoints were able to form lineage-committed progenitors. After 14 days in culture, representative images show CFU-E, GM and GEMM colonies from day

14 and day 18. Hence, adopting the spin EB method from EC was successful and was used to derive multipotent HSPCs from eA9^m cells.

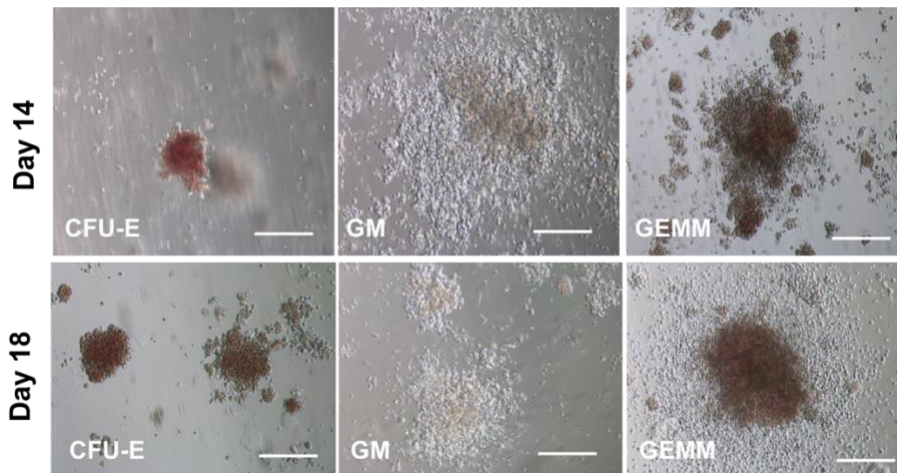


Figure 3.9 Lineage committed haematopoietic progenitors formed from eA9^m spin EB-derived HSPCs using the CFU assay.

Representative images of colonies formed from suspension cells harvested on day 14 and day 18, after 14 days in MethoCult™. BFU; blast-forming unit, G; Granulocyte, M; Macrophage, E; Erythroid, MM; monocyte megakaryocyte. Images were taken using a light microscope at 10x. Scale bar = 200 μm.

3.4 Streamlining the timing of mesoderm patterning and endothelial induction in spin EB differentiation

As stated previously (section 1.1.3), a key step of the spin EB protocol is the precise timing of mesoderm induction and patterning by inhibiting Activin/Nodal and stimulating Wnt. For the published protocol (Nafria et al., 2020b), this was achieved by adding an Activin inhibitor (SB431542) and Wnt agonist (CHIR99021), between 44-48h the differentiation of H9-ESC lines. SB and CHIR are widely used as Wnt signaling pathway. The authors noted however that this timing was not suitable for feeder-free iPSC cultures, such as RPATs. Earlier experiments in the laboratory showed optimal SB/CHIR addition for RPATs to be ~ 38-40h (EC). To further examine this, both timepoints were evaluated using RPATs (n=1 for both timepoints) and eA9^m cells (n=1 for 38h, n=3 for 40h).

3.4.1 Mesoderm patterning timing affects CD34 and CD90 expression of day 7 EBs

After treating RPATs and eA9^m cells with SB/CHIR for either 38h or 40h post seeding, EBs from both were collected on day 7 to investigate whether the timing affected haemato-vascular mesoderm formation. Cells were characterised for differences in surface marker expression using CD34, CD43 and CD90 (Figure 3.10, Figure 3.11) as before. Morphologically, EBs on day 7 from both treatments did not differ (Figure 3.10A). The 38h treatment generated ~9 % CD34 cells in RPATs and eA9^m cells. CD34 expression in both cell lines was ~ 2-fold higher on 40h- compared to 38h-treated EBs (Figure 3.10B,C). CD43 expression did not vary as much and ranged from ~ 3-7% across both cell lines. At this stage, low expression of CD43 is expected as HSPCs are not yet formed. Conversely, the fraction of CD90+ cells differed between both treatments, being higher (>40%) in 40h-treated EBs than 38h-treated EBs, which were 24% and 17% in RPATs and eA9^m cells, respectively (Figure 3.10B,C). Increased numbers of CD34+/CD90+ cells were observed in 40h-treated EBs (~ 21% and 14% in RPATs and eA9^m cells, respectively), compared to 38h-treated EBs (~ 8% and 2% in RPATs and eA9^m cells, respectively) but no co-expression of CD34 and CD43 was observed in day 7 EBs (Figure 3.11A). Although cell viability was > 50% for all samples a reduction in 40h treated eA9^m cells compared to the 38h counterpart was indicated (Figure 3.11B).

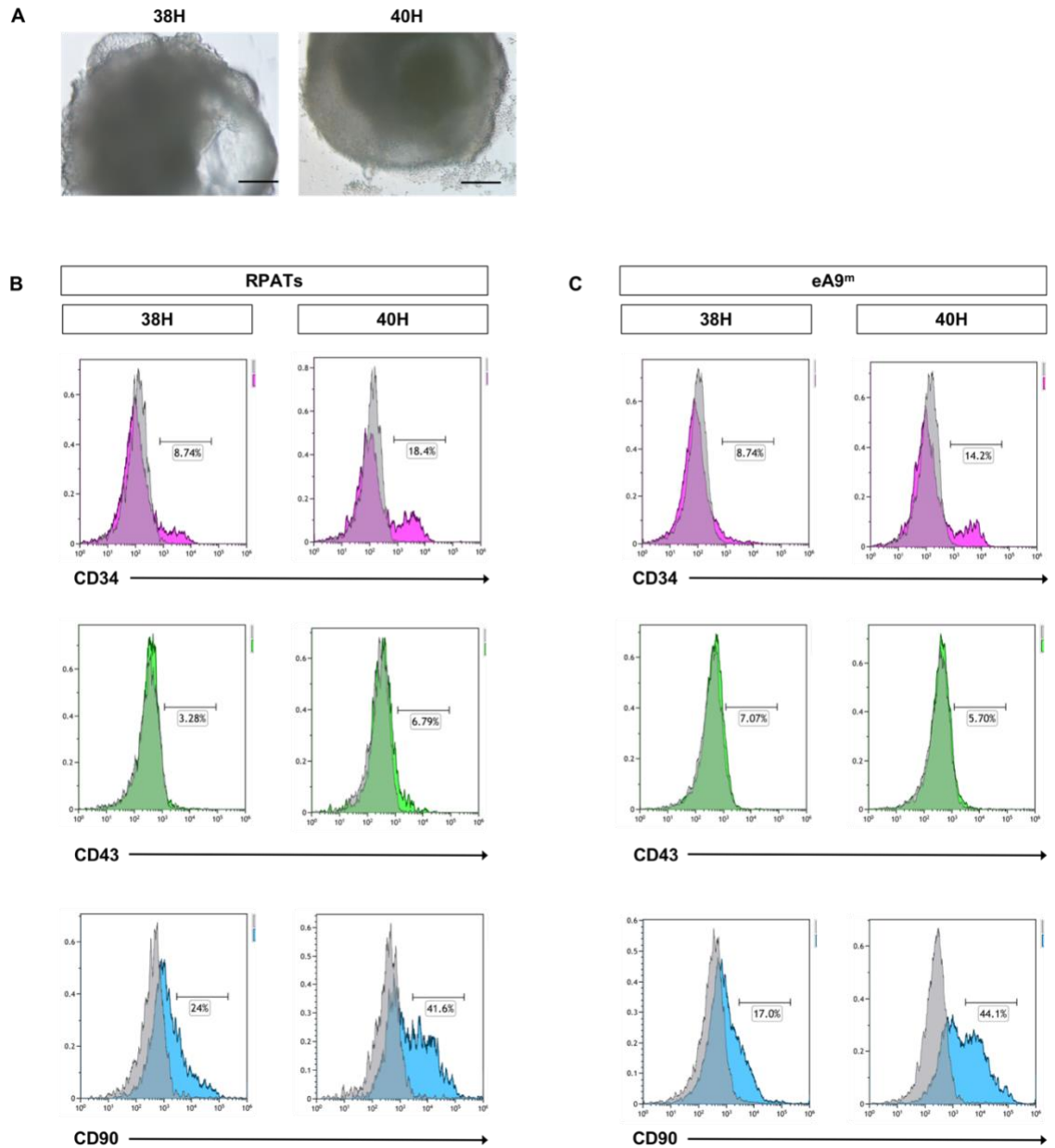


Figure 3.10 Comparative analysis of the effect of 38h or 40h SB/CHIR treatment on morphology and surface marker expression in day 7 EBs.

A. Phase contrast images showing the morphology of d7 EBs following addition of SB/CHIR 38h or 40h post cell seeding. Scale Bar= 200 μ m. **(B)** Histogram plots show changes in CD34, CD43 and CD90 expression in RPATs and **(C)** eA9^m. Background threshold was identified using isotype controls shown in grey. (n=1).

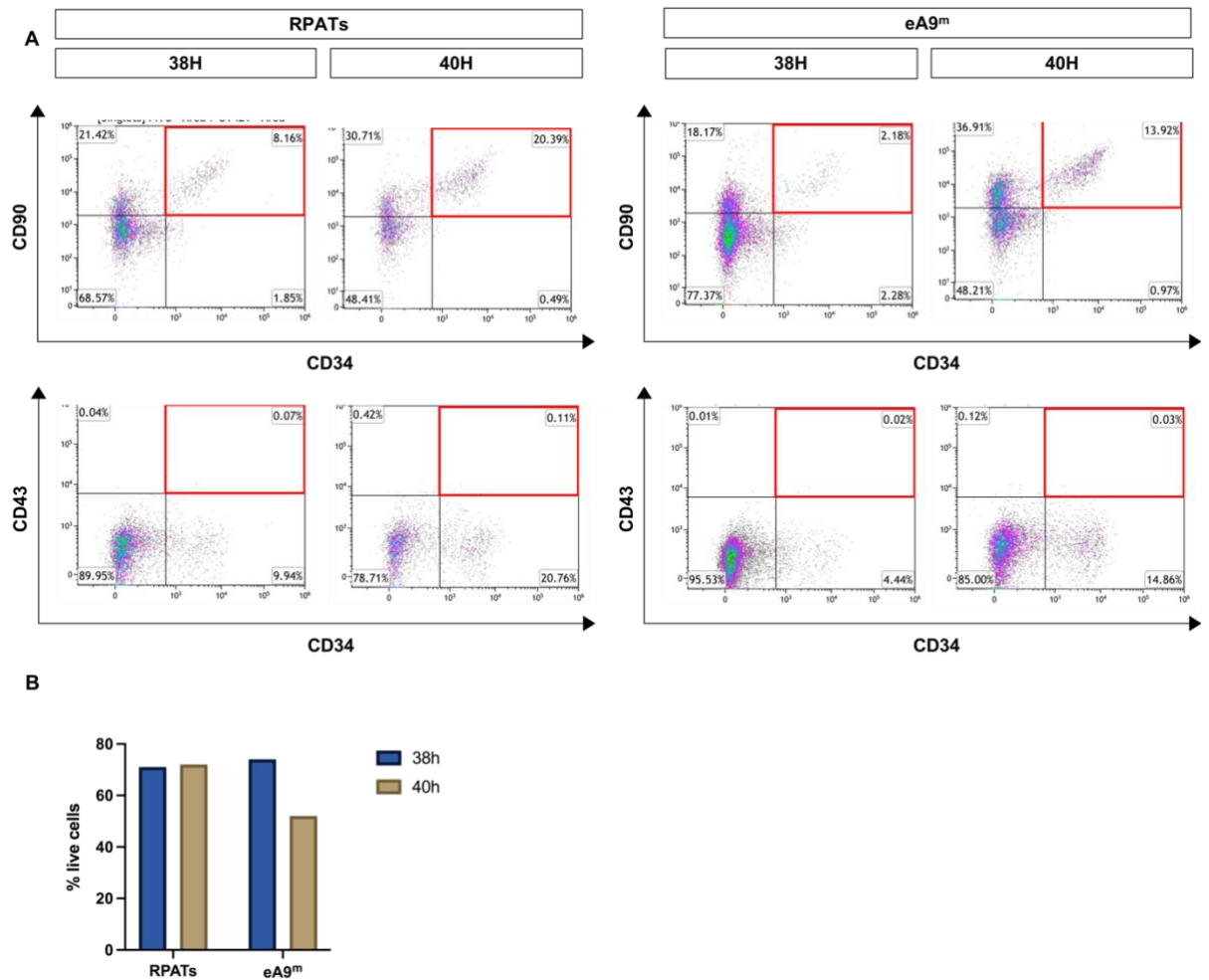


Figure 3.11 Comparative analysis of the effect of 38h and 40h SB/CHIR treatment on surface marker co-expression and viability in day 7 EBs.

A. Dot plots of double positive populations of haematopoietic markers in from day 7 RPATs and eA9^m (red boxes). **B.** Histogram plots show viability of day 7 EBs from both cell lines after addition of SB/CHIR at 38 or 40H post seeding. Background threshold was identified based on unstained samples. Viability was determined using Zombie NIR staining. (n=1).

3.4.2 Induction of mesoderm at 38h hinders HSPCs production

The effect of 38h or 40h SB/CHIR treatment of EBs on derivation of day 14 and day 18 suspension cells was subsequently examined. Both RPATs and eA9^m 38h-treated EBs produced low quantities of suspension cells on day 14 and day 18. Conversely, 40h-treated EBs derived from both cell lines produced many small, spherical, clustered suspension cells, characteristic of HSPCs, on both day 14 and day 18 (Figure 3.12A). For instance, $1.8 \pm 0.5 \times 10^5$ cells/mL and $9.8 \pm 0.2 \times 10^4$ were collected from RPATs differentiation (n=1) on day 14 and day 18, respectively. In eA9^m differentiations, on average (n=3), $1.9 \pm 0.7 \times 10^5$ cells/mL and $4.5 \pm 2.6 \times 10^5$ cells/mL were collected from day 14 and day 18, respectively.

The numbers of HSPCs produced from both differentiation protocols tested is shown in Table 3.3. Due to insufficient production of HSPCs from 38h-treated EBs, no further analysis was done on these cells. CFU assay confirmed haematopoietic activity of the HSPCs collected from 40h-treated EBs as they formed, GEMM and CFU-E colonies, after 9 days in MethoCult™ (Figure 3.12B).

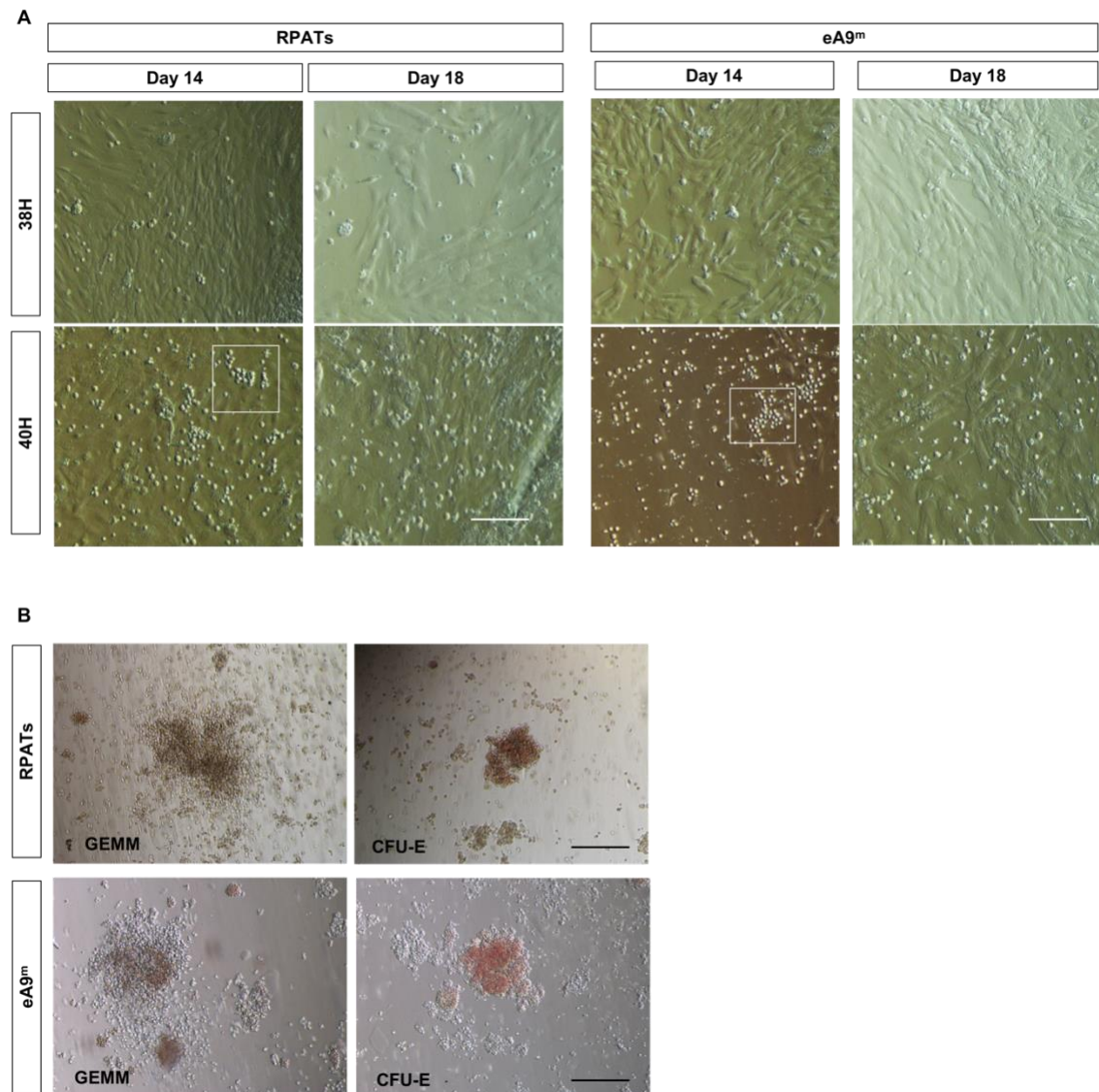


Figure 3.12 Comparative analysis of the effect of SB/CHIR treatment timing on generation and colony formation of day 14 and day 18 suspension cells.

A. Phase contrast images of suspension cells derived from 38h- or 40h- SB/CHIR treated EBs. Scale bar = 200 μ m. **B.** Images of haematopoietic colonies from suspension cells derived from 40h SB/CHIR treated EBs after 9 days in MethoCult™. (n=1). BFU; blast-forming unit, G; Granulocyte, M; Macrophage, E; Erythroid, MM; monocyte megakaryocyte.

Table 3.3 Number of HSPCs derived from RPATs and eA9^m

Cell line	Number of HSPCs (cells/mL)					
	STEMdiff™ kit		Spin EB differentiation			
	Day 12	Day 14	38h SB/CHIR		40h SB/CHIR	
			Day 14	Day 18	Day 14	Day 18
RPAT	-	-	-	-	$1.8 \pm 0.5 \times 10^5$	$9.8 \pm 0.2 \times 10^4$
eA9 ^m	$6.9 \pm 2 \times 10^4$	$5.5 \pm 1 \times 10^4$	-	-	$1.9 \pm 0.7 \times 10^5$	$4.5 \pm 2.6 \times 10^5$

3.4.3 Increased mesoderm induction enhances HSPC production

Flow cytometry analysis of surface marker expression (CD34, CD43, CD90 or CD38) was next applied to further assess the identity of the suspension cells harvested on day 14 and day 18 of the 40h-treated EB differentiations. The same background threshold strategy using isotype controls shown in Figure 3.7 was used here. Overall, cells possessed a CD34⁺CD43⁺CD90⁺CD38⁻ phenotype on both days, resembling the HSPCs expression profile (Figure 3.13A). RPATs showed increased numbers of CD43⁺ cells on both days, whereas eA9^m showed similar numbers to RPATs on day 18 only. In eA9^m, the number of CD34⁺ and CD43⁺ cells was higher on day 18 than day 14. RPATs showed similar numbers of cells expressing these haematopoietic markers on both days. Notably, the number of haematopoietic CD43⁺ eA9^m cells was doubled on day 18 (Figure 3.13A).

A higher proportion of haematopoietic progenitors (CD34⁺CD43⁺) was found in day 18 than day 14, in both cell lines (Figure 3.13B). In RPATs, 10% and ~56% of cells exhibited co-expression of CD34/CD43 on day 14 and day 18, respectively. Similarly, eA9^m cells co-expressed CD34/CD43 at almost 2-fold more in day 18 ($42 \pm 4\%$) compared to day 14 ($28 \pm 1\%$) cultures. Gain of CD43 confirmed that cells lost haemato-vascular phenotype (CD34⁺CD90⁺CD43⁻) and formed a haematopoietic-committed phenotype (CD34⁺CD90⁺CD43⁺) was feasible on both days. A similar variation was observed in the CD90⁺CD38⁻ fraction, wherein more cells possessed this phenotype on day 18 compared to day 14. On day 14, the RPATs fraction was ~38% and the eA9^m fraction was $53 \pm 2\%$. On day 18, the proportion of cells expressing CD90 and lacking CD38 increased to > 70% in both cell lines (Figure 3.13B). This indicates that during the differentiation, cells acquired the HSPCs phenotype gradually. In both cell lines, viability was higher on day 18 (~80%) than day 14 (~40-50%) (Figure 3.13C).

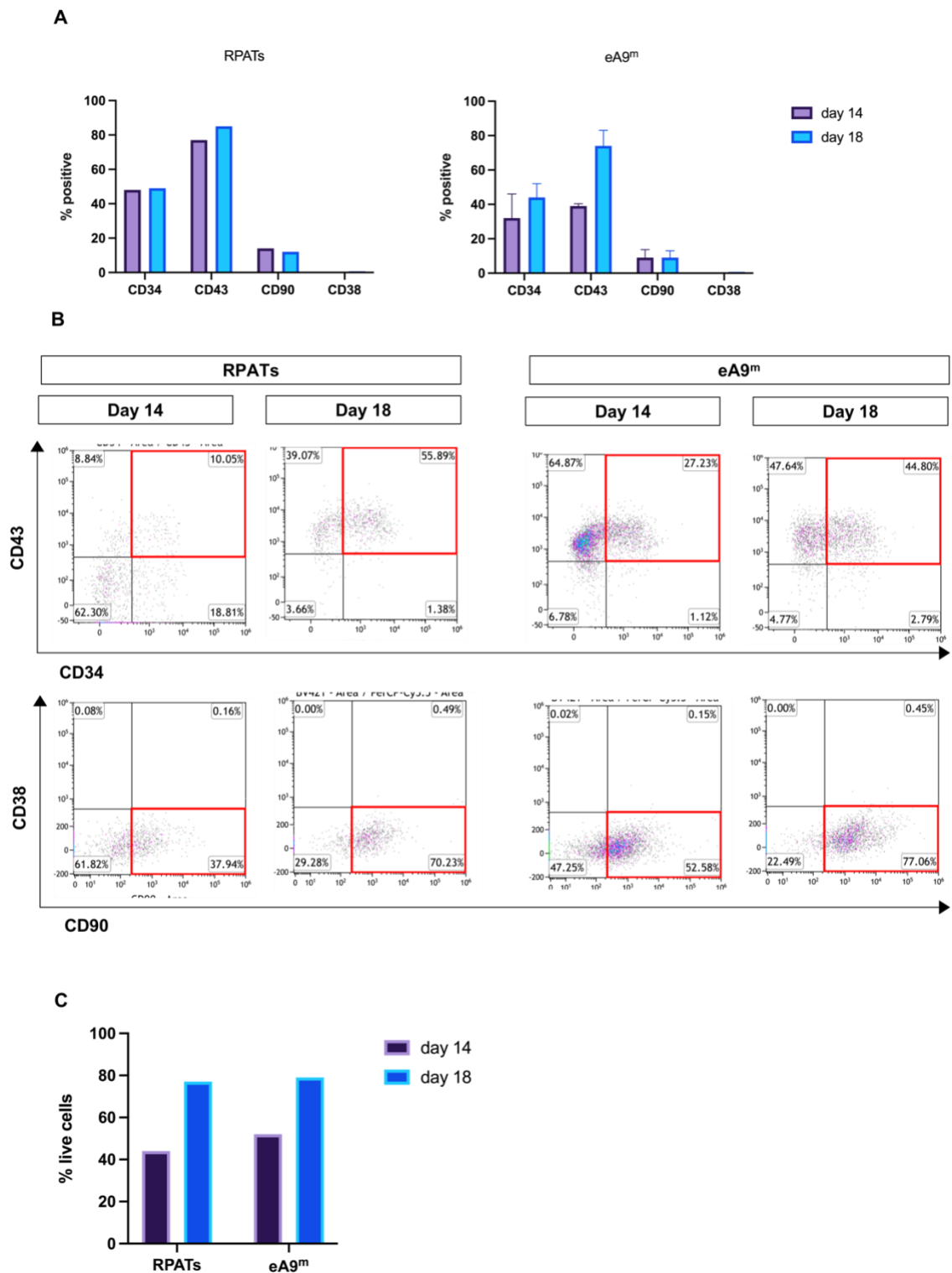


Figure 3.13 Analysis of HSPCs characterisation and viability derived from 40h-treated EBs.

A. Bar charts showing percentage of suspension cells, collected on day 14 and day 18 of the spin EB differentiation from RPATs (n=1) and eA9^m (n=3), expressing haematopoietic markers using flow cytometry analysis. **B.** Representative dot plots marking haematopoietic committed fraction (red boxes) from both cell lines on day 14 and day 18. **C.** Bar graphs showing viability of suspension cells identified using Zombie NIR staining. Results were gated using unstained controls (n=1).

3.5 Summary of results

Taken together, HSPCs possessing multipotential, colony-forming ability were successfully derived from RPAT-based iPSCs using both the STEMdiff™ kit and spin EB protocols. Single cell passaging and low density seeding in the presence of RC improved monolayer-based iPSCs haematopoietic differentiation using the STEMdiff™ kit. RC enabled maximum cell recovery after single cell passaging. Extending the STEMdiff™ kit culture time to 14 days indicated that an increased proportion of cells could still undergo HE specification and ultimately acquire haematopoietic fate, albeit with compromised viability. The CD34/CD43 profiling suggested that cells are shifted towards a haematopoietic profile, by gaining CD34 expression first (similar to HE cells) followed by CD43 expression which was enhanced with extended culture. The decrease in CD34+CD45+ cells could be resulting from stress-related factors, such as contact-inhibition from over confluency in cultures.

Despite being a commercial product, the STEMdiff™ kit generated low quantity of HSPCs using either the manufacturer's protocol or the approaches tested. The scalability of the process was hindered, as the components and concentrations of differentiation media was proprietary preventing the generation of in-house alternatives. These aspects were crucial for completion of other aims of the project. Moreover, the time and cost associated compared to the yield of HSPCs produced made the process inefficient. Thus, the spin EB differentiation method was applied. Compared to the STEMdiff™ kit, higher numbers of HSPCs were generated in all differentiation conditions, none of which were unsuccessful, unless due to technical issues. Mesoderm induction and patterning was induced at either 38h or 40h after initiation of spin EB differentiation to further examine the effect on the process. Although the haemato-vascular mesodermal population of cells did not show a major difference in day 7 EBs, SB/CHIR treatment of EBs at 40h instead of 38h was found to be more efficient in HSPCs production.

Therefore, the treatment of EBs with SB/CHIR at 40h was chosen for the remainder of this project on the premise of anticipated higher HSPC counts. Overall, the protocol was successful in generating multipotent HSPCs expressing CD34+CD43+CD90+CD38- markers with ability to form CFU-GEMM, GFU-G,

CFU-M and BFU-E colonies in methylcellulose. Consistent generation of HSPCs from eA9^m iPSCs was now established to create a platform for investigation of HOXA9 in eA9^m-derived haematopoiesis. As such, the detailed generation and further analysis of eA9^m-derived HSPCs is discussed in Chapter 4.

Chapter 4 Generation of a HOXA9-mScarlet reporter cell line

4.1 Brief background

As discussed in Chapter 1, HOXA9 plays a central role in haematopoiesis, embryogenesis and MLL-rearranged leukaemia initiation and progression. The primary aim of this chapter was to generate an iPSC-HOXA9 fluorescence reporter cell line capable of differentiating to HSPCs. With advances in genome editing techniques, as previously discussed, the endogenous *HOXA9* locus was targeted using CRISPR/Cas9 technology to generate a footprint-free knock-in of the red fluorescent protein, mScarlet-H (2.7).

In leukaemia, identifying the cell-of-origin for leukaemia initiation may provide opportunities for more specific and less toxic therapies. The use of reporter cell lines driven by expression of key oncogenic targets (such as HOXA9) may provide a tempo-spatial map of leukaemia and other cancer initiation. Hence, the proposed reporter cell line will be a useful tool for monitoring of *HOXA9* expression and protein-DNA binding, giving further insights into its molecular function and the ability to model diseases *in vitro*.

4.2 Gene targeting strategy of the endogenous HOXA9 locus in iPSCs

A schematic of the overall targeting strategy, after integration and excision of the PB cassette is summarised in Figure 4.1. The PB transposon system includes two sequential steps. First, the targeting vector is co-transfected with gRNA and Cas9, to promote genetic cleavage and homology-directed repair insertion into the endogenous *HOXA9* locus. To incorporate mScarlet-H (696 bp) in-frame and downstream of exon 2 of the *HOXA9* locus, the stop codon was replaced with the self-cleaving peptide T2A and mScarlet-H. T2A self-cleavage results in positioning a short peptide tag (18 amino acid) in frame with *HOXA9*.

Due to lack of adequate HOXA9 antibodies, informative molecular assays such as ChIP and protein pull-down assays may in the future be feasible using the reporter-tagged HOXA9.

Targeting was achieved using a gRNA and proximal PAM site motif (GGG) complimentary to this region of the *HOXA* locus (Figure 4.1A). The PB recombination sites flank the positive-negative drug selection cassette (puromycin and delta TK), all of which are located downstream to T2A and mScarlet-H (Figure 4.1B). This cassette (3939 bp) was then flanked on the left and right with *HOXA9* locus homology arms (1000 bp and 996 bp, respectively). The left homology arm (LHA) spans part of intron 1 and exon 2, and the right homology arm (RHA) is identical to a part of the 3' untranslated region (UTR). Figure 4.1B represents the *HOXA9* locus after integration of the cassette.

Positive puromycin selection identified RPATs clones that incorporated the cassette, thus possess resistance and survived. Out of these resistant clones, one clone (Clone 2 plus PB; C2+PB) was selected and expanded with former research colleague, Ben Johnson. This parental clone (C2+PB) was subsequently transfected with a transposase-expressing plasmid that induced recombination and deletion of the PB cassette at the sites indicated (Figure 4.1B). At the site of recombination, an endogenous quadra-nucleotide palindrome sequence, TTAA (PB-T2), is necessary for PB cassette excision. The *HOXA9* locus after excision of the resistance cassette, with PB-T2 remaining from the cassette and T2A-mScarlet downstream to *HOXA9*, is represented in Figure 4.1B. Following excision, negative antibiotic selection was achieved using ganciclovir, which kills cells expressing delta TK. Thus, 38 colonies, that survived excision of the antibiotic cassette were picked and expanded. The targeting vector used (pHOXA9-T2A-mScarlet) was generated by Genewiz (Figure 4.2A). The plasmid vector was sequenced to confirm all key elements are present and align with the plasmid sequence map (Figure 4.2B).

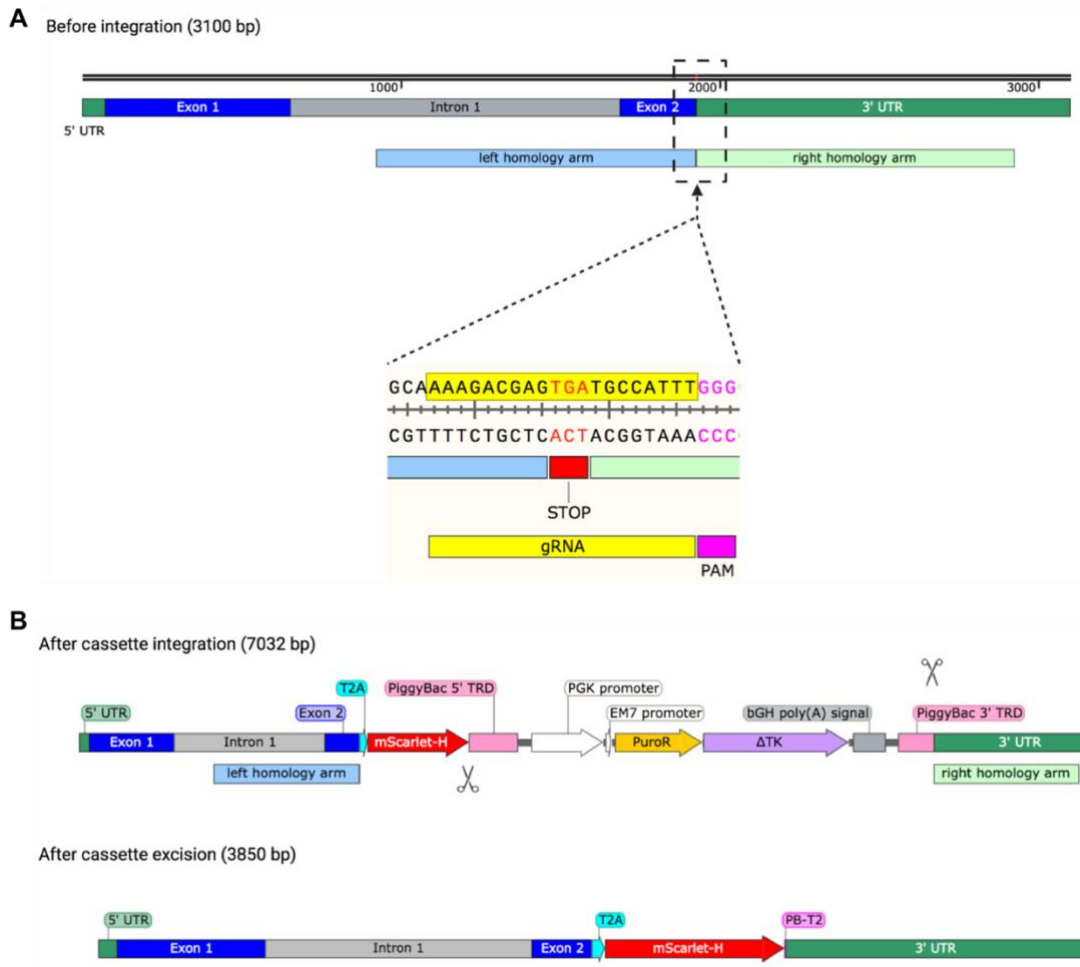


Figure 4.1 Strategy for the footprint-free targeting of the endogenous HOXA9 locus.

A. A schematic of the endogenous HOXA9 and the integration site (dotted black arrow) flanked by left and right arms homologous to exon 2, intron 1 and the 3' UTR of the HOXA9 locus, respectively. The magnified integration site (dotted square) shows location of the gRNA sequence (highlighted in yellow) and its respective PAM site (pink). The homologous arms flank the stop codon (red), which is present after exon 2. **B.** Following integration the stop codon is replaced by the cassette including PiggyBac recombination sites indicated using scissors, leaving a TTAA sequence (PB-T2) after excision of the cassette. After excision, the T2A peptide, mScarlet-H and PB-T2 sequence remain downstream to HOXA9. PAM, protospacer adjacent motif; UTR, untranslated region.

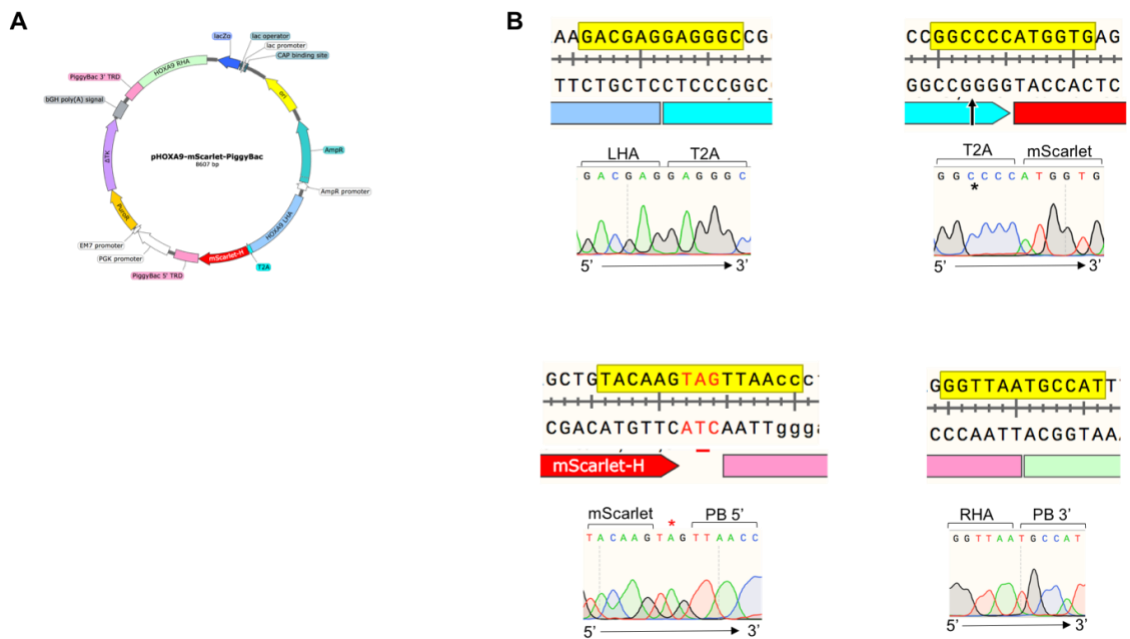


Figure 4.2 CRISPR/Cas9 targeting plasmid map.

A. Schematic of the targeting vector that contains a dual drug selection cassette (Puro- Δ TK) driven by EM7 and PGK promoters, respectively, flanked by PiggyBac TRD recombination sites and the HOXA9 homologous arms. mScarlet-H is downstream to HOXA9 LHA and separated by the T2A peptide. **B.** The targeting plasmid was generated by Genewiz and verified by Sanger sequencing. Chromatograms represent presence of the vector integration elements in the expected order. *T2A cleavage site; *mScarlet stop codon (TAG) labelled in red. TRD, terminal repeat domain; LHA, left homology arm; RHA, right homology arm; PB, PiggyBac. Plasmid map generated using Snapgene.

4.3 Molecular validation of HOXA9 targeting

After selection and expansion of individual clones, integration of the in-frame targeting of the reporter elements plus presence/absence of the PB cassette was validated. C2+PB genomic DNA was amplified using primers (A9.int F & Scar R), flanking the 5' integration site. These primers amplified part of intron 1, exon 2 and part of mScarlet-H (expected size 1752 bp) (Figure 4.3A). All primer sequences used in this section can be found in Table 2.7. A band of the expected size was observed in C2+PB gDNA and was absent in the negative control (RPATs) gDNA (Figure 4.3A). DNA from a Scarlet-expressing clone (iA9), previously generated by EC, acted as a positive control for the reporter. Primers Scar F and Scar R were used to confirm the presence of mScarlet-H in C2+PB and iA9, both showing a band of expected size (140 bp) (Figure 4.3B). No amplification of this band was observed in the negative control (RPATs) (Figure 4.3B). This confirms that the *HOXA9* locus was targeted at the intended location and mScarlet-H was present in the clone.

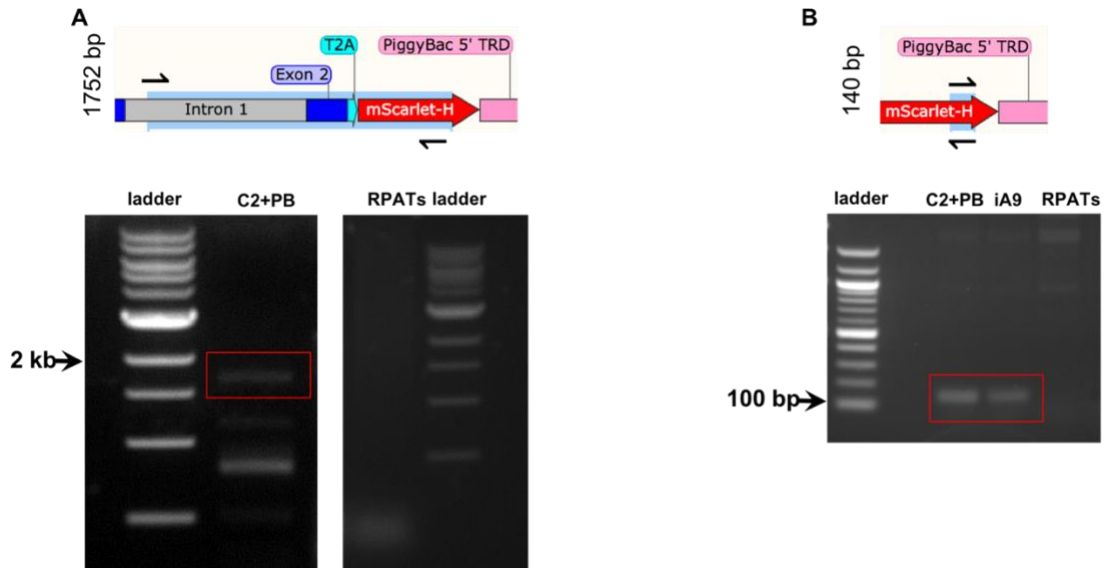


Figure 4.3 Validation of 5' integration and presence of mScarlet-H in HOXA9 locus.

A. Schematic indicates primer binding to amplify the region around the 5' integration site by PCR (upper panel), resulting in the expected 1752 bp band confirmed by the gel electrophoresis image (lower panel). **B.** Schematic of primer binding to amplify the region around mScarlet-H (upper panel), resulting in the expected 140 bp fragment, confirmed by the gel electrophoresis image (lower panel). Positive control (iA9); negative control (RPATs).

After the transposase treatment, DNA from the thirty-eight clones generated was first pooled and screened for presence of the excision, along with DNA from parental C2+PB. DNA from the targeting plasmid vector was used as a positive control. The primers used here (-PB F2 and -PB R2) bind in regions outside the PB cassette. Correct excision of the PB cassette results in the amplification of a 159 bp region instead of a 3440 bp as demonstrated in Figure 4.4. This amplification also verifies the 3' integration region as the reverse primer was designed to bind to the HOXA9 3' UTR. For classification, C2+PB DNA is denoted as “pre” and the pooled DNA from the 38 excised clones is denoted as “post” excision (Figure 4.4). Plasmid DNA showed a clear band larger than 3000 bp, similar to DNA from C2+PB. A faint band of similar size was visible in the pooled post-excision sample. This indicates that C2+PB possesses the full PB cassette, which may also be retained in the pooled post-excision sample. Unlike plasmid DNA, “pre” and “pooled” DNA samples had an additional band smaller than the expected size, potentially due to unspecific binding as a result of genomic DNA

complexity and size compared to plasmid DNA. Another small band, around 159 bp, was seen in the pooled post-excision sample, as expected. To further investigate the ~3440 bp band observed in the pooled sample (Figure 4.4), the pooled 'post' DNA sample was separated again on another agarose gel, alongside DNA amplification samples from all individual clones picked following excision (Figure 4.5). These clones were denoted numerically e.g. clone 10 (C10). After screening the DNA from the excised clones separately, the small 159 bp band was seen in most 'post' clones, validating excision of the PB cassette. The large band seen in the pooled 'post' sample in Figure 4.4 was not present in this gel (Figure 4.5), indicating that it could have been due to a technical issue. Two clones with clear bands at ~159 bp, C25 and C33, were excised from the gel and validated by Sanger sequencing Figure 4.6. For the purpose of this project, C25 was selected and expanded as it produced a single clear band of the expected size following PCR amplification and gel electrophoresis (Figure 4.5). This HOXA9-mScarlet reporter iPSCs cell line clone (eA9^m) was then used for all further downstream analysis.

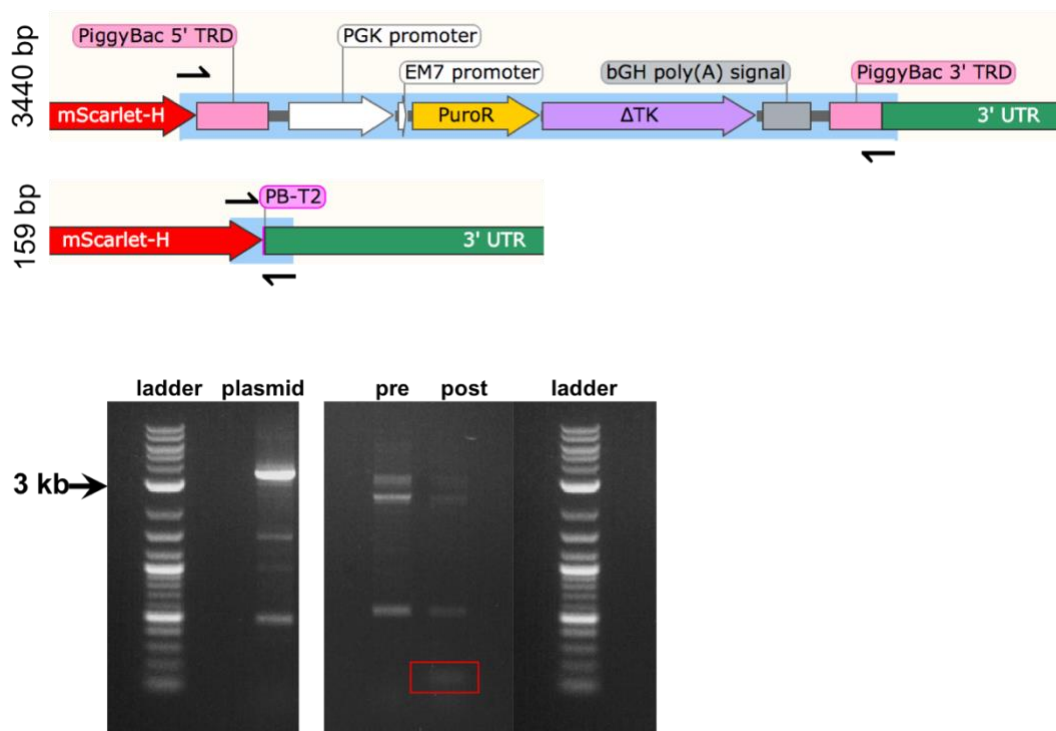


Figure 4.4 Validation of integration and excision of the PB cassette from the HOXA9 locus.

Schematic showing amplified region after cassette integration (3440 bp) and after cassette excision (159 bp). All DNA samples shown here were amplified using the -PB F2 and -PB R2 primers, denoted using black arrows (upper panel). The expected 159 bp band (red box) was confirmed in the 'post' sample by the gel

electrophoresis image (lower panel). pHOXA9-mScarlet-PiggBac; plasmid, C2+PB; pre, pooled sample; post.

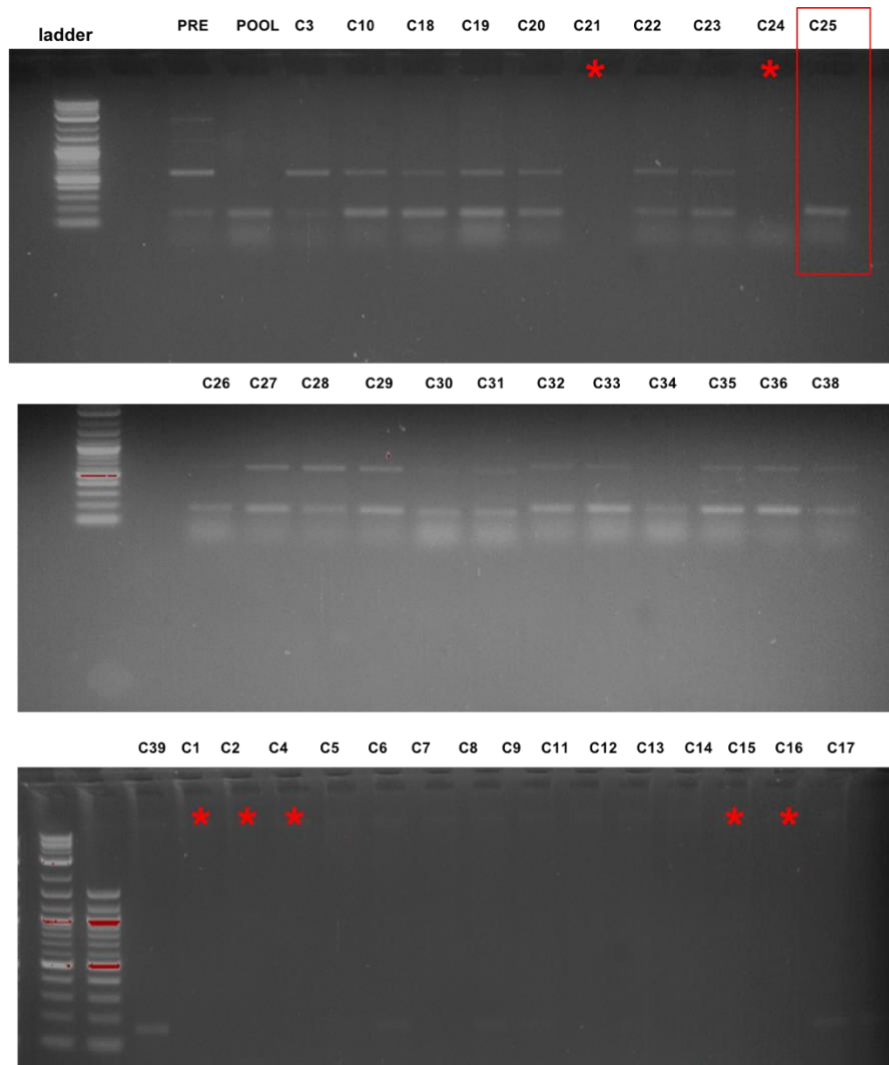


Figure 4.5 Validation of PB cassette excision after transposase treatment.

Images of amplification of the region flanking the PB cassette excision site (~159 bp) from genomic DNA of selected clones (C1-39) separated using gel electrophoresis. C2+PB (pre) and a pooled sample of all post-excision clones (pool) were also screened. Red asterisks are representative of lanes with no bands observed. One of the clones that showed a clear strong band was expanded (red box). Primers used to amplify all samples were -PB F2 and -PB R2.

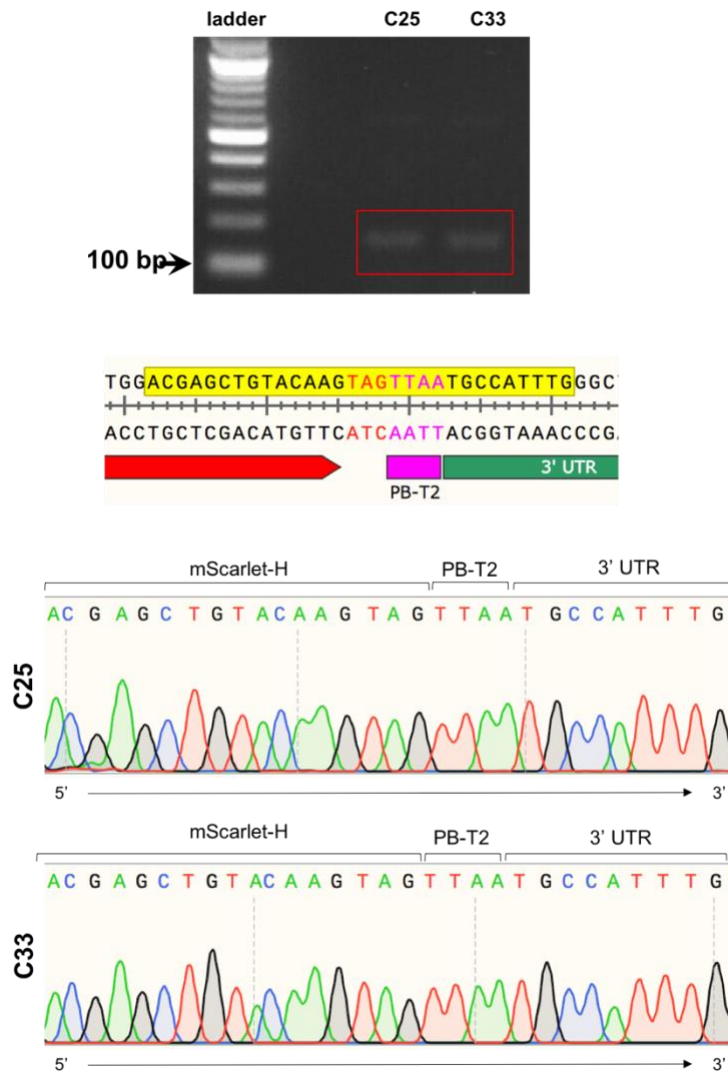


Figure 4.6 Validation of post excision clones by Sanger sequencing

Image of amplification of the PB cassette excision site (~159 bp) from genomic DNA of two post-excision clones, C25 and C33, separated using gel electrophoresis (upper panel). A schematic of a proportion of the expected PB cassette excision site sequence is shown. DNA bands from the gel shown were extracted and sequenced. Chromatograms represent the same sequence, highlighted in yellow, present in C25 and C33, confirming PB cassette excision (lower panel). Primers used were -PB F2 and -PB R2.

The editing efficiencies reported using this transposase approach range from 8%-93% (Kondrashov et al., 2018). We hypothesized that excision of the PB cassette was not wholly efficient, thus eA9^m may be heterozygous for deletion of the PB cassette. To validate whether eA9^m retained elements of the PB cassette, we designed further specific primer pairs (Table 2.7) that amplify short amplicons, shorter than 500 bp, of every element in the PB cassette (Figure 4.7A). The targeting plasmid was used as a positive control. The expected bands that were identical in eA9^m and the targeting plasmid (Figure 4.7B). These amplicons were

sequenced and chromatograms aligned with their respective sequences from the plasmid map (Figure 4.7C). This verified that albeit correctly targeted (Figure 4.6), eA9^m also retained all elements present in the PB cassette.

Together these data suggest that eA9^m may be heterozygous for the excision of the PB cassette, with one allele retaining the full PB cassette, and the second allele with only HOXA9-T2A-mScarlet. Alternatively, eA9^m could be a mixed clone, with some cells being “pre-excision” and others being “post-excision”. To examine these possibilities, a puromycin kill curve (up to 1 µg/mL) was conducted on eA9^m and RPATs (Figure 4.8). This demonstrated that both cell lines were sensitive to puromycin at these concentrations, particularly at the concentration used for clone selection (0.2 µg/mL). These findings indicate that eA9^m are not puromycin resistant, suggesting that the initial targeting was heterozygous and eA9^m retained a wildtype *HOXA9* allele. To confirm whether a wildtype allele is present, primers (WT fwd and WT rev) that amplify a region of *HOXA9* (spanning intron 1, exon 2 and the 3' UTR) were used, and bands of the expected size (~1210 bp) obtained and sequenced for validation (Figure 4.9A). RPATs were used as a positive control for the wild type locus, and showed a similar band to eA9^m. Sequencing results from RPATs and eA9^m were identical (Figure 4.9B). Aligning the chromatograms against the plasmid map confirmed that eA9^m is heterozygous for the gene edited *HOXA9* allele.

Together the validation PCR and sequencing indicates the presence of three forms of the *HOXA9* locus namely: wild type; HOXA9-T2A-Scarlet; and HOXA9-T2A-Scarlet-PB cassette. Monoallelic targeting by CRISPR/Cas9 is not unexpected and may in fact be preferential functionally as one allele of *HOXA9* remains intact. Retention of the PB cassette in the 3' UTR of *HOXA9* may have no significant impact on HOXA9 function beyond RNA stability. Therefore, eA9^m remained a viable clone to assess *HOXA9* expression during iPSC differentiation to HSPCs.

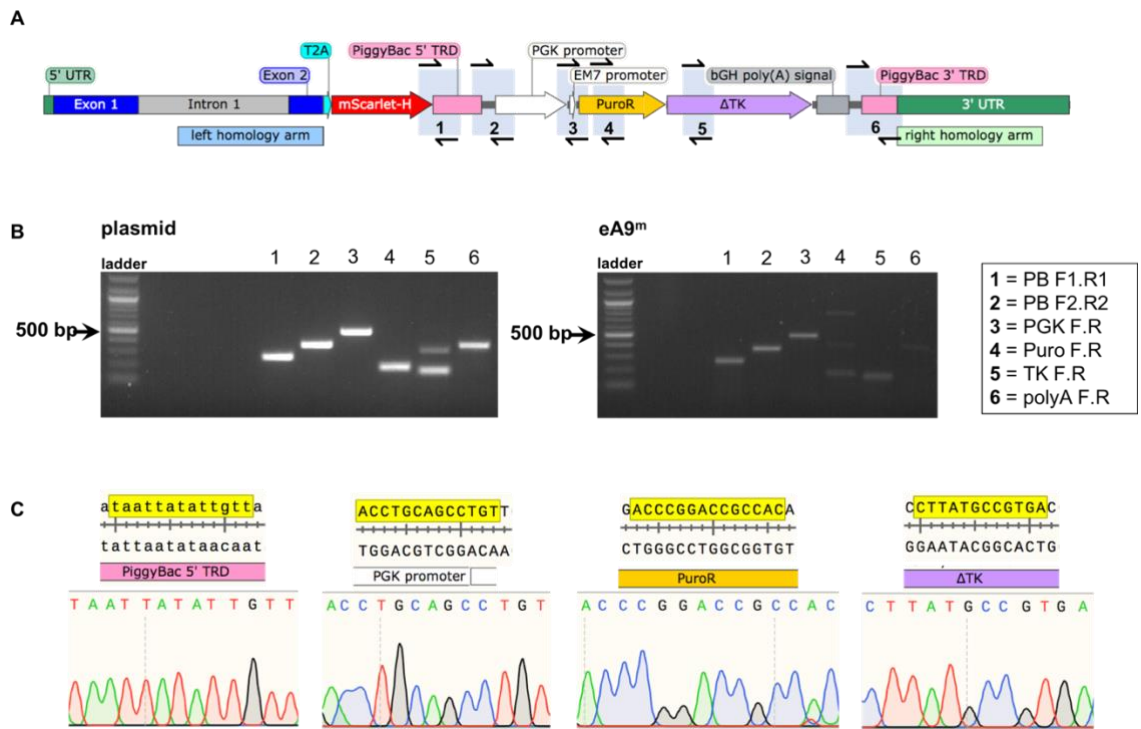


Figure 4.7 PiggyBac cassette elements are retained post-excision in eA9^m cells.

A. Schematic of the *HOXA9* locus, with full integration of the cassette is shown. PCR amplification of the six short regions indicated in grey boxes, and the corresponding primer pairs used are labelled 1-6 (Table 2.7). **B.** Images of PCR amplification products in agarose gels; targeting plasmid (pHOXA9-mScarlet-PiggyBac) used as positive control, showing all the expected bands, similar to eA9^m. **C.** DNA bands from **B** were extracted and sequenced. Chromatograms show representative regions of key elements in the cassette, and their corresponding sequence (highlighted in yellow).

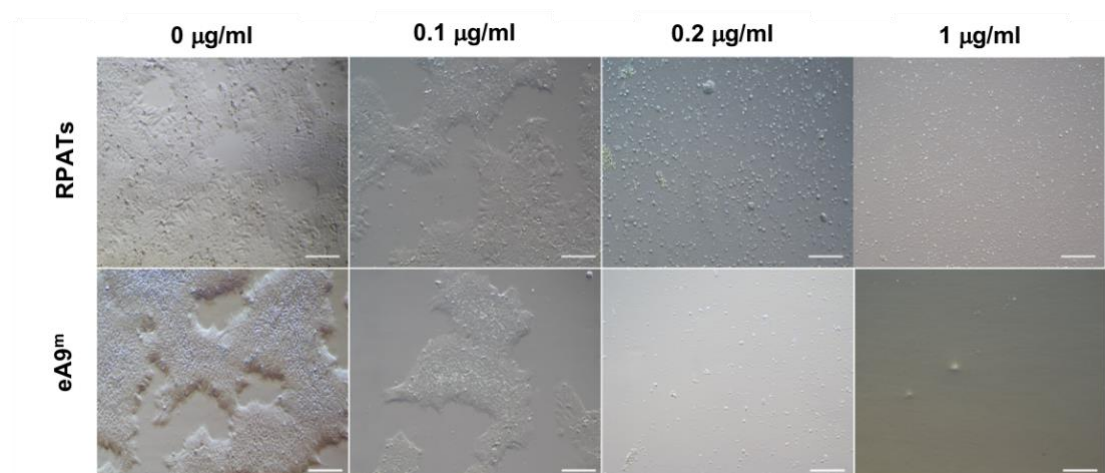


Figure 4.8 eA9^m are not resistant to puromycin.

Representative images (n=3) of eA9^m cells and RPATs controls after 48 hours in culture with puromycin at 0, 0.1, 0.2 and 1 µg/mL. Scale bar = 100 µm.

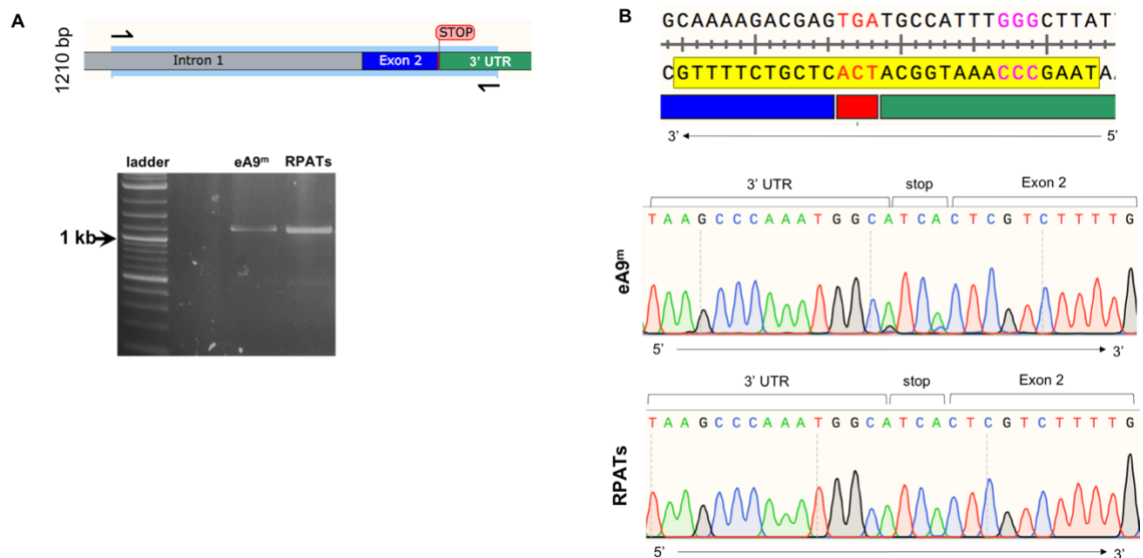


Figure 4.9 eA9^m retain a copy of the wildtype HOXA9 allele.

A. Schematic of the *HOXA9* locus. PCR amplification of the intron, non-targeted exon 2 and 3'untranslated region is highlighted in blue (upper panel). Image of PCR amplification products in agarose gels showing ~1210 bp products in both RPATs and eA9^m cells (lower panel). **B.** Schematic of the expected sequence of the wild type amplification product from A (upper panel). DNA bands from **A** were extracted and sequenced. Stop codon highlighted in red, PAM sequence highlighted in pink. Chromatograms confirm retention of the *HOXA9* stop codon in reverse strands of DNA obtained from both RPATs and eA9^m cells.

4.4 Functional validation through HOXA9 upregulation

After generation and molecular validation of the reporter cell line validation of functional upregulation of HOXA9 was done in eA9^m cells. If the clone was functional then upregulation of HOXA9 would be detected by increased expression of mScarlet-H. In this section, HOXA9 was upregulated using several approaches.

4.4.1 Upregulation of HOXA9 using Wnt pathway-related molecules

Firstly, the effect of supplementing SB and CHIR or RA in eA9^m normal growth media was examined. As discussed previously HOXA9 is not expressed in resting iPSCs (1.1). The expression of HOXA9 and mScarlet was evaluated after 24h and 48h of stimulation. Combined stimulation with SB, CHIR and RA was also tested to examine if a more robust upregulation of HOXA9 and mScarlet-H could be achieved in eA9^m.

Routinely, iPSCs are only cultured on Matrigel-coated tissue culture plasticware. To enable us to treat and image cells using confocal imaging, optimised seeding

and attachment of iPSCs to microscope coverslips was required. Prior to seeding, coverslips were coated with either Matrigel or fibronectin to test which formulation would aid cell attachment. After 24h, both cell lines showed regular morphology of iPSCs on both substrates, and attached to the coverslips (Figure 4.10).

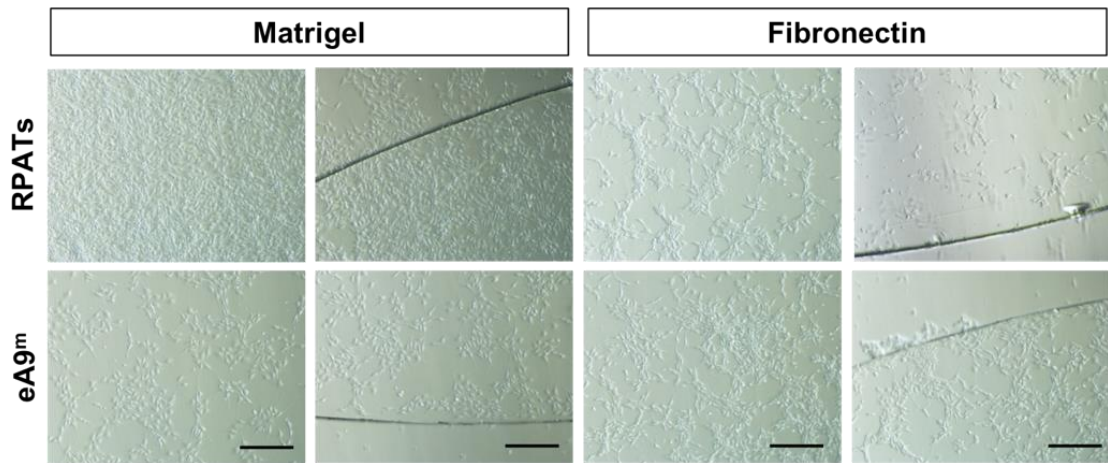


Figure 4.10 iPSC seeding and attachment on coverslips.

Representative images (n=3) of RPATs and eA9^m cells attached to coverslips coated with Matrigel or fibronectin (20 µg/ml), 24 hours after passaging. Scale bar = 200 µm. Attachment of cells at the centre of coverslips (left panels) and the edges (right panel) are demonstrated.

Both RPATs and eA9^m cells grew normally and covered the surface of Matrigel-coated coverslips. However, cells attached to fibronectin demonstrated a less confluent, clumped morphology indicating cell stasis or death. For this reason, Matrigel was chosen as coverslip substrate for further studies. Following 48h of seeding, iPSCs were treated with either SB and CHIR, RA alone, or all three in combination. Expression of *HOXA9* and *mScarlet-H* was analysed by qPCR. All samples collected after 24 hours showed no change in *HOXA9* or *mScarlet-H* expression. Although treatment with SB and CHIR was insufficient for *HOXA9* upregulation, an increase in expression was observed in cells that were treated with RA alone or as part of the combination after 48 hours (Figure 4.11A). Notably, a minor increase of ~4 fold was observed in *mScarlet-H* expression, compared to ~23 fold in *HOXA9*. The combination treatment was then repeated and samples taken for confocal imaging. RPATs were used as a negative control for mScarlet-H, to account for background fluorescence. eA9^m cells showed red fluorescence, that was absent in RPATs (Figure 4.11B).

The differential expression in *HOXA9* and *mScarlet-H* is potentially due in part to retention of the wildtype *HOXA9* allele shown in the molecular analysis. mRNA stability of the targeted allele may have also been compromised with retention of the PB cassette within the 3' UTR of *HOXA9*. Nevertheless, this proof-of-principle assay demonstrates that eA9^m cells can still function as a fluorescent reporter line for *HOXA9*.

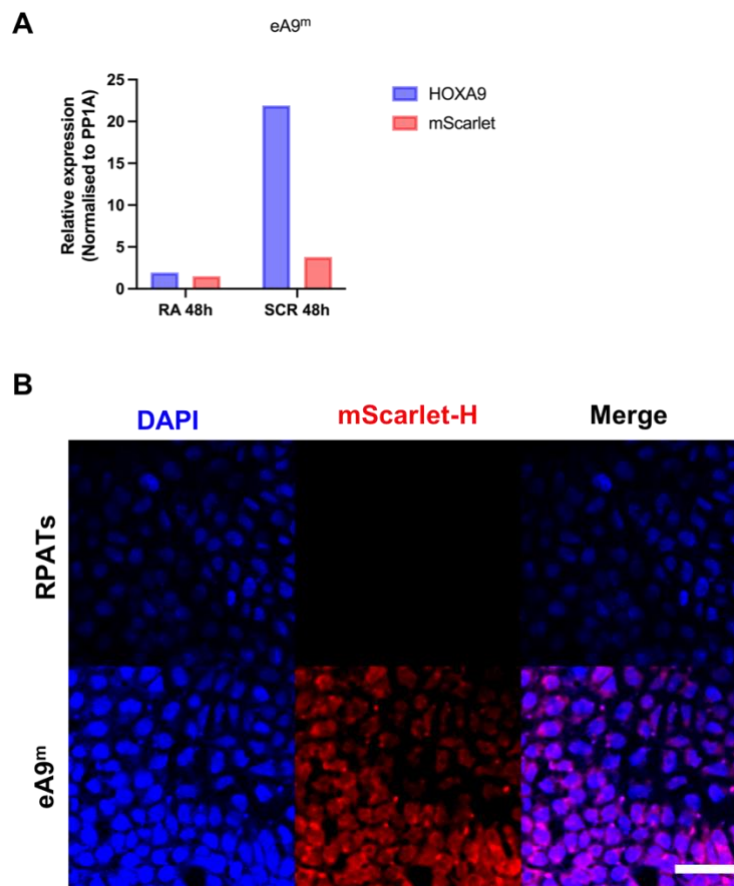


Figure 4.11 eA9^m cells show mScarlet-H fluorescence upon HOXA9 stimulation.

A. A bar chart showing the expression of *HOXA9* and *mScarlet-H* following treatment of eA9^m cells with RA alone or SB/CHIR/RA (SCR) for 48h determined using qPCR (n=1). All results are normalised to PP1A expression, and relative to undifferentiated eA9^m cells. **B.** Confocal images of cells stained with DAPI after treatment with a combination of SB (4 μ M), CHIR (3 μ M) and RA (3 μ M) for 48h. Endogenous mScarlet-H fluorescence was also visible after 48h. RPATs were used as a negative control for mScarlet-H fluorescence. Scale bar= 50 μ m.

4.4.2 Haematopoietic differentiation: HOXA9 vs RUNX1

Since *HOXA9* expression is reported to increase during haematopoiesis, the spin EB haematopoietic differentiation approach was next used to validate the function of eA9^m. The ability of eA9^m iPSCs to differentiate to functional HSPCs was

previously demonstrated (3.3). Therefore, EBs were collected from timepoints (day 4, 7, 14 and 18) of the differentiation, representative of key stages of HSPC formation, and the expression of *HOXA9* and *mScarlet-H* compared (Figure 4.12A). Expression of *HOXA9* was ~300 fold higher on day 4 than undifferentiated eA9^m cells with the greatest difference (2000-fold) observed on day 7. *HOXA9* expression was overall lower on day 14 and day 18, with only ~13 and 8.8 fold-increase over untreated eA9^m iPSCs, respectively (Figure 4.12A). This is consistent with the role of *HOXA9* in haematopoiesis. As observed for the SB/CHIR/RA combined treatment, the increased expression of *mScarlet-H* did not follow the degree of expression observed for *HOXA9* (e.g. only 2.5 fold-increase on day 7).

An extended time course study was then done on eA9^m cells, to identify the day of differentiation where *HOXA9* and potentially *mScarlet-H* would be most highly upregulated. A preliminary screen of qPCR expression was used as an indicator of the expression level needed to visualise a reporter line during the differentiation. eA9^m EBs were collected on each day of the differentiation, for the first 13 days, prior to the formation of HSPCs and changes in expression of *HOXA9*, *RUNX1* and *GATA2* was analysed (Figure 4.12B). Compared to *RUNX1* and *GATA2*, *HOXA9* is upregulated to much higher levels during the differentiation. We also confirmed that the largest increase in *HOXA9* expression occurs on day 7 of the differentiation, at the hemato-vascular mesodermal stage. *HOXA9* upregulation starts on day 4 and is downregulated after day 7. In contrast, *RUNX1* expression gradually increases and is highest after day 9 of the EB differentiation, as cells form HE and progress through EHT to form HSPCs. *GATA2* expression is similar to *HOXA9*, as it reaches the highest expression at day 6. It is expressed at early stages and then starts to decrease to almost no expression at all on day 8 onwards (Figure 4.12B).

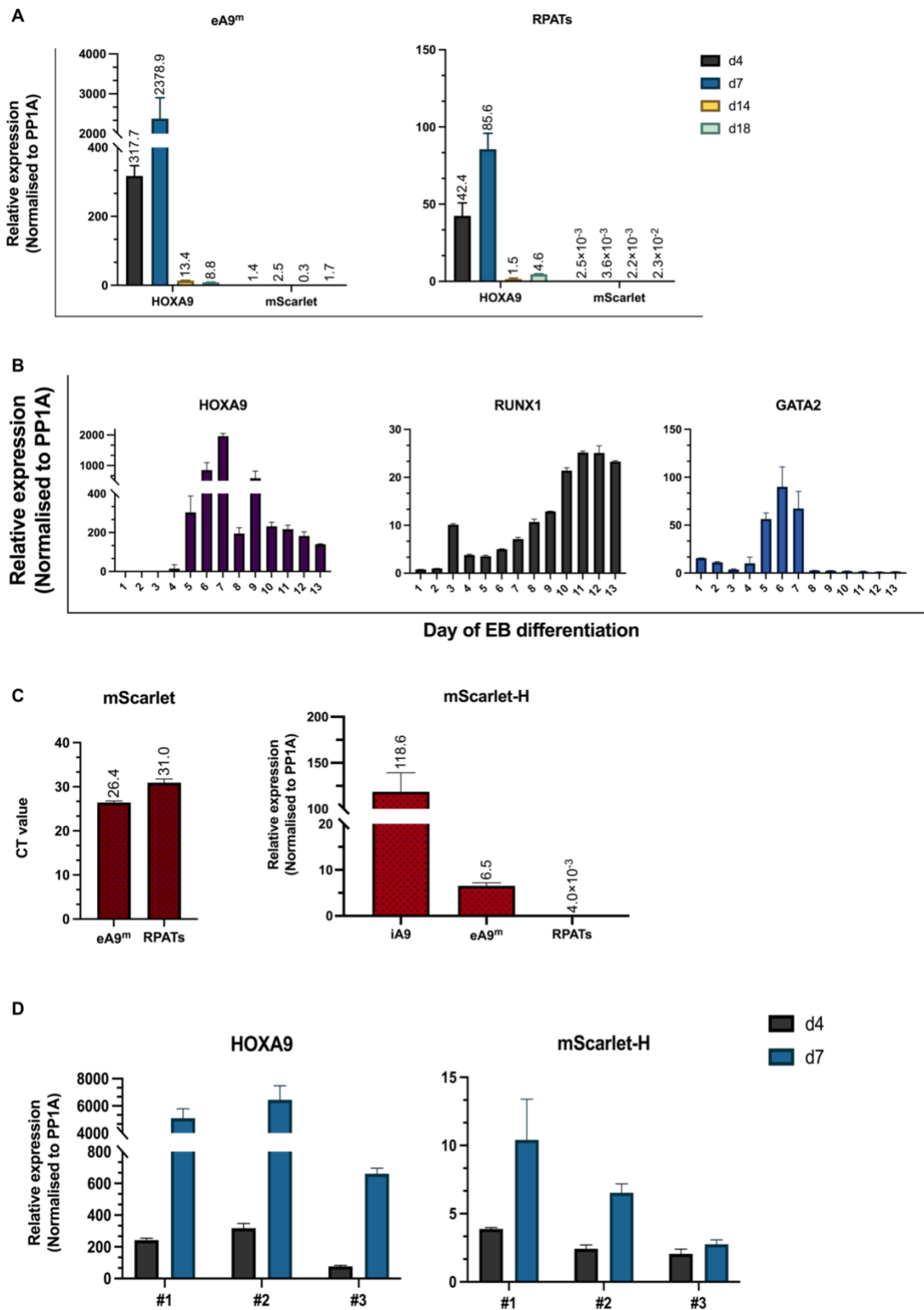


Figure 4.12 Differential gene expression of eA9^m and RPATs during EB differentiation.

A. Representative bar chart showing *HOXA9* and *mScarlet-H* expression on day 4, day 7, day 14 and day 18 of the spin EB differentiation, identified using qPCR. Primers, named mScarlet, were not able to detect mScarlet expression. **B.** Bar chart showing variation of *HOXA9*, *RUNX1* and *GATA2* expression in eA9^m from day 1-13 of the spin EB differentiation. Results are from three technical repeats

from the same differentiation. **C.** Left panel: bar chart of *mScarlet* CT values indicated issues with mScarlet primer function as shown in **B.** Right panel: Bar chart showing *mScarlet-H* gene expression in iA9, eA9^m and RPATs using another set of primers denoted mScarlet-H. **D.** Bar chart showing expression of *HOXA9* and *mScarlet-H* on day 4 and day 7 of three independent eA9^m differentiations (#1- #3). Results are mean of three technical repeats. All results are normalised to *PP1A* expression, and relative to undifferentiated iPSCs.

Using qPCR, lower *mScarlet* CT values were observed in undifferentiated eA9^m compared to RPATs, despite the expected lack of expression in both cell lines. To test if the lack of *mScarlet* amplification observed by qPCR was due to technical issues with the *mScarlet* primers (denoted mScarlet), a new set of primers were designed (denoted mScarlet-H) and used on the same day 7 cDNA samples from eA9^m and RPATs along with iA9 as a positive control (Figure 4.12A). The new primers showed more measurable expression in iA9, and similarly, although at expected lower values, in eA9^m (Figure 4.12C). Primer sequences are listed in Table 2.3. As expected, RPATs do not have *mScarlet-H* and no expression was observed. After validating the new primers, these were subsequently used for all other further qPCR experiments. *HOXA9* and *mScarlet-H* expression were examined on day 4 and day 7 from three independent EB differentiations, labelled #1- #3, and the same trend from both genes was observed, with cells expressing higher *HOXA9* and *mScarlet-H* on day 7 rather than day 4 (Figure 4.12D).

It is worth noting that between differentiations, the expression of each gene also varies. For instance, the expression of *HOXA9* on day 7 of differentiation #3 was approximately 100 fold lower than the other differentiations. Similarly, differentiation #3 possesses the lowest expression of *HOXA9* on day 4. This reflects the inherent variability in the constituents of EB formation that affects differentiation efficiency. Although *HOXA9* and *mScarlet-H* expression are aligned during eA9^m haematopoietic differentiation, the difference in levels indicate that not all *HOXA9* expression is reported by *mScarlet-H*. This is congruent with the molecular validation of three forms of the edited gene (section **Error! Reference source not found.4.3**).

4.5 MLL::AF9 treatment of eA9^m cells

MLL::AF9 is a known activator of *HOXA9* expression. As a potential goal of the eA9^m model is to generate a tractable leukaemia model, cells were exposed to MLL::AF9 by either nucleofection of MLL::AF9 containing plasmids or by transduction using MLL::AF9 lentiviral particles were applied to eA9^m cells and *HOXA9* and *mScarlet-H* expression assessed.

4.5.1 MLL::AF9 nucleofection of eA9^m iPSCs

eA9^m iPSCs were nucleofected with *MLL::AF9* (p2158, pMA9) or control (pCTRL) plasmid and cell morphology observed after 24 hours (Figure 4.13A). Details of source of plasmids used is in Table 2.2. Each plasmid was nucleofected once (single hit), or twice (double hit) consecutively, to attempt to increase the efficiency of nucleofection. The majority of cells survived a single nucleofection and represented the regular morphology of iPSCs, whereas double hit nucleofections resulted in significant cell death. While GFP expression was observed for the control plasmid (pGFPmax), mScarlet-H fluorescence was not detected after 48 hours in MLL::AF9 treated cells (Figure 4.13B). This may be due to the much larger size of the MLL::AF9 harbouring (> 12.4 kb) compared to control (3.486 kb) plasmids preventing integration into the eA9^m cells using the nucleofection process.

To further investigate if the eA9^m cells were nucleofected with MLL::AF9 plasmids the expression of *HOXA9* and *mScarlet-H* were analysed by qPCR (Figure 4.13C). In addition, the expression of other known MLL::AF9 target genes *HOXA5*, *HOXA7*, *cMYB* and *MECOM* were also evaluated. All genes, except *HOXA5*, showed upregulation after pMA9, pCTRL and p2158 nucleofection compared to untransfected eA9^m cells. RPATs were used as a negative control for gene expression, wherein all RQ values were below 2, confirming that upregulation observed across the plasmids was due to nucleofection (Figure 4.13C). Results show that *HOXA7* and *HOXA9* upregulation was highest after p2158 transfection. Conversely, p2158 resulted in minimum upregulation of *mScarlet-H* and *cMYB*. Surprisingly, peak expression in those genes was elucidated by pCTRL. *MECOM* expression was an exception, as all plasmids caused an upregulation to similar levels. Comparatively, pCTRL caused a stronger response than pMA9 across all genes. Overall, RQ values were lower

than 30 fold in this experiment. These findings suggest that eA9^m cells are sensitive to the nucleofection process itself which may have transiently influenced gene expression.

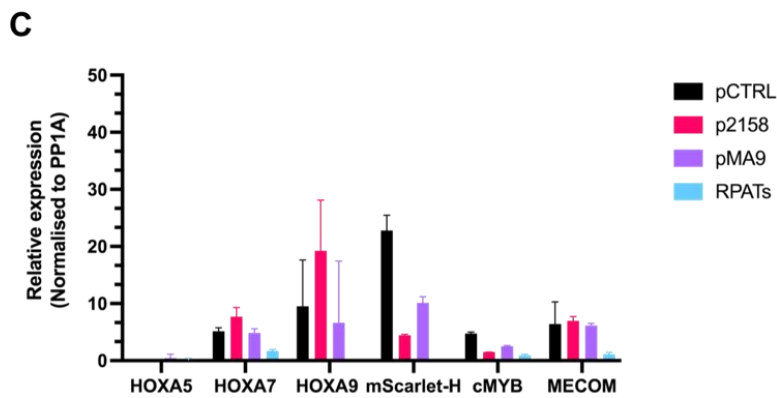
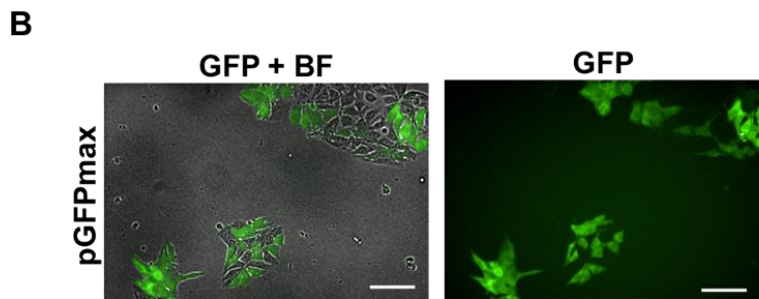
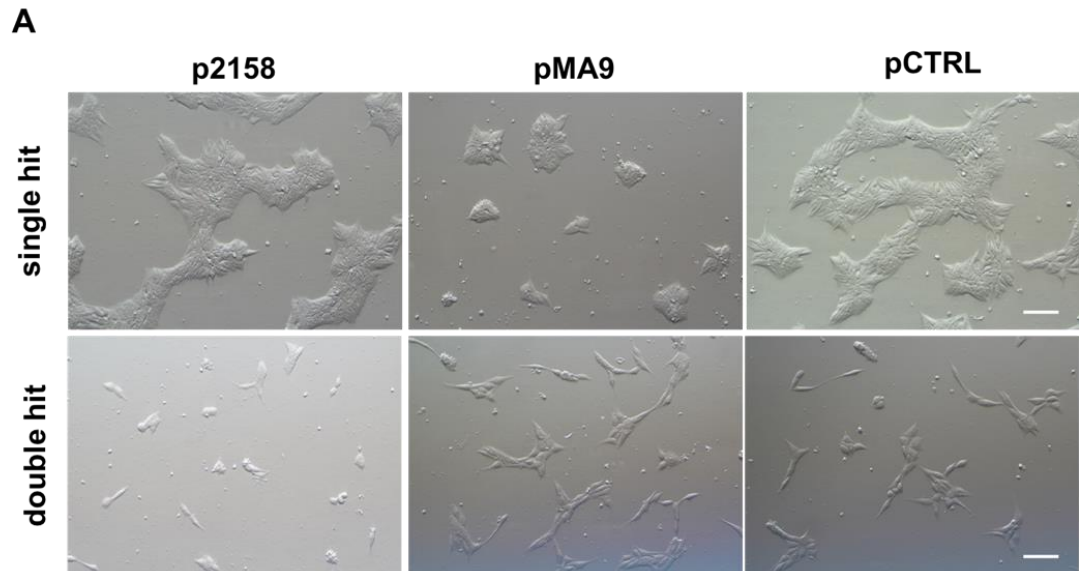


Figure 4.13 Nucleofection of MLL::AF9 plasmids in eA9^m cells.

A. Representative phase contrast images showing morphology of cells after 24h of single and double hit nucleofection with 1 μg of plasmids (pCTRL, pMA9, p2158). **B.** Representative fluorescence images of cells following 48h of transfection with pGFPmax as a positive control for nucleofection process. Transfection of pCTRL, pMA9, p2158 showed no fluorescence (images not shown). **C.** Bar chart showing changes in gene expression after 48h of nucleofection with pCTRL, pMA9 and p2158 using qPCR. Expression was normalised using *PP1A* gene and untreated eA9^m cells. Gene expression in untransfected RPATs is also shown as a negative control. Results are mean of three technical repeats. Scale bar = 100 μm .

4.5.2 MLL::AF9 lentiviral transduction of eA9^m iPSCs

Supernatants from MLL::AF9 and control lentiviral cultures were provided by Alexander Thompson (principal investigator). The presence of lentiviral particles (LVp) in the supernatants was confirmed by a viral titre assay (Figure 4.14). Manufacturer's guidelines (TakaraBio) were used to semi-quantify the amount of LVp present depending on intensity of indicator bands (Figure 4.14A). According to these images, an estimated amount of $\sim 4.6 \times 10^7$ IFU/mL was present in the supernatants (Figure 4.14B). Strong bands of similar intensities were seen in both titre tests, along with a strong fluorescent signal in HEK293Ts after production of LVp.

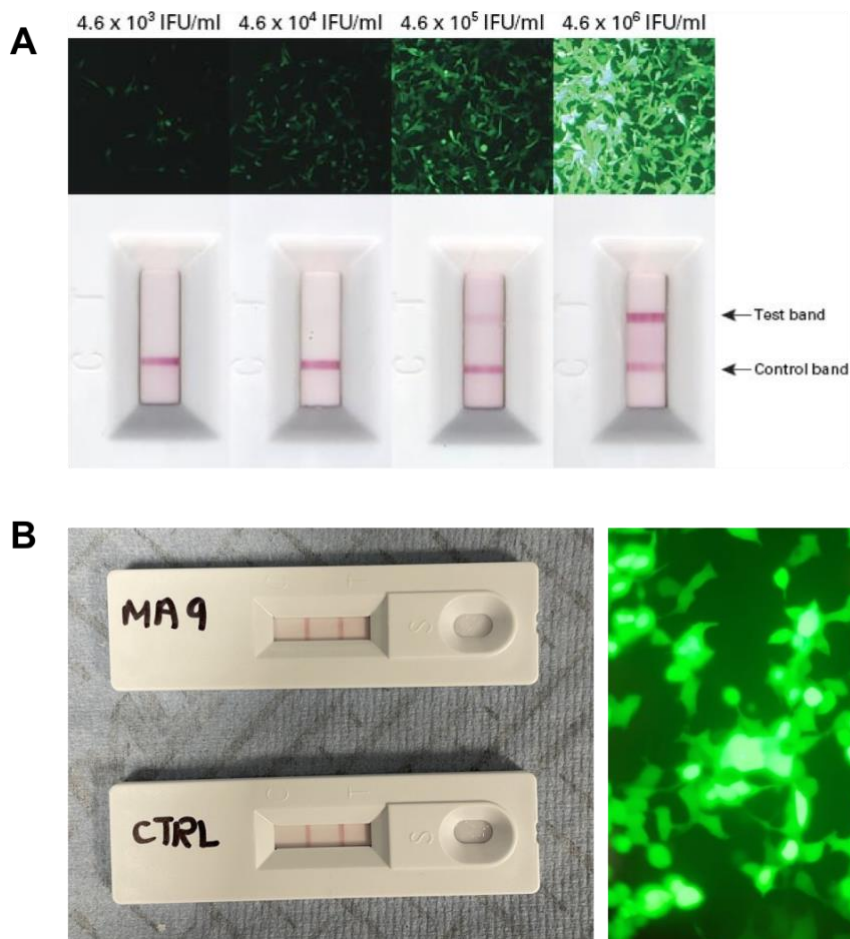


Figure 4.14 Measure of LVp using Lenti-X™ GoStix™ Plus.

A. Representative stock images of fluorescence intensity and viral titre as infectious units (IFU) per mL and intensity band (TakaraBio). **B.** Images from MLL::AF9 (MA9) and control (CTRL) LVp indicator test (left) and a representative fluorescence image of pCTRL LVp generating HEK293T cells (right).

After 48h of MA9 LVp transduction, eA9^m cells exhibited a stressed, round morphology, characteristic of apoptotic appearance, indicating that iPSCs may be sensitive to high titre LVp transduction (Figure 4.15). Preliminary flow cytometry analysis showed no difference in mScarlet-H fluorescence in eA9^m cells with and without MA9 LVp (Figure 4.15).

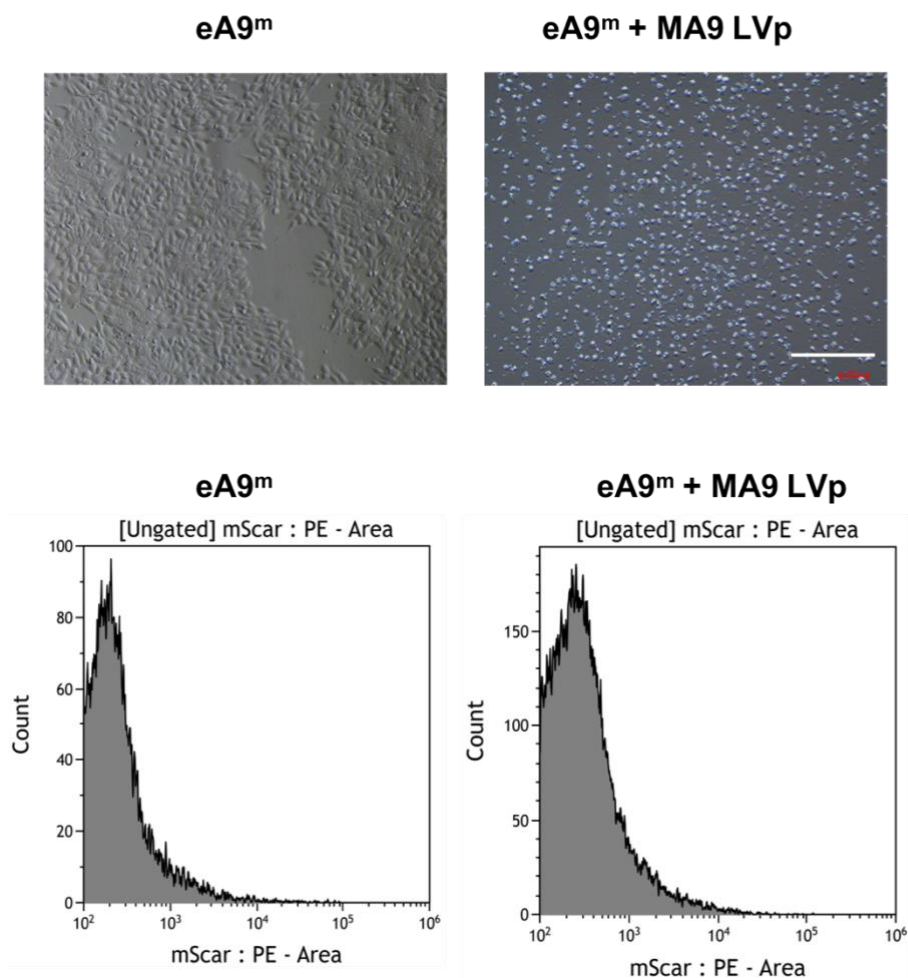


Figure 4.15 High-titre MLL::AF9 LVp transduction causes stress of eA9^m cells.

Representative phase contrast images (upper panel) and flow cytometry histogram plots (lower panel) of mScarlet-H expression in eA9^m cells with and without MA9 LVp addition after 48 hours. Scale bar= 200 μ m.

The addition of polybrene up to 5 μ g/mL was tolerated by the cells (Figure 4.16A). Titration of LVp with a range of concentrations (1 μ L/mL, 5 μ L/mL and 10 μ L/mL) in the presence of 5 μ g/mL polybrene was also tolerated by the eA9^m cells (Figure 4.16B). However increasing LVp concentration (MA9 and CTRL) resulted in loss of normal iPSC morphology indicating onset of cellular stress or apoptosis.

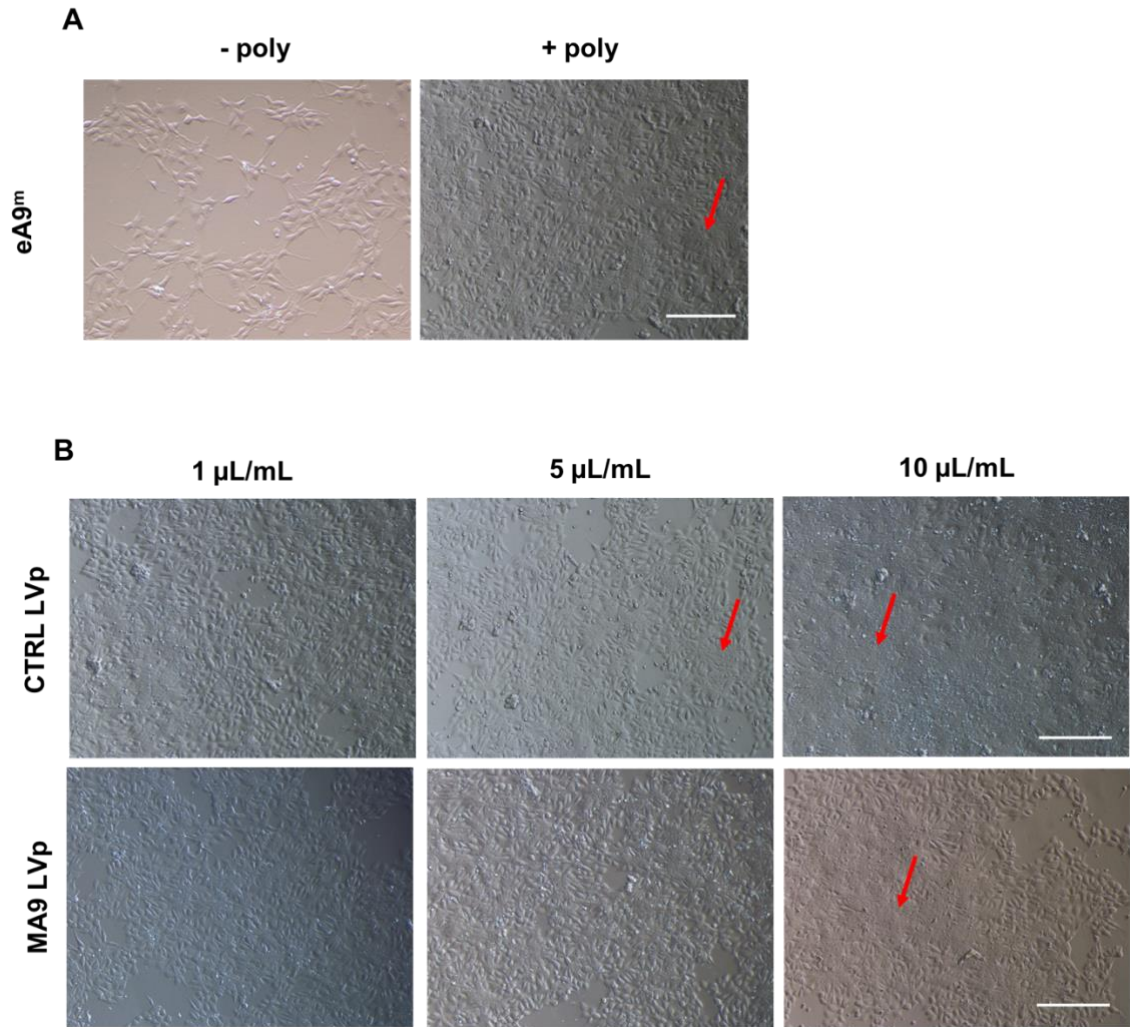


Figure 4.16 Effect of polybrene and LVp on morphology of eA9^m.

A. Representative phase contrast images of eA9^m cells cultured in the presence or absence of 5 µg/ml polybrene (poly). B. Representative phase contrast images of eA9^m cells cultured in the presence of polybrene and escalating dose of MA9 and CTRL LVp for 24 hours. Red arrows demonstrate loss of borders & morphology in treated cells. Scale bar= 200 µm, n=2.

As with the nucleofection strategy, mScarlet-H fluorescence was not detected following LVp exposure by fluorescence microscopy (data not shown), but differential gene expression was observed for the MLL::AF9 target genes by qPCR (Figure 4.17). *HOXA9* and *mScarlet-H* were upregulated more following CTRL LVp than MAF9 LVp and although the trend was similar in both approaches, the relative expression was much greater in the LVp treated cells compared to nucleofection (Figure 4.17 and Figure 4.13). LVp stimulation

resulted in upregulation of *HOXA5*, *HOXA7*, *HOXA9* and *mScarlet-H* and not *cMYB* and *MECOM*.

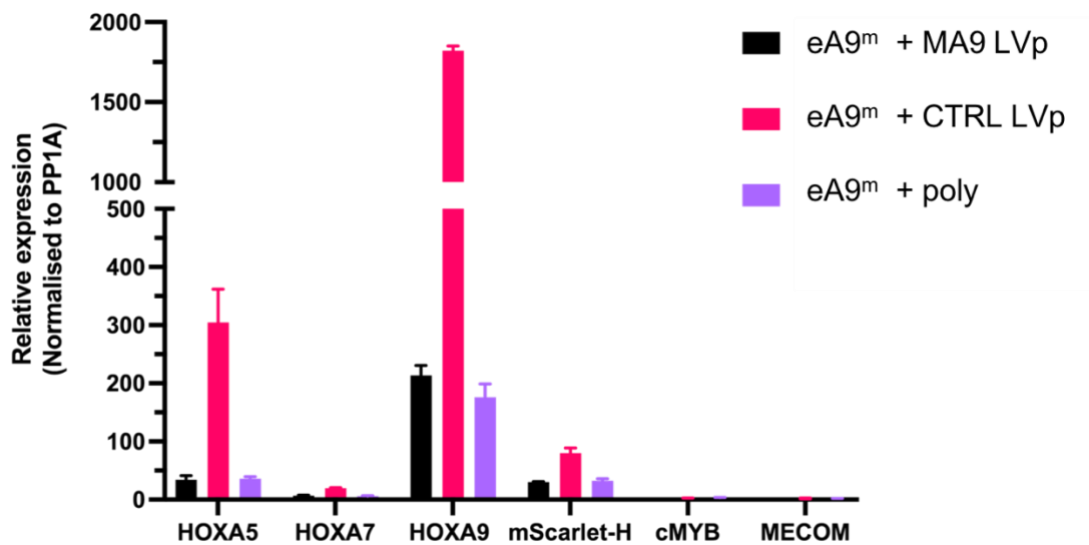


Figure 4.17 Effect of LVp transduction on gene expression in eA9^m.

Bar graph of relative expression in MLL-A9 target genes after 48 hours of MLL::AF9 (MA9) and control (CTRL) LVp treatment. Results are normalised to PP1A expression, and relative to untransduced eA9^m cells. Results are mean of three technical replicates.

To validate *mScarlet-H* expression, flow cytometry analysis following 48h exposure of eA9^m cells to 1 – 20 μ L/mL of each LVp showed limited but measurable fluorescence over control for both CTRL LVp (4.69% - 6.48%) and MA9 LVp (6% - 9.63%) treated samples (Figure 4.18). Together, the data indicates that upregulation of *HOXA9* following LVp transduction is achievable and measurable by gene expression and *mScarlet-H* expression.

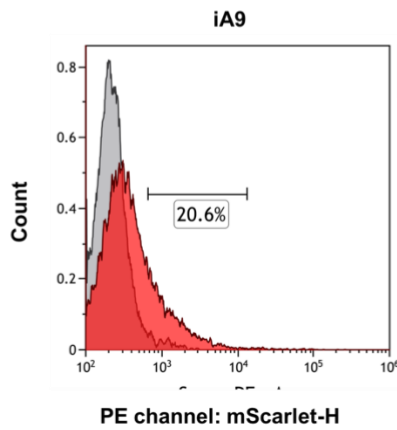
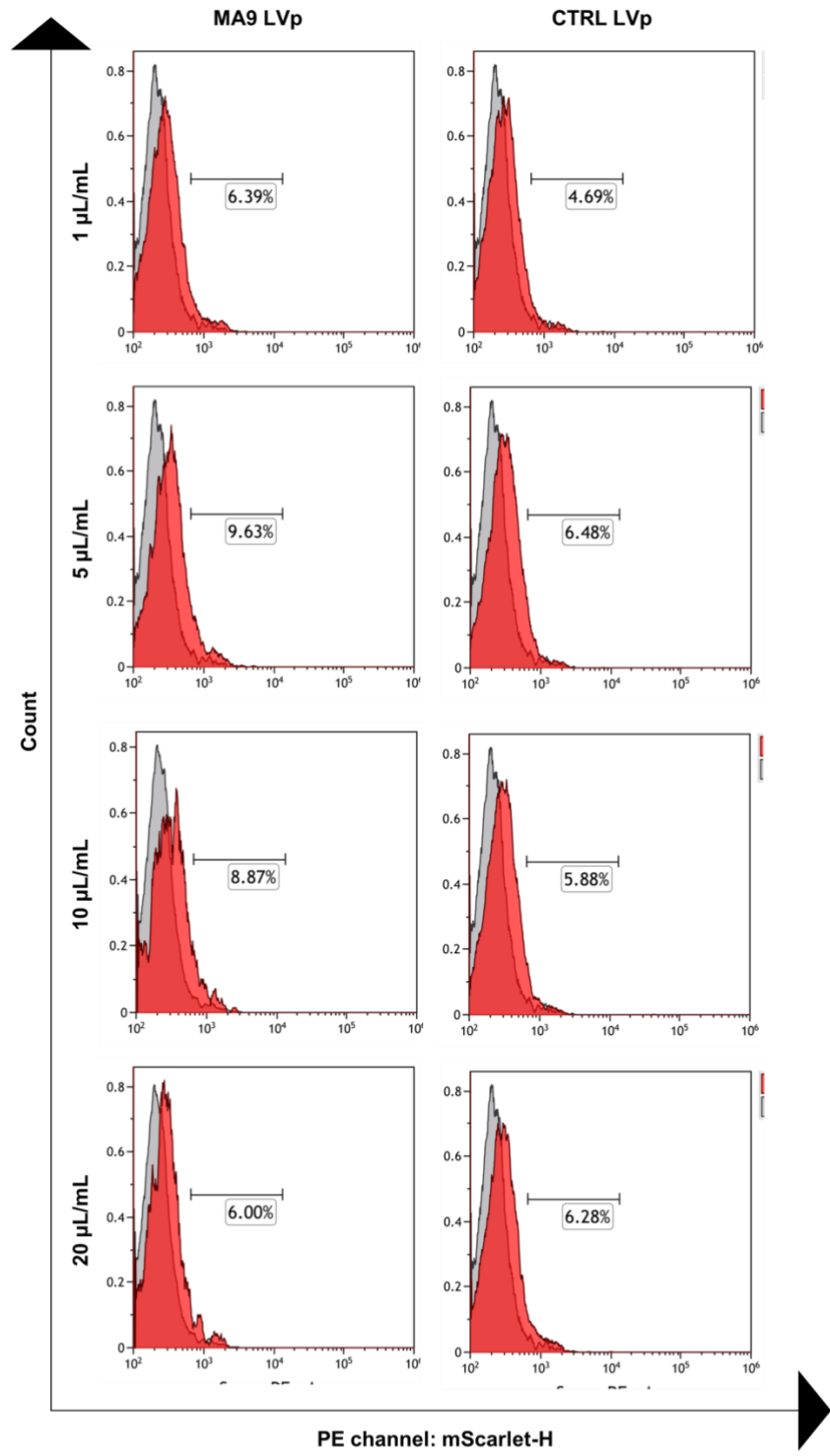


Figure 4.18 Expression of mScarlet after MLL::AF9 lentiviral transduction in eA9^m cells.

Flow cytometry histogram plots show measurable mScarlet expression in eA9^m cells treated with MLL::AF9 (MA9) and control (CTRL) LVp for 48h. The viral titration is shown on the left of the plots. Background/negative threshold was set using untreated eA9^m cells (grey). An mScarlet expressing cell line, iA9, was used as a positive control of fluorescence (n=1).

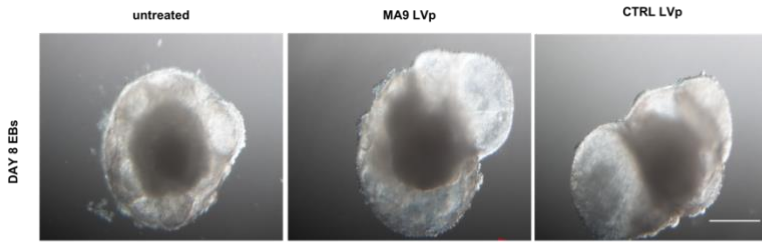
4.5.3 LVp addition during spin EB differentiation

To further test functionality of the endogenous reporter clone, a proof-of-principle study was performed by exposing eA9^m cells to MA9 and CTRL LVp during spin EB haematopoietic differentiation. Since endogenous *HOXA9* is highly expressed during EB differentiation, primarily at day 7, it was hypothesized that the *HOXA9* locus is more accessible at this stage of development. eA9^m EBs were transduced on day 7 and collected after 48h for flow cytometry analysis. EBs that were exposed to LVp increased in size and had an irregular appearance compared to untreated EBs (Figure 4.19A). The number of CD34⁺ cells was lower in MA9 and CTRL LVp-treated EBs (28.8% and 22.1%, respectively) compared to untreated EBs (38.6%) after 48 h of exposure (Figure 4.19B). The number of CD43⁺ cells were much lower after MA9 LVp exposure (~3.64%) compared to CTRL LVp (18.4%) or untreated EBs (19.6%) and the number of CD90⁺ cells was lower for both MA9 and CTRL LVp-treated EBs (20% and 21.2% respectively) compared to untreated EBs (29%) in day 9 EBs.

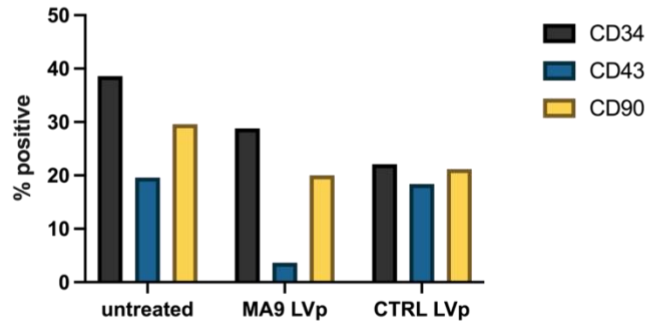
Since EB-derived cells co-express these surface markers at different stages of development, samples were also analysed for double positivity. Exposure to LVp resulted in decreased CD34⁺CD90⁺ double-positive populations in both MA9 and CTRL LVp treated EBs (10.2% and 8.6%, respectively) compared to untreated EBs (30%) at Day 9 (Figure 4.19C). Similarly, the number of CD34⁺CD43⁺ cells for MA9 (15.3%) and CTRL LVp (12%) treated EBs was lower than untreated EBs (29.3%) at Day 9 of the differentiation (Figure 4.19C). This indicates that the spin EB-based haematopoietic differentiation was blocked or delayed following LVp-treatment. Cell viability in Day 9 cultures was also negatively affected by LVp treatments for MA9 and CTRL (37% and 46% respectively) compared to untreated EBs (60%) (Figure 4.19D).

Together, this proof-of-principle data suggest that treatment of differentiating EBs with LVp after haemato-vascular mesoderm specification is feasible but may result in a block in or delayed onset of HE specification.

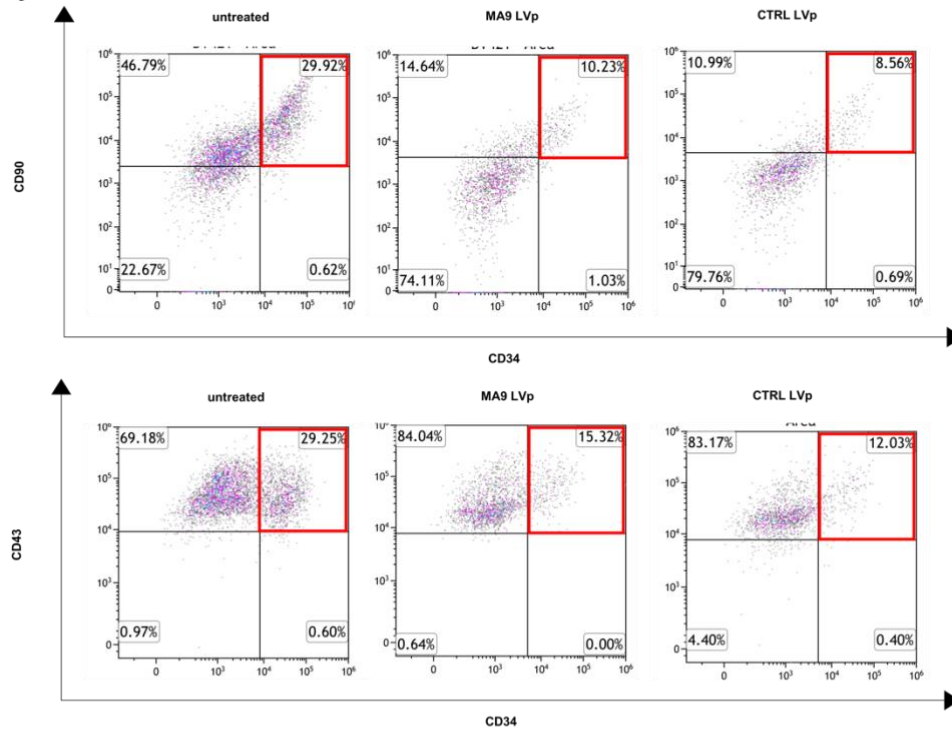
A



B



C



D

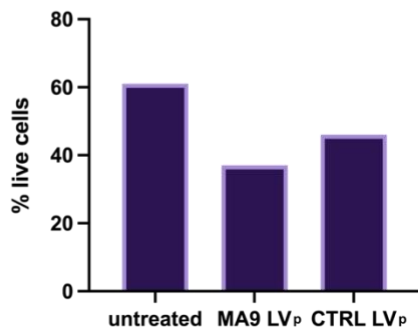


Figure 4.19 Effect of lentiviral transduction on morphology, haematopoietic markers expression and viability of EBs.

A. Images of eA9^m EBs following 24h treatment or not with MA9 or CTRL LVp. **B.** Bar charts of CD34, CD43 and CD90 expression in 48h-treated or untreated MA9 or CTRL day 9 EBs, determined using flow cytometry analysis. Positive expression was gated using isotype controls. **C.** Dot plots of double positive CD34+CD90+ and CD34+CD43+ populations (red boxes) in day 9 EBs, gated using unstained controls. **D.** Bar graph of cell viability (% live cells) of day 9 EBs after LVp transduction using Zombie NIR staining. Scale bar= 200 µm.

4.5.4 Effect of LVp addition on gene expression during the spin EB differentiation

To further investigate the effect of LVp addition on haematopoietic differentiation, the spin EB differentiations were repeated and extended to day 14. Expression of *HOXA* cluster (*HOXA5*, *HOXA7* and *HOXA9*), *RUNX1*, *GATA2*, *cMYB*, *MECOM* and *mScarlet-H* genes were evaluated on day 9 (Figure 4.20A). Variation in expression was observed across three independent EB differentiations (#1 - #3), although some trends were observed. MA9 LVp treated EBs demonstrated increased expression of all genes except *GATA2*, compared to untreated EBs in at least one differentiation and in 2/3 experiments for all but *GATA2* and *RUNX1*. CTRL LVp treatment resulted in upregulated expression of all genes except *HOXA5*, *HOXA7* and *GATA2* compared to untreated control in only one experiment (#3) (Figure 4.20A). *RUNX1* expression was highest on day 9 of differentiation #3, which may indicate premature haematopoietic specification leading to compromised HSPC production (Figure 4.20A). Samples in #3 differentiation were insufficient for *GATA2* expression analysis.

The same panel of eight genes were analysed on HSPCs collected on day 14 (Figure 4.20B). Only two differentiations (#1 and #2) survived to generate HSPCs. The overall trend was that day 14 MA9 LVp-treated EBs expressed lower *HOXA5*, *HOXA7*, *HOXA9*, *mScarlet-H*, *RUNX1*, *GATA2* and *MECOM* than untreated EB controls (Figure 4.20B). CTRL LVp-treated EBs showed similar decrease in gene expression except for *MECOM*. In both cases, MA9 LVp appeared to result in a greater decrease in expression than CTRL LVp, particularly for *HOXA5* and *HOXA9* (with associated reduction in *mScarlet-H*). Additional experiments are warranted to further assess this.

In summary, the observed altered gene expression appears to be due to variation in both the efficiency and quality of the differentiation and the response to LVp whether *MLL::AF9* is expressed or not. Additionally, the efficiency of LVp uptake by EBs may not have been consistent in all differentiations, due to the heterogenic nature of EBs.

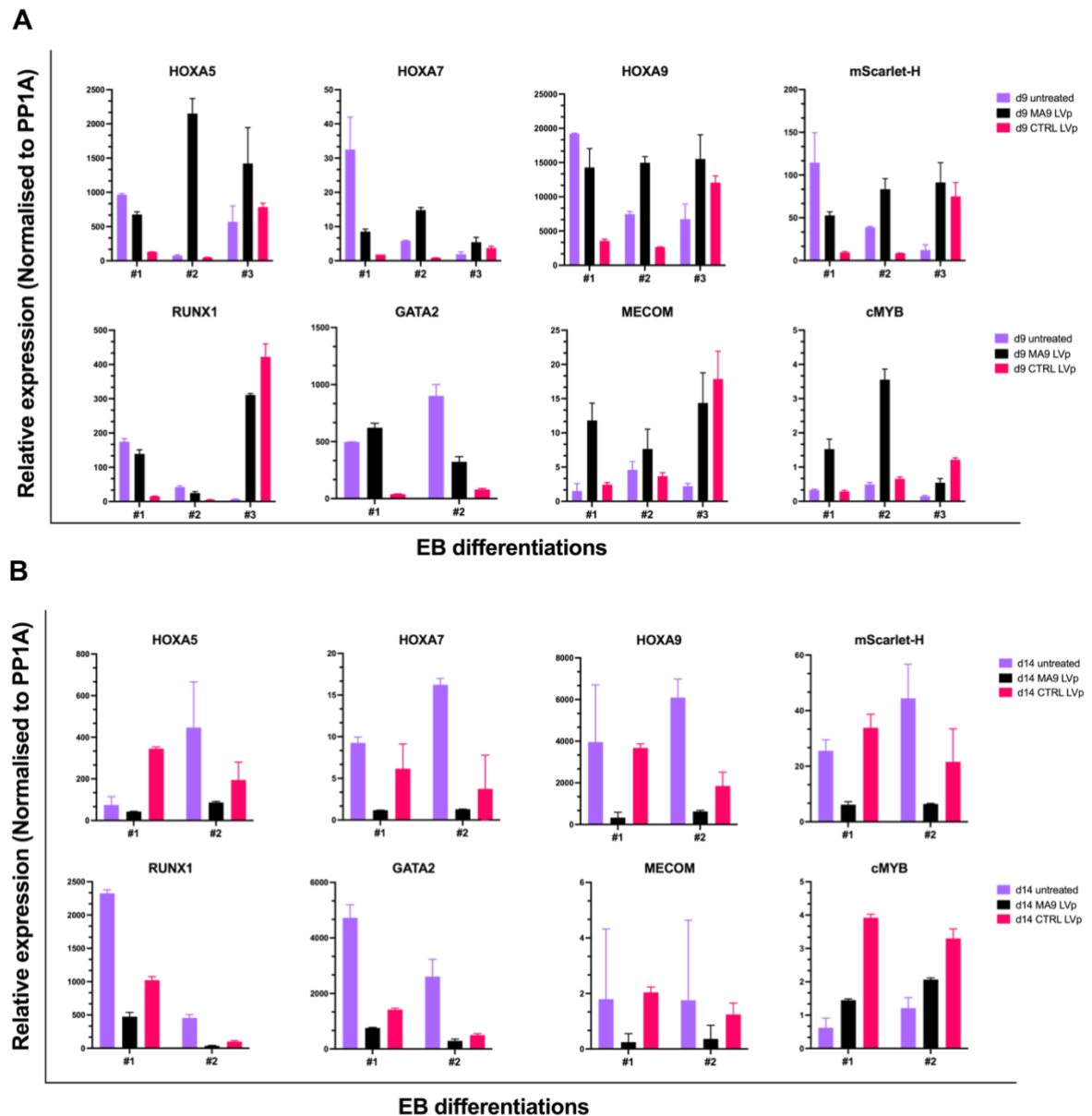


Figure 4.20 Differential gene expression following LVp induction of eA9^m-derived EBs during generation of HSPCs.

A. Bar graphs of haematopoietic gene expression from Day 9 harvested EBs treated or not on day 7 with *MLL::AF9* (MA9) or control (CTRL) LVp for 48h and **B.** HSPCs harvested on day 14 from the same treatments compared to untreated EBs. Expression was normalised using PP1A and undifferentiated eA9^m cells.

Results are mean \pm SD (n=3) of three independent differentiations labelled #1 - #3.

4.5.5 LVp exposure enhances production of HSPCs with myeloid lineage bias

Untreated, MA9 LVp and CTRL LVp eA9^m-derived HSPCs (day 14) were next examined for HSPC colony forming ability. Harvested HSPCs (Figure 4.21A) possessed colony-forming ability and produced various haematopoietic progenitors including CFU-GM, BFU-E and CFU-GEMM (Figure 4.21B). Notably, the size of BFU-E and CFU-GEMM colonies were smaller in LVp-treated cells than untreated cells (Figure 4.21B). A distinct increase in the number of BFU-E colonies was observed following either MA9 or CTRL LVp treatment with a loss of CFU-GEMMs (Figure 4.21C). These findings suggest that despite maintaining the multipotent ability of iPSC-derived HSPCs, exposure to either MA9 or CTRL LVp resulted in differentiation of the haematopoietic progenitors to more committed BFU-Es at the expense of multipotent GEMM colonies.

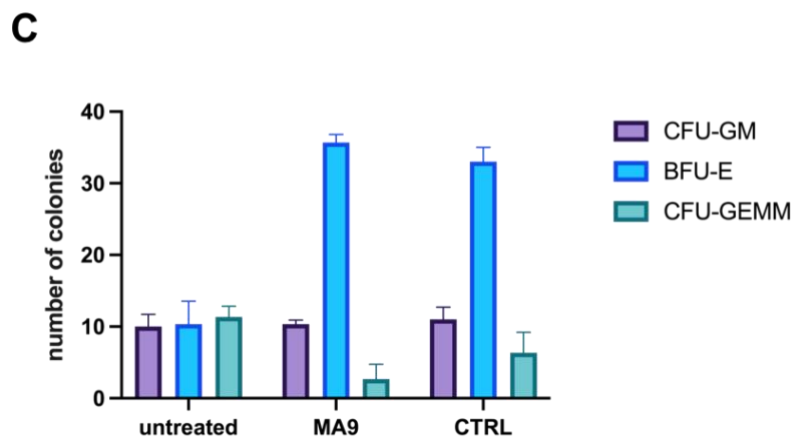
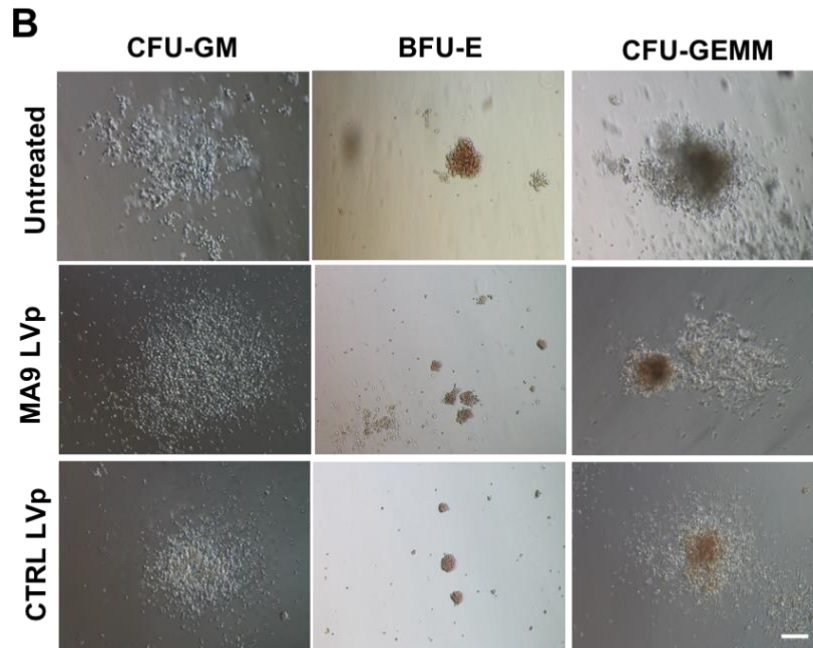
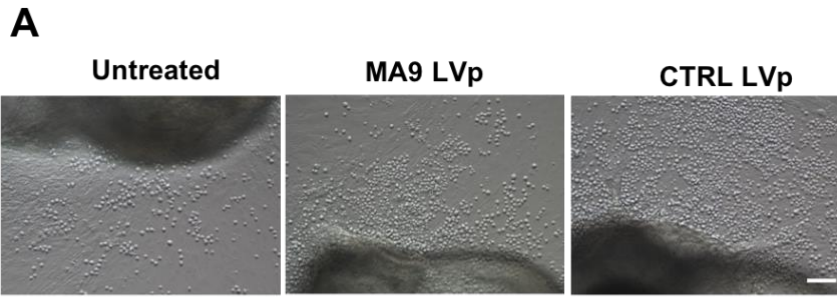


Figure 4.21 Colony forming potential of HSPCs after LVp exposure.

A. Representative images of morphology and quantity of HSPCs produced on day 14 of EB differentiation derived from EBs that were either untreated or LVp-treated on day 7. **B.** Representative images of day 8 colony formation from eA9^m-derived HSPCs. **C.** Bar chart showing quantification of haematopoietic progenitor colonies derived (per 3×10^3 cells plated). CFU colony-forming unit, BFU; blast-forming unit, G; Granulocyte, M; Macrophage, E; Erythroid, MM; monocyte megakaryocyte. Results are mean \pm SD (n=3). Scale bar= 100 μ m.

4.5.6 EBs show mScarlet-H fluorescence at varying intensities

To further examine the functionality of eA9^m cells, fluorescence of mScarlet-H was monitored in EBs. Day 2 EBs possess some autofluorescence when compared to RPATs (Figure 4.22A). The same contrast scale and intensity was also used to image EBs from both cell lines on day 4 of the differentiation. Representative images show a measurable increase in fluorescence on day 4, as opposed to day 2 in eA9^m. As expected, RPATs did not show any fluorescence on either day 2 or day 4 after compensation for autofluorescence. Next, the intensity of fluorescence from both RPAT- and eA9^m-derived EBs was measured at day 2, 4, 7 and 9 of standard spin EB differentiation along with day 9 EBs previously exposed to MA9 LVp or CTRL LVp for 48 h (Figure 4.22B). The intensities measured, across 3 EBs for each day and condition, are shown in Table 4.1. Across all days and conditions, eA9^m EBs had higher mean intensity fluorescence compared to day 2 EB baseline intensity (50 ± 3 a.u.). Mean fluorescence intensities for eA9^m cells ranged from 58.1 ± 9.7 a.u. to 80.9 ± 15.8 a.u. For RPATs, these intensities ranged from 53.7 ± 10.6 a.u. to 65.9 ± 10.5 a.u. The mean fluorescence intensity of day 4 and day 9 RPATs is above the threshold value set for day 2 EBs, possibly due to increased size and cell density of the older EBs.

Lower resolution imaging, to take account of EB density, showed a similar trend in fluorescence intensity with day 2 EBs possessing minimal autofluorescence, and a more prominent signal from eA9^m than RPATs on day 4 (Figure 4.22C). These observations support the presence of functional eA9^m reporter cells.

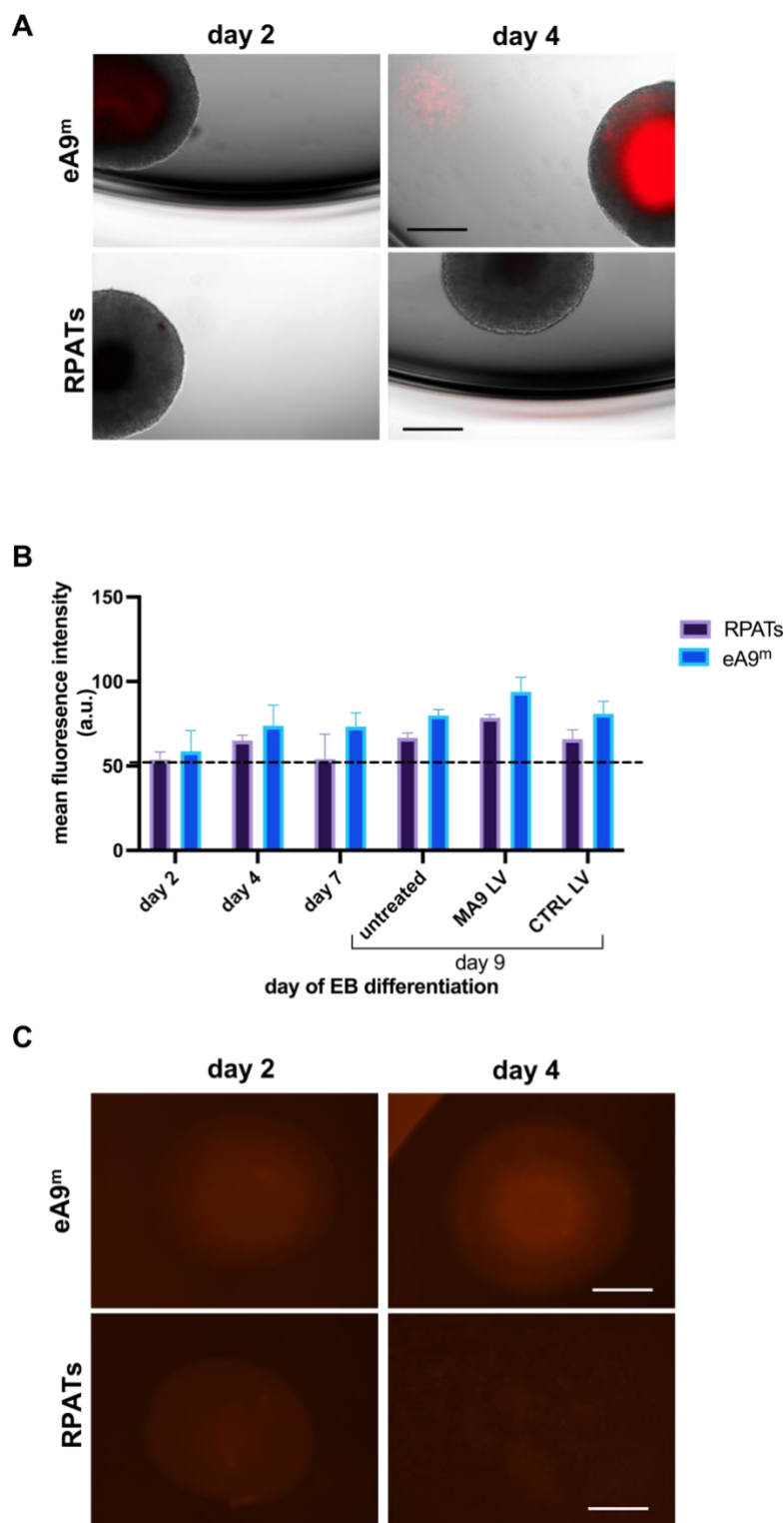


Figure 4.22 *mScarlet-H* expression in eA9^m EBs during spin EB haematopoietic differentiation.

A. Representative Operetta™ fluorescence images of RPATs and eA9^m day 2 and day 4 EBs. **B.** Bar graph of mean fluorescence intensities (a.u.) determined by Operetta™ software for treated or untreated EBs at different stages. Dotted line represents threshold intensity of autofluorescence observed in untreated day 2 EBs. Results are mean of n=3 EBs for each. **C.** Representative low resolution fluorescence images of EBs from eA9^m and RPATs imaged using EVOS

microscopy, on day 2 and 4 of the differentiation. Scale bar = 200 μ m. Same microscope parameters were used for all images.

Table 4.1 Intensity of *mScarlet-H* fluorescence in eA9^m EBs.

EB day	Mean intensity fluorescence (a.u.)	
	eA9 ^m	RPATs
Day 2	58.1 \pm 9.7	53.7 \pm 10.6
Day 4	73.8 \pm 25.5	65.0 \pm 7.6
Day 7	73.4 \pm 18.2	61.1 \pm 10.7
Untreated day 9	80.0 \pm 7.5	66.7 \pm 4.7
MA9 LVp day 9	94 \pm 20.3	78.5 \pm 4.3
CTRL LVp day 9	80.9 \pm 15.8	65.9 \pm 10.5

4.6 Summary of results

In this chapter, an endogenous HOXA9 reporter iPSCs line, eA9^m was generated using a combined CRISPR/Cas9 gene editing and transposase-based footprint-free PB approach, as previously reported (Kondrashov et al., 2018). *mScarlet-H* was incorporated as a fluorescence reporter and did not inhibit *HOXA9* expression. Fluctuations in *HOXA9* expression during the spin EB differentiation were unaffected in the reporter cell line. Molecular validation confirmed that the initial targeting of the *HOXA9* locus was achieved in the correct genomic location. However, heterozygous editing was achieved as wildtype copies of the *HOXA9* locus were retained. Transposase treatment resulted in heterogenous excision of the drug resistant element containing PB cassette. Sanger sequencing confirmed two different genotypes in eA9^m; a pre excision allele harbouring the full PB cassette and a post excision allele with the PB cassette deleted. Despite this, eA9^m contained *mScarlet-H* in both genotypes. Thus, several approaches were implemented to functionally validate the reporter cell line. The eA9^m reporter cell line retained its pluripotency and generated CD34⁺CD43⁺CD90⁺ HSPCs. *mScarlet* fluorescence was observed in monolayer, adhered eA9^m iPSCs following HOXA9 stimulation using a combination of SB/CHIR/RA. This confirmed that *mScarlet-H* expression and translation was functional in eA9^m iPSCs. To further show that *mScarlet-H* expression is under the control of the HOXA9 promoter, we exploited the spatial and temporal expression patterns of HOXA9 that is mimicked in the spin EB differentiation. As confirmation, *mScarlet-H* expression levels varied in line with *HOXA9* levels, particularly on day 4 and day 7.

To examine functionality in a potential disease setting, eA9^m iPSCs were exposed to oncogenic MLL::AF9 containing plasmids using nucleofection and lentiviral transduction. The viability and morphology of eA9^m iPSCs was compromised by nucleofection and transduction with either MA9 or control plasmids. To overcome this MLL::AF9 and Control LVp were applied to eA9^m generated EBs, in a proof-of-principle study, during differentiation to HSPCs. Increased *mScarlet-H* expression along with *HOXA9* and other MLL::AF9 target genes was observed during haematopoietic specification and differentiation. Confirmation of m-Scarlet fluorescence was observed by confocal microscopy following untreated spin EB differentiation of eA9^m cells compared to control RPATs.

Together, the data generated supports the generation of a molecularly and functionally validated endogenous HOXA9-mScarlet reporter iPSC line for future generation of human isogenic leukaemic *in vitro* models. Such advanced models would be a step change in de-risking candidate anti-leukaemic drugs prior to clinical evaluation by directly assessing potential toxicity in a genetically equivalent normal cell.

Potential candidate anti-leukaemic drugs were identified and validated in traditional models in Chapter 5.

Chapter 5 Investigation of the efficacy of FDA-approved drugs in AML

5.1 Brief background

Prior to joining the laboratory, conditional deletion of the *HOXA* cluster in a mouse model of *MLL::AF9* was used to generate a *Hoxa*^{del} signature by Illumina BeadArray (Kettyle et al., 2019). A systematic approach, connectivity mapping, was used to detect functional connections between this *Hoxa*^{del} signature and small molecules and drugs. This approach identified candidate FDA-approved drugs that mimic the *Hoxa* deletion, thus potentially possessing anti-leukaemic effects. Out of this list, five drugs were initially chosen: homoharringtonine (HHT), atorvastatin (ATV), albendazole, glycopyrrolate and fluocinonide and their effect on cell viability in *MLLr* leukaemias was investigated. HHT and ATV were chosen for further study based on preliminary data prior to the start of this project.

HHT, originally extracted from *Cephalotaxus hainanensis*, has been approved for treatment of chronic myeloid leukaemia (cited in Yakhni et al., 2019). Studies revealed that HHT inhibits protein synthesis by binding to the small ribosome subunit, and activating the TGF- β pathway leading to cell cycle arrest (Chen et al., 2017). HHT is particularly effective in tyrosine kinase inhibitor-induced resistant malignancies (Alvandi et al., 2014; Cao et al. 2014; Weng et al., 2018). ATV is a tissue selective hydroxymethylglutaryl coenzyme A (HMG-CoA) inhibitor, commonly used for hypercholesterolemia (Abolghasemi et al., 2022). It is a potent, well-tolerated, lipophilic, FDA-approved drug, available at low cost as Lipitor (Roth, 2002). It was recently recognised as an anti-cancer agent due to its pleiotropic effects on rapidly dividing cells (Shaghaghi et al., 2022). In particular, ATV has shown efficacy in breast cancer (Abolghasemi et al., 2022; Marti et al., 2021).

The efficacy of HHT and ATV on four leukaemic cell lines: THP1, MV4-11, OCI-AML3 and HL60 was examined *in vitro*. The panel of cells were selected to incorporate both *MLL* rearrangements (*MLLr*) i.e THP1 and MV4-11 or non-*MLLr* (OCI-AML3 and HL60) (Table 5.1). All cell lines have an associated upregulation in *HOXA* genes. Dose response assays, CFU assays, RNA sequencing analysis and validation were used to evaluate the anti-leukaemic effect of both candidate drugs.

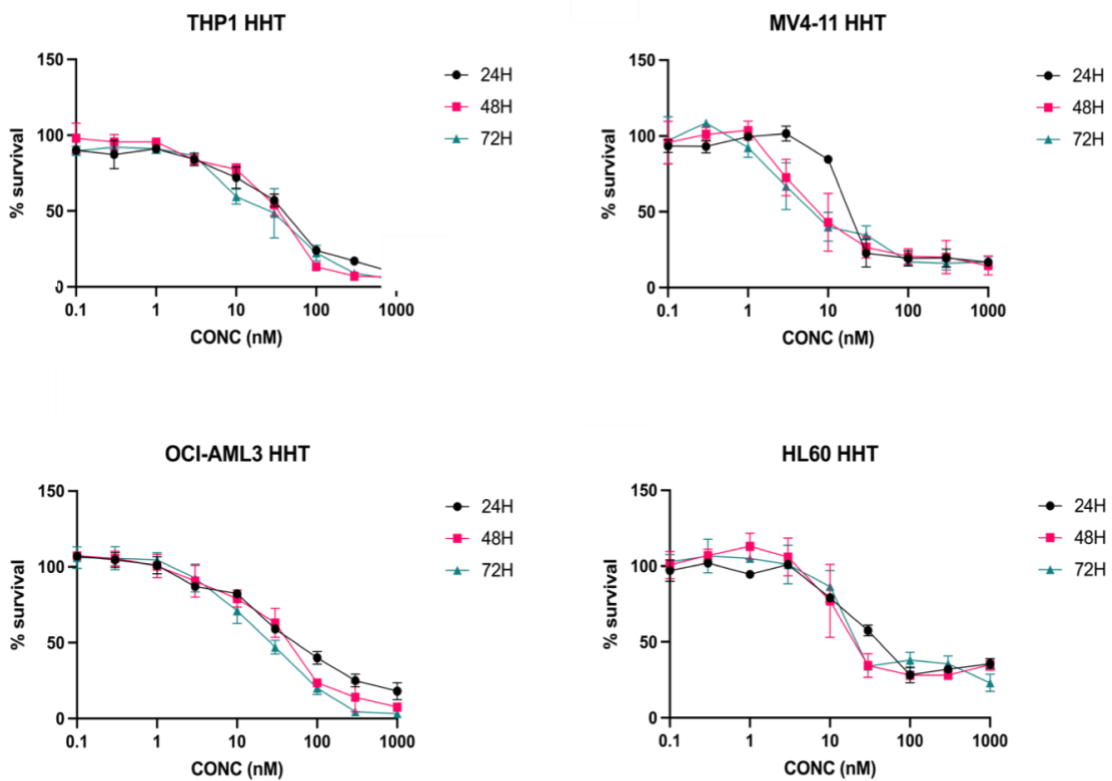
Table 5.1 Common mutations in AML cell lines

Cell line	Mutation
THP1	MLL rearrangement (MLL::AF9)
MV4-11	MLL rearrangement (MLL::AF4)
OCI-AML3	NPM1 type A mutation
HL60	Amplified MYC gene

5.2 Effect of FDA-approved drugs on cell viability of leukaemic cell lines

5.2.1 Homoharringtonine (HHT)

Due to its high potency demonstrated in previous studies, leukaemic cell lines were treated with HHT at a range of nine low concentrations (0.1 to 1000 nM) in liquid culture. Cell viability of all cell lines after 24h, 48h and 72h were obtained as a percentage of DMSO control (Figure 5.1A). The dose response curves generated show a gradual decrease in cell viability in all cell lines with increasing HHT concentrations. Cell lines tested also exhibit greater sensitivity in a time-dependent manner. At concentrations higher than 100 nM, HHT demonstrated measurable potency against all cell lines at all time points. Similar 50% inhibitory concentration (IC₅₀) values were obtained at 24h, for both THP-1 and OCI-AML3 (36.93 ± 6.11 and 33.24 ± 6.71, respectively) (Figure 5.1B). IC₅₀ values of MV4-11 and HL60 were slightly lower, at 15.07 ± 1.46 and 19.51 ± 2.73, respectively. Consistent with the 24h timepoint, MV4-11 showed the highest sensitivity to HHT at 48h and 72h, with IC₅₀ values of approximately 5 nM. Conversely, THP-1 and OCI-AML3 showed higher IC₅₀ values compared to MV4-11 and HL60 after 48h and 72h of treatment, represent less sensitivity to HHT. Cell viability of MV4-11 and HL60 reaches plateau after 30 nM with minimum change at higher doses, whereas the viability of THP-1 and OCI-AML3 continues to decrease to nearly 0%. All cell lines showed similar responses and conferred sensitivity to HHT in a time and dose dependent manner at the concentrations used. This data confirms that HHT is a promising candidate for treatment of AML, and not restricted to *MLLr* mutations.

A**B**

Homoharringtonine				
IC50 (nM)	THP1	MV4-11	OCI-AML3	HL60
24h	36.93±6.11	15.07±1.46	33.24±6.71	19.51±2.73
48h	30.20±3.18	5.45±1.19	35.10±6.81	11.33±1.58
72h	27.00±5.68	4.13±0.10	22.10±2.89	12.52±3.53

Figure 5.1 Effect of HHT on the viability of leukaemic cell lines.

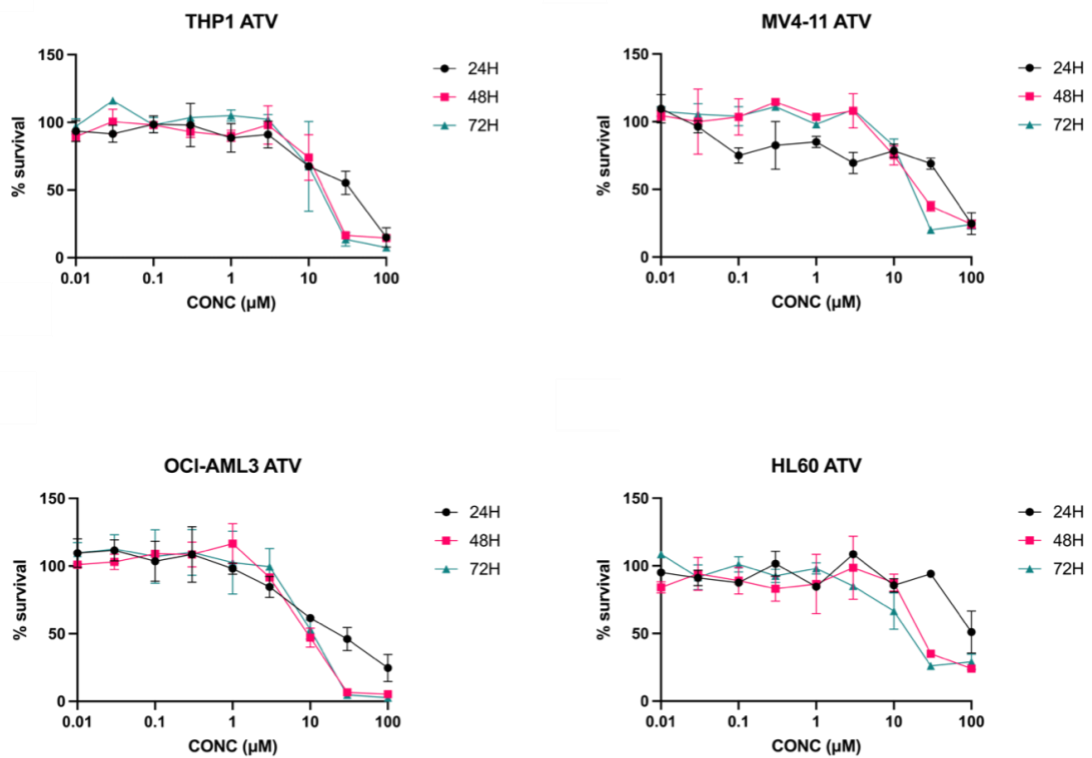
A. Dose-response curves of cells treated with HHT at nine concentrations ranging from 0.0001 μ M to 1 μ M. Cell viability was assessed using Real-TimeGlo™ and measured every 24 hours using FLUOstar® plate reader. Cell viability is represented as a percentage of survival compared to 0.01% DMSO vehicle control. Results are mean of three technical repeats from n=4 experiments. **B.** Table showing the IC50 values and uncertainty/deviation at each time point, determined using GraphPad prism nonlin-fit agonist vs. response- variable slope (four parameters).

5.2.2 Atorvastatin (ATV)

Based on preliminary observations, leukaemic cell lines were treated with ATV concentrations that ranged from 0.01 μ M to 100 μ M. Low ATV doses of less than 10 μ M did not show an effect on cell viability in all cell lines except for OCI-AML3

at 24h (Figure 5.2A). ATV possessed a minimal effect on cell viability at concentrations up to 10 μM . Higher concentrations of ATV were required to exhibit an inhibitory effect on cell viability across all cell lines tested at all timepoints. Viability of the majority of cell lines reached $\sim 0\%$ following 30 μM ATV treatment at 48h and 72h. At 24h of ATV treatment, THP1, MV4-11 and HL60 did not achieve IC₅₀ values. This indicates that $>100 \mu\text{M}$ of ATV is needed to achieve IC₅₀ values at 24h for these cell lines. In contrast, OCI-AML3 cells showed an IC₅₀ value of $13.05 \pm 11.42 \mu\text{M}$ after 24h of ATV treatment. OCI-AML3 also showed the highest sensitivity to ATV at 48h and 72h of treatment compared to all cell lines tested, with IC₅₀ values of $8.27 \pm 0.87 \mu\text{M}$ and $9.60 \pm 1.24 \mu\text{M}$, respectively. The 48h-IC₅₀ value of HL60 was $21.62 \pm 8.60 \mu\text{M}$, displaying the lowest sensitivity to ATV, and a 72h-IC₅₀ value of $10.41 \pm 2.09 \mu\text{M}$. THP1 and MV4-11, exhibited similar IC₅₀ values of ATV of approximately $13 \pm 3 \mu\text{M}$ at 48h of treatment. At 72h of ATV treatment, THP1 had an IC₅₀ value of $11.88 \pm 1.89 \mu\text{M}$, whereas MV4-11 IC₅₀ value was $10.73 \mu\text{M}$. Compared to HHT, ATV was much less potent as higher concentrations were needed to achieve IC₅₀ values in all leukaemic cell lines used (Figure 5.2B).

A



B

Atorvastatin				
IC50 (μM)	THP1	MV4-11	OCI-AML3	HL60
24h	-	-	14.33±11.42	-
48h	12.57±3.30	13.05±2.46	8.27±0.87	21.62±8.60
72h	11.88±1.89	10.73±	9.60±1.24	10.41±2.09

Figure 5.2 Effect of ATV on the viability of leukaemic cell lines.

A. Dose-response curves of cells treated with ATV at nine concentrations ranging from 0.01 μM to 100 μM. Cell viability was assessed using Real-TimeGlo™ and measured every 24 hours using FLUOstar® plate reader. Cell viability is represented as a percentage of survival compared to 0.01% DMSO vehicle control. Results are mean ± SD from n=4 experiments. Three technical repeats performed in each. **B.** Table showing the IC50 values and uncertainty/deviation at each time point, determined using GraphPad prism nonlin-fit agonist vs. response- variable slope (four parameters).

5.3 Effect of atorvastatin and homoharringtonine on colony formation

Colony forming assays were used to assess whether ATV and HHT affect the clonogenicity of leukaemic cell lines. Leukaemic cell lines were treated with their respective 48h-IC50 values identified in the dose response assays prior to seeding the cells in methylcellulose medium. Changes in colony formation and number using the CFU assay were monitored for 7 days (Figure 5.3). Representative images of colonies formed after 7 days in culture show a decrease in colony size in OCI-AML3 and HL60 that were treated with ATV compared to vehicle control (Figure 5.3A). Conversely, the size of THP1 and MV4-11 colonies treated with ATV did not show a marked change in colony size compared to DMSO vehicle control. All cell lines that were treated with HHT did not form any colonies after 7 days, indicating that HHT either disrupted the clonogenicity of the leukaemic cell lines tested or all cells were killed in the assay. No significant change in colony number of the cell lines was observed after ATV treatment relative to DMSO vehicle control ($p > 0.5$) using one-way ANOVA and Tukey's multiple comparison test (Figure 5.3B). These results demonstrate that ATV does not significantly impair colony formation at the doses used.

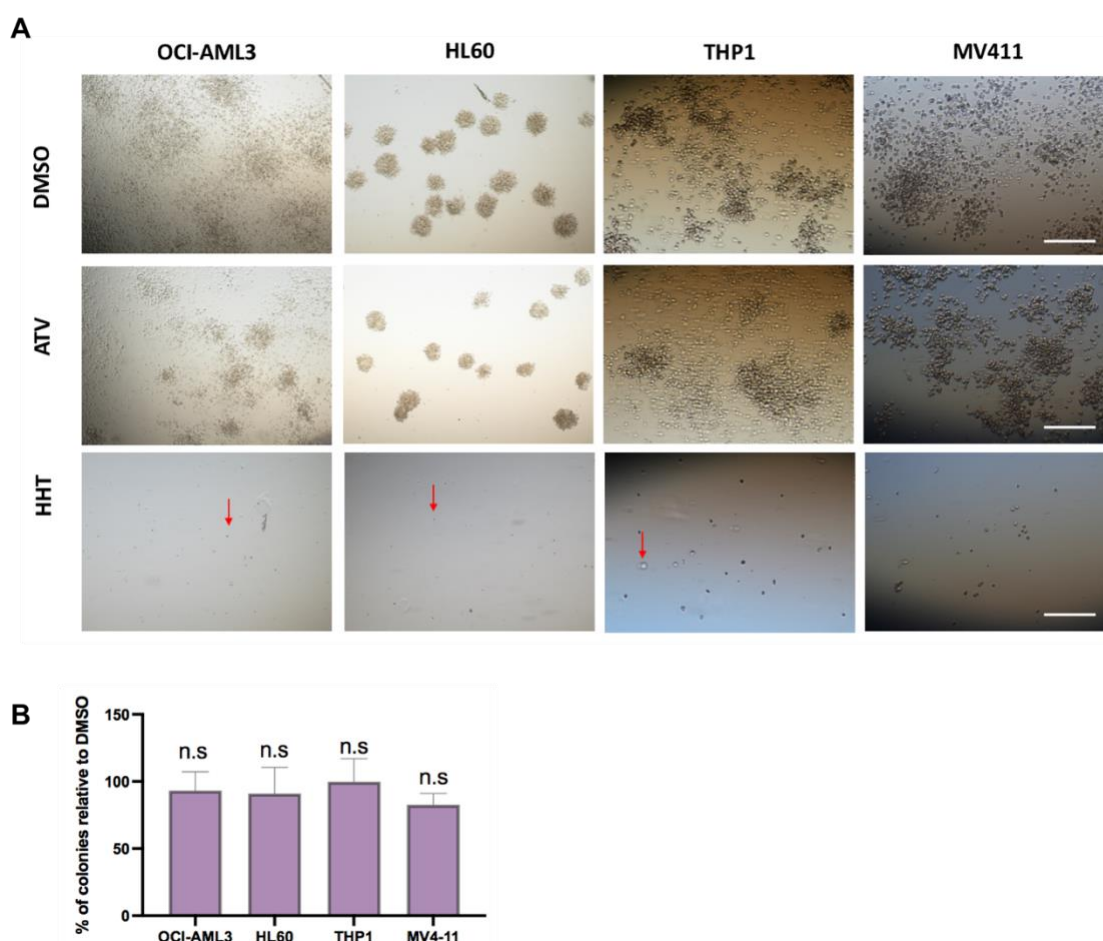


Figure 5.3 Effect of HHT and ATV treatment on colony formation in leukaemic cell lines.

A. Representative images of colonies formed from cell lines that were seeded into methylcellulose medium containing the 48h IC₅₀ values of HHT or ATV. Cells that did not form colonies are also shown (red arrows). **B.** Bar chart showing percentage of colonies from A relative to 0.01% DMSO vehicle control, formed after 7 days. Results are mean \pm SD of n=3 experiments. Statistical analysis showed changes in ATV-treated colonies were not significant (n.s) ($p > 0.5$), using one-way ANOVA along with Tukey's multiple comparison test. Scale bar = 200 μ m.

5.4 Gene expression profiling of IC₅₀-treated leukaemic cell lines

To better understand the effect of ATV and HHT on molecular processes of the leukaemic cell lines (THP1, OCI-AML3, MV4-11 and HL60), transcriptome analysis was performed using RNA sequencing following 48h IC₅₀-treatments. Differences between biological replicates (denoted as 1 or 2) were also investigated. To demonstrate the relationship between the different treatments in leukaemic cell lines, principal component analysis (PCA) was used (Figure 5.4). PCA analysis confirmed that matched cell lines and treatments could be separated along at least one axis, indicating differential gene expression. The

clustering shown indicates good reproducibility for all conditions except HL60_H1 and HL60_H2. This indicates a degree of technical or intrinsic biological variation at the time of sample preparation or treatment, respectively. Consistent with the functional differences observed, HHT-treated replicas clustered further away than ATV- and DMSO-treated samples, as demonstrated by OCI-AML3 and THP1 samples. This illustrates the significant transcriptional changes imposed on the cells by HHT compared to ATV. All MV4-11 samples clustered together in the same location on the plot, representing highest correlation in the transcriptome of the samples. These results are in line with the influence of these drugs identified in 5.2 on the leukaemic cell lines tested, with HHT holding a more profound effect on gene expression compared to ATV.

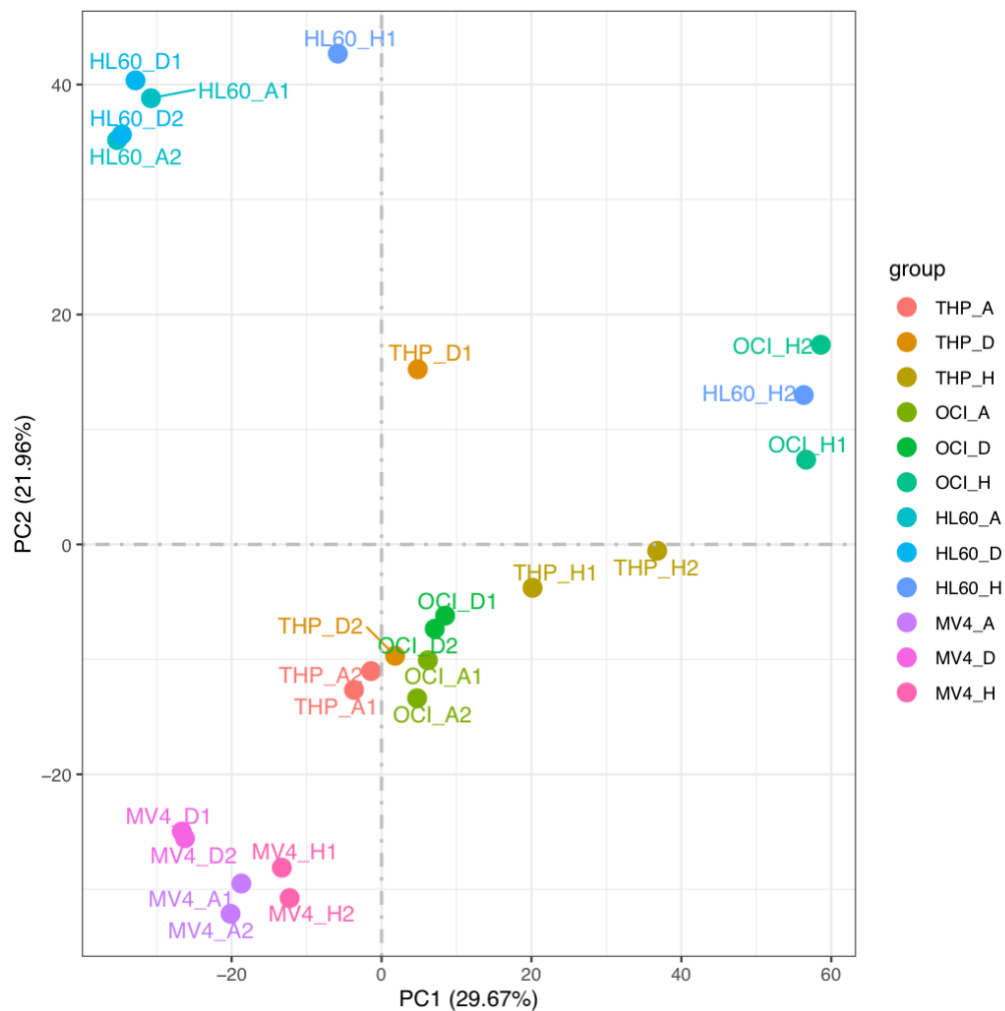


Figure 5.4 Gene expression relationship between treated leukaemic cell lines.

PCA plot demonstrates the clustering between THP1, MV4-11, OCI-AML3 and HL60 after 48h of treatment with DMSO, HHT and ATV based on similarities in their expression profiles. DMSO was used at 0.01%, and HHT and ATV were used at the 48h-IC50 doses. Two biological replicates for each treatment is

shown. Plot shows most variation between THP1_D and HL60_H. D= DMSO; H= HHT; A= ATV.

5.5 Differential expression in IC50-treated leukaemic cell lines

Transcriptome was further analysed by quantifying the differentially expressed genes (DEGs) based on a $\log_2\text{FoldChange} > 1$ and $\text{padj} < 0.05$. Volcano plots reflect the differences in gene expression between the different treatments (Figure 5.5, Figure 5.6). In total, HHT-treated MLLr cell lines, THP1 and MV4-11, showed the least number of DEGs (939 and 1720, respectively), whereas the HHT-treated non-MLLr cell lines, OCI-AML3 and HL60, had the highest number of DEGs (6302 and 4369, respectively). As represented in the PCA plot, OCI-AML3 cells had the highest number of DEGs compared to the other cell lines (Figure 5.5C). In contrast, HHT treatment resulted in the lowest number of upregulated and downregulated genes in THP1 cells amongst the leukaemic cell lines (Figure 5.5A). Values of DEGs in MV4-11 and HL60 fall in similar ranges to THP1 and OCI-AML3 cells, respectively (Figure 5.5B,D).

As observed for HHT, lowest variation in gene expression was found in ATV-treated THP1 cells (148 DEGs) compared to other ATV-treated cell lines (Figure 5.6A), ATV-treated MV4-11 showed the highest number of DEGs (1124) (Figure 5.6B). OCI-AML3 and HL60 cells treated with ATV had relatively low number of DEGs (242 and 332, respectively) (Figure 5.6C,D). These results highlight the level of variation between the cell lines and drugs used, with HHT having a more significant effect on gene expression compared to ATV. Extended analysis of the identified DEGs showed genes that are mutually co-expressed or exclusively between all the leukaemic cell lines (Figure 5.7).

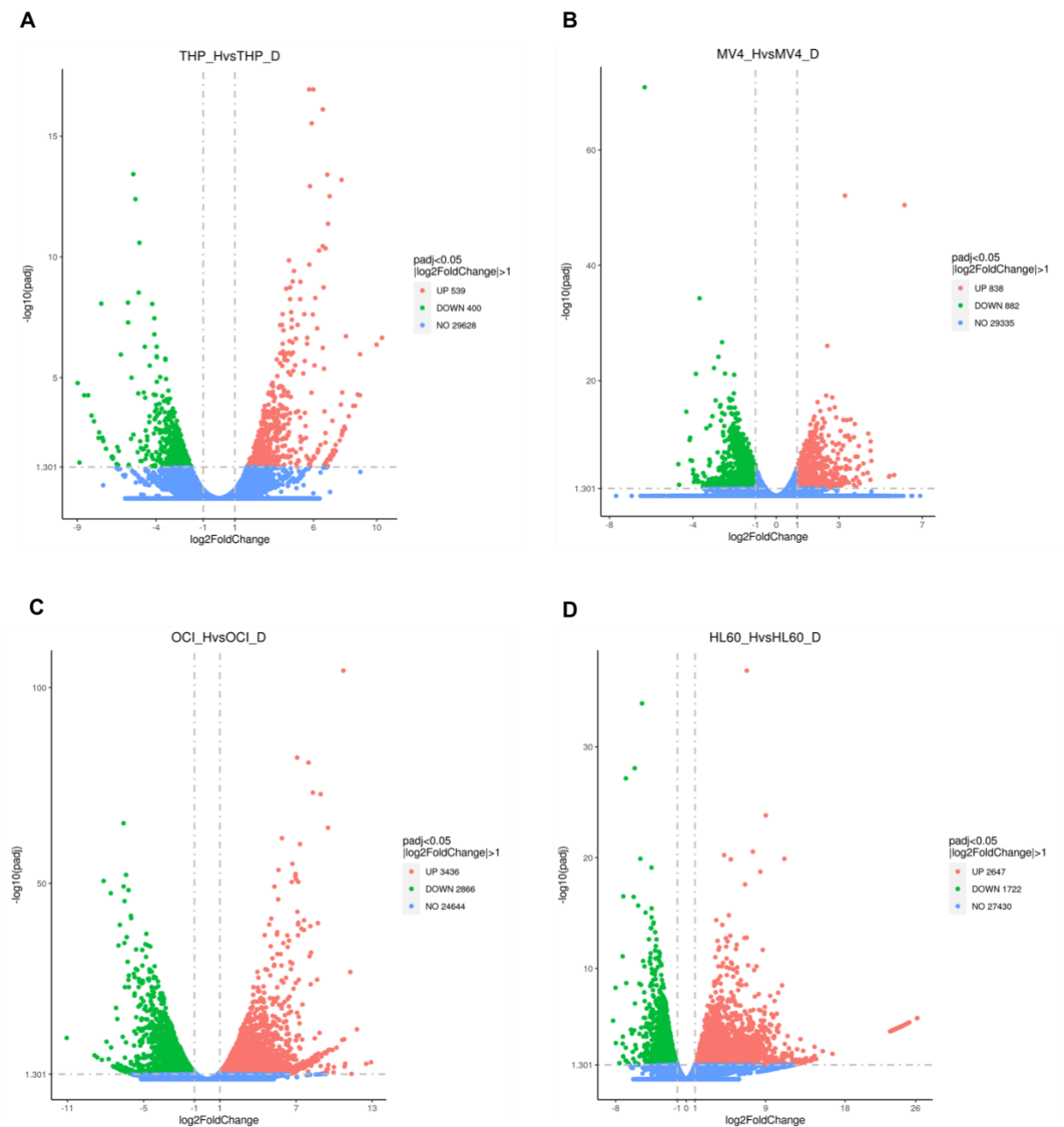


Figure 5.5 Differential gene expression of leukaemic cell lines treated with HHT.

A-D. Volcano plots show the number of DEGs that were upregulated or downregulated between comparative treatments with 48h-IC50 dose of HHT or 0.01% DMSO, on THP1, MV4-11, OCI-AML3 and HL60. It also shows the number of genes that showed no change (NO). DEGs are based on a threshold of $\log_2\text{FoldChange} > 1$ and $\text{padj} < 0.05$. Results are from two biological replicates. Figures were generated by Novogene. D= DMSO; H= HHT; A= ATV.

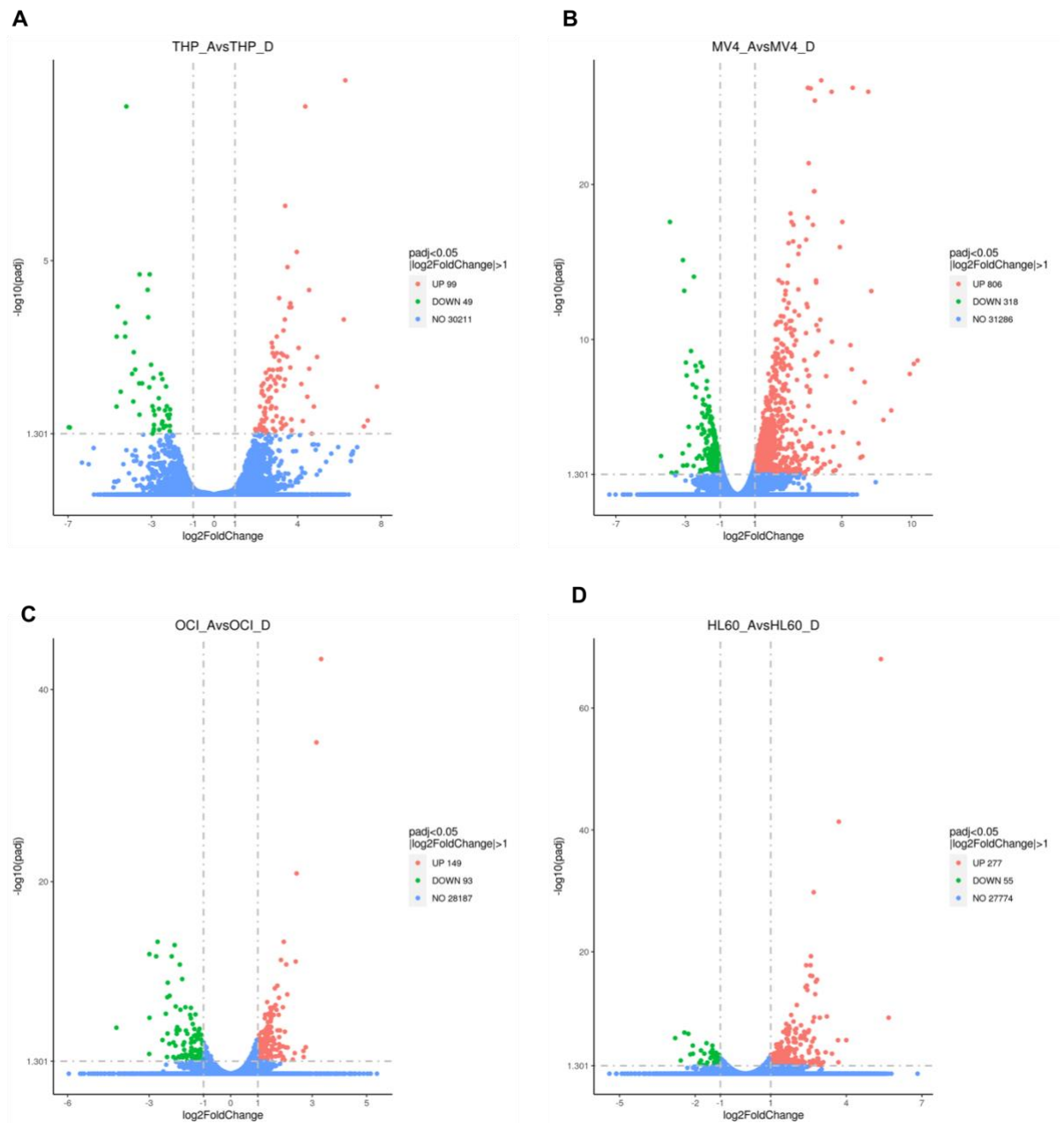


Figure 5.6 Differential gene expression of leukaemic cell lines treated with ATV.

A-D. Volcano plots show the number of DEGs that were upregulated or downregulated between comparative treatments with 48h-IC50 dose of ATV or 0.01% DMSO, on THP1, MV4-11, OCI-AML3 and HL60. It also shows the number of genes that showed no change (NO). DEGs are based on a threshold of log₂FoldChange >1 and padj < 0.05. Results are from two biological replicates. Figures were generated by Novogene. D= DMSO; H= HHT; A= ATV.

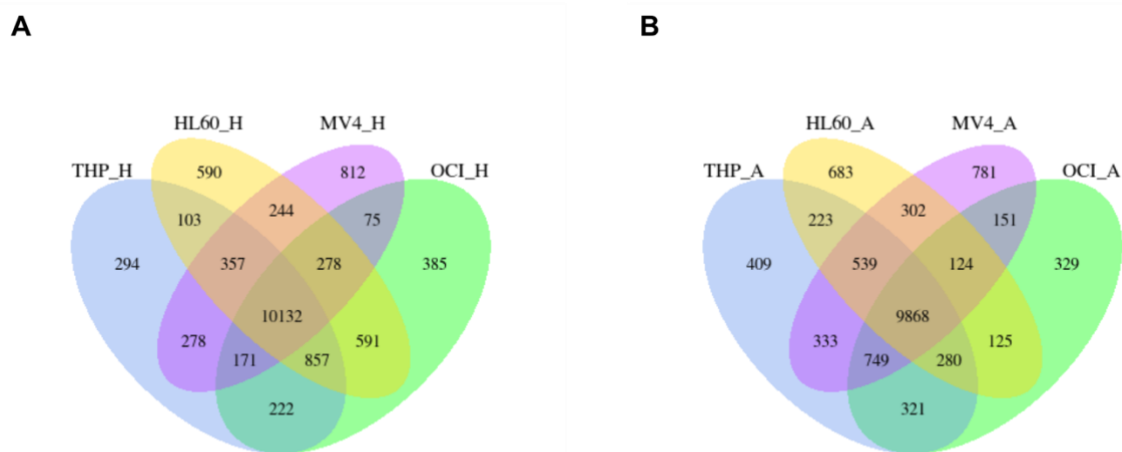


Figure 5.7 Schematic representation of co-expressed genes in treated leukaemic cell lines.

Venn diagrams illustrate the number of genes mutually or exclusively expressed in leukaemic cell lines that were treated with the 48h-IC50 doses of HHT (**A**) or ATV (**B**) for 48h. H= HHT; A= ATV.

5.6 Pathway analysis of IC50-treated leukaemic cell lines

Kyoto encyclopedia of genes and genomes (KEGG) pathway analysis was performed on the DEGs that were either upregulated or downregulated after treatment with HHT or ATV. As expected, the top 20 pathways identified varied for individual cell lines (Figure 5.8, Figure 5.9, Figure 5.10 and Figure 5.11). However, some recurring pathways between cell lines or treatments were identified. These include the IL-17 signalling pathway, PI3K-Akt signalling pathway, systemic lupus erythematosus and rheumatoid arthritis (Table 5.2). The false discovery rate (FDR) and enrichment score (ES) associated with these KEGG pathways were not significantly enriched based on a cut-off of < 0.05 . The IL-17 signalling and rheumatoid arthritis were both highlighted in THP1 cells treated with HHT and in OCI-AML3 cells treated with ATV, indicating a potential.

ATV treatment of THP1 and OCI-AML3 cells resulted in differential expression of genes associated with the PI3K-Akt signalling pathway. Genes associated with systemic lupus erythematosus were affected by HHT treatment in all cell lines except MV4-11. Indeed, none of the aforementioned pathways were identified in MV4-11 after either treatments. Several signalling pathways were also enriched following ATV and HHT treatments, such as p53 signalling pathway, cAMP signalling pathway, TNF signalling pathway and HIF-1 signalling pathway. KEGG

pathways specific to cellular mechanisms such as cell cycle, DNA replication and similarly, pathways related to cancers like breast, prostate, lung and leukaemia were also enriched.

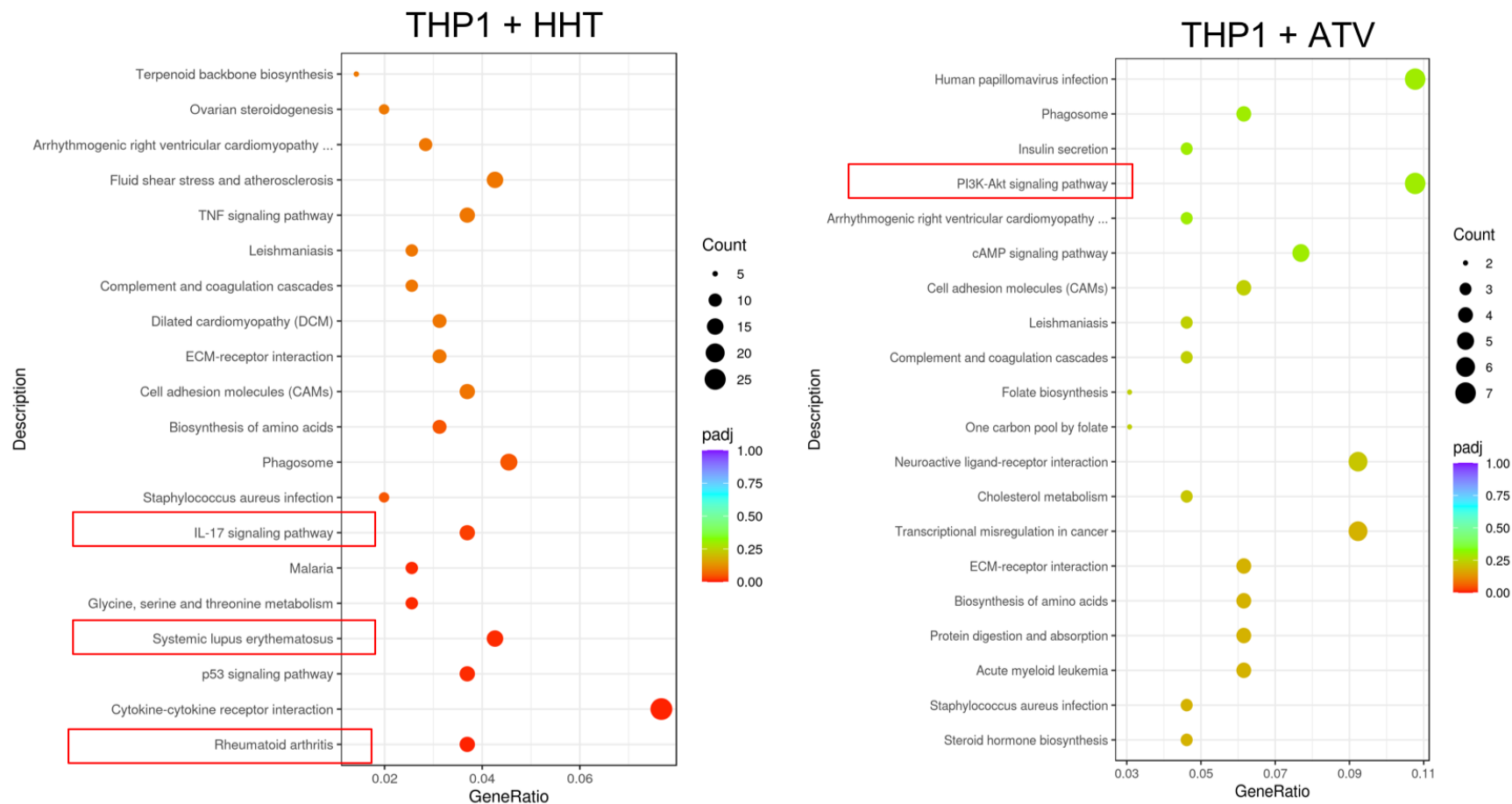


Figure 5.8 Pathway analysis of differentially expressed genes in THP1 treated with HHT or ATV.

A-D. Dot plots show the KEGG pathways that were enriched following treatment of THP1 with either HHT or ATV. Pathways of interest, recurring between cell lines are marked (red box). Results are from two biological replicates. Figures were generated by Novogene.

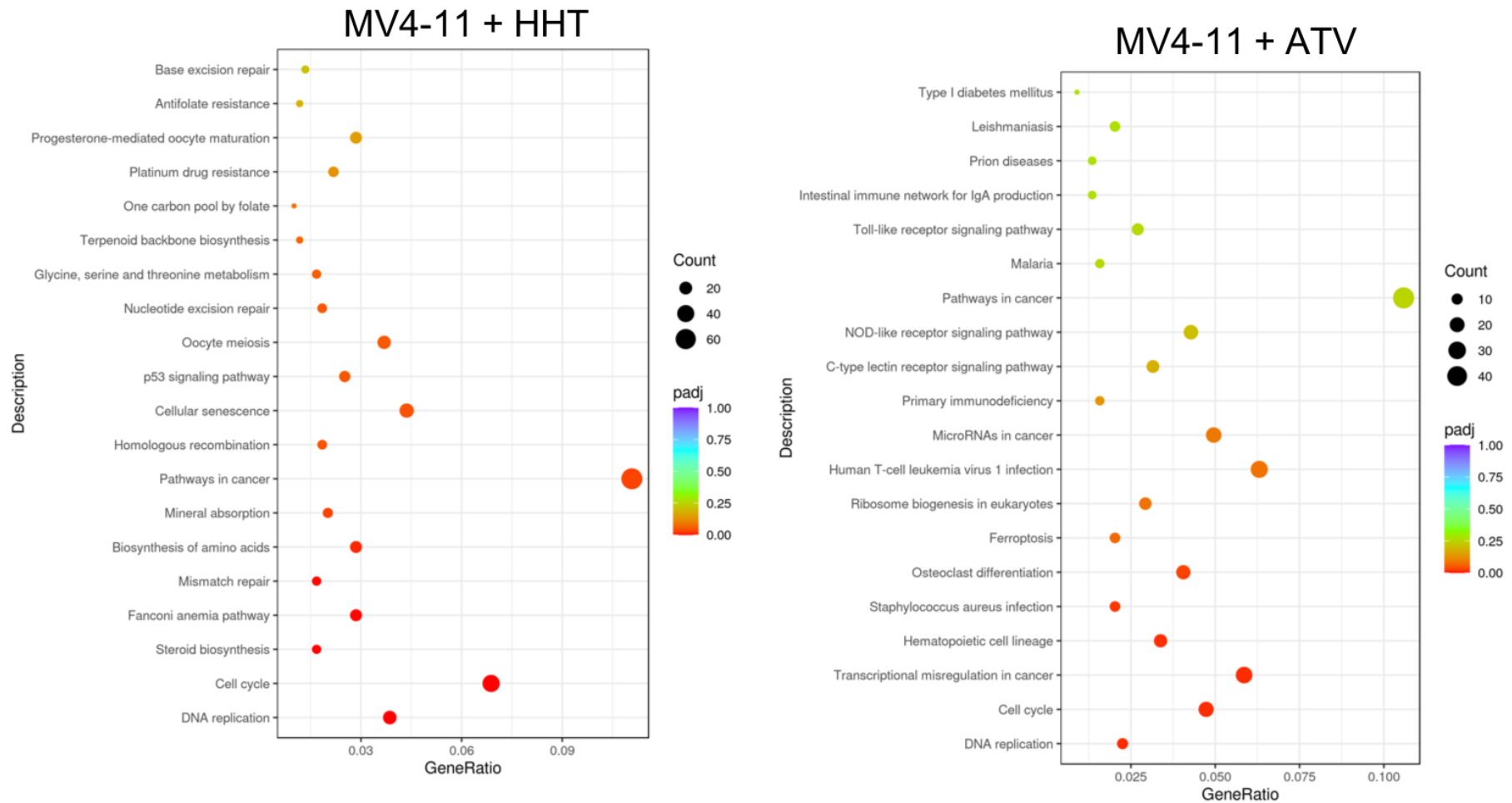


Figure 5.9 Pathway analysis of differentially expressed genes in MV4-11 treated with HHT or ATV.

A-D. Dot plots show the KEGG pathways that were enriched following treatment of MV4-11 with either HHT or ATV. Pathways of interest, recurring between cell lines are marked (red box). Results are from two biological replicates. Figures were generated by Novogene.

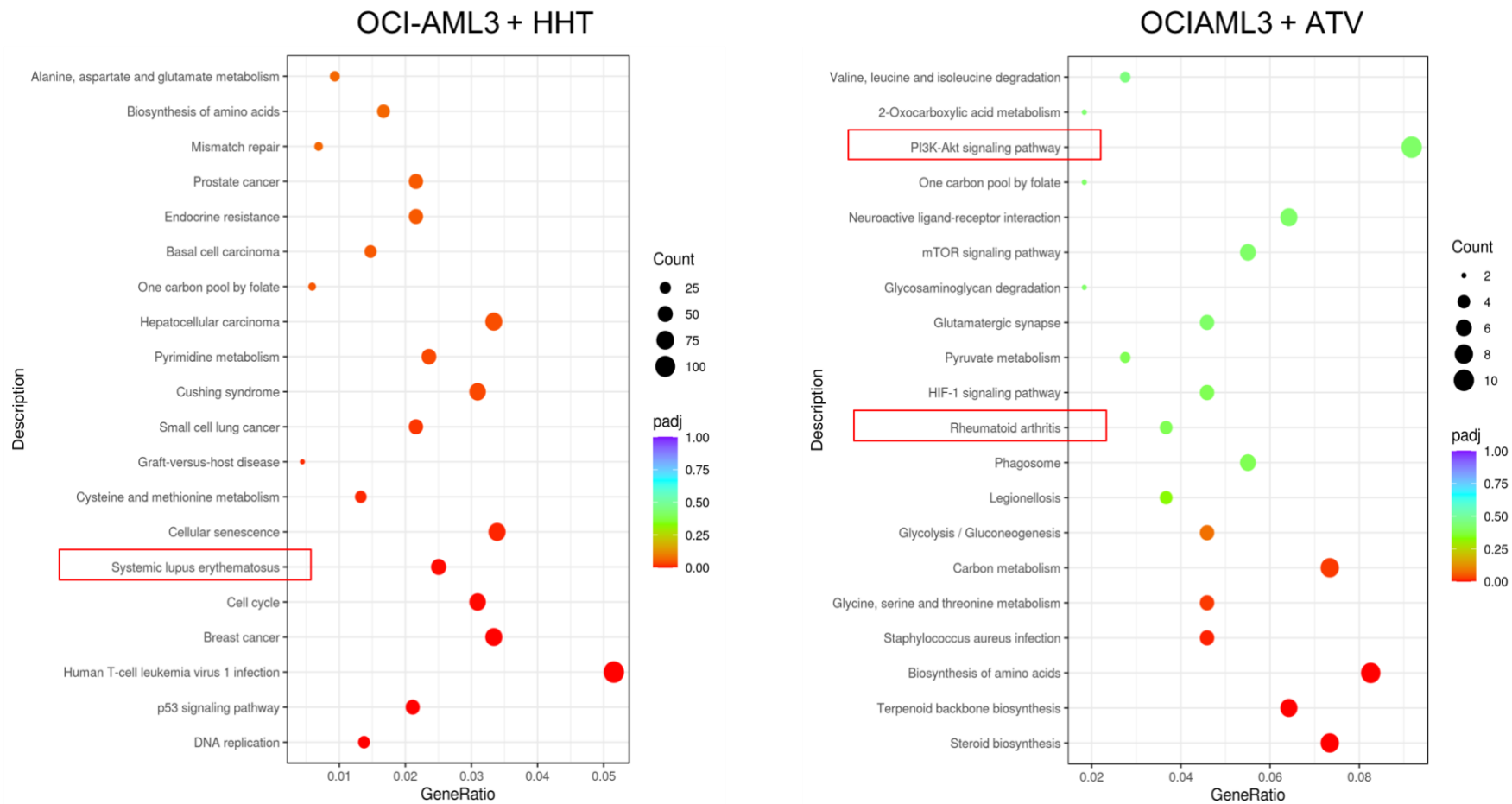


Figure 5.10 Pathway analysis of differentially expressed genes in OCI-AML3 treated with HHT or ATV.

A-D. Dot plots show the KEGG pathways that were enriched following treatment of OCI-AML3 with either HHT or ATV. Pathways of interest, recurring between cell lines are marked (red box). Results are from two biological replicates. Figures were generated by Novogene.

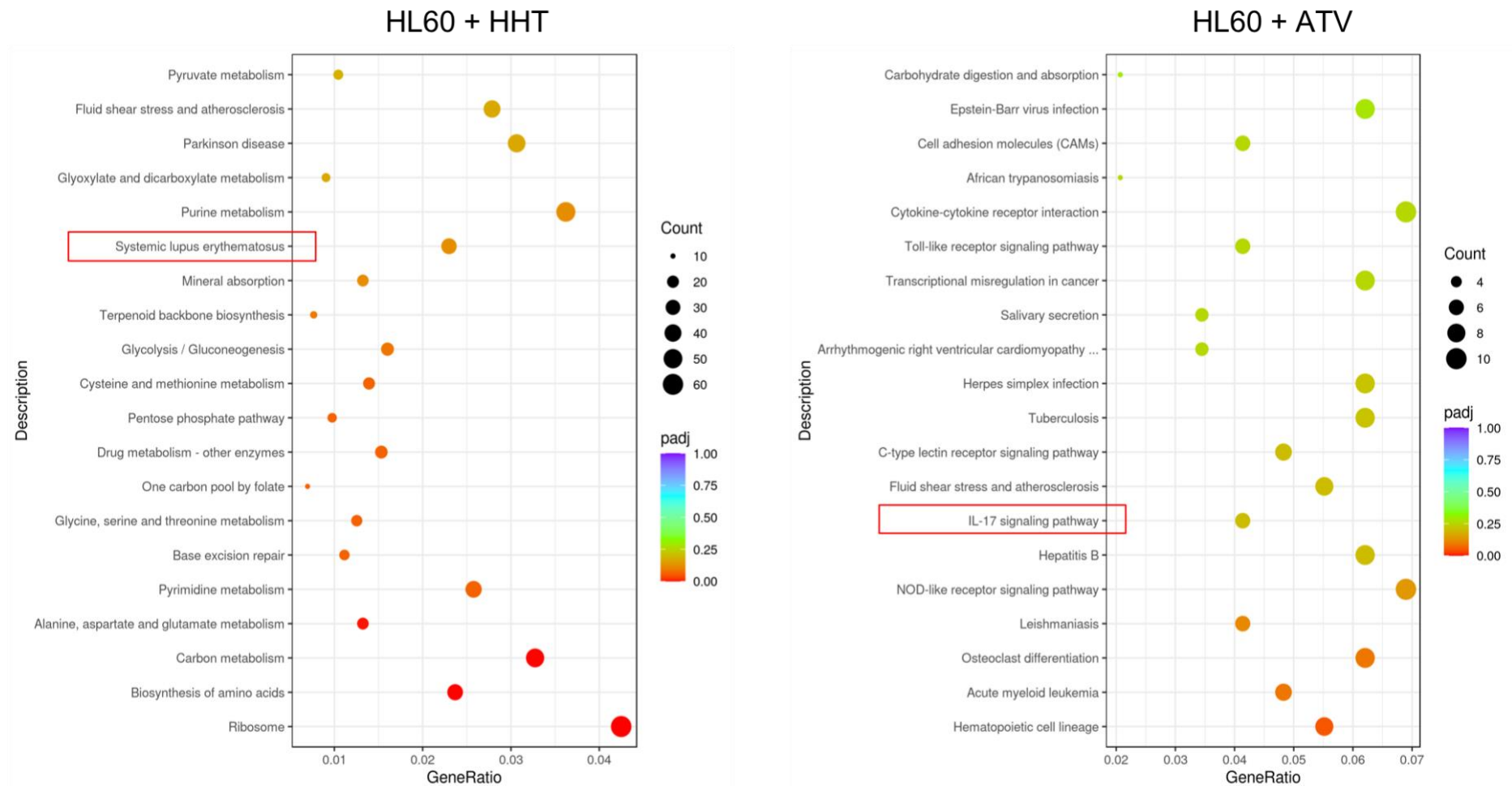


Figure 5.11 Pathway analysis of differentially expressed genes in HL60 treated with HHT or ATV.

A-D. Dot plots show the KEGG pathways that were enriched following treatment of HL60 with either HHT or ATV. Pathways of interest, recurring between cell lines are marked (red box). Results are from two biological replicates. Figures were generated by Novogene.

Table 5.2 Significance of KEGG pathways selected for validation

KEGG pathway	ATV		HHT	
	FDR (q-val)	ES	FDR	ES
Systemic lupus erythematosus				
THP1	0.31082758	0.42292172	0.17500001	0.7592949
HL60	0.45959458	0.43321872	0.6175084	0.6236965
OCI-AML3	0.3233853	0.5026722	0.25014848	0.7919585
MV4-11	0.1824831	0.531510	1	0.3753790
Rheumatoid arthritis				
THP1	0.44429392	0.33817112	0.17500003	0.65379685
HL60	0.58611506	0.28496087	-	-
OCI-AML3	0.48503816	0.2474653	0.34692833	0.72065634
MV4-11	0.27369946	0.39812186	1	0.24374826
IL-17 signalling				
THP1	0.26265362	0.36803398	0.17500012	0.70301634
HL60	0.5897613	0.26724064	0.6040312	0.4482906
OCI-AML3	0.4356982	0.29206333	0.28748772	0.6958927
MV4-11	0.3966217	0.36525035	1	0.23264502
PI3K-Akt signalling				
THP1	0.30525237	0.34023243	0.19558547	0.5328552
HL60	0.6885749	0.20130648	-	-
OCI-AML3	0.20315225	0.5030166	0.2513489	0.6482511
MV4-11	0.32442763	0.2829288	1	0.26844406

*FDR= false discovery rate, *ES= enrichment score

5.7 Validation of DEGs identified using RNA sequencing by qPCR

To validate the KEGG analysis, 3-4 DEGs were selected from each pathway were selected for quantification (Table 5.3). These genes were *BCL2*, *MMP9*, *IL1B*, *CD86*, *CDKN1A*, *CSF1*, *CXCL6*, *EIF4EBP1*, *H2AFZ* and *HIST1H3H*. Transcriptional changes of the selected DEGs were initially determined based on the fragments per kilobase of exon per million mapped (FPKM) extracted from the RNA sequencing data. These changes are denoted as either upregulated or downregulated relative to the FPKM of each gene in DMSO-treated samples (Table 5.4). Validation of these findings were achieved by examining the fold changes in expression using qPCR (Figure 5.12). The relative expression of these genes was found using DMSO-treated samples as a reference and

normalised to *B2M* expression. The same RNA samples used for RNA sequencing were also used for qPCR validation.

Table 5.3 Genes from four pathways and at least 3 cell lines were selected for validation by qPCR

Pathway	Drug	DEG	THP1	MV4-11	OCI-AML3	HL60
Systemic lupus erythematosus	HHT	CD86	✓	✓	✓	✓
		H2AFZ	✓	✓	✓	✓
		HIST1H3H	✓	✓	✓	✓
Rheumatoid arthritis	ATV and HHT	CD86	✓	✓	✓	✓
		IL1B	✓		✓	✓
		CXCL6	✓		✓	✓
		CSF1		✓	✓	✓
IL-17 signalling	ATV and HHT	IL1B	✓		✓	✓
		CXCL6	✓		✓	✓
		MMP9	✓		✓	✓
PI3K-Akt signalling	ATV	BCL2	✓		✓	✓
		CDKN1A	✓	✓	✓	✓
		E1F4EBP1	✓	✓	✓	✓

Table 5.4 Gene expression changes identified from RNA sequencing data

Gene	HHT				ATV			
	THP1	MV4_11	OCI-AML3	HL60	THP1	MV4_11	OCI-AML3	HL60
BCL2	down	no	down	down	down	no	down	no
MMP9	up	up	up	up	up	up	no	up
IL1B	up	no	up	up	down	up	down	up
CD86	up	up	up	up	up	up	no	up
CDKN1A	up	up	up	up	up	up	no	up
CSF1	up	down	up	no	down	up	down	no
CXCL6	up	0	up	up	no	0	no	0
EIF4EBP1	down	down	down	down	down	down	down	down
H2AFZ	down	down	down	down	down	down	no	down
HIST1H3H	up	down	up	up	no	up	up	no

Consistent with the RNA sequencing data, *BCL2* did not show upregulation by qPCR in all treated cell lines (Figure 5.12A). RNA sequencing, showed upregulation in *MMP9*, *CD86* and *CDKN1A* in all samples, except ATV-treated OCI-AML3 (Table 5.4). *MMP9* expression changes were also validated in the qPCR data for all samples except ATV-treated MV4-11 cells (Figure 5.12B). Upregulation of *CDKN1A* and *CXCL6* occurred in all samples after both treatments, which was also observed across several samples by qPCR. The expression of *EIF4EBP1* and *H2AFZ* was downregulated in all RNA sequencing samples, with no change in *H2AFZ* expression occurring in ATV-treated OCI-AML3. qPCR data confirmed that *EIF4EBP1* was not upregulated in most of these samples. Overall, the expression pattern of *EIF4EBP1* and *H2AFZ* from both assays were matching. Variations between the transcriptional data from RNA sequencing and qPCR in the remaining genes could be due to technical errors from primer design causing unspecific amplification (upregulation) or primer binding difficulties (downregulation) in the gene of interest. Another explanation is the differences in sensitivity levels of both assays, leading to missed identification of minor changes by one or other. These discrepancies warrant further assays and biological replicates to be performed.

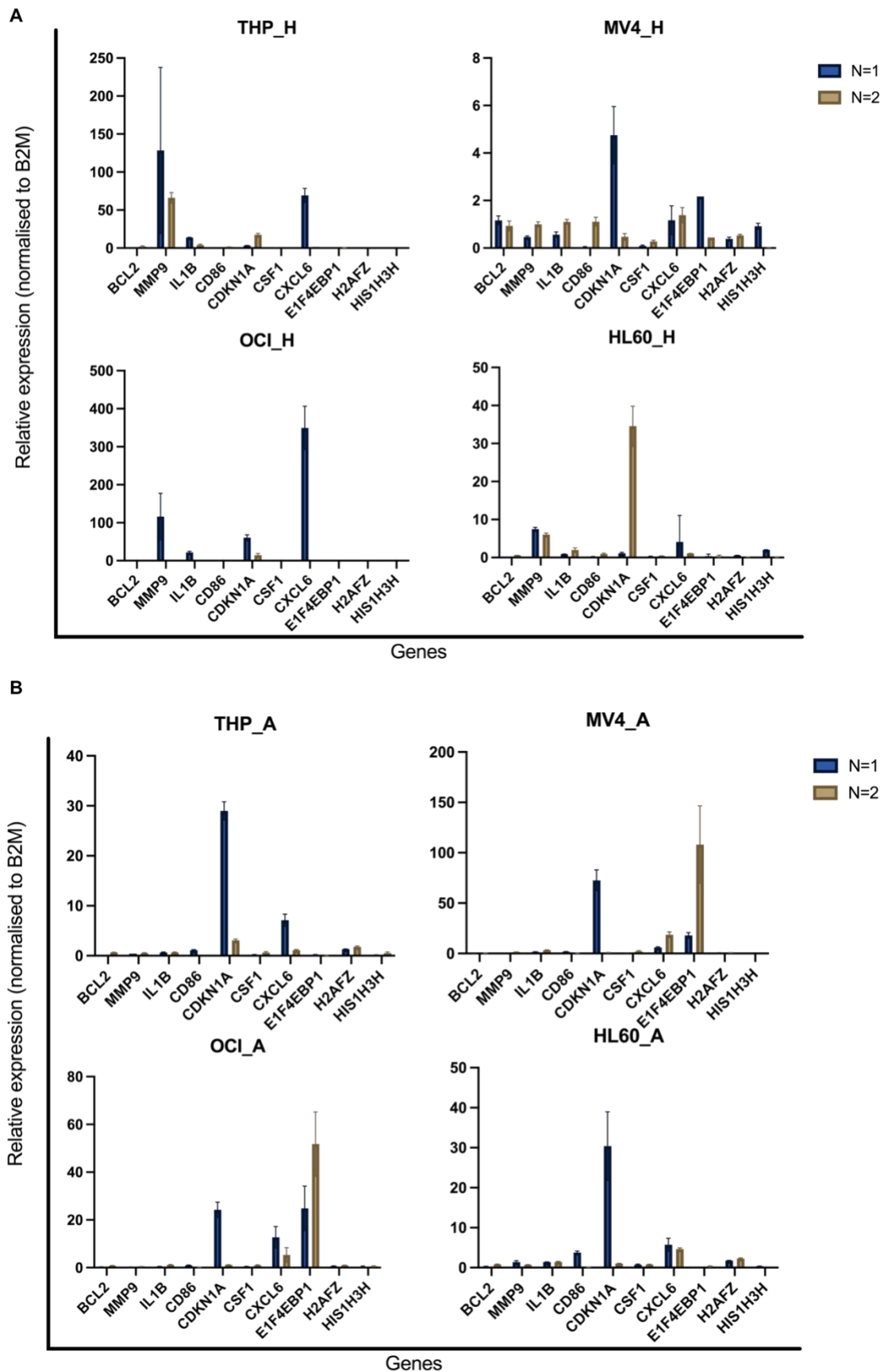


Figure 5.12 Validation of DEGs in treated leukaemic cell lines by qPCR.

Bar graphs show fold changes in expression of genes identified using qPCR following HHT (A) or ATV (B) treatment. Candidate genes were selected from RNA sequencing data. Data from biological replicates is shown separately, N=1

and N=2, due to variation. Results are mean \pm SD (n=3). Expression is normalized to *B2M* expression, relative to the DMSO-treated corresponding leukaemic cell line. H; HHT, A; ATV.

5.8 Discussion

In this chapter, the effective use of connectivity mapping as a means of identifying potential anti-leukaemic drugs has been validated. Feasibility of repurposed FDA-approved drugs has been demonstrated through successful eradication of MLLr and non-MLLr cell lines using HHT and ATV. HHT was shown to be highly effective in reducing leukaemic cell viability in all four cell lines tested, and inhibited growth *in vitro* after 24h of HHT exposure using concentrations previously reported to be achievable in human plasma after subcutaneous administration of the drug (Yakhni et al., 2019). HHT was shown to be more potent than ATV across all cell lines tested. This was further reflected using the CFU assay, where HHT inhibited self-renewal capacity and colony formation of all cell lines tested. Conversely, IC50 concentrations of ATV did not inhibit colony formation ability of any cell line, indicating that the mode of reduced cell viability observed is not at the level of leukaemia stem cell. RNA sequencing analysis demonstrated that HHT had the most profound effect on transcription of the non-MLLr cell line, OCI-AML3, whereas ATV mostly affected the transcriptome of an MLLr cell line, MV4-11. Notably, THP1, demonstrated the lowest effect on the transcriptome for both HHT and ATV treatments.

Anti-cancer properties of HHT are reported to primarily be exerted by inhibiting synthesis of cell survival proteins and onco-drivers such as Bcr-abl in chronic myeloid leukaemia (Gandhi et al., 2014). HHT has also been shown to kill lung cancer and breast cancer cells through IL6/JAK/STAT pathway and anti-apoptotic protein reduction, respectively (Cao et al., 2015; Yakhni et al., 2019). In line with this, RNA sequencing showed that the anti-apoptotic protein, BCL2, was downregulated after HHT and ATV treatment. Together, this suggests that inhibition of cell growth occurred in part by stimulating apoptosis. Cell stress could also be a prominent factor as these drugs are likely activating an inflammatory response in cells. This is because *IL1B* was upregulated in most of the cell lines following either treatment. ATV is known to enhance pro-inflammatory cytokines such as *IL6*, *TNF α* and *IL1B* (reviewed in Shaghghi et al., 2022). Upregulation of *CD86*, a marker of monocyte-committed blast cells (Re et al., 2002), was also

demonstrated, suggesting that cell stress-induced differentiation has taken place following the drug treatments. Similarly, upregulation of *MMP9* across all cell lines could be in response to cell stress, via the *CXCL1* upregulation shown or represent differentiation. Research has shown that *CXCR4*-ligand engagement upregulates *MMP9* as a response in B-cell chronic lymphoid leukaemia (Redondo-Muñoz et al., 2006). The anti-leukaemic potential of these drugs was also demonstrated by reduction in *EIF4EBP1* and *H2AFZ* expression. *EIF4EBP1* is linked to poor survival in hepatocellular cancer and an indicator of tumour oncogenic activity (Cha et al., 2015) and is also reported as an oncogene in breast cancer (Rutovsky et al., 2019). Similarly, *H2AFZ* overexpression is associated with tumour malignancy and poor prognosis in several cancers, particularly during the metastatic stage (Dong et al., 2021; Li et al., 2022). However, having indirectly targeted the *HOXA* cluster, it would be beneficial to observe the effect of ATV and HHT on the expression of candidate genes involved in the *Hoxa^{del}* signature used to initially identify these drugs.

To enhance drug-cell interactions, as in the case of ATV which is lipophilic, the concentrations of ATV tested can be loaded in nanostructured lipid carriers (NLCs) (Gambhire et al., 2018). Another effective approach could be using combination treatments. Studies have shown that therapeutic yield index was improved when ATV was used in combination with Trastuzumab in gastric cancer cells (Lee et al., 2019). Recently, ATV was also found to possess protective effects to chemotherapy, enlarging its area of exploitation (Marti et al., 2021; Juan et al., 2021).

To further exploit these promising therapeutic agents, the validated genes and pathways could be directly targeted using small molecules or inhibitors. Overall, treatment with HHT and ATV has revealed that both drugs resulted in measurable transcriptomic changes between cell lines, regardless of the *MLL* and possibly *HOXA* gene status. HL60 possess the lowest expression of *HOXA* genes, particularly *HOXA9* amongst the cell lines examined, however, it showed sensitivity to both drugs tested. Cell lines possess distinct biological characteristics such as cell of origin and mutational burden, ultimately leading to functional differences reflected in the variable drug responses observed.

This highlights the importance of advanced models for drug discovery and development and reinforces the need for generating isogenic leukaemia and iPSC-derived HSPCs to better test these and other candidate drugs .

Chapter 6 General Discussion

The focus of this thesis was to target HOXA in normal and malignant haematopoiesis using an endogenous tagged-HOXA9 iPSC line and leukaemic cell lines, respectively. Due to the vital role of particularly *HOXA9* in haematopoietic specification and development, a crucial pre-requisite was the ability to routinely and efficiently produce HSPCs from iPSCs. To this end, two haematopoietic differentiation protocols were tested and optimised; a monolayer- and a 3D spin EB-based protocol. The consistency and efficiency of the monolayer-based protocol was improved by using single cells to prepare iPSCs for differentiation as a suitable alternative to aggregates. Extending culture time in this protocol showed promising results as cells continued to gain a haematopoietic CD34+CD43+ profile beyond 12 days of differentiation, provided cultures are replenished with fresh media to avoid the compromised viability observed. However, the scalability of the monolayer-based protocol remained an obstacle despite these improvements, making this approach only suitable for experiments where high HSPCs quantity is not needed. For this reason, the 3D spin EB-based protocol was adapted, which was more robust and efficient, by producing higher HSPCs count and consistent results. Challenges in iPSCs maintenance and ability to further upscale the process were not circumvented. Nevertheless, the spin EB protocol allowed other areas of the project to be explored. In this approach, it was highlighted that relatively small changes in the timing of Activin and Wnt modulation can affect HSPC specification and potential differentiation. However, further study was warranted to examine which timepoint could potentially enhance HSPCs generation.

In line with previous studies, generation of *bona fide* HSPCs was proven to be challenging and the fine tuning of the protocols involved play a major role in the quality and maturity of HSPCs produced (primitive vs. definitive). Hence, the HSPCs derived using both protocols could be further analysed to examine whether they are functionally distinct. This could be achieved by adding more surface marker expression to the panel of characterisation. It is also worth sorting the CD34+CD43+ iPSC-HSPCs produced.

Following successful derivation of HSPCs from iPSCs, the endogenous *HOXA9* locus in human iPSCs was tagged with a fluorescent reporter, mScarlet-H, using

a footprint free CRISPR/Cas9 approach coupled with the PB transposase system. The reporter cell line generated, eA9^m, retained a *HOXA9* wild type allele due to the expected monoallelic targeting of CRISPR/Cas9. Two more genotypes of the *HOXA9* locus were also identified by Sanger sequencing; HOXA9-T2A-mScarlet and HOXA9-T2A-mScarlet-PB cassette, defining eA9^m as heterozygous. In theory, another possibility is that eA9^m could be a mixed clone, with some cells being “pre-excision” and others being “post-excision”. This is likely due to technical error during colony selection. Pre-excision cells harbouring PB resistance elements should still be resistant to puromycin treatment. Preliminary data showed that eA9^m is not resistant to puromycin. Whole genome sequencing of the targeted locus is crucial. From a range of 38 clones, C25 was selected to generate the eA9^m cell line. Hence, investigation of the remaining post-excision clones available remains a worthy goal as the PB cassette retention was validated in two clones only, C25 and C33, due to time restrictions. In the case of similarities in all remaining clones, PB transposase treatment and clone selection of the parental clone, C2+PB, should be repeated. This is also to ensure an early cell passage of the clone is being used, as it may subject the cell line to further limitations.

Although retention of the PB cassette in the clone was an unexpected finding, it was not found to have a major impact on the function of *HOXA9*. Thus, allowing it to be exploited as an iPSC model for *HOXA9* expression, particularly during haematopoiesis. Following molecular validation of eA9^m, the focus of this thesis was to assess the functionality of the reporter cell line relative to *HOXA9* expression. We first confirmed that genetic editing did not affect the stemness of eA9^m and it retained its pluripotency by generating CD34⁺CD43⁺ HSPCs. During this process, monitoring and tracking *HOXA9* expression was feasible without interference of the fluorescent reporter in its expression or function. This was demonstrated using the spin EB differentiation, where expected fluctuations of *HOXA9* were not affected and were mirrored by mScarlet-H expression, predominantly at early stages of the differentiation (day 4 and day 7). We also demonstrated the ability to attach and image eA9^m iPSCs using confocal microscopy. Due to the monolayer nature of this approach, we have shown that stimulation of *HOXA9* in eA9^m iPSCs by SB/CHIR/RA was reported by mScarlet-H.

As previously discussed, *MLLr* acts as an oncogenic driver and leads to dysregulation of the *HOXA* cluster. To this end, we attempted to further stimulate *HOXA9* expression using several approaches. Initially, we exploited the use of nucleofection to transfect eA9^m iPSCs with *MLL::AF9*-containing plasmids. Our results showed that transfection of these large (>10 kb) plasmids was feasible in eA9^m iPSCs, despite their sensitivity and the morphological stress noted. Indeed, upregulation of *HOXA9*, *mScarlet-H*, *cMYB* and *HOXA7* was observed after transfection. In myeloid leukaemia, deregulation of *cMYB* expression is a downstream effect of expression of TFs like *Hoxa9* and *Meis1* (Dassé et al., 2012). It is a pro-leukaemic target containing cis-regulatory elements that are bound by *HOXA9* (Dassé et al., 2012). Although, this confirmed that the transfection prompted a response in eA9^m, mScarlet-H fluorescence was not observed, which could be due to only a small proportion of cells incorporating the plasmids, making it technically challenging to find using a microscope. It is worth noting that these transcriptional changes were also observed using the control (empty) plasmid. This could be due to its smaller size (lack of *MLL::AF9* cDNA), hence efficiency of transfection was enhanced.

In parallel, few published studies involve efficient transduction of iPSCs, indicating that it has been challenging (Friedel et al., 2016). Previous results led us to generate LV using the nucleofection plasmids, pMA9 and pCTRL (MA9 LV and CTRL LV) and transduce eA9^m iPSCs. We attempted LVp transduction using various methods, either by the suspension method, where cells were seeded in their maintenance medium containing LVp and left in the incubator to attach, or to top up the medium with LVp after cell passaging and attachment. Due to ability of cells to survive the transduction, we attempted to enrich for the transduced cells by treating cells with puromycin, but no cells survived in this experiment. As such, results showed that eA9^m iPSCs transduction using these methods could be detrimental and was not considered a suitable approach.

Extensive research carried out in *MLLr* leukaemias has shown that the exact timing and cell of origin in which the leukaemic insult elucidates the disease is critical and still not fully clear. In a proof-of-principle study, we investigated the effect of *MLL::AF9* treatment of EBs during the EB differentiation using the

generated LV particles. We initiated the LVp induction during the hemato-vascular mesoderm stage (day 7 of the differentiation), as previous data showed the highest expression of *HOXA9* on that day, thus increasing the chances of *HOXA9* locus accessibility. *HOXA* genes are predominantly expressed in myeloid cells (Bhatlekar et al., 2018). Thus, exposure to LVp containing MLL::AF9 rearrangement has caused a dysregulation in gene expression, particularly in the *HOXA* cluster genes, *HOXA5*, *HOXA7* and *HOXA9*. Expression of these genes was downregulated on day 14 after MA9 LVp exposure, compared to untreated cells. These *HOXA* genes are targeted by *MLL* fusions and contribute to leukaemogenesis (Collins and Hess, 2016). An increase in *RUNX1*, *MYB* and *GATA2* are indicative of EHT and an emerging haematopoietic lineage (Alsayegh et al., 2019). *GATA2* is required for EHT and HSCs generation (de Pater et al., 2013). Therefore, the reduction in upregulation of these genes observed following MA9 LVp addition suggests that haematopoietic differentiation has been disturbed. Notably, both LVp triggered gene expression changes in these experiments. We propose that it could be a result of the LVp insult on iPSCs, warranting further investigation. Together with the nucleofection experiment findings, sequencing of the plasmid vectors, pMA9 and pCTRL, used to generate the LV particles is also essential.

In line with these conclusions, we demonstrated that the population of cells that integrated the LVp and expressed mScarlet-H was very low by flow cytometry. This reflects the issue with observing mScarlet-H in real-time. Moreover, we have also identified that due to the morphological 3D structure of EBs, autofluorescence was a technical issue in confocal imaging. Quantitatively, eA9^m EBs possessed higher fluorescence compared to RPATs EBs due to mScarlet-H expression. Thus, the relatively low percentage of *mScarlet-H* expression obtained from the endogenous targeting compared to the doxycycline induced AAVS-1 targeting clone, iA9, may have contributed to lack of detection with the fluorescence microscope.

Results from the CFU assay strongly dictates that LVp exposure has disturbed haematopoietic specification and development in eA9^m EBs. We have observed a shift towards the myeloid lineage, wherein the HSPCs derived from LVp-treated EBs were restricted to formation of BFU-E colonies only. These findings are

supported by the literature, which shows that viral infection of HSCs *in vivo* resulted in inflammatory stress that affected the functionality of HSCs, favouring the myeloid lineage (Hirche et al., 2017). Indeed, inflammatory signals promote differentiation of HSCs *in vivo*. Further investigation of these results will help determine if the responses observed are due to an inflammatory response from LVp exposure or the MLL::AF9 insult. This can be achieved by inducing inflammatory responses in EBs using combined exposure to cytokine molecules such as Toll-like receptor ligands, IL-6, tumour necrosis factor and CC motif chemokine ligand 2 (Chen et al., 2010; Takizawa et al., 2011).

However, inconsistency of the effect on HSPCs generation requires further examination and experimental repeats. These experiments reflected that iPSCs are hard to transfect, due to their aggressive immune responses and stringent membrane poration inhibiting the entry of viral vectors (Kalidasan et al., 2021). This highlights the need for testing other non-viral delivery vectors such as glycosaminoglycan-binding enhanced transduction peptides (Power et al., 2022).

Finally, we demonstrated the efficiency of using connectivity mapping for the identification of potential anti-cancer drugs. The efficacy of two potential anti-AML drugs were investigated, HHT and ATV. Drug responses between the leukaemic cell lines used were variable, which reflects the intrinsic differences that ultimately result in functional variations. These conclusions are supported by the transcriptome changes found in the RNA sequencing analysis performed. Similarly, current pre-clinical models do not fully recapitulate disease pathology in humans, as discussed in 1.4. To this end, eA9^m can be used to generate novel iPSC-derived AML and their isogenic HSPCs as an ideal platform for pre-clinical drug discovery studies. *In vivo* studies remain indispensable to fully examine the toxicity of these drugs against normal HSCs. Overall, we demonstrated the feasibility of utilising eA9^m iPSCs as a tool to study HOXA9 function in haematologic disorders through haematopoietic differentiation.

Findings from this project provide a robust platform for the generation of more advanced *in vitro* models of MLLr leukaemia. This could be achieved using gene editing tools such as CRISPR/Cas9 to induce chromosomal translocation, such as MLL::AF9, in iPSCs at stage-specific timepoints during the spin EB

haematopoietic differentiation. This would provide insights on the mechanism of initiation of the disease. In cancer studies, it will accelerate the route to *in vivo* studies and clinical trials. This is because it can help identify the effect of drugs, such as the ones identified in this project, on normal and *MLL::AF9*-harbouring iPSCs from the same cell line. Overall, this would reduce drug discovery failure rates and dependency on other *in vitro* models.

References

- Abolghasemi, R., Ebrahimi-Barough, S., Bahrami, N., & Ai, J. (2022). Atorvastatin Inhibits Viability and Migration of MCF7 Breast Cancer Cells. *Asian Pacific Journal of Cancer Prevention*, 23(3), 867–875. <https://doi.org/10.31557/APJCP.2022.23.3.867>
- Advani, A. S. (2006). Targeting the c-kit receptor in the treatment of acute myelogenous leukemia. *Current Hematologic Malignancy Reports*, 1(2), 101–107. <https://doi.org/10.1007/s11899-006-0020-9>
- Alharbi, R. A., Pettengell, R., Pandha, H. S., & Morgan, R. (2013). The role of HOX genes in normal hematopoiesis and acute leukemia. In *Leukemia* (Vol. 27, Issue 5, pp. 1000–1008). <https://doi.org/10.1038/leu.2012.356>
- Alsayegh, K., Cortés-Medina, L. v., Ramos-Mandujano, G., Badraiq, H., & Li, M. (2019). Hematopoietic Differentiation of Human Pluripotent Stem Cells: HOX and GATA Transcription Factors as Master Regulators. *Current Genomics*, 20(6), 438–452. <https://doi.org/10.2174/1389202920666191017163837>
- Alvandi, F., Kwitkowski, V. E., Ko, C.-W., Rothmann, M. D., Ricci, S., Saber, H., Ghosh, D., Brown, J., Pfeiler, E., Chikhale, E., Grillo, J., Bullock, J., Kane, R., Kaminskas, E., Farrell, A. T., & Pazdur, R. (2014). U.S. Food and Drug Administration Approval Summary: Omacetaxine Mepesuccinate as Treatment for Chronic Myeloid Leukemia. *The Oncologist*, 19(1), 94–99. <https://doi.org/10.1634/theoncologist.2013-0077>
- Arber, D. A., Orazi, A., Hasserjian, R. P., Borowitz, M. J., Calvo, K. R., Kvasnicka, H.-M., Wang, S. A., Bagg, A., Barbui, T., Branford, S., Bueso-Ramos, C. E., Cortes, J. E., Dal Cin, P., DiNardo, C. D., Dombret, H., Duncavage, E. J., Ebert, B. L., Estey, E. H., Facchetti, F., ... Tefferi, A. (2022). International Consensus Classification of Myeloid Neoplasms and Acute Leukemias: integrating morphologic, clinical, and genomic data. *Blood*, 140(11), 1200–1228. <https://doi.org/10.1182/blood.2022015850>
- Arber, D. A., Orazi, A., Hasserjian, R., Thiele, J., Borowitz, M. J., le Beau, M. M., Bloomfield, C. D., Cazzola, M., & Vardiman, J. W. (2016). The 2016 revision to the World Health Organization classification of myeloid neoplasms and acute

- leukemia. *Blood*, 127(20), 2391–2405. <https://doi.org/10.1182/blood-2016-03-643544>
- Aregger, M., Chandrashekhar, M., Tong, A. H. Y., Chan, K., & Moffat, J. (2019). *Pooled Lentiviral CRISPR-Cas9 Screens for Functional Genomics in Mammalian Cells* (pp. 169–188). https://doi.org/10.1007/978-1-4939-8805-1_15
- Argiropoulos, B., & Humphries, R. K. (2007). Hox genes in hematopoiesis and leukemogenesis. In *Oncogene* (Vol. 26, Issue 47, pp. 6766–6776). <https://doi.org/10.1038/sj.onc.1210760>
- Aryal, S., Zhang, Y., Wren, S., Li, C., & Lu, R. (2023). Molecular regulators of HOXA9 in acute myeloid leukemia. *The FEBS Journal*, 290(2), 321–339. <https://doi.org/10.1111/febs.16268>
- Bach, C., Buhl, S., Mueller, D., García-Cuellar, M.-P., Maethner, E., & Slany, R. K. (2010). Leukemogenic transformation by HOXA cluster genes. *Blood*, 115(14). <https://doi.org/10.1182/blood-2009-04-216606>
- Baron, M. H., Isern, J., & Fraser, S. T. (2012). The embryonic origins of erythropoiesis in mammals. *Blood*, 119(21), 4828–4837. <https://doi.org/10.1182/blood-2012-01-153486>
- Belyavsky, A., Petinati, N., & Drize, N. (2021). Hematopoiesis during Ontogenesis, Adult Life, and Aging. *International Journal of Molecular Sciences*, 22(17), 9231. <https://doi.org/10.3390/ijms22179231>
- Bhat, A. A., Nisar, S., Mukherjee, S., Saha, N., Yarravarapu, N., Lone, S. N., Masoodi, T., Chauhan, R., Maacha, S., Bagga, P., Dhawan, P., Akil, A. A.-S., El-Rifai, W., Uddin, S., Reddy, R., Singh, M., Macha, M. A., & Haris, M. (2022). Integration of CRISPR/Cas9 with artificial intelligence for improved cancer therapeutics. *Journal of Translational Medicine*, 20(1), 534. <https://doi.org/10.1186/s12967-022-03765-1>
- Bhatlekar, S., Fields, J. Z., & Boman, B. M. (2018). Role of HOX Genes in Stem Cell Differentiation and Cancer. *Stem Cells International*, 2018, 1–15. <https://doi.org/10.1155/2018/3569493>
- Bindels, D. S., Haarbosch, L., van Weeren, L., Postma, M., Wiese, K. E., Mastop, M., Aumonier, S., Gotthard, G., Royant, A., Hink, M. A., & Gadella, T. W. J. (2016). MScarlet: A bright monomeric red fluorescent protein for cellular imaging. *Nature Methods*, 14(1), 53–56. <https://doi.org/10.1038/nmeth.4074>
- Bock, C., Datlinger, P., Chardon, F., Coelho, M. A., Dong, M. B., Lawson, K. A., Lu, T., Maroc, L., Norman, T. M., Song, B., Stanley, G., Chen, S., Garnett, M., Li, W.,

- Moffat, J., Qi, L. S., Shapiro, R. S., Shendure, J., Weissman, J. S., & Zhuang, X. (2022). High-content CRISPR screening. *Nature Reviews Methods Primers*, 2(1), 8. <https://doi.org/10.1038/s43586-021-00093-4>
- Böiers, C., Carrelha, J., Lutteropp, M., Luc, S., Green, J. C. A., Azzoni, E., Woll, P. S., Mead, A. J., Hultquist, A., Swiers, G., Perdiguero, E. G., Macaulay, I. C., Melchiori, L., Luis, T. C., Kharazi, S., Bouriez-Jones, T., Deng, Q., Pontén, A., Atkinson, D., ... Jacobsen, S. E. W. (2013). Lymphomyeloid Contribution of an Immune-Restricted Progenitor Emerging Prior to Definitive Hematopoietic Stem Cells. *Cell Stem Cell*, 13(5), 535–548. <https://doi.org/10.1016/j.stem.2013.08.012>
- Brabetz, O., Alla, V., Angenendt, L., Schliemann, C., Berdel, W. E., Arteaga, M.-F., & Mikesch, J.-H. (2017). RNA-Guided CRISPR-Cas9 System-Mediated Engineering of Acute Myeloid Leukemia Mutations. *Molecular Therapy - Nucleic Acids*, 6, 243–248. <https://doi.org/10.1016/j.omtn.2016.12.012>
- Braekeleer, E. de, Douet-Guilbert, N., Basinko, A., Bris, M.-J. le, Morel, F., & Braekeleer, M. de. (2014). *Hox* gene dysregulation in acute myeloid leukemia. *Future Oncology*, 10(3). <https://doi.org/10.2217/fon.13.195>
- Buechele, C., Breese, E. H., Schneidawind, D., Lin, C.-H., Jeong, J., Duque-Afonso, J., Wong, S. H. K., Smith, K. S., Negrin, R. S., Porteus, M., & Cleary, M. L. (2015). MLL leukemia induction by genome editing of human CD34+ hematopoietic cells. *Blood*, 126(14), 1683–1694. <https://doi.org/10.1182/blood-2015-05-646398>
- Buske, C., Feuring-Buske, M., Antonchuk, J., Rosten, P., Hogge, D. E., Eaves, C. J., & Humphries, R. K. (2001). Overexpression of HOXA10 perturbs human lymphomyelopoiesis in vitro and in vivo. *Blood*, 97(8). <https://doi.org/10.1182/blood.V97.8.2286>
- Campos-Sanchez, E., Martínez-Cano, J., del Pino Molina, L., López-Granados, E., & Cobaleda, C. (2019). Epigenetic Deregulation in Human Primary Immunodeficiencies. *Trends in Immunology*, 40(1), 49–65. <https://doi.org/10.1016/j.it.2018.11.005>
- Canu, G., & Ruhrberg, C. (2021). First blood: the endothelial origins of hematopoietic progenitors. *Angiogenesis*, 24(2), 199–211. <https://doi.org/10.1007/s10456-021-09783-9>
- Cao, W., Liu, Y., Zhang, R., Zhang, B., Wang, T., Zhu, X., Mei, L., Chen, H., Zhang, H., Ming, P., & Huang, L. (2015). Homoharringtonine induces apoptosis and inhibits STAT3 via IL-6/JAK1/STAT3 signal pathway in Gefitinib-resistant lung cancer cells. *Scientific Reports*, 5(1), 8477. <https://doi.org/10.1038/srep08477>

- Cha, Y.-L., Li, P.-D., Yuan, L.-J., Zhang, M.-Y., Zhang, Y.-J., Rao, H.-L., Zhang, H.-Z., Zheng, X. F. S., & Wang, H.-Y. (2015). EIF4EBP1 Overexpression Is Associated with Poor Survival and Disease Progression in Patients with Hepatocellular Carcinoma. *PLOS ONE*, *10*(2), e0117493. <https://doi.org/10.1371/journal.pone.0117493>
- Chen, C., Liu, Y., Liu, Y., & Zheng, P. (2010). Mammalian target of rapamycin activation underlies HSC defects in autoimmune disease and inflammation in mice. *Journal of Clinical Investigation*, *120*(11), 4091–4101. <https://doi.org/10.1172/JCI43873>
- Chen, W., Kumar, A. R., Hudson, W. A., Li, Q., Wu, B., Staggs, R. A., Lund, E. A., Sam, T. N., & Kersey, J. H. (2008). Malignant Transformation Initiated by Mll-AF9: Gene Dosage and Critical Target Cells. *Cancer Cell*, *13*(5), 432–440. <https://doi.org/10.1016/j.ccr.2008.03.005>
- Cheng, H., Zheng, Z., & Cheng, T. (2020). New paradigms on hematopoietic stem cell differentiation. *Protein & Cell*, *11*(1), 34–44. <https://doi.org/10.1007/s13238-019-0633-0>
- Chiarella, E., Carrá, G., Scicchitano, S., Codispoti, B., Mega, T., Lupia, M., Pelaggi, D., Marafioti, M. G., Aloisio, A., Giordano, M., Nappo, G., Spoletti, C. B., Grillone, T., Giovannone, E. D., Spina, R., Bernaudo, F., Moore, M. A. S., Bond, H. M., Mesuraca, M., & Morrone, G. (2014). Umg lenti: Novel lentiviral vectors for efficient transgene- And reporter gene expression in human early hematopoietic progenitors. *PLoS ONE*, *9*(12). <https://doi.org/10.1371/journal.pone.0114795>
- Chiaretti, S., Gianfelici, V., Ceglie, G., & Foà, R. (2014). Genomic Characterization of Acute Leukemias. *Medical Principles and Practice*, *23*(6), 487–506. <https://doi.org/10.1159/000362793>
- Collins, C. T., & Hess, J. L. (2016). Deregulation of the HOXA9/MEIS1 axis in acute leukemia. In *Current Opinion in Hematology* (Vol. 23, Issue 4, pp. 354–361). Lippincott Williams and Wilkins. <https://doi.org/10.1097/MOH.0000000000000245>
- Collins, E. C., Pannell, R., Simpson, E. M., Forster, A., & Rabbitts, T. H. (2000). Inter-chromosomal recombination of *Mll* and *Af9* genes mediated by cre- *loxP* in mouse development. *EMBO Reports*, *1*(2), 127–132. <https://doi.org/10.1093/embo-reports/kvd021>
- Conlon, F. L., Lyons, K. M., Takaesu, N., Barth, K. S., Kispert, A., Herrmann, B., & Robertson, E. J. (1994). A primary requirement for nodal in the formation and

- maintenance of the primitive streak in the mouse. *Development*, 120(7), 1919–1928. <https://doi.org/10.1242/dev.120.7.1919>
- Corral, J., Lavenir, I., Impey, H., Warren, A. J., Forster, A., Larson, T. A., Bell, S., McKenzie, A. N. J., King, G., & Rabbitts, T. H. (1996). An MII–AF9 Fusion Gene Made by Homologous Recombination Causes Acute Leukemia in Chimeric Mice: A Method to Create Fusion Oncogenes. *Cell*, 85(6), 853–861. [https://doi.org/10.1016/S0092-8674\(00\)81269-6](https://doi.org/10.1016/S0092-8674(00)81269-6)
- Cortés, F., Debacker, C., Péault, B., & Labastie, M.-C. (1999). Differential expression of KDR/VEGFR-2 and CD34 during mesoderm development of the early human embryo. *Mechanisms of Development*, 83(1–2), 161–164. [https://doi.org/10.1016/S0925-4773\(99\)00030-1](https://doi.org/10.1016/S0925-4773(99)00030-1)
- Daga, A., Podesta, M., Capra, M. C., Piaggio, G., Frassoni, F., & Corte, G. (2000). The retroviral transduction of HOXC4 into human CD34+ cells induces an in vitro expansion of clonogenic and early progenitors. *Experimental Hematology*, 28(5), 569–574. [https://doi.org/10.1016/S0301-472X\(00\)00135-1](https://doi.org/10.1016/S0301-472X(00)00135-1)
- Dassé, E., Volpe, G., Walton, D. S., Wilson, N., Del Pozzo, W., O'Neill, L. P., Slany, R. K., Frampton, J., & Dumon, S. (2012). Distinct regulation of c-myb gene expression by HoxA9, Meis1 and Pbx proteins in normal hematopoietic progenitors and transformed myeloid cells. *Blood Cancer Journal*, 2(6), e76–e76. <https://doi.org/10.1038/bcj.2012.20>
- de Kouchkovsky, I., & Abdul-Hay, M. (2016). 'Acute myeloid leukemia: a comprehensive review and 2016 update.' *Blood Cancer Journal*, 6(7), e441–e441. <https://doi.org/10.1038/bcj.2016.50>
- Dong, M., Chen, J., Deng, Y., Zhang, D., Dong, L., & Sun, D. (2021). H2AFZ Is a Prognostic Biomarker Correlated to TP53 Mutation and Immune Infiltration in Hepatocellular Carcinoma. *Frontiers in Oncology*, 11. <https://doi.org/10.3389/fonc.2021.701736>
- Doss, M. X., & Sachinidis, A. (2019). Current Challenges of iPSC-Based Disease Modeling and Therapeutic Implications. *Cells*, 8(5), 403. <https://doi.org/10.3390/cells8050403>
- Dou, D. R., Calvanese, V., Sierra, M. I., Nguyen, A. T., Minasian, A., Saarikoski, P., Sasidharan, R., Ramirez, C. M., Zack, J. A., Crooks, G. M., Galic, Z., & Mikkola, H. K. A. (2016). Medial HOXA genes demarcate haematopoietic stem cell fate during human development. *Nature Cell Biology*, 18(6), 595–606. <https://doi.org/10.1038/ncb3354>

- Doulatov, S., Notta, F., Laurenti, E., & Dick, J. E. (2012). Hematopoiesis: A Human Perspective. *Cell Stem Cell*, 10(2), 120–136. <https://doi.org/10.1016/j.stem.2012.01.006>
- Drynan, L. F., Pannell, R., Forster, A., Chan, N. M. M., Cano, F., Daser, A., & Rabbits, T. H. (2005). Mll fusions generated by Cre-loxP-mediated de novo translocations can induce lineage reassignment in tumorigenesis. *The EMBO Journal*, 24(17), 3136–3146. <https://doi.org/10.1038/sj.emboj.7600760>
- el Chaer, F., Keng, M., & Ballen, K. K. (2020). MLL-Rearranged Acute Lymphoblastic Leukemia. *Current Hematologic Malignancy Reports*, 15(2), 83–89. <https://doi.org/10.1007/s11899-020-00582-5>
- Elliott, E. K., Haupt, L. M., & Griffiths, L. R. (2021). Mini review: genome and transcriptome editing using CRISPR-cas systems for haematological malignancy gene therapy. *Transgenic Research*, 30(2), 129–141. <https://doi.org/10.1007/s11248-020-00232-9>
- Enciso, J., Mendoza, L., & Pelayo, R. (2015). Normal vs. Malignant hematopoiesis: the complexity of acute leukemia through systems biology. *Frontiers in Genetics*, 6, 290. <https://doi.org/10.3389/fgene.2015.00290>
- Erfurth, F. E., Popovic, R., Grembecka, J., Cierpicki, T., Theisler, C., Xia, Z.-B., Stuart, T., Diaz, M. O., Bushweller, J. H., & Zeleznik-Le, N. J. (2008). MLL protects CpG clusters from methylation within the *Hoxa9* gene, maintaining transcript expression. *Proceedings of the National Academy of Sciences*, 105(21), 7517–7522. <https://doi.org/10.1073/pnas.0800090105>
- Evseenko, D., Zhu, Y., Schenke-Layland, K., Kuo, J., Latour, B., Ge, S., Scholes, J., David, G., Li, X., MacLellan, W. R., & Crooks, G. M. (2010). Mapping the first stages of mesoderm commitment during differentiation of human embryonic stem cells. *Proceedings of the National Academy of Sciences*, 107(31), 13742–13747. <https://doi.org/10.1073/pnas.1002077107>
- Faber, J., Krivtsov, A. v., Stubbs, M. C., Wright, R., Davis, T. N., van den Heuvel-Eibrink, M., Zwaan, C. M., Kung, A. L., & Armstrong, S. A. (2009). HOXA9 is required for survival in human MLL-rearranged acute leukemias. *Blood*, 113(11). <https://doi.org/10.1182/blood-2007-09-113597>
- Ferkowicz, M. J., & Yoder, M. C. (2005). Blood island formation: longstanding observations and modern interpretations. *Experimental Hematology*, 33(9), 1041–1047. <https://doi.org/10.1016/j.exphem.2005.06.006>

- Flamme, I., Breier, G., & Risau, W. (1995). Vascular Endothelial Growth Factor (VEGF) and VEGF Receptor 2(flk-1) Are Expressed during Vasculogenesis and Vascular Differentiation in the Quail Embryo. *Developmental Biology*, 169(2), 699–712. <https://doi.org/10.1006/dbio.1995.1180>
- Forster, A., Pannell, R., Drynan, L. F., McCormack, M., Collins, E. C., Daser, A., & Rabbitts, T. H. (2003). Engineering de novo reciprocal chromosomal translocations associated with Mll to replicate primary events of human cancer. *Cancer Cell*, 3(5), 449–458. [https://doi.org/10.1016/S1535-6108\(03\)00106-5](https://doi.org/10.1016/S1535-6108(03)00106-5)
- Frame, J. M., McGrath, K. E., & Palis, J. (2013). Erythro-myeloid progenitors: “Definitive” hematopoiesis in the conceptus prior to the emergence of hematopoietic stem cells. *Blood Cells, Molecules, and Diseases*, 51(4), 220–225. <https://doi.org/10.1016/j.bcmed.2013.09.006>
- Friedel, T., Jung-Klawitter, S., Sebe, A., Schenk, F., Modlich, U., Ivics, Z., Schumann, G. G., Buchholz, C. J., & Schneider, I. C. (2016). CD30 Receptor-Targeted Lentiviral Vectors for Human Induced Pluripotent Stem Cell-Specific Gene Modification. *Stem Cells and Development*, 25(9), 729–739. <https://doi.org/10.1089/scd.2015.0386>
- Frisch, B. J., & Calvi, L. M. (2014). *Hematopoietic Stem Cell Cultures and Assays* (pp. 315–324). https://doi.org/10.1007/978-1-62703-989-5_24
- Gambhire, V. M., Salunkhe, S. M., & Gambhire, M. S. (2018). Atorvastatin-loaded lipid nanoparticles: antitumor activity studies on MCF-7 breast cancer cells. *Drug Development and Industrial Pharmacy*, 44(10), 1685–1692. <https://doi.org/10.1080/03639045.2018.1492605>
- Gandhi, V., Plunkett, W., & Cortes, J. E. (2014). Omacetaxine: A Protein Translation Inhibitor for Treatment of Chronic Myelogenous Leukemia. *Clinical Cancer Research*, 20(7), 1735–1740. <https://doi.org/10.1158/1078-0432.CCR-13-1283>
- Gao, X., Xu, C., Asada, N., & Frenette, P. S. (2018). The hematopoietic stem cell niche: from embryo to adult. *Development*, 145(2). <https://doi.org/10.1242/dev.139691>
- Genomic and Epigenomic Landscapes of Adult De Novo Acute Myeloid Leukemia. (2013). *New England Journal of Medicine*, 368(22), 2059–2074. <https://doi.org/10.1056/NEJMoa1301689>
- Golub, T. R., Slonim, D. K., Tamayo, P., Huard, C., Gaasenbeek, M., Mesirov, J. P., Coller, H., Loh, M. L., Downing, J. R., Caligiuri, M. A., Bloomfield, C. D., & Lander, E. S. (1999). Molecular Classification of Cancer: Class Discovery and Class

- Prediction by Gene Expression Monitoring. *Science*, 286(5439).
<https://doi.org/10.1126/science.286.5439.531>
- Gomes, A. M., Kurochkin, I., Chang, B., Daniel, M., Law, K., Satija, N., Lachmann, A., Wang, Z., Ferreira, L., Ma'ayan, A., Chen, B. K., Papatsenko, D., Lemischka, I. R., Moore, K. A., & Pereira, C.-F. (2018). Cooperative Transcription Factor Induction Mediates Hemogenic Reprogramming. *Cell Reports*, 25(10), 2821-2835.e7. <https://doi.org/10.1016/j.celrep.2018.11.032>
- González-Romero, E., Martínez-Valiente, C., García-Ruiz, C., Vázquez-Manrique, R. P., Cervera, J., & Sanjuan-Pla, A. (2019). CRISPR to fix bad blood: a new tool in basic and clinical hematology. *Haematologica*, 104(5), 881–893. <https://doi.org/10.3324/haematol.2018.211359>
- Gori, J. L., Butler, J. M., Chan, Y.-Y., Chandrasekaran, D., Poulos, M. G., Ginsberg, M., Nolan, D. J., Elemento, O., Wood, B. L., Adair, J. E., Rafii, S., & Kiem, H.-P. (2015). Vascular niche promotes hematopoietic multipotent progenitor formation from pluripotent stem cells. *Journal of Clinical Investigation*, 125(3), 1243–1254. <https://doi.org/10.1172/JCI79328>
- Grier, D., Thompson, A., Kwasniewska, A., McGonigle, G., Halliday, H., & Lappin, T. (2005). The pathophysiology of HOX genes and their role in cancer. *The Journal of Pathology*, 205(2). <https://doi.org/10.1002/path.1710>
- Gunaseeli, I., Doss, M., Antzelevitch, C., Hescheler, J., & Sachinidis, A. (2010). Induced Pluripotent Stem Cells as a Model for Accelerated Patient- and Disease-specific Drug Discovery. *Current Medicinal Chemistry*, 17(8), 759–766. <https://doi.org/10.2174/092986710790514480>
- Hannon, G. J., & Rossi, J. J. (2004). Unlocking the potential of the human genome with RNA interference. *Nature*, 431(7006), 371–378. <https://doi.org/10.1038/nature02870>
- Hay, M., Thomas, D. W., Craighead, J. L., Economides, C., & Rosenthal, J. (2014). Clinical development success rates for investigational drugs. *Nature Biotechnology*, 32(1), 40–51. <https://doi.org/10.1038/nbt.2786>
- Hess, J., Yu, B., Li, B., Hanson, R., & Korsmeyer, S. (1997). Defects in yolk sac hematopoiesis in Mll-null embryos. *Blood*, 90(5).
- Hirche, C., Frenz, T., Haas, S. F., Döring, M., Borst, K., Tegtmeyer, P.-K., Brizic, I., Jordan, S., Keyser, K., Chhatbar, C., Pronk, E., Lin, S., Messerle, M., Jonjic, S., Falk, C. S., Trumpp, A., Essers, M. A. G., & Kalinke, U. (2017). Systemic Virus Infections Differentially Modulate Cell Cycle State and Functionality of Long-Term

- Hematopoietic Stem Cells In Vivo. *Cell Reports*, 19(11), 2345–2356. <https://doi.org/10.1016/j.celrep.2017.05.063>
- Horiuchi, K., Perez-Cerezales, S., Papasaikas, P., Ramos-Ibeas, P., López-Cardona, A. P., Laguna-Barraza, R., Fonseca Balvís, N., Pericuesta, E., Fernández-González, R., Planells, B., Viera, A., Suja, J. A., Ross, P. J., Alén, F., Orio, L., Rodríguez de Fonseca, F., Pintado, B., Valcárcel, J., & Gutiérrez-Adán, A. (2018). Impaired Spermatogenesis, Muscle, and Erythrocyte Function in U12 Intron Splicing-Defective Zrsr1 Mutant Mice. *Cell Reports*, 23(1), 143–155. <https://doi.org/10.1016/j.celrep.2018.03.028>
- Huang, X., Wang, Y., Yan, W., Smith, C., Ye, Z., Wang, J., Gao, Y., Mendelsohn, L., & Cheng, L. (2015). Production of Gene-Corrected Adult Beta Globin Protein in Human Erythrocytes Differentiated from Patient iPSCs After Genome Editing of the Sickle Point Mutation. *Stem Cells*, 33(5), 1470–1479. <https://doi.org/10.1002/stem.1969>
- Huang, Y., Sitwala, K., Bronstein, J., Sanders, D., Dandekar, M., Collins, C., Robertson, G., MacDonald, J., Cezard, T., Bilenky, M., Thiessen, N., Zhao, Y., Zeng, T., Hirst, M., Hero, A., Jones, S., & Hess, J. L. (2012). Identification and characterization of Hoxa9 binding sites in hematopoietic cells. *Blood*, 119(2), 388–398. <https://doi.org/10.1182/blood-2011-03-341081>
- Ishida, J., Konishi, M., Ebner, N., & Springer, J. (2016). Repurposing of approved cardiovascular drugs. *Journal of Translational Medicine*, 14(1), 269. <https://doi.org/10.1186/s12967-016-1031-5>
- Ivanovs, A., Rybtsov, S., Ng, E. S., Stanley, E. G., Elefanty, A. G., & Medvinsky, A. (2017). Human haematopoietic stem cell development: from the embryo to the dish. *Development*, 144(13), 2323–2337. <https://doi.org/10.1242/dev.134866>
- Jang, I. H., Lu, Y.-F., Zhao, L., Wenzel, P. L., Kume, T., Datta, S. M., Arora, N., Guiu, J., Lagha, M., Kim, P. G., Do, E. K., Kim, J. H., Schlaeger, T. M., Zon, L. I., Bigas, A., Burns, C. E., & Daley, G. Q. (2015). Notch1 acts via Foxc2 to promote definitive hematopoiesis via effects on hemogenic endothelium. *Blood*, 125(9), 1418–1426. <https://doi.org/10.1182/blood-2014-04-568170>
- Jeong, J., Jager, A., Domizi, P., Pavel-Dinu, M., Gojenola, L., Iwasaki, M., Wei, M. C., Pan, F., Zehnder, J. L., Porteus, M. H., Davis, K. L., & Cleary, M. L. (2019). High-efficiency CRISPR induction of t(9;11) chromosomal translocations and acute leukemias in human blood stem cells. *Blood Advances*, 3(19), 2825–2835. <https://doi.org/10.1182/bloodadvances.2019000450>

- Jing, L., Tamplin, O. J., Chen, M. J., Deng, Q., Patterson, S., Kim, P. G., Durand, E. M., McNeil, A., Green, J. M., Matsuura, S., Ablain, J., Brandt, M. K., Schlaeger, T. M., Huttenlocher, A., Daley, G. Q., Ravid, K., & Zon, L. I. (2015). Adenosine signaling promotes hematopoietic stem and progenitor cell emergence. *Journal of Experimental Medicine*, 212(5), 649–663. <https://doi.org/10.1084/jem.20141528>
- Jude, C. D., Climer, L., Xu, D., Artinger, E., Fisher, J. K., & Ernst, P. (2007). Unique and Independent Roles for MLL in Adult Hematopoietic Stem Cells and Progenitors. *Cell Stem Cell*, 1(3), 324–337. <https://doi.org/10.1016/j.stem.2007.05.019>
- Kalidasan, V., Ng, W. H., Ishola, O. A., Ravichantar, N., Tan, J. J., & Das, K. T. (2021). A guide in lentiviral vector production for hard-to-transfect cells, using cardiac-derived c-kit expressing cells as a model system. *Scientific Reports*, 11(1), 19265. <https://doi.org/10.1038/s41598-021-98657-7>
- Kang, H., Mesquitta, W.-T., Jung, H. S., Moskvina, O. v., Thomson, J. A., & Slukvin, I. I. (2018). GATA2 Is Dispensable for Specification of Hemogenic Endothelium but Promotes Endothelial-to-Hematopoietic Transition. *Stem Cell Reports*, 11(1), 197–211. <https://doi.org/10.1016/j.stemcr.2018.05.002>
- Kantarjian, H., Kadia, T., DiNardo, C., Daver, N., Borthakur, G., Jabbour, E., Garcia-Manero, G., Konopleva, M., & Ravandi, F. (2021). Acute myeloid leukemia: current progress and future directions. *Blood Cancer Journal*, 11(2), 41. <https://doi.org/10.1038/s41408-021-00425-3>
- Kennedy, M., Awong, G., Sturgeon, C. M., Ditadi, A., LaMotte-Mohs, R., Zúñiga-Pflücker, J. C., & Keller, G. (2012). T Lymphocyte Potential Marks the Emergence of Definitive Hematopoietic Progenitors in Human Pluripotent Stem Cell Differentiation Cultures. *Cell Reports*, 2(6), 1722–1735. <https://doi.org/10.1016/j.celrep.2012.11.003>
- Kettyle, L. M., Lebert-Ghali, C. É., Grishagin, I. v., Dickson, G. J., O'reilly, P. G., Simpson, D. A., Bijl, J. J., Mills, K. I., Sauvageau, G., & Thompson, A. (2019). Pathways, processes, and candidate drugs associated with a hoxa cluster-dependency model of leukemia. *Cancers*, 11(12). <https://doi.org/10.3390/cancers11122036>
- Kim, J. J. (2015). Applications of iPSCs in Cancer Research. *Biomarker Insights*, 10s1, BMI.S20065. <https://doi.org/10.4137/BMI.S20065>

- Ko, H. C., & Gelb, B. D. (2014). Concise Review: Drug Discovery in the Age of the Induced Pluripotent Stem Cell. *Stem Cells Translational Medicine*, 3(4), 500–509. <https://doi.org/10.5966/sctm.2013-0162>
- Kondrashov, A., Hoang, M. D., Smith, J. G. W., Bhagwan, J. R., Duncan, G., Mosqueira, D., Munoz, M. B., Vo, N. T. N., & Denning, C. (2018). Simplified Footprint-Free Cas9/CRISPR Editing of Cardiac-Associated Genes in Human Pluripotent Stem Cells. *Stem Cells and Development*, 27(6), 391–404. <https://doi.org/10.1089/scd.2017.0268>
- Krenz, D., Aivazidou, F., Bosio, A., Knöbel, S., & Bissels, U. (2017). Efficient isolation of human CD34+CD38- hematopoietic stem cells using immunomagnetic sorting. *Experimental Hematology*, 53, S124. <https://doi.org/10.1016/j.exphem.2017.06.311>
- Krivtsov, A. v., & Armstrong, S. A. (2007). MLL translocations, histone modifications and leukaemia stem-cell development. *Nature Reviews Cancer*, 7(11), 823–833. <https://doi.org/10.1038/nrc2253>
- Krivtsov, A. v, Figueroa, M. E., Sinha, A. U., Stubbs, M. C., Feng, Z., Valk, P. J. M., Delwel, R., Döhner, K., Bullinger, L., Kung, A. L., Melnick, A. M., & Armstrong, S. A. (2013). Cell of origin determines clinically relevant subtypes of MLL-rearranged AML. *Leukemia*, 27(4), 852–860. <https://doi.org/10.1038/leu.2012.363>
- Krivtsov, A. v., Twomey, D., Feng, Z., Stubbs, M. C., Wang, Y., Faber, J., Levine, J. E., Wang, J., Hahn, W. C., Gilliland, D. G., Golub, T. R., & Armstrong, S. A. (2006). Transformation from committed progenitor to leukaemia stem cell initiated by MLL–AF9. *Nature*, 442(7104), 818–822. <https://doi.org/10.1038/nature04980>
- Kroon, E. (1998). Hoxa9 transforms primary bone marrow cells through specific collaboration with Meis1a but not Pbx1b. *The EMBO Journal*, 17(13). <https://doi.org/10.1093/emboj/17.13.3714>
- Kumar, B., Garcia, M., Weng, L., Jung, X., Murakami, J. L., Hu, X., McDonald, T., Lin, A., Kumar, A. R., DiGiusto, D. L., Stein, A. S., Pullarkat, V. A., Hui, S. K., Carlesso, N., Kuo, Y.-H., Bhatia, R., Marcucci, G., & Chen, C.-C. (2018). Acute myeloid leukemia transforms the bone marrow niche into a leukemia-permissive microenvironment through exosome secretion. *Leukemia*, 32(3), 575–587. <https://doi.org/10.1038/leu.2017.259>
- Laboratories Inc, C. (n.d.). *Lenti-X™ GoStix™ Protocol-at-a-Glance*. www.clontech.com

- Lamb, J., Crawford, E. D., Peck, D., Modell, J. W., Blat, I. C., Wrobel, M. J., Lerner, J., Brunet, J.-P., Subramanian, A., Ross, K. N., Reich, M., Hieronymus, H., Wei, G., Armstrong, S. A., Haggarty, S. J., Clemons, P. A., Wei, R., Carr, S. A., Lander, E. S., & Golub, T. R. (2006). The Connectivity Map: Using Gene-Expression Signatures to Connect Small Molecules, Genes, and Disease. *Science*, *313*(5795), 1929–1935. <https://doi.org/10.1126/science.1132939>
- Lange, L., Morgan, M., & Schambach, A. (2021a). The hemogenic endothelium: a critical source for the generation of PSC-derived hematopoietic stem and progenitor cells. *Cellular and Molecular Life Sciences*, *78*(9), 4143–4160. <https://doi.org/10.1007/s00018-021-03777-y>
- Lange, L., Morgan, M., & Schambach, A. (2021b). The hemogenic endothelium: a critical source for the generation of PSC-derived hematopoietic stem and progenitor cells. *Cellular and Molecular Life Sciences*, *78*(9), 4143–4160. <https://doi.org/10.1007/s00018-021-03777-y>
- Lapidot, T., Sirard, C., Vormoor, J., Murdoch, B., Hoang, T., Caceres-Cortes, J., Minden, M., Paterson, B., Caligiuri, M. A., & Dick, J. E. (1994). A cell initiating human acute myeloid leukaemia after transplantation into SCID mice. *Nature*, *367*(6464), 645–648. <https://doi.org/10.1038/367645a0>
- Laurenti, E., & Göttgens, B. (2018). From haematopoietic stem cells to complex differentiation landscapes. *Nature*, *553*(7689), 418–426. <https://doi.org/10.1038/nature25022>
- Lawrence, H. J., Christensen, J., Fong, S., Hu, Y.-L., Weissman, I., Sauvageau, G., Humphries, R. K., & Largman, C. (2005). Loss of expression of the Hoxa-9 homeobox gene impairs the proliferation and repopulating ability of hematopoietic stem cells. *Blood*, *106*(12). <https://doi.org/10.1182/blood-2005-05-2003>
- Lawrence, J., Cameron, D., & Argyle, D. (2015). Species differences in tumour responses to cancer chemotherapy. *Philosophical Transactions of the Royal Society B: Biological Sciences*, *370*(1673), 20140233. <https://doi.org/10.1098/rstb.2014.0233>
- Lebert-Ghali, C.-É., Fournier, M., Kettyle, L., Thompson, A., Sauvageau, G., & Bijl, J. J. (2016). Hoxa cluster genes determine the proliferative activity of adult mouse hematopoietic stem and progenitor cells. *Blood*, *127*(1). <https://doi.org/10.1182/blood-2015-02-626390>
- Lee, S., Lee, H.-J., Kang, H., Kim, E.-H., Lim, Y.-C., Park, H., Lim, S. M., Lee, Y. J., Kim, J. M., & Kim, J. S. (2019). Trastuzumab Induced Chemobrain, Atorvastatin

- Rescued Chemobrain with Enhanced Anticancer Effect and without Hair Loss-Side Effect. *Journal of Clinical Medicine*, 8(2), 234. <https://doi.org/10.3390/jcm8020234>
- Li, M., & Belmonte, J. C. I. (2017). Ground rules of the pluripotency gene regulatory network. *Nature Reviews Genetics*, 18(3), 180–191. <https://doi.org/10.1038/nrg.2016.156>
- Li, X., Sun, B., Qian, H., Ma, J., Paolino, M., & Zhang, Z. (2022). A high-efficiency and versatile CRISPR/Cas9-mediated HDR-based biallelic editing system. *Journal of Zhejiang University-SCIENCE B*, 23(2), 141–152. <https://doi.org/10.1631/jzus.B2100196>
- Li, Z., Hu, M., Qiu, J., Feng, J., Zhang, R., Wu, H., Hu, G., & Ren, J. (2021). H2A Histone Family Member Z (H2AFZ) Serves as a Prognostic Biomarker in Lung Adenocarcinoma: Bioinformatic Analysis and Experimental Validation. *Medical Science Monitor*, 27. <https://doi.org/10.12659/MSM.933447>
- Li, Z., Huang, H., Li, Y., Jiang, X., Chen, P., Arnovitz, S., Radmacher, M. D., Maharry, K., Elkahlon, A., Yang, X., He, C., He, M., Zhang, Z., Dohner, K., Neilly, M. B., Price, C., Lussier, Y. A., Zhang, Y., Larson, R. A., ... Chen, J. (2012). Up-regulation of a HOXA-PBX3 homeobox-gene signature following down-regulation of miR-181 is associated with adverse prognosis in patients with cytogenetically abnormal AML. *Blood*, 119(10), 2314–2324. <https://doi.org/10.1182/blood-2011-10-386235>
- Lim, W. F., Inoue-Yokoo, T., Tan, K. S., Lai, M. I., & Sugiyama, D. (2013). Hematopoietic cell differentiation from embryonic and induced pluripotent stem cells. *Stem Cell Research & Therapy*, 4(3), 71. <https://doi.org/10.1186/scrt222>
- Lin, M. I., Price, E. N., Boatman, S., Hagedorn, E. J., Trompouki, E., Sathishchandran, S., Carspecken, C. W., Uong, A., DiBiase, A., Yang, S., Canver, M. C., Dahlberg, A., Lu, Z., Zhang, C. C., Orkin, S. H., Bernstein, I. D., Aster, J. C., White, R. M., & Zon, L. I. (2015). Angiopoietin-like proteins stimulate HSPC development through interaction with notch receptor signaling. *ELife*, 4. <https://doi.org/10.7554/eLife.05544>
- Lis, R., Karrasch, C. C., Poulos, M. G., Kunar, B., Redmond, D., Duran, J. G. B., Badwe, C. R., Schachterle, W., Ginsberg, M., Xiang, J., Tabrizi, A. R., Shido, K., Rosenwaks, Z., Elemento, O., Speck, N. A., Butler, J. M., Scandura, J. M., & Rafii, S. (2017). Conversion of adult endothelium to immunocompetent

- haematopoietic stem cells. *Nature*, 545(7655), 439–445.
<https://doi.org/10.1038/nature22326>
- Liu, P., Wakamiya, M., Shea, M. J., Albrecht, U., Behringer, R. R., & Bradley, A. (1999). Requirement for Wnt3 in vertebrate axis formation. *Nature Genetics*, 22(4), 361–365. <https://doi.org/10.1038/11932>
- Livak, K. J., & Schmittgen, T. D. (2001). Analysis of Relative Gene Expression Data Using Real-Time Quantitative PCR and the 2- $\Delta\Delta$ CT Method. *Methods*, 25(4), 402–408. <https://doi.org/10.1006/meth.2001.1262>
- Löwenberg, B., Ossenkoppele, G. J., van Putten, W., Schouten, H. C., Graux, C., Ferrant, A., Sonneveld, P., Maertens, J., Jongen-Lavrencic, M., von Lilienfeld-Toal, M., Biemond, B. J., Vellenga, E., Kooy, M. van M., Verdonck, L. F., Beck, J., Döhner, H., Gratwohl, A., Pabst, T., & Verhoef, G. (2009). High-Dose Daunorubicin in Older Patients with Acute Myeloid Leukemia. *New England Journal of Medicine*, 361(13), 1235–1248.
<https://doi.org/10.1056/NEJMoa0901409>
- Mark, M., Rijli, F. M., & Chambon, P. (1997). Homeobox Genes in Embryogenesis and Pathogenesis. *Pediatric Research*, 42(4), 421–429.
<https://doi.org/10.1203/00006450-199710000-00001>
- Marti, J. L. G., Beckwitt, C. H., Clark, A. M., & Wells, A. (2021a). Atorvastatin facilitates chemotherapy effects in metastatic triple-negative breast cancer. *British Journal of Cancer*, 125(9), 1285–1298. <https://doi.org/10.1038/s41416-021-01529-0>
- Marti, J. L. G., Beckwitt, C. H., Clark, A. M., & Wells, A. (2021b). Atorvastatin facilitates chemotherapy effects in metastatic triple-negative breast cancer. *British Journal of Cancer*, 125(9), 1285–1298. <https://doi.org/10.1038/s41416-021-01529-0>
- Mestas, J., & Hughes, C. C. W. (2004). Of Mice and Not Men: Differences between Mouse and Human Immunology. *The Journal of Immunology*, 172(5), 2731–2738. <https://doi.org/10.4049/jimmunol.172.5.2731>
- Metzeler, K. H., Herold, T., Rothenberg-Thurley, M., Amler, S., Sauerland, M. C., Görlich, D., Schneider, S., Konstandin, N. P., Dufour, A., Bräundl, K., Ksienzyk, B., Zellmeier, E., Hartmann, L., Greif, P. A., Fiegl, M., Subklewe, M., Bohlander, S. K., Krug, U., Faldum, A., ... Spiekermann, K. (2016). Spectrum and prognostic relevance of driver gene mutations in acute myeloid leukemia. *Blood*, 128(5), 686–698. <https://doi.org/10.1182/blood-2016-01-693879>
- Meyer, C., Burmeister, T., Gröger, D., Tsauro, G., Fehina, L., Renneville, A., Sutton, R., Venn, N. C., Emerenciano, M., Pombo-de-Oliveira, M. S., Barbieri Blunck, C.,

- Almeida Lopes, B., Zuna, J., Trka, J., Ballerini, P., Lapillonne, H., de Braekeleer, M., Cazzaniga, G., Corral Abascal, L., ... Marschalek, R. (2018a). The MLL recombinome of acute leukemias in 2017. *Leukemia*, 32(2), 273–284. <https://doi.org/10.1038/leu.2017.213>
- Meyer, C., Burmeister, T., Gröger, D., Tsaur, G., Fehina, L., Renneville, A., Sutton, R., Venn, N. C., Emerenciano, M., Pombo-De-Oliveira, M. S., Barbieri Blunck, C., Almeida Lopes, B., Zuna, J., Trka, J., Ballerini, P., Lapillonne, H., de Braekeleer, M., Cazzaniga, G., Corral Abascal, L., ... Marschalek, R. (2018b). The MLL recombinome of acute leukemias in 2017. *Leukemia*, 32(2), 273–284. <https://doi.org/10.1038/leu.2017.213>
- Meyer, C., Hofmann, J., Burmeister, T., Gröger, D., Park, T. S., Emerenciano, M., Pombo de Oliveira, M., Renneville, A., Villarese, P., Macintyre, E., Cavé, H., Clappier, E., Mass-Malo, K., Zuna, J., Trka, J., de Braekeleer, E., de Braekeleer, M., Oh, S. H., Tsaur, G., ... Marschalek, R. (2013). The MLL recombinome of acute leukemias in 2013. *Leukemia*, 27(11), 2165–2176. <https://doi.org/10.1038/leu.2013.135>
- Meyer, C., Schneider, B., Jakob, S., Strehl, S., Attarbaschi, A., Schnittger, S., Schoch, C., Jansen, M. W. J. C., van Dongen, J. J. M., den Boer, M. L., Pieters, R., Ennas, M.-G., Angelucci, E., Koehl, U., Greil, J., Griesinger, F., zur Stadt, U., Eckert, C., Szczepański, T., ... Marschalek, R. (2006). The MLL recombinome of acute leukemias. *Leukemia*, 20(5), 777–784. <https://doi.org/10.1038/sj.leu.2404150>
- Milne, T. A. (2017). Mouse models of MLL leukemia: recapitulating the human disease. *Blood*, 129(16), 2217–2223. <https://doi.org/10.1182/blood-2016-10-691428>
- Mojica, F. J. M., Díez-Villaseñor, C., García-Martínez, J., & Almendros, C. (2009). Short motif sequences determine the targets of the prokaryotic CRISPR defence system. *Microbiology*, 155(3), 733–740. <https://doi.org/10.1099/mic.0.023960-0>
- Mojica, F. J. M., Ferrer, C., Juez, G., & Rodríguez-Valera, F. (1995). Long stretches of short tandem repeats are present in the largest replicons of the Archaea *Haloferax mediterranei* and *Haloferax volcanii* and could be involved in replicon partitioning. *Molecular Microbiology*, 17(1), 85–93. https://doi.org/10.1111/j.1365-2958.1995.mmi_17010085.x
- Muntean, A. G., & Hess, J. L. (2012). The Pathogenesis of Mixed-Lineage Leukemia. *Annual Review of Pathology: Mechanisms of Disease*, 7(1), 283–301. <https://doi.org/10.1146/annurev-pathol-011811-132434>

- Nakamuta, A., Yoshido, K., & Naoki, H. (2022). Stem cell homeostasis regulated by hierarchy and neutral competition. *Communications Biology*, 5(1), 1268. <https://doi.org/10.1038/s42003-022-04218-7>
- Ng, E. S., Davis, R. P., Hatzistavrou, T., Stanley, E. G., & Elefanty, A. G. (2008). Directed Differentiation of Human Embryonic Stem Cells as Spin Embryoid Bodies and a Description of the Hematopoietic Blast Colony Forming Assay. *Current Protocols in Stem Cell Biology*, 4(1). <https://doi.org/10.1002/9780470151808.sc01d03s4>
- Nicholson, M. W., Ting, C.-Y., Chan, D. Z. H., Cheng, Y.-C., Lee, Y.-C., Hsu, C.-C., Huang, C.-Y., & Hsieh, P. C. H. (2022a). Utility of iPSC-Derived Cells for Disease Modeling, Drug Development, and Cell Therapy. *Cells*, 11(11), 1853. <https://doi.org/10.3390/cells11111853>
- Nicholson, M. W., Ting, C.-Y., Chan, D. Z. H., Cheng, Y.-C., Lee, Y.-C., Hsu, C.-C., Huang, C.-Y., & Hsieh, P. C. H. (2022b). Utility of iPSC-Derived Cells for Disease Modeling, Drug Development, and Cell Therapy. *Cells*, 11(11), 1853. <https://doi.org/10.3390/cells11111853>
- North, T. E., de Bruijn, M. F. T. R., Stacy, T., Talebian, L., Lind, E., Robin, C., Binder, M., Dzierzak, E., & Speck, N. A. (2002). Runx1 Expression Marks Long-Term Repopulating Hematopoietic Stem Cells in the Midgestation Mouse Embryo. *Immunity*, 16(5), 661–672. [https://doi.org/10.1016/S1074-7613\(02\)00296-0](https://doi.org/10.1016/S1074-7613(02)00296-0)
- North, T., Gu, T. L., Stacy, T., Wang, Q., Howard, L., Binder, M., Marin-Padilla, M., & Speck, N. A. (1999). Cbfa2 is required for the formation of intra-aortic hematopoietic clusters. *Development*, 126(11), 2563–2575. <https://doi.org/10.1242/dev.126.11.2563>
- Osaki, H., Walf-Vorderwülbecke, V., Mangolini, M., Zhao, L., Horton, S. J., Morrone, G., Schuringa, J. J., de Boer, J., & Williams, O. (2013). The AAA+ ATPase RUVBL2 is a critical mediator of MLL-AF9 oncogenesis. *Leukemia*, 27(7), 1461–1468. <https://doi.org/10.1038/leu.2013.42>
- Palis, J., Robertson, S., Kennedy, M., Wall, C., & Keller, G. (1999). Development of erythroid and myeloid progenitors in the yolk sac and embryo proper of the mouse. *Development*, 126(22), 5073–5084. <https://doi.org/10.1242/dev.126.22.5073>
- Palis, J., & Yoder, M. C. (2001). Yolk-sac hematopoiesis. *Experimental Hematology*, 29(8), 927–936. [https://doi.org/10.1016/S0301-472X\(01\)00669-5](https://doi.org/10.1016/S0301-472X(01)00669-5)

- Palumbo, A., Facon, T., Sonneveld, P., Bladè, J., Offidani, M., Gay, F., Moreau, P., Waage, A., Spencer, A., Ludwig, H., Boccadoro, M., & Harousseau, J.-L. (2008). Thalidomide for treatment of multiple myeloma: 10 years later. *Blood*, *111*(8), 3968–3977. <https://doi.org/10.1182/blood-2007-10-117457>
- Pammolli, F., Magazzini, L., & Riccaboni, M. (2011). The productivity crisis in pharmaceutical R&D. *Nature Reviews Drug Discovery*, *10*(6), 428–438. <https://doi.org/10.1038/nrd3405>
- Pantziarka, P., Bouche, G., Meheus, L., Sukhatme, V., Sukhatme, V. P., & Vikas, P. (2014). The Repurposing Drugs in Oncology (ReDO) Project. *Ecancermedicalscience*, *8*, 442. <https://doi.org/10.3332/ecancer.2014.442>
- Park, S., Cho, B. S., & Kim, H.-J. (2020a). New agents in acute myeloid leukemia (AML). *BLOOD RESEARCH*, *55*(S1), S14–S18. <https://doi.org/10.5045/br.2020.S003>
- Park, S., Cho, B. S., & Kim, H.-J. (2020b). New agents in acute myeloid leukemia (AML). *BLOOD RESEARCH*, *55*(S1), S14–S18. <https://doi.org/10.5045/br.2020.S003>
- Pearson, S., Cuvertino, S., Fleury, M., Lacaud, G., & Kouskoff, V. (2015). In Vivo Repopulating Activity Emerges at the Onset of Hematopoietic Specification during Embryonic Stem Cell Differentiation. *Stem Cell Reports*, *4*(3), 431–444. <https://doi.org/10.1016/j.stemcr.2015.01.003>
- Pearson, S., Sroczynska, P., Lacaud, G., & Kouskoff, V. (2008). The stepwise specification of embryonic stem cells to hematopoietic fate is driven by sequential exposure to Bmp4, activin A, bFGF and VEGF. *Development*, *135*(8), 1525–1535. <https://doi.org/10.1242/dev.011767>
- Pelayo, R., Dorantes-Acosta, E., Vadillo, E., & Fuentes-P, E. (2012). From HSC to B-Lymphoid Cells in Normal and Malignant Hematopoiesis. In *Advances in Hematopoietic Stem Cell Research*. InTech. <https://doi.org/10.5772/32213>
- Pittermann, E., Lachmann, N., MacLean, G., Emmrich, S., Ackermann, M., Göhring, G., Schlegelberger, B., Welte, K., Schambach, A., Heckl, D., Orkin, S. H., Cantz, T., & Klusmann, J.-H. (2017). Gene correction of HAX1 reversed Kostmann disease phenotype in patient-specific induced pluripotent stem cells. *Blood Advances*, *1*(14), 903–914. <https://doi.org/10.1182/bloodadvances.2016003798>
- Pollyea, D. A., Gutman, J. A., Gore, L., Smith, C. A., & Jordan, C. T. (2014). Targeting acute myeloid leukemia stem cells: a review and principles for the development

- of clinical trials. *Haematologica*, 99(8), 1277–1284.
<https://doi.org/10.3324/haematol.2013.085209>
- Power, R. N., Cavanagh, B. L., Dixon, J. E., Curtin, C. M., & O'Brien, F. J. (2022). Development of a Gene-Activated Scaffold Incorporating Multifunctional Cell-Penetrating Peptides for pSDF-1 α Delivery for Enhanced Angiogenesis in Tissue Engineering Applications. *International Journal of Molecular Sciences*, 23(3), 1460. <https://doi.org/10.3390/ijms23031460>
- Pushpakom, S., Iorio, F., Eyers, P. A., Escott, K. J., Hopper, S., Wells, A., Doig, A., Guilliams, T., Latimer, J., McNamee, C., Norris, A., Sanseau, P., Cavalla, D., & Pirmohamed, M. (2019). Drug repurposing: progress, challenges and recommendations. *Nature Reviews Drug Discovery*, 18(1), 41–58. <https://doi.org/10.1038/nrd.2018.168>
- Ramos-Mejía, V., Navarro-Montero, O., Ayllón, V., Bueno, C., Romero, T., Real, P. J., & Menendez, P. (2014). HOXA9 promotes hematopoietic commitment of human embryonic stem cells. *Blood*, 124(20), 3065–3075. <https://doi.org/10.1182/blood-2014-03-558825>
- Rathe, S. K., Moriarity, B. S., Stoltenberg, C. B., Kurata, M., Aumann, N. K., Rahrmann, E. P., Bailey, N. J., Melrose, E. G., Beckmann, D. A., Liska, C. R., & Largaespada, D. A. (2014). Using RNA-seq and targeted nucleases to identify mechanisms of drug resistance in acute myeloid leukemia. *Scientific Reports*, 4(1), 6048. <https://doi.org/10.1038/srep06048>
- Re, F., Arpinati, M., Testoni, N., Ricci, P., Terragna, C., Preda, P., Ruggeri, D., Senese, B., Chirumbolo, G., Martelli, V., Urbini, B., Baccarani, M., Tura, S., & Rondelli, D. (2002). Expression of CD86 in acute myelogenous leukemia is a marker of dendritic/monocytic lineage. *Experimental Hematology*, 30(2), 126–134. [https://doi.org/10.1016/S0301-472X\(01\)00768-8](https://doi.org/10.1016/S0301-472X(01)00768-8)
- Redaelli, A., Laskin, B. I., Stephens, J. M., Botteman, M. F., & Pashos, C. I. (2005). A systematic literature review of the clinical and epidemiological burden of acute lymphoblastic leukaemia (ALL). *European Journal of Cancer Care*, 14(1), 53–62. <https://doi.org/10.1111/j.1365-2354.2005.00513.x>
- Redondo-Muñoz, J., Escobar-Díaz, E., Samaniego, R., Terol, M. J., García-Marco, J. A., & García-Pardo, A. (2006). MMP-9 in B-cell chronic lymphocytic leukemia is up-regulated by $\alpha 4\beta 1$ integrin or CXCR4 engagement via distinct signaling pathways, localizes to podosomes, and is involved in cell invasion and migration. *Blood*, 108(9), 3143–3151. <https://doi.org/10.1182/blood-2006-03-007294>

- Richardson, C., & Jasin, M. (2000). Frequent chromosomal translocations induced by DNA double-strand breaks. *Nature*, *405*(6787), 697–700. <https://doi.org/10.1038/35015097>
- Rix, B., Maduro, A. H., Bridge, K. S., & Grey, W. (2022). Markers for human haematopoietic stem cells: The disconnect between an identification marker and its function. *Frontiers in Physiology*, *13*. <https://doi.org/10.3389/fphys.2022.1009160>
- Roth, B. D. (2002). *1 The Discovery and Development of Atorvastatin, A Potent Novel Hypolipidemic Agent* (pp. 1–22). [https://doi.org/10.1016/S0079-6468\(08\)70080-8](https://doi.org/10.1016/S0079-6468(08)70080-8)
- Roth, J. J., Crist, R. C., & Buchberg, A. M. (2009). Might as well face it: MLL's addicted to HOX. *Blood*, *113*(11). <https://doi.org/10.1182/blood-2009-01-197616>
- Ruiz, J. P., Chen, G., Haro Mora, J. J., Keyvanfar, K., Liu, C., Zou, J., Beers, J., Bloomer, H., Qanash, H., Uchida, N., Tisdale, J. F., Boehm, M., & Larochelle, A. (2019). Robust generation of erythroid and multilineage hematopoietic progenitors from human iPSCs using a scalable monolayer culture system. *Stem Cell Research*, *41*, 101600. <https://doi.org/10.1016/j.scr.2019.101600>
- Rutkovsky, A. C., Yeh, E. S., Guest, S. T., Findlay, V. J., Muise-Helmericks, R. C., Armeson, K., & Ethier, S. P. (2019). Eukaryotic initiation factor 4E-binding protein as an oncogene in breast cancer. *BMC Cancer*, *19*(1), 491. <https://doi.org/10.1186/s12885-019-5667-4>
- Rybtsov, S., Ivanovs, A., Zhao, S., & Medvinsky, A. (2016). Concealed expansion of immature precursors underpins acute burst of adult HSC activity in foetal liver. *Development*, *143*(8), 1284–1289. <https://doi.org/10.1242/dev.131193>
- Sauvageau, G., Lansdorp, P. M., Eaves, C. J., Hogge, D. E., Dragowska, W. H., Reid, D. S., Largman, C., Lawrence, H. J., & Humphries, R. K. (1994). Differential expression of homeobox genes in functionally distinct CD34+ subpopulations of human bone marrow cells. *Proceedings of the National Academy of Sciences*, *91*(25), 12223–12227. <https://doi.org/10.1073/pnas.91.25.12223>
- Scavone, C., Brusco, S., Bertini, M., Sportiello, L., Rafaniello, C., Zoccoli, A., Berrino, L., Racagni, G., Rossi, F., & Capuano, A. (2020). Current pharmacological treatments for COVID-19: What's next? *British Journal of Pharmacology*, *177*(21), 4813–4824. <https://doi.org/10.1111/bph.15072>
- Schneidawind, C., Jeong, J., Schneidawind, D., Kim, I.-S., Duque-Afonso, J., Wong, S. H. K., Iwasaki, M., Breese, E. H., Zehnder, J. L., Porteus, M., & Cleary, M. L.

- (2018). MLL leukemia induction by t(9;11) chromosomal translocation in human hematopoietic stem cells using genome editing. *Blood Advances*, 2(8), 832–845. <https://doi.org/10.1182/bloodadvances.2017013748>
- Schwaller, J. (2020a). Learning from mouse models of MLL fusion gene-driven acute leukemia. *Biochimica et Biophysica Acta (BBA) - Gene Regulatory Mechanisms*, 1863(8), 194550. <https://doi.org/10.1016/j.bbagr.2020.194550>
- Schwaller, J. (2020b). Learning from mouse models of MLL fusion gene-driven acute leukemia. *Biochimica et Biophysica Acta (BBA) - Gene Regulatory Mechanisms*, 1863(8), 194550. <https://doi.org/10.1016/j.bbagr.2020.194550>
- Scialdone, A., Tanaka, Y., Jawaid, W., Moignard, V., Wilson, N. K., Macaulay, I. C., Marioni, J. C., & Göttgens, B. (2016). Resolving early mesoderm diversification through single-cell expression profiling. *Nature*, 535(7611), 289–293. <https://doi.org/10.1038/nature18633>
- Shaghghi, Z., Alvandi, M., Farzipour, S., Dehbanpour, M. R., & Nosrati, S. (2022a). A review of effects of atorvastatin in cancer therapy. *Medical Oncology*, 40(1), 27. <https://doi.org/10.1007/s12032-022-01892-9>
- Shaghghi, Z., Alvandi, M., Farzipour, S., Dehbanpour, M. R., & Nosrati, S. (2022b). A review of effects of atorvastatin in cancer therapy. *Medical Oncology*, 40(1), 27. <https://doi.org/10.1007/s12032-022-01892-9>
- Shi, J., Wang, E., Milazzo, J. P., Wang, Z., Kinney, J. B., & Vakoc, C. R. (2015). Discovery of cancer drug targets by CRISPR-Cas9 screening of protein domains. *Nature Biotechnology*, 33(6), 661–667. <https://doi.org/10.1038/nbt.3235>
- Singh, T. U., Parida, S., Lingaraju, M. C., Kesavan, M., Kumar, D., & Singh, R. K. (2020). Drug repurposing approach to fight COVID-19. *Pharmacological Reports*, 72(6), 1479–1508. <https://doi.org/10.1007/s43440-020-00155-6>
- Slany, R. K. (2009). The molecular biology of mixed lineage leukemia. *Haematologica*, 94(7). <https://doi.org/10.3324/haematol.2008.002436>
- Soares-da-Silva, F., Freyer, L., Elsaid, R., Burlen-Defranoux, O., Iturri, L., Sismeiro, O., Pinto-do-Ó, P., Gomez-Perdiguerro, E., & Cumano, A. (2021). Yolk sac, but not hematopoietic stem cell-derived progenitors, sustain erythropoiesis throughout murine embryonic life. *Journal of Experimental Medicine*, 218(4). <https://doi.org/10.1084/jem.20201729>
- Sochacka-Ćwikła, A., Mączyński, M., & Regiec, A. (2021). FDA-Approved Drugs for Hematological Malignancies—The Last Decade Review. *Cancers*, 14(1), 87. <https://doi.org/10.3390/cancers14010087>

- Somervaille, T. C. P., & Cleary, M. L. (2006). Identification and characterization of leukemia stem cells in murine MLL-AF9 acute myeloid leukemia. *Cancer Cell*, 10(4), 257–268. <https://doi.org/10.1016/j.ccr.2006.08.020>
- Song, B., Fan, Y., He, W., Zhu, D., Niu, X., Wang, D., Ou, Z., Luo, M., & Sun, X. (2015). Improved Hematopoietic Differentiation Efficiency of Gene-Corrected Beta-Thalassemia Induced Pluripotent Stem Cells by CRISPR/Cas9 System. *Stem Cells and Development*, 24(9), 1053–1065. <https://doi.org/10.1089/scd.2014.0347>
- Stavropoulou, V., Kaspar, S., Brault, L., Sanders, M. A., Juge, S., Morettini, S., Tzankov, A., Iacovino, M., Lau, I.-J., Milne, T. A., Royo, H., Kyba, M., Valk, P. J. M., Peters, A. H. F. M., & Schwaller, J. (2016). MLL-AF9 Expression in Hematopoietic Stem Cells Drives a Highly Invasive AML Expressing EMT-Related Genes Linked to Poor Outcome. *Cancer Cell*, 30(1), 43–58. <https://doi.org/10.1016/j.ccell.2016.05.011>
- Sterner, R. C., & Sterner, R. M. (2021). CAR-T cell therapy: current limitations and potential strategies. *Blood Cancer Journal*, 11(4), 69. <https://doi.org/10.1038/s41408-021-00459-7>
- Studd, J. B., Cornish, A. J., Hoang, P. H., Law, P., Kinnersley, B., & Houlston, R. (2021). Cancer drivers and clonal dynamics in acute lymphoblastic leukaemia subtypes. *Blood Cancer Journal*, 11(11), 177. <https://doi.org/10.1038/s41408-021-00570-9>
- Sturgeon, C. M., Ditadi, A., Awong, G., Kennedy, M., & Keller, G. (2014). Wnt signaling controls the specification of definitive and primitive hematopoiesis from human pluripotent stem cells. *Nature Biotechnology*, 32(6), 554–561. <https://doi.org/10.1038/nbt.2915>
- Sugimura, R., Jha, D. K., Han, A., Soria-Valles, C., da Rocha, E. L., Lu, Y.-F., Goettel, J. A., Serrao, E., Rowe, R. G., Malleshaiah, M., Wong, I., Sousa, P., Zhu, T. N., Ditadi, A., Keller, G., Engelman, A. N., Snapper, S. B., Doulatov, S., & Daley, G. Q. (2017). Haematopoietic stem and progenitor cells from human pluripotent stem cells. *Nature*, 545(7655), 432–438. <https://doi.org/10.1038/nature22370>
- Sumi, T., Tsuneyoshi, N., Nakatsuji, N., & Suemori, H. (2008). Defining early lineage specification of human embryonic stem cells by the orchestrated balance of canonical Wnt/ β -catenin, Activin/Nodal and BMP signaling. *Development*, 135(17), 2969–2979. <https://doi.org/10.1242/dev.021121>

- Takahashi, K., & Yamanaka, S. (2006). Induction of Pluripotent Stem Cells from Mouse Embryonic and Adult Fibroblast Cultures by Defined Factors. *Cell*, 126(4), 663–676. <https://doi.org/10.1016/j.cell.2006.07.024>
- Takizawa, H., Regoes, R. R., Boddupalli, C. S., Bonhoeffer, S., & Manz, M. G. (2011). Dynamic variation in cycling of hematopoietic stem cells in steady state and inflammation. *Journal of Experimental Medicine*, 208(2), 273–284. <https://doi.org/10.1084/jem.20101643>
- Takizawa, H., Schanz, U., & Manz, M. (2011). Ex vivo expansion of hematopoietic stem cells: mission accomplished? *Swiss Medical Weekly*. <https://doi.org/10.4414/smw.2011.13316>
- Tavian, M., Robin, C., Coulombel, L., & Péault, B. (2001). The Human Embryo, but Not Its Yolk Sac, Generates Lympho-Myeloid Stem Cells. *Immunity*, 15(3), 487–495. [https://doi.org/10.1016/S1074-7613\(01\)00193-5](https://doi.org/10.1016/S1074-7613(01)00193-5)
- Tsakaneli, A., & Williams, O. (2021). Drug Repurposing for Targeting Acute Leukemia With KMT2A (MLL)—Gene Rearrangements. *Frontiers in Pharmacology*, 12. <https://doi.org/10.3389/fphar.2021.741413>
- Tursky, M. L., Loi, T. H., Artuz, C. M., Alateeq, S., Wolvetang, E. J., Tao, H., Ma, D. D., & Molloy, T. J. (2020). Direct Comparison of Four Hematopoietic Differentiation Methods from Human Induced Pluripotent Stem Cells. *Stem Cell Reports*, 15(3), 735–748. <https://doi.org/10.1016/j.stemcr.2020.07.009>
- Valletta, S., Dolatshad, H., Bartenstein, M., Yip, B. H., Bello, E., Gordon, S., Yu, Y., Shaw, J., Roy, S., Scifo, L., Schuh, A., Pellagatti, A., Fulga, T. A., Verma, A., & Boulwood, J. (2015). *ASXL1* mutation correction by CRISPR/Cas9 restores gene function in leukemia cells and increases survival in mouse xenografts. *Oncotarget*, 6(42), 44061–44071. <https://doi.org/10.18632/oncotarget.6392>
- Vodyanik, M. A., Thomson, J. A., & Slukvin, I. I. (2006). Leukosialin (CD43) defines hematopoietic progenitors in human embryonic stem cell differentiation cultures. *Blood*, 108(6), 2095–2105. <https://doi.org/10.1182/blood-2006-02-003327>
- Weng, T.-Y., Wu, H. F., Li, C.-Y., Hung, Y.-H., Chang, Y.-W., Chen, Y.-L., Hsu, H.-P., Chen, Y.-H., Wang, C.-Y., Chang, J.-Y., & Lai, M.-D. (2018). Homoharringtonine induced immune alteration for an Efficient Anti-tumor Response in Mouse Models of Non-small Cell Lung Adenocarcinoma Expressing Kras Mutation. *Scientific Reports*, 8(1), 8216. <https://doi.org/10.1038/s41598-018-26454-w>

- Whiteley, A. E., Price, T. T., Cantelli, G., & Sipkins, D. A. (2021). Leukaemia: a model metastatic disease. *Nature Reviews Cancer*, 21(7), 461–475. <https://doi.org/10.1038/s41568-021-00355-z>
- Winnier, G., Blessing, M., Labosky, P. A., & Hogan, B. L. (1995). Bone morphogenetic protein-4 is required for mesoderm formation and patterning in the mouse. *Genes & Development*, 9(17), 2105–2116. <https://doi.org/10.1101/gad.9.17.2105>
- Winters, A. C., & Bernt, K. M. (2017). MLL-Rearranged Leukemias—An Update on Science and Clinical Approaches. *Frontiers in Pediatrics*, 5. <https://doi.org/10.3389/fped.2017.00004>
- Xia, A.-L., He, Q.-F., Wang, J.-C., Zhu, J., Sha, Y.-Q., Sun, B., & Lu, X.-J. (2019). Applications and advances of CRISPR-Cas9 in cancer immunotherapy. *Journal of Medical Genetics*, 56(1), 4–9. <https://doi.org/10.1136/jmedgenet-2018-105422>
- Xiang, P., Wei, W., Hofs, N., Clemans-Gibbon, J., Maetzig, T., Lai, C. K., Dhillon, I., May, C., Ruschmann, J., Schneider, E., Rosten, P., Hu, K., Kuchenbauer, F., Hoodless, P. A., & Humphries, R. K. (2017). A knock-in mouse strain facilitates dynamic tracking and enrichment of MEIS1. *Blood Advances*, 1(24), 2225–2235. <https://doi.org/10.1182/bloodadvances.2017010355>
- Yakhni, M., Briat, A., el Guerrab, A., Furtado, L., Kwiatkowski, F., Miot-Noirault, E., Cachin, F., Penault-Llorca, F., & Radosevic-Robin, N. (2019). Homoharringtonine, an approved anti-leukemia drug, suppresses triple negative breast cancer growth through a rapid reduction of anti-apoptotic protein abundance. *American Journal of Cancer Research*, 9(5), 1043–1060.
- Yen, C.-T., Fan, M.-N., Yang, Y.-L., Chou, S.-C., Yu, I.-S., & Lin, S.-W. (2016). Current animal models of hemophilia: the state of the art. *Thrombosis Journal*, 14(S1), 22. <https://doi.org/10.1186/s12959-016-0106-0>
- Yoder, M. C. (2014). Inducing definitive hematopoiesis in a dish. *Nature Biotechnology*, 32(6), 539–541. <https://doi.org/10.1038/nbt.2929>
- Yokoyama, A., Somerville, T. C. P., Smith, K. S., Rozenblatt-Rosen, O., Meyerson, M., & Cleary, M. L. (2005). The Menin Tumor Suppressor Protein Is an Essential Oncogenic Cofactor for MLL-Associated Leukemogenesis. *Cell*, 123(2), 207–218. <https://doi.org/10.1016/j.cell.2005.09.025>
- Zeisig, B. B., Milne, T., García-Cuellar, M.-P., Schreiner, S., Martin, M.-E., Fuchs, U., Borkhardt, A., Chanda, S. K., Walker, J., Soden, R., Hess, J. L., & Slany, R. K. (2004). Hoxa9 and Meis1 Are Key Targets for MLL-ENL-Mediated Cellular

- Immortalization. *Molecular and Cellular Biology*, 24(2).
<https://doi.org/10.1128/MCB.24.2.617-628.2004>
- Zeng, J., Yi, D., Sun, W., Liu, Y., Chang, J., Zhu, L., Zhang, Y., Pan, X., Dong, Y., Zhou, Y., Lai, M., Bian, G., Zhou, Q., Liu, J., Chen, B., & Ma, F. (2021). Overexpression of HOXA9 upregulates NF-κB signaling to promote human hematopoiesis and alter the hematopoietic differentiation potentials. *Cell Regeneration*, 10(1), 9. <https://doi.org/10.1186/s13619-020-00066-0>
- Zhang, P., Li, J., Tan, Z., Wang, C., Liu, T., Chen, L., Yong, J., Jiang, W., Sun, X., Du, L., Ding, M., & Deng, H. (2008). Short-term BMP-4 treatment initiates mesoderm induction in human embryonic stem cells. *Blood*, 111(4), 1933–1941. <https://doi.org/10.1182/blood-2007-02-074120>
- Zhang, Z., Zhou, L., Xie, N., Nice, E. C., Zhang, T., Cui, Y., & Huang, C. (2020). Overcoming cancer therapeutic bottleneck by drug repurposing. *Signal Transduction and Targeted Therapy*, 5(1), 113. <https://doi.org/10.1038/s41392-020-00213-8>
- Zhou, Y., Zhu, S., Cai, C., Yuan, P., Li, C., Huang, Y., & Wei, W. (2014). High-throughput screening of a CRISPR/Cas9 library for functional genomics in human cells. *Nature*, 509(7501), 487–491. <https://doi.org/10.1038/nature13166>
- Zini, G., & Bennett, J. M. (2023). <sc>ICC</sc> -2022 versus <sc>WHO</sc> - 2022 classification systems for acute leukemias and myeloid neoplasms: The perspective from two classical morphologists. *American Journal of Hematology*. <https://doi.org/10.1002/ajh.26963>
- Zovein, A. C., Hofmann, J. J., Lynch, M., French, W. J., Turlo, K. A., Yang, Y., Becker, M. S., Zanetta, L., Dejana, E., Gasson, J. C., Tallquist, M. D., & Iruela-Arispe, M. L. (2008). Fate Tracing Reveals the Endothelial Origin of Hematopoietic Stem Cells. *Cell Stem Cell*, 3(6), 625–636. <https://doi.org/10.1016/j.stem.2008.09.018>